POLYAROMATIC ANTICANCER PLATINUM COMPLEXES: SYNTHESIS AND ANALYSIS OF DNA BINDING

Benjamin James Pages

B.Sc. (Hons)

School of Science and Health

Western Sydney University

A thesis presented to Western Sydney University in

fulfilment of the requirements for the degree of

Doctor of Philosophy (Science)

January 2018

Statement of Authenticity

This thesis is submitted in fulfilment of the requirements of the Doctor of Philosophy (Science) course at Western Sydney University, School of Science and Health. The work presented in this thesis is, to the best of my knowledge, original except as acknowledged in the text. All journal publications are included with the permission of their respective publishers. I hereby declare that I have not previously submitted this material, either in whole or in part, for a degree at this or any other institution.

16/01/18

Benjamin Pages

Acknowledgements

I would not have been able to complete this project without the help of many people, all of whom I would like to thank. First and foremost, I would like to thank my supervisors Professor Janice Aldrich-Wright, Professor William Price, and Dr Gang Zheng, for their support over the years. They have always been present to help with all inquiries and issues I have approached them with. In particular, Janice has been the cornerstone of my support for this project. Without her constant enthusiasm for all projects, even the failed ones, and her capacity to come up with new solutions and ideas, I would not have made it this far. Janice has also provided me with countless opportunities to travel overseas to both conduct research and to attend conferences, allowing me to become part of the international scientific community. She has also been there for me in tough personal times and for that I am truly grateful.

I would also like to thank past and present research students from Janice's group and others for their help and support over the years. Thank you to the past students Dr Benjamin Harper and Dr Neville Ng, PhD students Dale Ang, Aleksandra Bjelosevic, Krishant Deo, Samuel Frost and Lawson Spare, and the Masters students Ankita Dhiman, Jason Holland, Aleen Khoury, Lisa Lam, Brondwyn McGhie, Adeline Rajamanickam and Joseph Tadros. You have all made the office and lab a wonderful place to work these past four years. Thank you for any assistance you have provided, whether it is proof-reading work of mine, helping to solve lab or office issues, or just providing a huge helping of humour every day. I will remember each of you fondly in the years to come.

The work in this thesis would not be possible without the help of many international collaborators. Firstly, I would like to thank the Australian government and Scope Global for providing me with an Endeavour Fellowship, allowing me to travel to the UK for four months of work. A big thank you to Prof Alison Rodger for supervising me during my time at the University of Warwick, and being very patient with me when it came to writing our paper. Similar thanks to Dr Nikola Chmel for his supervision and help with my biophysical experiments. Thank you to all the members of Alison's group for their company and assistance during my time there – particularly Don Praveen Amarasinghe, Daniela Lobo, Meropi Sklepari and Dr Alan Wemyss. I also thank collaborators at other European universities for their assistance when I visited – Dr Sharon Kelly at Glasgow University for her help with isothermal titration calorimetry, Dr Nykola Jones at Aarhus University for assistance with synchrotron radiation circular dichroism and Dr James Hall of the University

of Reading for his help with DNA crystallisation. From other countries, I would like to thank Dr James Crowley of the University of Otago and Prof James Hoeschele from Eastern Michigan University for providing compounds from which I could synthesise new platinum complexes and publish new papers.

I would also like to thank several Australian academics for their assistance – from Calvary Mater Hospital Newcastle, Drs Jennette Sakoff and Jayne Gilbert for testing the cytotoxicity of so many of our compounds; from the Australian Nuclear Science and Technology Organisation, Dr Yingjie Zhang for obtaining X-ray crystal structures of our compounds; from Western Sydney University, Dr Feng Li for crystallography assistance, Drs Alan Torres and Scott Willis for their help with NMR, Dr Christopher Gordon for helping with flow chemistry and Dr David Harman for assistance with mass spectrometry.

For allowing the reproduction of my publications in this document, I would like to thank the publishers Elsevier, John Wiley & Sons and the Royal Society of Chemistry.

I am indebted to Western Sydney University for their financial support provided through several scholarships throughout my candidature.

Finally, I would like to thank my friends and family for their support over the years, and for their interest, or feigned interest, in this project! There have been many up and downs and I am very grateful for all their support. In particular, I would like to thank my parents Christine and Alan for supporting me no matter what path I take, and for not kicking me out of the house at 25 years old! I would also like to thank my partner Brondwyn for her continued love and support during my last year. Thank you to each and every one of my loved ones for keeping me on track and for your support during my journey.

Abstract

Chemotherapy is a primary source of treatment for victims of cancer, a globally prominent disease that affects millions. The platinum(II) agents cisplatin, carboplatin and oxaliplatin are used in approximately half of all chemotherapy treatment schemes. These drugs kill cancerous cells by binding covalently to DNA and preventing replication, which leads to apoptosis. Despite the success of these drugs they have many debilitating side effects such as nephrotoxicity, myelotoxicity, nausea and vomiting. Furthermore, many cancers are resistant to treatment from these drugs, often through DNA repair mechanisms.

To overcome these issues, researchers are developing platinum complexes (PCs) that kill cancerous cells through different mechanisms of action to cisplatin. A promising series of PCs in this field are those of the type $[Pt(P_L)(A_L)]^{2+}$, in which P_L is a polyaromatic heterocyclic ligand and A_L is a cyclic diamine. Relative to cisplatin, these polyaromatic PCs (PPCs) are more cytotoxic to cancer cells, kill these cells through different mechanisms, and bind to DNA through noncovalent interactions. Due to these characteristics, PPCs have the potential to surpass traditional platinum drugs as chemotherapy candidates. This potential is further amplified when they are oxidised from platinum(II) to platinum(IV), resulting in complexes of the type $[Pt(P_L)(A_L)(X)_2]^{2+}$, where X is an axial ligand such as hydroxide or succinimide. The PCs can be tuned, through modification of these axial ligands, to target cancer cells selectively, improve bloodstream stability, and to selectively reduce to the active platinum(II) form once inside a cancer cell.

In this work, reported in four published journal articles together with some additional experiments, several novel PPCs have been synthesised and tested for their viability as DNA binders and anticancer agents. Several P_L and A_L combinations were explored, most of which were new to this series of PCs. All PPCs were characterised through nuclear magnetic resonance, elemental microanalysis, ultraviolet (UV) spectroscopy, electrospray ionisation mass spectrometry (ESIMS), and, where applicable, circular dichroism (CD) and X-ray crystallography. Most of the PCs adopted a square-planar coordination geometry, although the geometry of 2-(2'-pyridyl)quinoxaline complexes was distorted, leading to unusual CD, diffusion and crystal packing activity. All PPCs were produced with desirable purity and yield.

The anticancer potential of the PPCs was assessed in several human cancer cell lines, revealing high *in vitro* cytotoxicity across a wide variety of cancers, often higher than that of cisplatin, oxaliplatin and carboplatin. Most of the PCs were particularly active against Du145

prostate cancer, HT29 colon carcinoma and SJ-G2 glioblastoma cells. It was found that while both the choice of P_L and A_L affected activity, the A_L choice was more impactful. Considering that the P_L is the component of the PPCs responsible for DNA binding, this is suggestive that DNA interactions are not the primary mechanism of action of these complexes.

The DNA binding of some PCCs was assessed through several biophysical methods, including UV spectroscopy, synchrotron radiation CD, linear dichroism (LD), isothermal titration calorimetry (ITC), fluorescence spectroscopy and ESIMS. The complexes studied incorporated 1*S*, 2*S*-diaminocyclohexane (*SS*-dach) as an A_L and one of the following P_Ls: phen, 5,6-dimethyl-phen ($56Me_2$phen), 2,2'-bipyridine (bpy), 4,4'-dimethyl-bpy ($44Me_2$bpy), dipyrido[3,2-*f*:2',3'-*h*]quinoxaline (dpq) or 2,3-dimethyl-dpq ($23Me_2$dpq). It was found that each PPC could bind to DNA through intercalation, with binding constants between 10^4 and 10^6 M^{-1}. While each biophysical method provided unique information about the binding of these PPCs with DNA, it was determined that ITC and LD provide the most useful information regarding thermodynamics and binding mode, respectively. The order of DNA affinity based upon P_L was $56Me_2$phen > $23Me_2$dpq ≥ dpq ≥ $44Me_2$bpy = phen > bpy. This suggests that $56Me_2$phen is the optimum P_L size for PPC interactions with DNA. Cytotoxicity and DNA affinity did not correlate for the dpq and $23Me_2$dpq complexes, yet it did for the rest; the $56Me_2$phen and bpy complexes were the most and least potent, respectively, while the phen and $44Me_2$bpy complexes were at the midpoint of DNA affinity and cytotoxicity. Additionally, the DNA binding of complexes of *cis*-1,4-diaminocyclohexane (1,4-dach) was also assessed by ITC, revealing slightly higher DNA affinity than the complexes of *SS*-dach. However, the 1,4-dach complexes were not very toxic to cancer cells, leaving no correlation between DNA affinity and cytotoxicity.

Finally, platinum(IV) complexes of the type $[Pt(P_L)(A_L)(OH)_2]^{2+}$ and $[Pt(P_L)(A_L)(OH)(OOCCH_3)]^{2+}$ were also synthesised, and the latter complex was bound to a moiety that can target prostate-specific membrane antigen (PSMA). The synthesis of these complexes required some optimisation to achieve desirable yields and purity, and the results confirm that further axial ligand addition to PPCs is possible. These preliminary experiments will provide the foundation from which further functionalisation of PPCs and more detailed biological testing of these complexes can occur in the future, leading to the development of new chemotherapy candidates.

Table of Contents

List of Figures

List of Tables

Selected Abbreviations and Acronyms

1,2-dach	1,2-diaminocyclohexane
1,4-dach	*cis*-1,4-diaminocyclohexane
23Me$_2$dpq	2,3-dimethyl-dipyrido[3,2-f:2',3'-h]quinoxaline
2pq	2-(2'-pyridyl)quinoxaline
44Me$_2$bpy	4,4'-dimethyl-2,2'-bipyridine
56Me$_2$phen	5,6-dimethyl-1,10-phenanthroline
5Mephen	5-methyl-1,10-phenanthroline
A_L	Ancillary ligand
AT	Adenine-thymine
bpy	2,2'-bipyridine
CD	Circular dichroism
Cisplatin	*cis*-diamminedichloroplatinum(II)
d	Doublet
DCL	*N*-{*N*-[(*S*)-1,3-dicarboxypropyl]carbamoyl}-(*S*)-L-lysine
DCM	Dichloromethane
dd	Doublet of doublets
DIPEA	*N*,*N*-diisopropylethylamine
DMF	Dimethylformamide
DNA	Deoxyribonucleic acid
dpq	dipyrido[3,2-*f*:2',3'-*h*]quinoxaline
ER(+)	Oestrogen-receptor positive
ESIMS	Electrospray ionisation mass spectrometry
EtBr	Ethidium bromide
GC	Guanine-cytosine
HBTU	2-(1*H*-benzotriazol-1-yl)-1,1,3,3-tetramethyluronium hexafluorophosphate
HMQC	Heteronuclear multiple quantum correlation
HOBt	1-Hydroxybenzotriazole
HPLC	High-performance liquid chromatography
IC_{50}	Half maximal inhibitory concentration
Iproplatin	*cis*,*trans*,*cis*-Dichloridodihydroxidobis(isopropylamine)platinum-(IV)

ITC	Isothermal titration calorimetry
K	Binding constant
LD	Linear dichroism
m	Multiplet
MTT	3-[4,5-dimethylthiazol-2-yl]-2,5-diphenyl-tetrazoliumbromide
N	Number of bound ligands
n	Number of binding sites
NMR	Nuclear magnetic resonance
Ormaplatin	Tetrachlorido(1,2-cyclohexanediamine-*N*,*N*')platinum(IV)
PC	Platinum Complex
phen	1,10-phenanthroline
P_L	Polyaromatic ligand
PPC	Polyaromatic platinum complex
PSMA	Prostrate-specific membrane antigen
R-pytri	pyridyl-1,2,3-triazole
RR-dach	1*R*,2*R*-diaminocyclohexane
s	Singlet
Satraplatin	Bis(acetato-*O*)amminedichlorido(cyclohexylamine)platinum(IV)
SR	Synchrotron radiation
SRCD	Synchrotron radiation circular dichroism
SS-dach	1*S*,2*S*-diaminocyclohexane
TEA	Triethylamine
terpy	2,2':6',2''-terpyridine
TLC	Thin-layer chromatography
T_M	Melting point
UV	ultraviolet-visible
Δ*G*	Gibbs free energy change
Δ*H*	Enthalpy change
Δ*S*	Entropy change

Publications

Journal Articles – Direct Thesis Contributors

I. **Pages, B. J.**; Zhang, Y.; Li, F.; Sakoff, J.; Gilbert, J.; Aldrich-Wright, J. R. Cytotoxicity and Structural Analyses of 2,2'-Bipyridine-, 4,4'-Dimethyl-2,2'-bipyridine- and 2-(2'-Pyridyl)quinoxalineplatinum(II) Complexes. *European Journal of Inorganic Chemistry* 2015, 4167-4175. DOI: 10.1002/ejic.201500754 (Impact Factor 2.444, 13 citations).

II. **Pages, B. J.**; Sakoff, J.; Gilbert, J.; Rodger, A.; Chmel, N. P.; Jones, N. C.; Kelly, S. M.; Ang, D. L.; Aldrich-Wright, J. R. Multifaceted studies of the DNA interactions and in vitro cytotoxicity of potent polyaromatic platinum(II) complexes. *Chemistry – A European Journal* 2016, **22**, 8943-8954. DOI: 10.1002/chem.201601221 (Impact Factor 5.317, 10 citations).

III. **Pages, B. J.**; Sakoff, J.; Gilbert, J.; Zhang, Y.; Li, F.; Preston, D.; Crowley, J.; Aldrich-Wright, J. R. Investigating the cytotoxicity of platinum(II) complexes incorporating bidentate pyridyl-1,2,3-triazole "click" ligands. *Journal of Inorganic Biochemistry* 2016, **165**, 92-99. DOI: 10.1016/j.jinorgbio.2016.06.017 (Impact Factor 3.348, 7 citations).

IV. **Pages, B. J.**; Sakoff, J.; Gilbert, J.; Zhang, Y.; Hoeschele, J. D.; Kelly, S. M.; Aldrich-Wright, J. R. Combining the platinum(II) drug candidate kiteplatin with 1,10-phenanthroline analogues. *Dalton Transactions* 2018, Accepted. DOI: 10.1039/C7DT04108J (Impact Factor 4.029, 0 citations).

Journal Articles – Indirect Thesis Contributors

V. **Pages, B. J.**; Li, F.; Wormell, P.; Ang, D. L.; Clegg, J. K.; Kepert, C. J.; Spare, L. K.; Danchaiwijit, S.; Aldrich-Wright, J. R. Synthesis and analysis of the anticancer activity of platinum(II) complexes incorporating dipyridoquinoxaline variants. *Dalton Transactions* 2014, **43**, 15566-15575. DOI: 10.1039/C4DT02133A (Impact Factor 4.029, 19 citations).

VI. Macias, F. J.; Deo, K. M.; **Pages, B. J.**; Wormell, P.; Clegg, J. K.; Zhang, Y.; Li, F.; Zheng, G.; Sakoff, J.; Gilbert, J.; Aldrich-Wright, J. R. Synthesis and Analysis of the Structure, Diffusion and Cytotoxicity of Heterocyclic Platinum(IV) Complexes. *Chemistry – A European Journal* 2015, **21**, 16990-17001. DOI: 10.1002/chem.201502159 (Impact Factor 5.317, 10 citations).

VII. **Pages, B. J**.; Ang, D. L.; Wright, E. P.; Aldrich-Wright, J. R. Metal complex interactions with DNA. *Dalton Transactions* 2015, **44**, 3505-3526. DOI: 10.1039/C4DT02700K (Impact Factor 4.029, 66 citations).

VIII. Deo, K.;[†] **Pages, B.J.**;[†] Ang, D.; Gordon, C.; Aldrich-Wright, J. Transition Metal Intercalators as Anticancer Agents – Recent Advances. *International Journal of Molecular Sciences,* 2016, **17**, 1818-1834. DOI: 10.3390/ijms17111818 (Impact Factor 3.226, 9 citations). ([†]: the authors contributed equally)

IX. **Pages, B. J.**; Garbutcheon-Singh, K. B.; Aldrich-Wright, J. R. Platinum intercalators of DNA as anticancer agents. *European Journal of Inorganic Chemistry* 2017, 1613-1624. DOI: 10.1002/ejic.201601204 (Impact Factor 2.444, 1 citation).

X. Bjelosevic, A.; **Pages, B. J.**; Spare, L. K.; Deo, K.; Ang, D. L.; Aldrich-Wright, J. R. Exposing "bright" metals: promising advances in photoactivated anticancer transition metal complexes. *Current Medicinal Chemistry* 2018, **25**, 478-492. DOI:10.2174/0929867324666170530085123 (Impact Factor 3.249, 0 citations).

XI. Deo, K. M.; Ang, D. L.; McGhie, B.S.; Rajamanickam, A.; Dhiman, A.; Khoury, A.; Holland, J.; Bjelosevic, A.; **Pages, B. J.**; Gordon C.; Aldrich-Wright, J. R. Platinum Coordination Compounds with Potent Anticancer Activity. Coordination Chemistry Reviews, 2018, Accepted. DOI: CCR112609 (Impact Factor 13.324, 0 citations).

Presentations

Oral Presentations

I. **Pages, B. J.**; Sakoff, J.; Gilbert, J.; Zhang, Y.; Chmel, N. P.; Rodger, A.; Aldrich-Wright, J. R. Cytotoxic, structural and biophysical analyses of polyaromatic platinum(II) complexes. *EU/UK Annual CD User Group Meeting,* **2015**, Coventry, United Kingdom.

II. Harper, B. W.; Vilar, R.; Jones, N. C., Hoffmann, S. V.; Ang, D. L.; **Pages**, **B**. **J**.; Aldrich-Wright, J. R. G-quadruplex DNA interactions of dinuclear Pt(II) complexes. *The International Chemical Congress of Pacific Basin Societies (Pacifichem),* **2015**, Honolulu, Hawaii, USA.

III. **Pages, B. J.**; Sakoff, J.; Gilbert, J.; Li, F.; Zhang, Y.; Kelly, S. M.; Chmel, N. P.; Rodger, A.; Crowley, J. D.; Aldrich-Wright, J. R. Polyaromatic platinum complexes – new iterations and detailed biophysical DNA analyses. *8th Asian Biological Inorganic Chemistry Conference,* **2016**, Auckland, New Zealand.

Poster Presentations

I. **Pages, B. J.**; Jones, N. C.; Zhang, Y.; Li, F.; Aldrich-Wright, J. R. Using synchrotron radiation to determine the X-ray structure and CT-DNA affinity of platinum anticancer complexes. *Australian Synchrotron User Meeting,* **2014**, Melbourne, NSW, Australia.

II. **Pages, B. J.**; Sakoff, J.; Gilbert, J.; Jones, N. C.; Kelly, S. M.; Chmel, N. P.; Rodger, A.; Aldrich-Wright, J. R. Multifaceted studies of the cytotoxicity and DNA binding of polyaromatic platinum(II) complexes. *International Symposium on Clinical and Experimental Metallodrugs in Medicine,* **2015**, Honolulu, Hawaii, USA.

III. **Pages, B. J.**; Sakoff, J.; Gilbert, J.; Rodger, A.; Chmel, N. P.; Kelly, S. M.; Zhang, Y.; Hoeschele, J. D.; Aldrich-Wright, J. R. Polyaromatic Platinum Complexes: Synthesis and Analysis of DNA Binding. *12th International Symposium on Platinum Coordination Compounds in Cancer Chemotherapy,* **2017**, Coogee, New South Wales, Australia.

CHAPTER 1. INTRODUCTION

1.1 Cancer

1.1.1 Cancer and chemotherapy

Cancer is one of the most deadly and impactful diseases in existence. In western civilisations, it is the second highest cause of death behind heart disease, with a lifelong diagnostic rate of approximately 40-50%.[1, 2] The disease is characterised by the uncontrolled replication of cells, which eventually form tumours. These tumours can interfere with organ function and can also metastasise, leading to widespread damage throughout the body and causing death.[1] To treat cancer, combinations of surgery and chemotherapy have been used since the 1950s,[3] and there are many drugs available for this purpose. While the majority of chemotherapeutic agents are organic, many chemotherapy schemes utilise platinum anticancer drugs at some point, whether alone or in combination with other drugs.[4] Most agents will kill cancer cells by halting their DNA replication or interfering with other cellular processes, often at different cell cycle stages depending on the drug(s) used.[5, 6] A preliminary test used to assess the viability of potential anticancer drugs determines *in vitro* cytotoxicity, usually though determination of the half maximal inhibitory concentration (IC_{50}). This is the concentration of a drug that is required to halt cellular replication by 50%.[7] Compounds that produce low IC_{50} values for a variety of cancer cell lines are often considered to have good potential as chemotherapeutic agents.

1.1.2 Prostate cancer and prostate-specific membrane antigen

Prostate cancer is the most commonly diagnosed cancer in Australia, with over 16 000 new diagnoses in 2017.[1] Radiation, surgery and androgen deprivation are the usual methods of treating prostate cancer,[8] however with each of these treatments comes the risk of in undesirable side effects such as loss of urinary control, impotence and toxicity.[9, 10] Chemotherapy is available for some cancers using drugs such as mitoxantrone, prednisone and docetaxel, however their survival benefit is small.[11, 12] In order to synthesise more effective agents to fight prostate cancer, research has turned toward targeted therapy that allows for selective delivery of drugs. This would allow for a greater percentage of the administered drug to reach its intended target and fewer side effects for healthy cells. Prostate-specific membrane antigen (PSMA) is a membrane glycoprotein that is commonly found on the surface of prostate cells, and occasionally in other cells in the brain, kidneys, liver and small intestine.[13-15] The major role of PSMA is still largely unknown, although it is known to function as a neuropeptidase and folate hydrolase.[13] PSMA is overexpressed in all stages of prostate cancer and acts as a marker of tumour progression.[16-18] The antigen is restricted to the cell membrane and it does not enter circulation,[18, 19] internalises any bound

species through clathrin-mediated endocytosis,[15, 20] and is recycled to the cell surface after doing so.[19] Additionally, studies have shown that each cancer cell expresses up to 10^6 PSMAs on their surface and that uptake of PSMA binding agents is rapid.[21] All of these factors make PSMA an attractive candidate for targeted therapy and diagnostics. Urea-based binders, in particular the peptide moiety *N*-{*N*-[(*S*)-1,3-dicarboxypropyl]carbamoyl}-(*S*)-*L*-lysine (DCL), have proven to be very effective as radiolabelled imaging agents, and have shown some promise in delivering anticancer drugs (Figure 1.1.1).[22, 23] These have the potential to be tethered to platinum(IV) species in order to create prodrugs (see section 1.4.2).

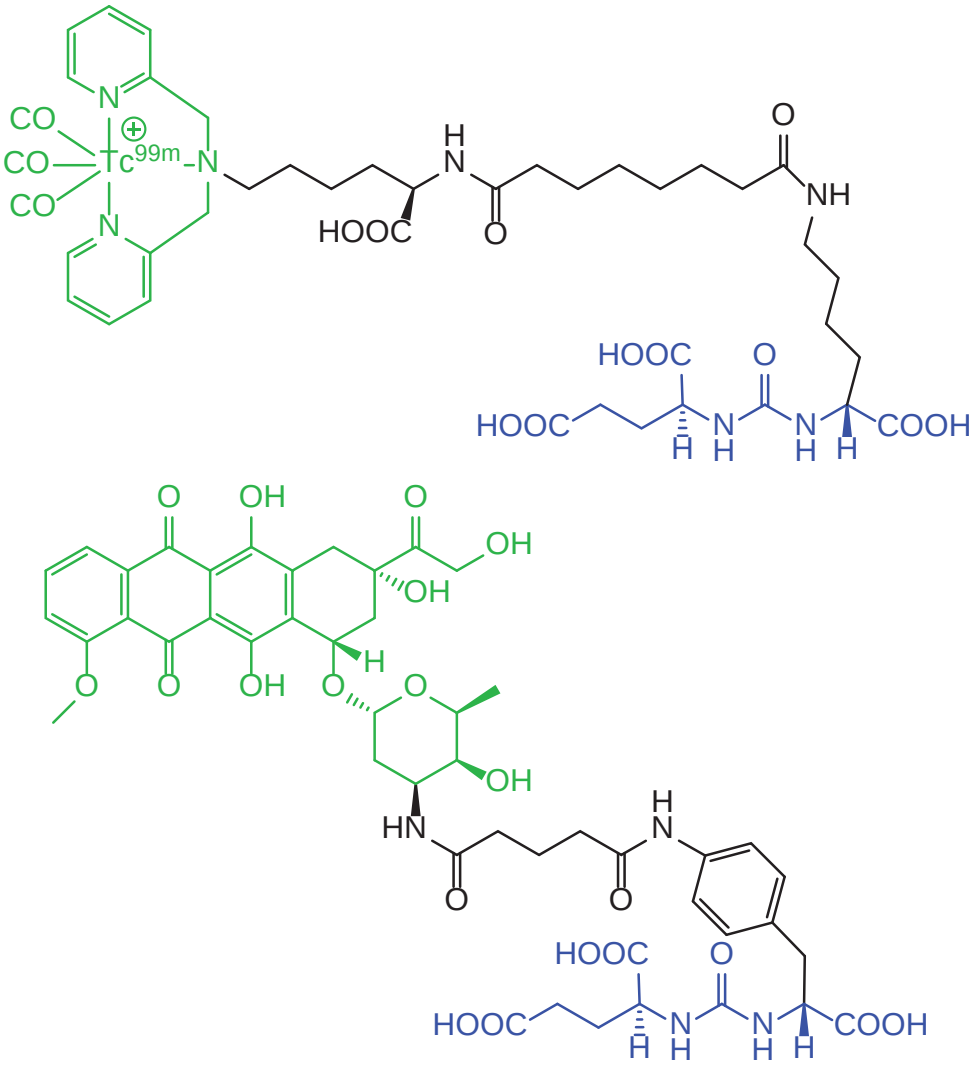

Figure 1.1.1. Chemical structures of two compounds tethered to DCL: a ^{99m}Tc radioactive diagnostic agent (top) and a doxorubicin anticancer compound (bottom).[22, 23] DCL is shown in blue and active component in green.

1.2 Platinum Anticancer Agents

1.2.1 Cisplatin and derivatives

In 1965, the cytotoxicity of platinum was first reported by the group of Barnett Rosenberg, where it was found to inhibit bacterial cell growth.[24] These experiments identified platinum

complexes (PCs) as potential anticancer drugs, particularly the complex *cis*-diamminedichloroplatinum(II) (cisplatin).[25] It was approved for clinical use to treat testicular cancer among many others in 1978.[26] Early anticancer PCs consisted of a platinum(II) centre, coordinated to inert amine ligands and one or two leaving groups. These complexes can be taken up into cells *via* both passive and active transport paths.[27] Upon entry to the cell, the drug can bind to several intracellular compounds such as DNA, ribonucleic acid, phospholipids, detoxifying thiols and cytoskeletal microfilaments.[27-29] However, the most important target of these drugs is DNA.[30] The binding of these complexes to DNA results in unwinding, bending, and/or cross-linking of the strand, which triggers a series of cellular processes leading eventually to apoptosis (Figure 1.2.1).[31] For binding to occur, the chloride leaving groups of cisplatin must be hydrolysed; this is easily achieved within cells where chloride concentrations are much lower than they are extracellularly (~4-20 mM and 100 mM, respectively).[32, 33]

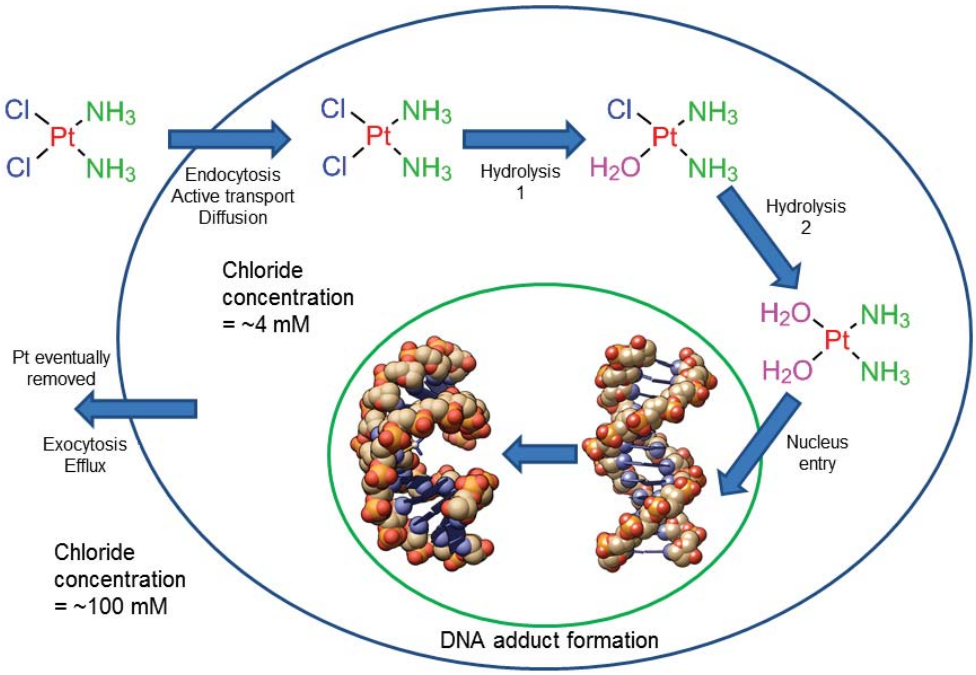

Figure 1.2.1. Depiction of the hydrolysis of cisplatin *in vitro* and subsequent DNA binding, demonstrating the kink formed in the phosphate backbone. DNA images sourced from protein data bank files 1AIO and 1D86.

Aside from cisplatin, two other PCs have been accepted for use as chemotherapy agents worldwide (Figure 1.2.2). Carboplatin was the second globally approved platinum-based chemotherapeutic agent; this drug has a similar spectrum of activity to cisplatin, however the side-effects of carboplatin treatment are different to that of cisplatin, and often less severe.[34] Oxaliplatin was the third drug to be approved, as it was found to be cytotoxic in several cancer types that are resistant to cisplatin. It is thought that the 1*R*,2*R*-diaminocyclohexane ligand helps to overcome some DNA resistance and repair mechanisms.[35]

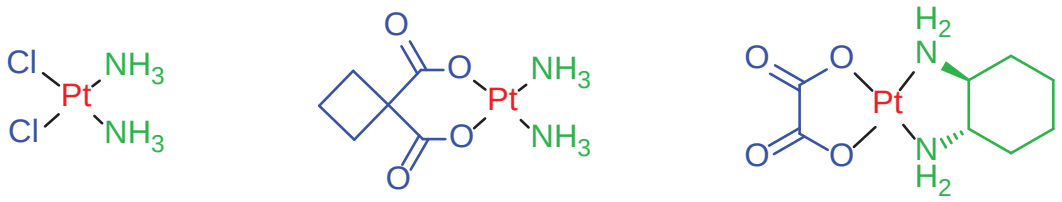

Cisplatin Carboplatin Oxaliplatin

Figure 1.2.2. The chemical structures of cisplatin, oxaliplatin and carboplatin, showing the labile ligands in blue, platinum centre in red and ancillary amines in green.

1.2.2 Kiteplatin

Inspired by the successes of the cisplatin analogues carboplatin and oxaliplatin, kiteplatin was developed in the 1990's as a DNA adduct forming chemotherapy candidate.[36] Kiteplatin incorporates the ligand *cis*-1,4-diaminocyclohexane (1,4-dach) and has the formula [Pt(1,4-dach)Cl_2] (Figure 1.2.3). The binding of the 1,4-dach ligand to the platinum centre results in a locked-boat conformation in which a seven-membered chelate ring is formed between the ligand and platinum. This also results in a wider chloride-platinum-chloride angle of approx. 93° rather than 90°.[37] Studies of the DNA binding of kiteplatin have revealed similar sequence preference and major adducts to cisplatin; however, DNA adducts of kiteplatin were found to inhibit DNA polymerase I, and thus DNA replication processes (such as the Polη-catalysed synthesis), with greater efficiency than those of cisplatin.[38, 39] This may be the reason why kiteplatin is cytotoxic to many cell lines that are resistant to oxaliplatin and cisplatin.[40] In mice models, administration of kiteplatin results in approximately the same tumour shrinkage as cisplatin, with considerably less side effects.[40] Due to these advantages kiteplatin continues to be a relevant platinum drug candidate with potential for clinical use.

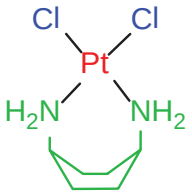

Figure 1.2.3. The chemical structure of kiteplatin, showing the labile ligands in blue, platinum centre in red and 1,4-dach ligand in green.

1.2.3 Issues with current platinum drugs

Despite the recognised success of cisplatin and its derivatives as clinical drugs,[35] treatment often results in toxic side effects, and drug resistance is a common issue that affects their efficacy. Cisplatin is assimilated by cells that rapidly divide, such as tumours, but also by other rapidly-dividing cells such as bone marrow cells, which can lead to myelotoxicity.[4] There are many other possible toxic side effects such as ototoxicity and nephrotoxicity.[41] Additionally, tumours can resist cisplatin treatment, either intrinsically or through repeated exposure. Resistance mechanisms can include higher expression of proteins and peptides that bind to cisplatin such as glutathione, increased efflux of cisplatin and increased DNA repair activity.[35, 42] While carboplatin and oxaliplatin are superior to cisplatin in some situations, they also exhibit drawbacks in terms of toxicity and resistance.[4] In order to overcome these issues, a large body of research is dedicated to the development of novel anticancer agents that have less treatment side-effects than cisplatin and are active in cancer cells that are resistant to cisplatin.[43] Aside from the aforementioned drugs, no other platinum complex has been globally approved for use in chemotherapy, with some being approved only for use in specific countries while many others have failed in the later stages of clinical trials.[4] Many of these drugs are analogues of cisplatin, carboplatin and oxaliplatin, as in they also induce apoptosis in cancerous cells *via* the formation of DNA adducts.[35] Researchers are now focusing on metal complexes with vastly different structures and mechanisms of action to cisplatin. These compounds have demonstrated both the ability to bypass traditional cell resistance mechanisms and to be higher in cytotoxicity than cisplatin.[44, 45] They may bind to DNA through a different mechanism such as groove binding or intercalation,[46-49] or they could attack cancerous cells through other pathways. The continued study and development of these complexes is vital to the improvement of metal-based chemotherapy.[50]

1.3 Platinum Intercalators

Intercalation was first described in 1961 by Lerman as the insertion of planar moieties between consecutive DNA base-pairs.[51] This reversible form of DNA binding is driven by π-stacking interactions between the planar aromatic rings of the base-pairs and the intercalator.[52] A positive charge is also required for the intercalator, to balance the negative charge of the DNA strand.[53] This base-pair insertion causes lengthening and unwinding of the DNA strand;[54, 55] the unwinding angle can be as high as 26° for binders such as ethidium bromide.[56] Intercalation can render DNA unable to participate in several physiological processes including replication.[57-59] For example, many intercalators stop DNA from interacting with type II topoisomerase, an enzyme that cleaves the helix to manage tangles and supercoils.[60] This is the mechanism of action through which clinically approved organic intercalators such

as Amsacrine, Doxorubicin, Daunorubicin and Mitoxantrone kill cancerous cells.[60] The anticancer potency of these intercalators has inspired their inclusion in inorganic chemotherapy research. Intercalators bound to a platinum centre (Figure 1.3.1) are of particular interest due to the known anticancer properties of platinum. PCs incorporating polyaromatic moieties such as 2,2':6',2''-terpyridine (terpy), 1,10-phenanthroline (phen), 2,2'-bipyridine (bpy) and several acridines exhibit anticancer potential.[46, 61-63]

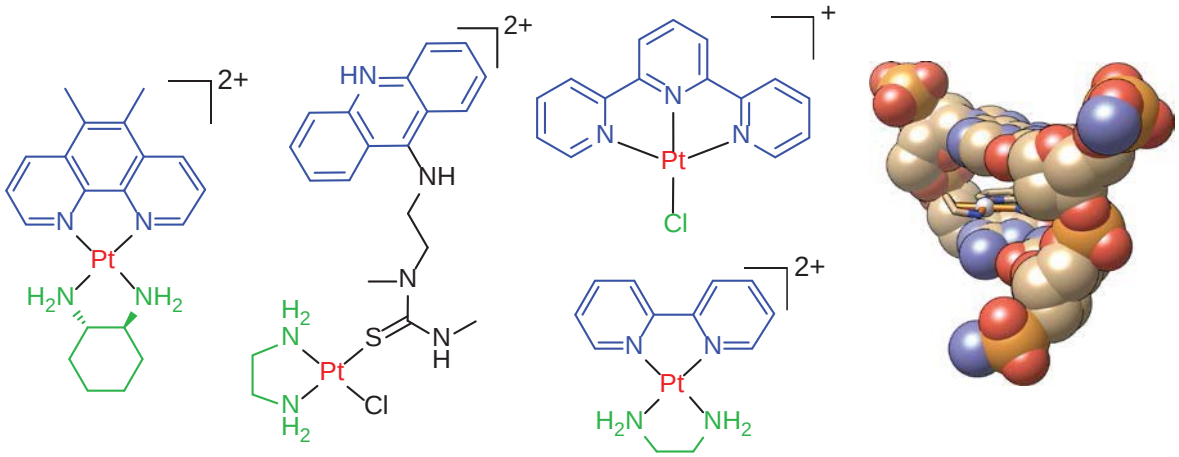

Figure 1.3.1. Left: examples of platinum intercalators incorporating terpy, phen, bpy and acridine derivatives, showing the polyaromatic intercalating ligand moiety in blue, platinum centre in red and ancillary ligand in green. Right: molecular representation of $[Pt(4\text{-methyl-phen})(ethylenediamine)]^{2+}$ intercalating with the minor groove of DNA sequence $d(GTCGAC)_2$ (T_2 and C_3 base pairs shown only).[46]

These polyaromatic platinum complexes (PPCs) have been in development since the 1970s, with many modern examples that are more active than cisplatin against many cancers.[45, 62, 64] A series of particularly cytotoxic PPCs are those of the type $[Pt(P_L)(A_L)]^{2+}$, where P_L is a polyaromatic ligand such as phen and A_L is a diamine such as 1,2-diaminocyclohexane (1,2-dach). Unlike cisplatin, these PPCs are positively charged, allowing for high DNA affinity and water solubility.[65, 66] These complexes bind to DNA by intercalation, and solution studies of $[Pt(5\text{-methyl-phen})(1S,2S\text{-dach})]^{2+}$ and $[Pt(4\text{-methyl-phen})(ethylenediamine)]^{2+}$ (Figure 1.3.1) have shown this occurs through the minor groove of the helix.[46, 67] The most cytotoxic complex in this series is [(5,6-dimethyl-phen)(1*S*,2*S*-diaminocyclohexane)platinum(II)] dichloride (56MESS), which is more cytotoxic than cisplatin in all cell lines tested,[45, 68] including those that are cisplatin-resistant.[45] There are many types of PPCs in this family utilising different P_L and A_L combinations, all of which exhibit a broad range of cytotoxicity. However, the mechanism of action of these complexes is difficult to elucidate.[67, 69] Using 1,2-dach as an example, PPCs that incorporate the *S*,*S* isomer (*SS*-dach) are more cytotoxic than those with the *R*,*R* isomer (*RR*-dach).[67] However, this trend is reversed when the A_L used is 1,2-diaminocyclopentane.[70] Cellular uptake is not related to cytotoxicity, as uptake rates for

56MESS and its *R,R* enantiomer are the same despite large differences in IC_{50} values.[68] There are many other factors that have been considered for these complexes,[45, 71-73] yet there is no clear answer regarding the mechanism of action. To know more about the way these compounds kill cells, more biological studies and new PPCs need to be synthesised to expand the range of active complexes available for chemotherapy.

1.4 Platinum(IV) Complexes

1.4.1 Properties and history

Platinum(IV) complexes are becoming an increasingly attractive option over platinum(II) complexes due to their unique properties. The low spin $5d^6$ electron configuration of platinum(IV) complexes results in an octahedral geometry, rather than the $5d^8$ square planar configuration of platinum(II). Subsequently platinum(IV) complexes are more kinetically inert, resistant to ligand attack, and have a coordination number of six instead of four.[74] These properties potentially give platinum(IV) compounds distinct advantages *in vivo* by increasing bloodstream survivability and allowing for additional functionality.[75-77] Functionality can include tumour-targeting ligands to increase cell penetration, fluorescent ligands to allow tracking of the complex, charged ligands to adjust solubility, hydrophobic groups to increase lipophilicity, extra cytotoxic compounds for intracellular release, and more.[29, 78-81] The lower reactivity of these complexes has the potential to decrease their cytotoxicity, however the complexes can be tuned to reduce to their active platinum(II) form in an intracellular environment (Figure 1.4.1); platinum(IV) compounds therefore have the potential to be potent prodrugs.[75-77]

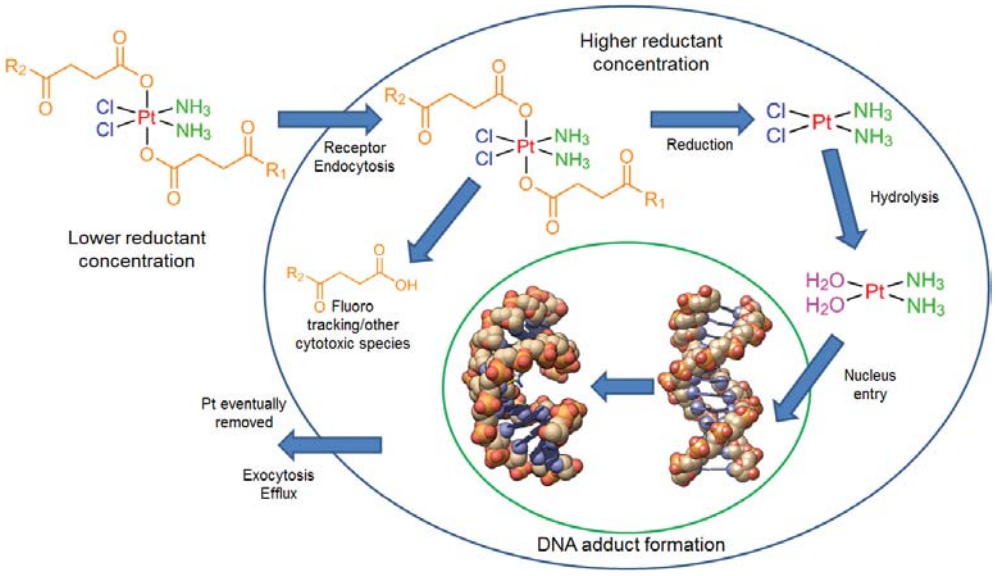

Figure 1.4.1. Schematic showing the cellular penetration of a platinum(IV) complex and subsequent reduction to the active platinum(II) species. R_1 and R_2 represent a variety of different moieties.

Despite the reported advantages of platinum(IV) over platinum(II) when it comes to anticancer efficacy, no platinum(IV) complexes have gained marketing approval. The first complex to be approved for clinical trials was *cis*,*trans*,*cis*-dichloridodihydroxidobis(isopropylamine)platinum-(IV) (iproplatin); over 1000 patients were treated with iproplatin in a variety of phase I and II trials, as well as one phase III trial.[4] Unfortunately, patients suffered from thrombocytopenia as a result of treatment, and the drug failed to show efficacy greater than cisplatin in all cancers assessed.[82, 83] Tetrachlorido(1,2-cyclohexanediamine-*N*,*N* ')platinum(IV) (ormaplatin) was subjected to phase I trials, however severe neurotoxicity in its patients prevented further progression.[84, 85] *Bis*(acetato-*O*)amminedichlorido(cyclohexylamine)platinum(IV) (satraplatin) is currently the most successful platinum(IV) drug; it is the first complex to be administered orally rather than intravenously, and its mild success in phase III clinical trials against prostate cancer resulted in an application for accelerated FDA approval. However, this application was denied as the overall survival benefit of treatment was not certain.[4] Satraplatin is currently undergoing further trials against a variety of cancers in combination with other drugs.[86, 87] These complexes (Figure 1.4.2) demonstrate the potential that platinum(IV) compounds have as anticancer agents, although measures to increase their *in-vivo* efficacy need to be taken.

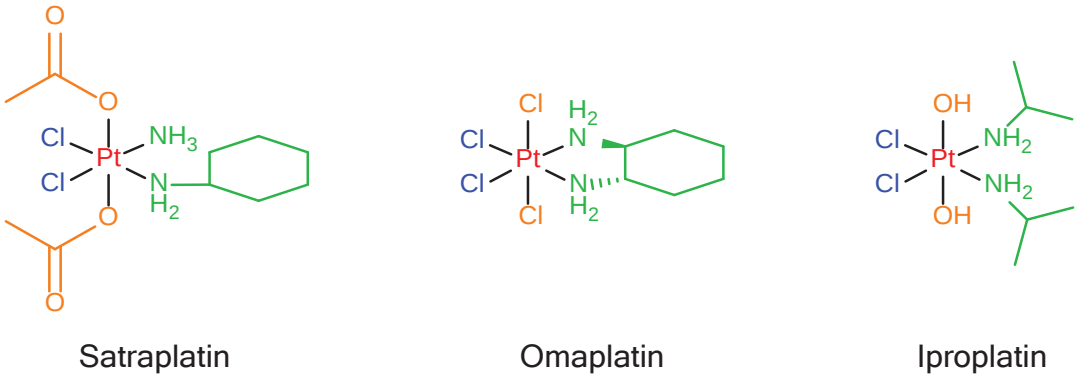

Figure 1.4.2 The chemical structures of satraplatin, omaplatin and iproplatin, showing the labile ligands in blue, platinum centre in red, ancillary amines in green and axial ligands in orange.

1.4.2 Improving functionality

The improved functionalisation of platinum(IV) complexes through modulation of their axial ligands may be the key to increasing their *in vivo* efficacy. By doing so, the structure of the equatorial ligands can remain unchanged, allowing for the release of the cytotoxic platinum(II) species upon intracellular reduction.[29] The first platinum(IV) complexes were synthesised *via* oxidation using chlorine gas or hydrogen peroxide to produce dichlorido or dihydroxido complexes.[88-90] The hydroxido complexes were found to be nucleophilic enough to undergo carboxylation with anhydrides and other carboxylic acids using carbodiimides or

uronium salts such as 2-(1*H*-benzotriazol-1-yl)-1,1,3,3-tetramethyluronium hexafluorophosphate (HBTU).[91-94] The optimal strategy of this type is the use of cyclic anhydrides, as the final product contains a free carboxyl group that can be further functionalised;[95] this strategy has allowed the tethering of a wide array of compounds to platinum(IV) centres (Figure 1.4.3). As an example, oestrogen-tethered complexes have been developed with axial ligands that can sensitise cancerous cells toward the platinum(II) "warhead"; these target oestrogen-receptor positive (ER(+)) cancers.[96] Upon intracellular reduction, two oestradiol molecules are released, which upregulate the expression of HMGB1, a protein that inhibits the repair of DNA adducts;[97] this allowed the cisplatin warhead to more effectively damage DNA, resulting in higher cytotoxicity in ER(+) cell lines. A common axial ligand type seen in platinum(IV) are those that are designed to target the surface of cancerous cells, thereby increasing the cellular accumulation of the cytotoxic platinum(II) component. Peptides are the most common tethers for this purpose; platinum(IV) complexes incorporating folate,[79] RGD (Arg-Gly-Asp)[98] and pNT (Lys-Lys-Pro-Tyr-Ile-Leu)[99] have each seen success in the targeting of proteins that are overexpressed in cancerous cells.[100, 101] Each compound was able to penetrate the target and exhibited cytotoxicity equal to or greater than cisplatin.

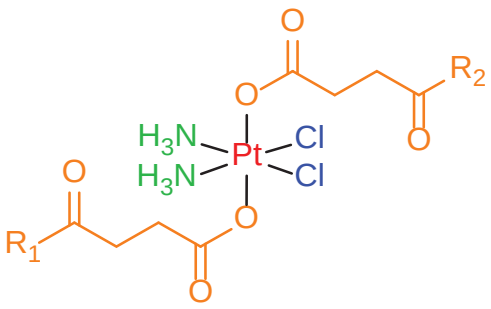

Targeting complexes: R_1, R_2= oestrogen, RGD or pNT
Carbon nanotube carrier: R_1,= folate, R_2 = single-walled carbon nanotube
Polymer: complex is one unit, connected through R_1 and R_2 (ethylenediamine or piperazine)

Figure 1.4.3. General structure of a cisplatin platinum(IV) complex with functional groups tethered *via* succinato moieties. Examples are given from a variety of studies.[79, 96, 98, 99, 102]

Another strategy is to tether large macromolecules to the platinum centre. This can be effective, as the fast proliferation of cancer cells leads to an increased uptake of macromolecules within tumours.[103] To this end, researchers have successfully tethered polymers,[102] nanoparticles[104] and carbon nanotubes[105] to cisplatin centres, resulting in complexes with higher efficacy than cisplatin alone in many cell lines. It is clear that there are many avenues through which axial ligand functionalisation can improve the efficacy of platinum complexes against cancer. However, most of these strategies have only employed

cisplatin analogues as the platinum(II) warhead, and so research into the use of platinum(IV) functionalisation with complexes such as polyaromatic PCs has potential.

1.5 Biophysical Methods of Studying DNA Interactions

1.5.1 Circular dichroism

Circular dichroism is the measurement of the difference in absorption of light that is circularly polarised to the right and left of an orientation axis.[106] A chiral compound will absorb either left or right polarised light more than the other, which produces a CD spectrum; the CD spectra of two enantiomers will be the exact mirror images of each other (Figure 1.5.1). Many biomolecules such as proteins and DNA are chiral due to complex structural motifs, and so CD is often used to investigate the structure and reactions of these molecules.[107-112] Binding events and changes of solution conditions can change the conformation of these biomolecules, thus producing measurable changes in the CD spectrum; this allows for valuable data such as binding constants to be obtained.[46, 113, 114]

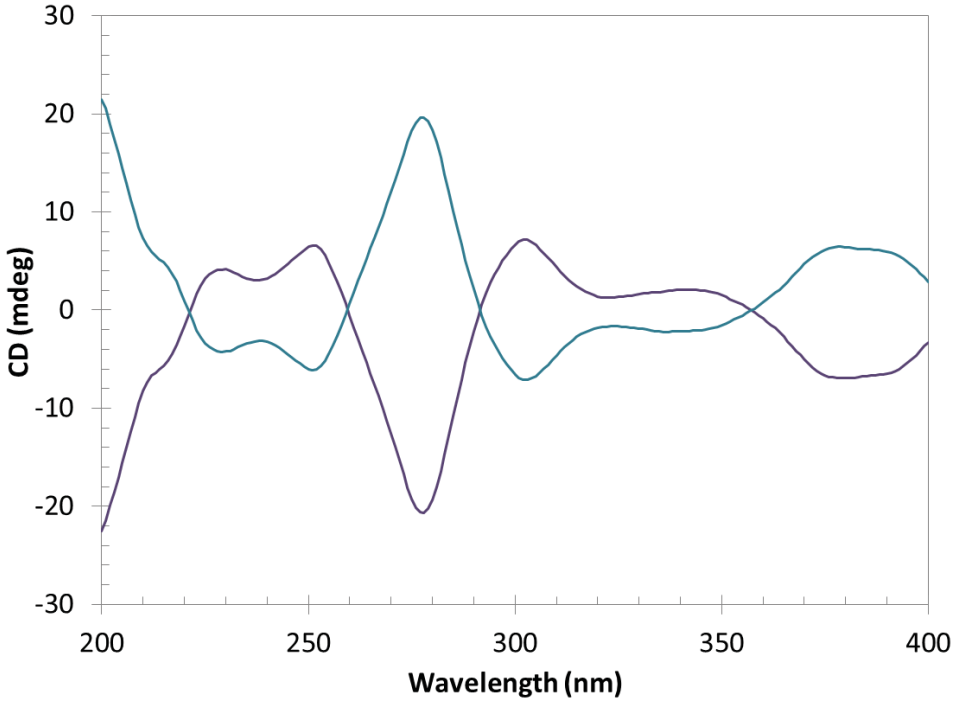

Figure 1.5.1. CD spectra of [Pt{2-(2-pyridyl)quinoxaline}(*SS*-dach)]Cl_2 (purple) and its enantiomer (blue).[115]

While X-ray crystallography and similar solid-state techniques can provide very accurate structures of biomolecules, CD spectra are obtained in solution under a wide variety of conditions, allowing for structural information to be obtained in more physiologically accurate conditions.[116] CD also sets itself apart from other solution spectroscopy techniques such as ultraviolet-visible (UV) spectroscopy as it often provides more information than those techniques, although CD spectra can be less directly interpretable than UV spectra. For example, DNA strands produce one peak in their UV spectrum while producing as many as

five peaks in their CD spectrum. CD is a powerful tool for studying the interactions of PCs with DNA. The binding of PCs to DNA produces a measureable change in the location and intensity of the CD peaks; by titrating a PC into a solution of DNA and measuring the signal between titrations, a binding curve can be generated from which a binding constant (*K*) can be determined.[46, 67, 117] This is a quantitative measure of the affinity of the complex for DNA, and can be compared with the *K* of other complexes to observe relative affinity. Aside from titration experiments, binding data can also be obtained from melting experiments, in which the variable is not PPC concentration, but temperature. As DNA is heated, the secondary structure will unravel or 'melt', leading to a loss of CD signal (Figure 1.5.2).[117] For simple structures such as B-DNA, all CD signals will decrease at the same rate with increasing temperature; however, for more complex structures such as G-quadruplexes, the peaks may decrease at different rates. This indicates that the peaks represent different structural motifs, and that the motifs are gradually unfolding at higher temperatures.[118-120] Similarly to binding curves, the attenuation of each peak can be plotted against temperature to produce a melting curve, of which the point of inflexion is the 'melting point' (T_M) of the DNA structure.[121] When a complex intercalates with DNA, the structure is stabilised and the melting point is increased.[122] Complexes that induce large increases in the DNA T_M are considered to be effective DNA binders.

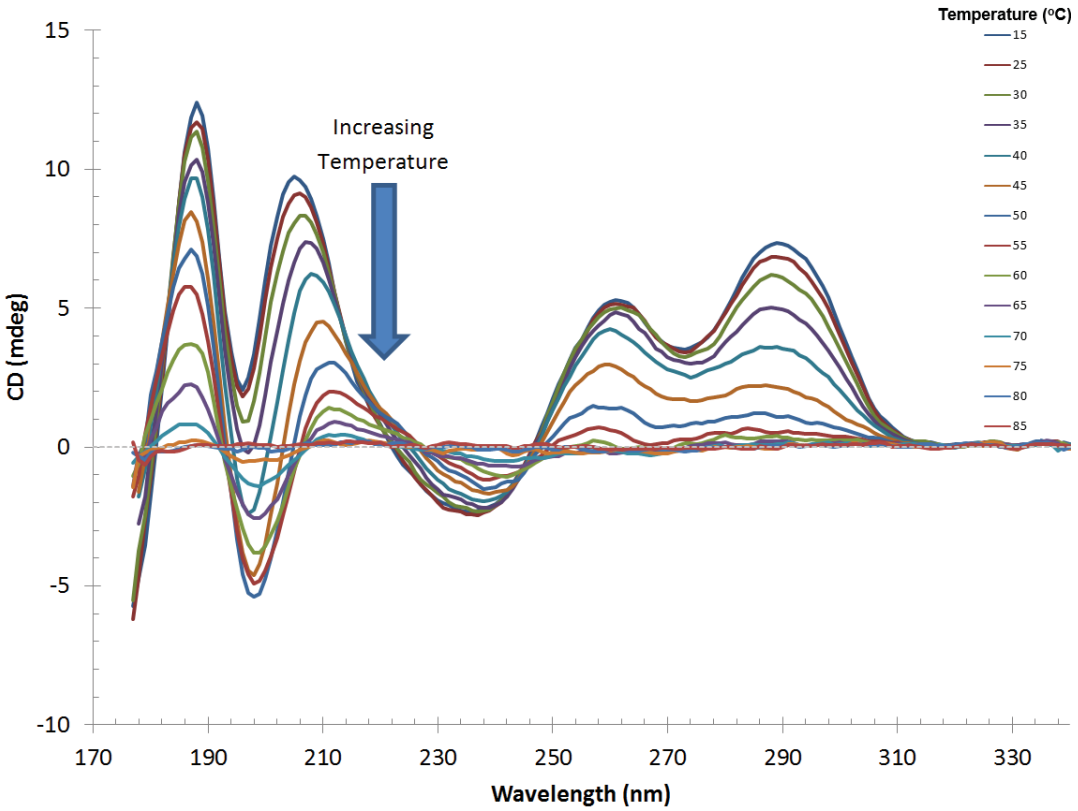

Figure 1.5.2. CD spectra of a G-quadruplex sequence at various temperatures. The CD signal is attenuated as the temperature increases.[123]

1.5.2 Synchrotron radiation circular dichroism

Synchrotron radiation CD (SRCD) is a specialised technique in which the typical xenon lamp CD light source is replaced by radiation produced from a synchrotron, allowing the flux from the light source to be much higher than conventional CD at low wavelengths.[124] This overcomes the issue of low signal-to-noise ratio at low wavelengths, evident in bench top CD spectra; conventional spectropolarimeters normally cannot collect data past ~190 nm, while SRCD instruments can collect as low as 140 nm.[125, 126] The SRCD spectra of biomolecules such as DNA (Figure 1.5.3) are enhanced relative to regular CD spectra as more peaks are produced, from which additional data can be extracted.

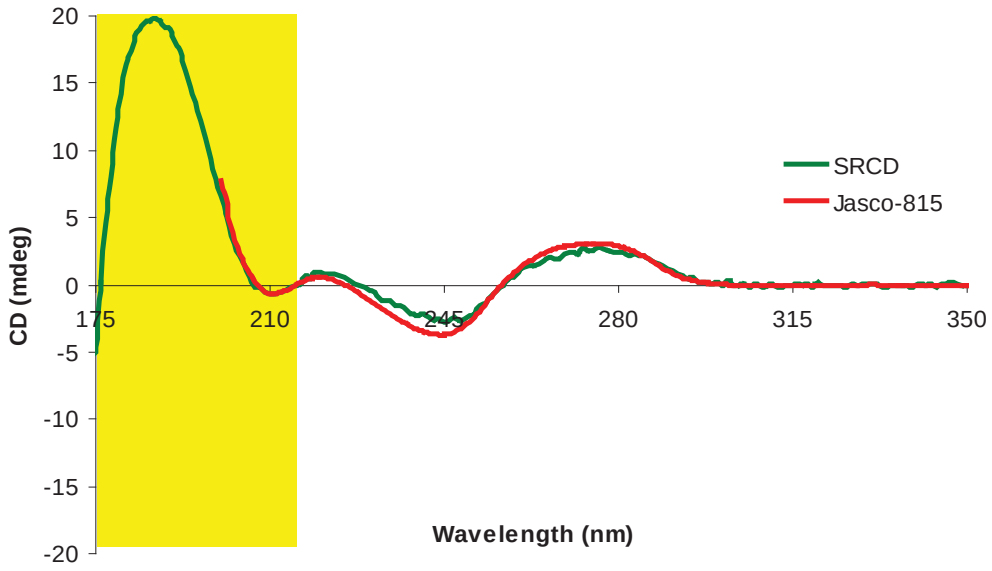

Figure 1.5.3. Comparison of the CD spectra of calf-thymus DNA, obtained with a conventional instrument (red) and with an SRCD instrument (green), demonstrating the extended wavelength range provided by SRCD.[119] The SRCD spectrum would typically be smoother, although in this case it was obtained using fewer repetitions than the CD spectrum (3 and 30, respectively).

1.5.3 Linear dichroism

In contrast to CD, linear dichroism (LD) is a technique that measures the difference in absorption of light that is polarised parallel and perpendicular to the orientation axis of the sample.[106] For an orientation axis to exist, the sample must be linearly aligned;[127] this can be achieved through the adsorption of the sample onto a stretchable film,[128] or more commonly, through the use of a Couette flow cell (Figure 1.5.4).[129] In this cell, the sample solution is placed in a chamber between two transparent cylinders, one of which rotates during measurement. This rotation exerts a shear force upon the sample that results its alignment of along the direction of the flow.[129] The advantage of this alignment is that only large molecules with a high aspect ratio are affected by the shear force; smaller compounds such as platinum complexes are not aligned due to shear flow and thus do not produce LD peaks.[127] This allows

for the study of the interactions of chiral compounds with chiral macromolecules without the need to discriminate between the dichroism signals of both species.[114] In addition to measuring the changes in structure of biomolecules, LD can also provide information regarding the nature of the change; for example, the LD spectra of DNA bound with an groove-binding compound will respond differently to that of DNA bound with an intercalating compound.[130] LD therefore can provide valuable information regarding the interactions of PCs with high aspect ratio biomolecules.

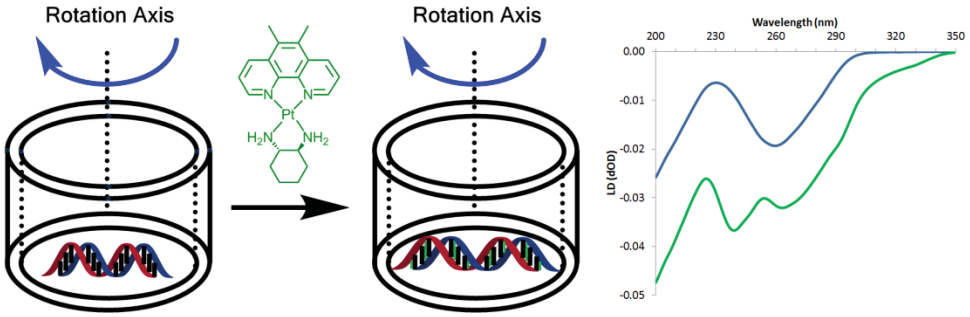

Figure 1.5.4. Demonstration of the lengthening of DNA upon the addition of 56MESS within a Couette flow cell (left). The LD spectra (right) demonstrate the signal of calf-thymus DNA (blue) and DNA bound with 56MESS (green).

1.5.4 Fluorescence spectroscopy

Fluorescence spectroscopy involves the excitation of a fluorescent species at a specific wavelength, followed by the measurement of radiation emitted when the excitation ends.[131] For a compound to be capable of fluorescence (a fluorophore), it typically needs to contain a conjugated π system, or a transition metal.[132-134] The emission of a fluorophore is often changed depending on the solvation shell, and this shell is often affected during DNA or protein binding interactions.[135-137] To examine the binding interactions of non-fluorescent species, one can competitively displace a binding-dependent fluorophore from a binding site and measure the attenuation of emission. A common fluorophore used for this purpose is ethidium bromide (EtBr); when bound with DNA, the emission of EtBr is greatly amplified.[138] The addition of a competitive binder such as a PPC will eject EtBr from the site, resulting in attenuation of fluorescence (Figure 1.5.5) in an experiment known as a fluorescence intercalator displacement FID assay.[139-141] The attenuation of EtBr fluorescence can be plotted as a binding curve from which binding constants can be calculated.

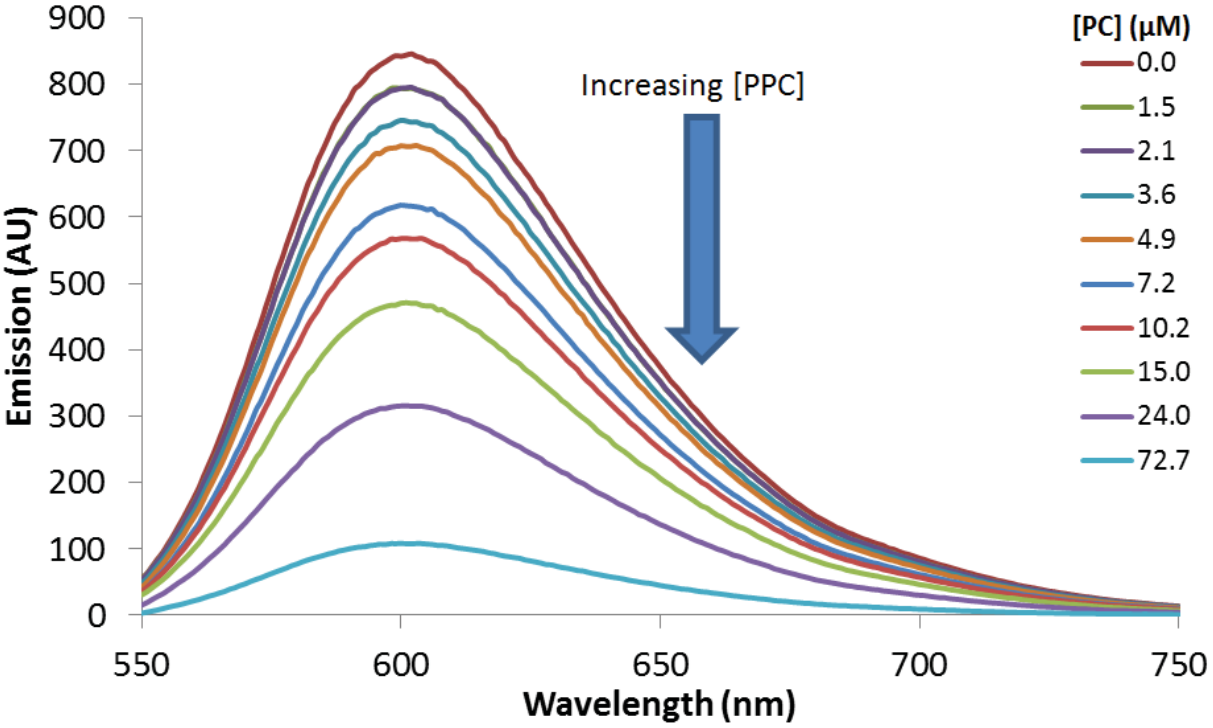

Figure 1.5.5. Fluorescence spectra of EtBr bound with DNA, with increasing concentration of 56MESS. The EtBr emission is quenched with increasing 56MESS concentration.[142]

1.5.5 Isothermal titration calorimetry

Isothermal titration calorimetry (ITC) is a biophysical technique in which the thermodynamics of the interaction between a biologically active compound and a macromolecule can be measured; this occurs through the highly sensitive measurement of the heat of enthalpy of the interaction.[143] This type of analysis is used to study the binding of ligands to proteins;[144-146] however, ITC has also been used to study the interactions of compounds with DNA,[113, 147, 148] with metal complex-DNA interactions reported as early as the nineties.[147, 149-151] ITC is the only technique that can determine the binding constant (K), enthalpy change (ΔH), entropy change (ΔS), Gibbs free energy change (ΔG), and the number of bound ligands (N) in the same experiment.[152] ITC is also particularly useful because it can be applied to any biological interaction that produces a heat signal, which is the very large majority of interactions.[153] Similarly to CD, ITC does not require the addition of any reagents that may interfere with the interaction, allowing for unperturbed binding.[154] In ITC analysis, the biologically active compound is titrated into a solution of the macromolecule. This results in the temperature of the solution changing, and the instrument uses power to bring the solution temperature back to equilibrium. The instrument power usage is plotted and the thermodynamic parameters determined from this data (Figure 1.5.6).[152]

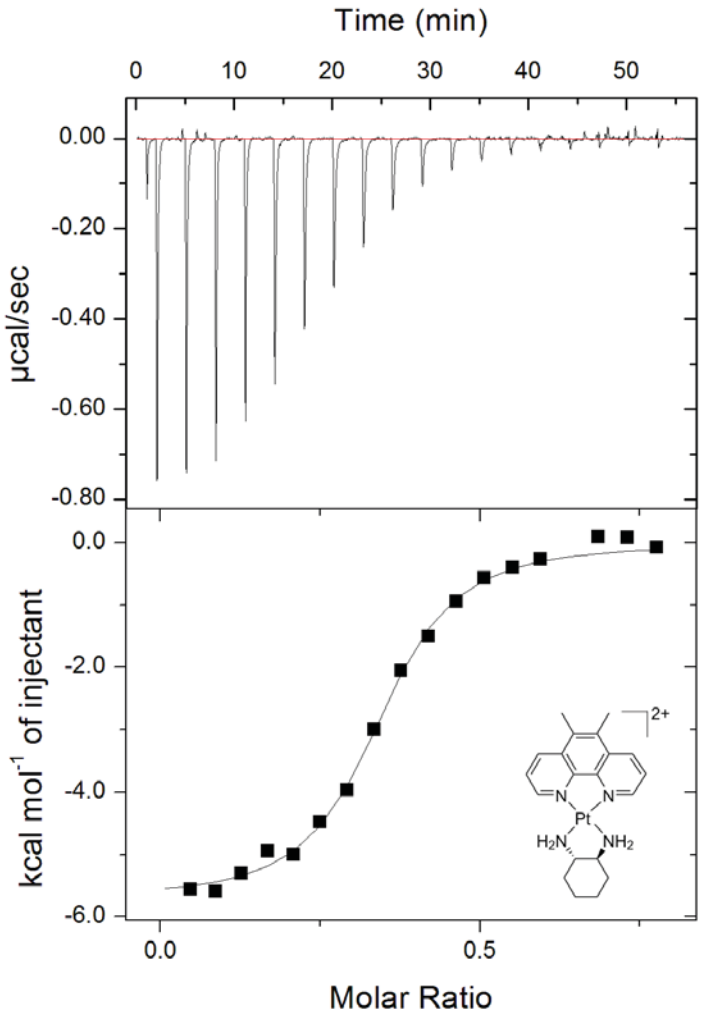

Figure 1.5.6. ITC trace (top) and binding curve (bottom) of the titration of 56MESS (600 µM) into calf-thymus DNA (160 µM base pair).

1.6 Aims and Objectives

This project aimed to build upon the research into polyaromatic PCs (PPCs) with anticancer activity in several ways. The first objective, which was continuous throughout this project, was the synthesis of novel platinum(II) agents (Figure 1.8.1), resulting in a well-rounded library of complexes that could be carried into further studies in international collaboration with other research groups. This was to be achieved through a variety of synthesis and purification methods depending on the nature of the intended product. These complexes incorporated ligands not previously used in the PPC library, including bpy, 4,4'-dimethyl-bpy (44Me$_2$bpy), 2-(2'-pyridyl)quinoxaline (2pq), a variety of pyridyl-1,2,3-triazole (R-pytri) ligands, and 1,4-dach. The second objective was the determination of a relationship, if any, between the aromatic surface area, DNA binding affinity, and cytotoxicity of a series of PPCs. Six PCs were chosen for this study, each with the same A_L of *SS*-dach and either bpy, 44Me$_2$bpy, phen, 5,6-dimethyl-phen (56Me$_2$phen), dipyrido[3,2-*f*:2',3'-*h*]quinoxaline (dpq) or 2,3-dimethyl-dpq (23Me$_2$dpq) as a P_L (Figure 1.6.1).

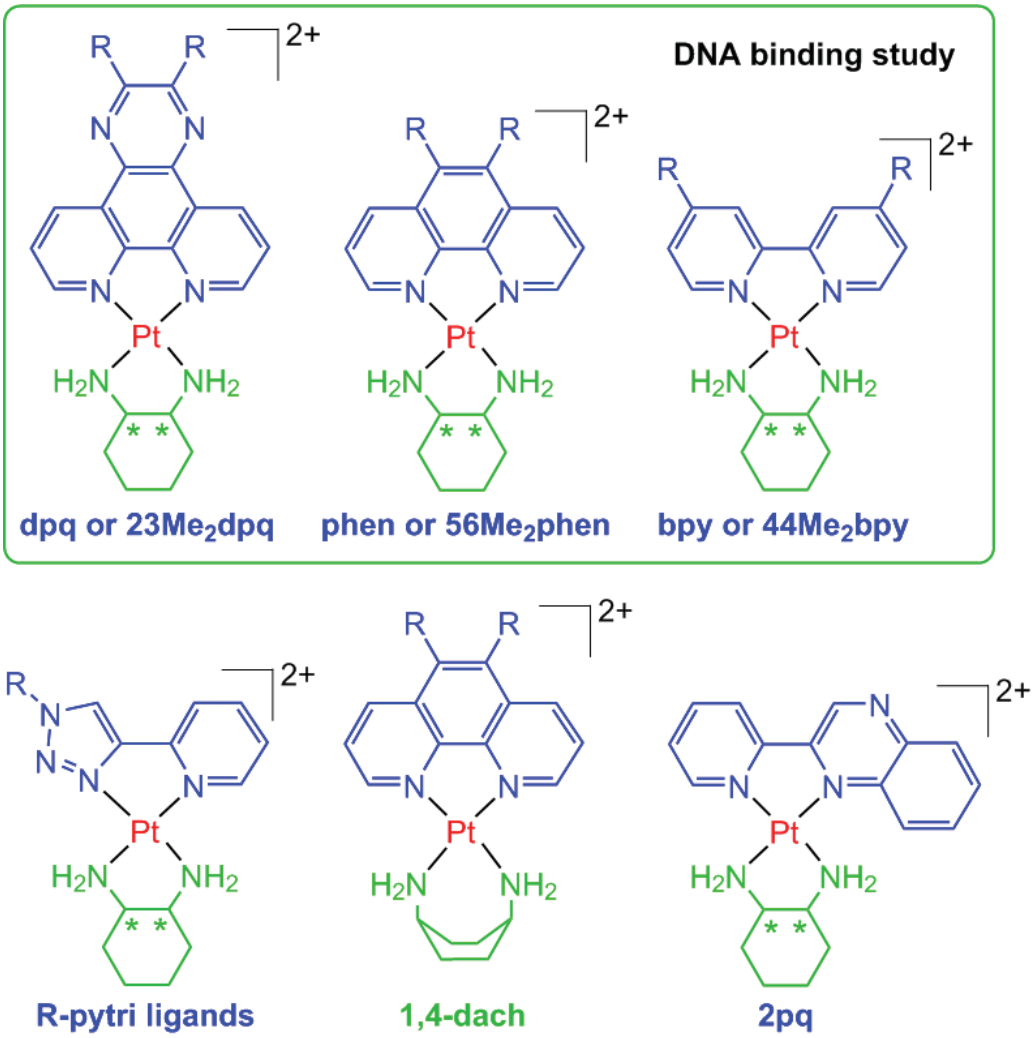

Figure 1.6.1. General structures of the platinum (II) complexes in this study, showing the P_L in blue, platinum centre in red and A_L in green. * indicates a stereocentre, either *S*,*S* or *R*,*R*, and counter-ions have been omitted for clarity. The 1,4-dach complexes are racemic. 'R' represents either a hydrogen or methyl substituent. Under each complex is the abbreviated name of the P_L or A_L, whichever is more noteworthy. The *S*,*S* isomers of the top row were used in the DNA binding study for the second objective.

The investigation would utilise a variety of biophysical assays, allowing for a comparison of the data obtained from each technique and the determination of the optimal technique(s) to study platinum-DNA interactions. The techniques utilised were UV spectroscopy, fluorescence, LD, SRCD, electrospray ionisation mass spectrometry (ESIMS) and ITC. The third objective was the development of platinum(IV) variations of highly-active platinum(II) complexes (Figure 1.6.2). Initial studies involved the synthesis of relatively simple dihydroxido analogues in to compare platinum(II) and platinum(IV) cytotoxicity. The final goal was the synthesis of a platinum(IV) prodrug incorporating a platinum(II) "payload" and an axial ligand that can target PSMA on the surface of prostate tumours through the use of the DCL moiety. All synthesised platinum(II) complexes underwent cytotoxicity testing against several different cancer cell lines, including but not limited to: L1210 murine leukaemia,

HT29 human colon carcinoma and U87 human glioblastoma cell lines. A variety of cell lines were tested to assess the versatility and cross-resistances of each PC. Chapter 2 summarises the results of four first-author publications in which the first two objectives regarding platinum(II) were fulfilled. Chapter 3 is a summary of unpublished progress toward the platinum (IV) objectives, while Chapter 4 makes concluding statements and summarises the project.

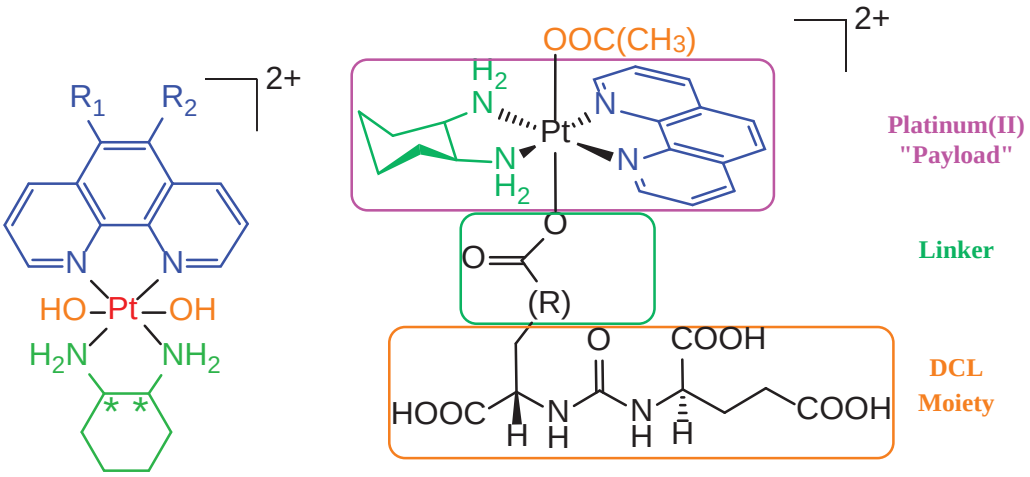

Figure 1.6.2 General structures of the platinum (IV) complexes in this study, showing the P_L in blue, platinum centre in red, A_L in green and axial ligands in orange. * indicates a stereocentre, either *S*,*S* or *R*,*R*, and counter-ions have been omitted for clarity. The compound on the right represents the final platinum(IV) prodrug goal.

CHAPTER 2. PUBLICATION SUMMARY

2.1 Foreword

This chapter briefly summarises the work contained in the four publications that directly contribute to this thesis. To improve coherency and avoid repetition, the papers will not be discussed separately; instead, the synthesis and characterisation, cytotoxicity and DNA binding from all papers will be summarised in respective sections. In terms of author contributions, Drs Jennette Sakoff and Jayne Gilbert performed cytotoxicity assays for all papers, and Dr Yingjie Zhang collected X-ray crystallography data where applicable. This author completed the large majority of other laboratory work with minor input from other listed authors, and prepared over 95% of each manuscript. The publications are listed below and will be referred to as Paper I, Paper II etc. Papers I-IV are included in full at the end of the chapter. The papers that indirectly contributed to this thesis, Papers V-XI, are also listed.

I. **Pages, B. J.**; Zhang, Y.; Li, F.; Sakoff, J.; Gilbert, J.; Aldrich-Wright, J. R. Cytotoxicity and Structural Analyses of 2,2'-Bipyridine-, 4,4'-Dimethyl-2,2'-bipyridine- and 2-(2'-Pyridyl)quinoxalineplatinum(II) Complexes. *European Journal of Inorganic Chemistry* 2015, 4167-4175. DOI: 10.1002/ejic.201500754 (Impact Factor 2.444, 13 citations).

II. **Pages, B. J.**; Sakoff, J.; Gilbert, J.; Rodger, A.; Chmel, N. P.; Jones, N. C.; Kelly, S. M.; Ang, D. L.; Aldrich-Wright, J. R. Multifaceted studies of the DNA interactions and in vitro cytotoxicity of potent polyaromatic platinum(II) complexes. *Chemistry – A European Journal* 2016, **22**, 8943-8954. DOI: 10.1002/chem.201601221 (Impact Factor 5.317, 10 citations).

III. **Pages, B. J.**; Sakoff, J.; Gilbert, J.; Zhang, Y.; Li, F.; Preston, D.; Crowley, J.; Aldrich-Wright, J. R. Investigating the cytotoxicity of platinum(II) complexes incorporating bidentate pyridyl-1,2,3-triazole "click" ligands. *Journal of Inorganic Biochemistry* 2016, **165**, 92-99. DOI: 10.1016/j.jinorgbio.2016.06.017 (Impact Factor 3.348, 7 citations).

IV. **Pages, B. J.**; Sakoff, J.; Gilbert, J.; Zhang, Y.; Hoeschele, J. D.; Kelly, S. M.; Aldrich-Wright, J. R. Combining the platinum(II) drug candidate kiteplatin with 1,10-phenanthroline analogues. *Dalton Transactions* 2018, Accepted. DOI: 10.1039/C7DT04108J (Impact Factor 4.029, 0 citations).

2.2 Synthesis and Characterisation

Throughout papers I, III and IV, fifteen PPCs were synthesised, fourteen of which were novel. The purpose was to expand the library of PPCs of the type $[Pt(P_L)(A_L)]^{2+}$ beyond that of complexes incorporating phen derivatives as a P_L and 1,2-dach as an A_L, and to probe the

anticancer activity of these complexes. In Papers I and III, studies are described of complexes incorporating either *SS*-dach or *RR*-dach as an A_L, and one of bpy, 44Me$_2$bpy, 2pq (Paper I) or R-pytri ligands (Paper III) as a P_L. Paper IV introduced complexes incorporating racemic 1,4-dach as an A_L and either phen, 5-methyl-phen (5Mephen) or 56Me$_2$phen as a P_L. The general structures of these PPCs are shown in Figure 1.8.1. Synthesis of these complexes was achieved using the previously published methods of the Aldrich-Wright group, although in each case some modifications were made. In brief, potassium tetrachloroplatinate is reacted with the A_L in water to precipitate the intermediate [Pt(A_L)Cl$_2$]. This product is then refluxed with the P_L in water to form the crude product, which is then purified through C-18 reverse-phase chromatography.[70] A summary of the reaction scheme for each complex archetype is shown in Figure 2.2.1.

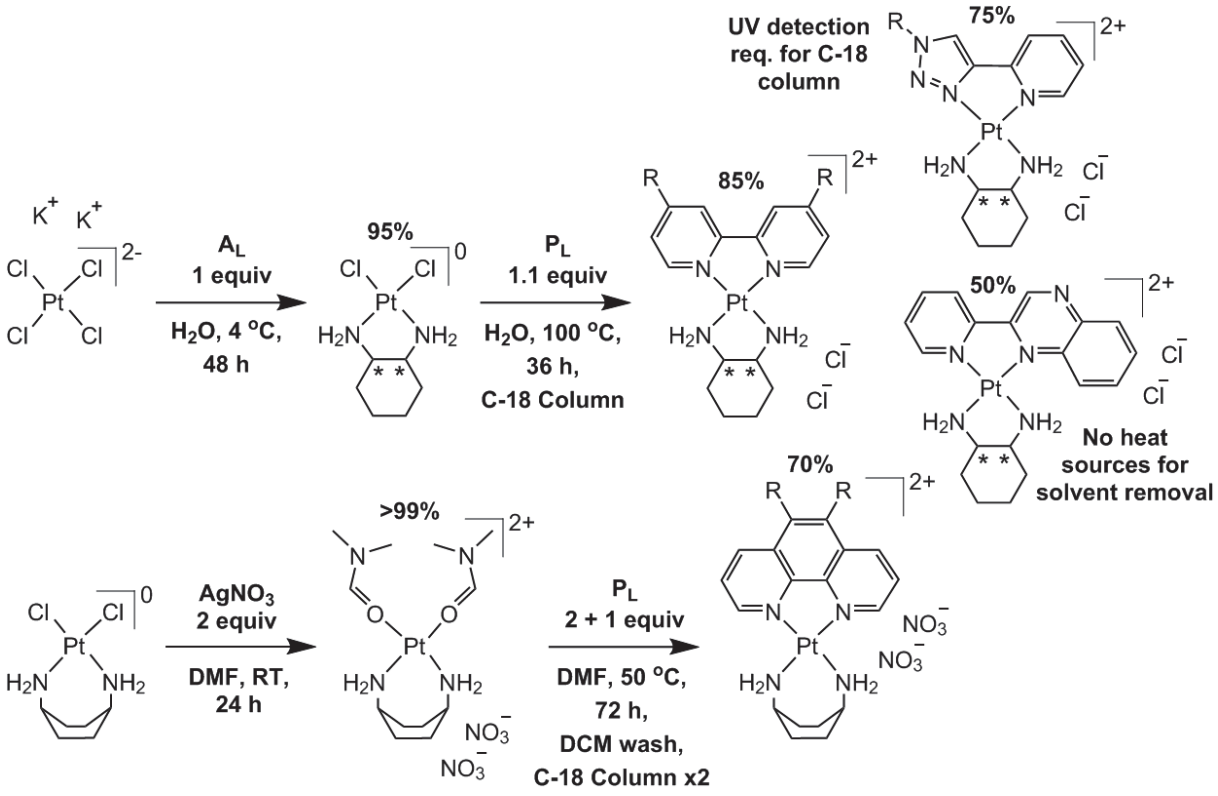

Figure 2.2.1. Summary of the synthesis of [Pt(P_L)(A_L)]$^{2+}$ complexes in this project. * indicates a stereocentre, either *S* or *R*. R is either H or CH_3.

There were some challenges to the synthesis method for most complexes. Complexes of bpy and 44Me$_2$bpy were made without modification to the method, however complexes of 2pq were found to be heat sensitive; this required all solvent removal to done through lyophilisation rather than rotary evaporation. The R-pytri reaction products were white instead of the typical yellow colour, meaning that column fractions required UV monitoring to confirm the presence of the product. The complex [Pt(1,4-dach)Cl$_2$] degraded under reflux conditions, and so an alternative method was developed based on previous work.[67] The

complex was reacted with silver chloride in dimethylformamide (DMF) to form [Pt(1,4-dach)$(DMF)_2$]$(NO_3)_2$; the DMF leaving groups of this complex are easier to displace than chloride ligands. This intermediate was then reacted with the P_L at 50 °C to form the crude product, which was then purified by column chromatography. The PPCs produced from these methods were very pure, with elemental microanalysis results deviating between 0.1-0.4% from the expected values. Yields varied between 50% and ~85% depending on the length of the purification process and stability of the product. PPC characterisation was achieved through nuclear magnetic resonance (NMR), UV spectra, CD spectra (where appropriate) mass spectrometry, elemental microanalysis (C, H, N) and x-ray crystallography. Some structural features determined through X-ray crystallography are discussed here; data from other spectroscopic characterisation can be found in Papers, I, III and IV.

X-ray crystal data obtained for bpy, 44Me_2bpy and R-pytri complexes revealed typical platinum coordination geometries in which the P_L was planar and the A_L adopted a chair conformation. Similar geometry was observed for the 1,4-dach complex (Figure 2.2.2, Table 2.2.1), however the A_L was in a twist-boat conformation due to coordination through the 1 and 4 positions of the ring rather than 1 and 2. Due to a steric clash between the peripheral ring of the 2pq ligand and the amine of the 1,2-dach ligand, the P_L was non-planar and the coordination geometry of the complex was distorted as a result. This was thought to be the cause of the instability of these complexes under heat and their low cytotoxicity. The chirality of the A_L affected the direction in which the 2pq P_L was distorted, and so the P_L was also chiral; interestingly, this lead to some very intense CD spectra as the P_L is much more absorbent than the A_L (see Paper I). The effect of different A_L and P_L combinations on the geometries of the platinum centre can be observed in Figure 2.2.2 and Table 2.2.1, in which complexes of 44Me_2bpy, 2pq and 1,4-dach are compared. The Pt-N bond lengths of each complex are similar, while differences emerge for some bond angles of the P_L (the 2pq complex) and A_L (the 1,4-dach complex). The synthesis of these complexes was an overall success, and many of the PPCs exhibited high cytotoxicity against several cell lines (Section 2.3), as well as high DNA affinity (Section 2.4).

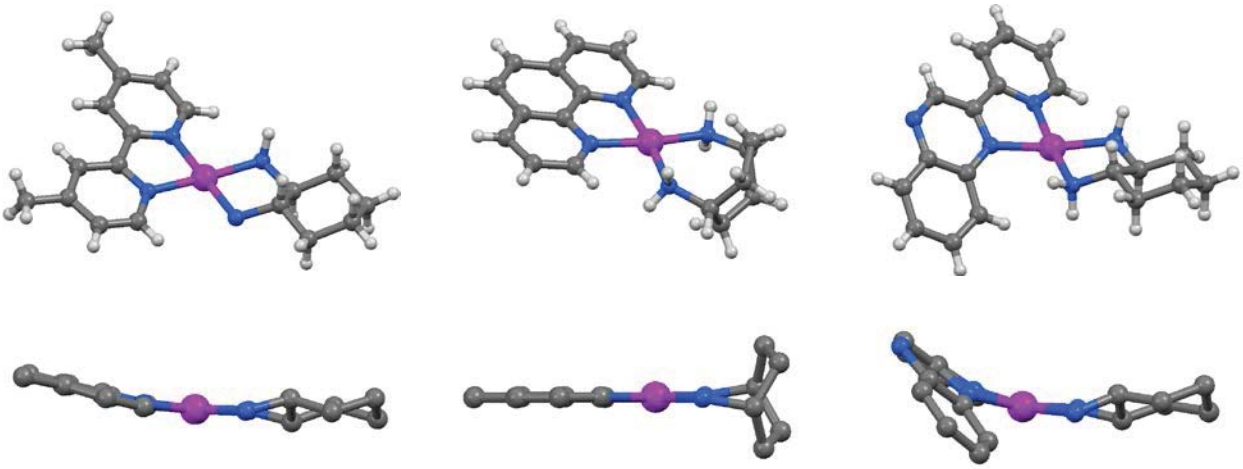

Figure 2.2.2. Comparison of the X-ray crystal structures of $[Pt(44Me_2bpy)(SS\text{-dach})]^{2+}$ (left), $[Pt(phen)(1,4\text{-dach})]^{2+}$ (middle) and $[Pt(2pq)(SS\text{-dach})]^{2+}$ (right), showing the differences in platinum coordination geometry. Platinum centres are shown in purple, nitrogen atoms in blue and carbon in grey. Hydrogen atoms (for the side views), solvents of hydration and counter-ions have been removed for clarity.

Table 2.2.1. Comparison of selected bond lengths and angles of complexes $[Pt(44Me_2bpy)(SS\text{-dach})]^{2+}$ (44MEBSS), $[Pt(phen)(1,4\text{-dach})]^{2+}$ (PHENK) and $[Pt(2pq)(SS\text{-dach})]^{2+}$ (2PQSS). Standard deviation is shown in parentheses.

	Complex		
Bond length (Å)	**44MEBSS**	**PHENK**	**2PQSS**
Pt-N (P_L)	2.03(2)	2.062(4)	2.020(5)
Pt-N (A_L)	2.07(2)	2.072(4)	2.050(5)
Bond angle (°)	**44MEBSS**	**PHENK**	**2PQSS**
N-Pt-N (P_L)	80.6(7)	81.7(2)	79.8(2)
N-Pt-N (A_L)	83.2(7)	96.3(3)	81.9(2)
Pt-N-C (A_L)	109(1)	125.6(4)	109.1(4)
Torsion angle (°)	**44MEBSS**	**PHENK**	**2PQSS**
N-C-C-N (P_L)	-1(3)	0.7(8)	-6(8)

2.3 *In Vitro* Cytotoxicity

Each complex synthesised in Papers I, III and IV was tested in a variety of human cancer cell lines to screen their viability as anticancer agents. The protocol utilised to determine the IC_{50} value is described in detail in Papers I-IV. In brief, the cancer cells were grown for 24 hours, before the test PPC was added. After 72 more hours, cell growth was assessed using the 3-[4,5-dimethylthiazol-2-yl]-2,5-diphenyl-tetrazoliumbromide (MTT) assay and the IC_{50} value was calculated, representing the concentration of PPC required to reduce cell growth by 50%. All PPCs from Papers I, III and IV were tested, as well as several complexes from the indirect

contributor Paper V (see Section 2.5, Figure 2.3.1). The chemotherapeutic drugs cisplatin, carboplatin and oxaliplatin were also assessed, as well as several published phen and 56Me$_2$phen PPCs that did not have cytotoxicity data for these lines. Several of the most cytotoxic PPCs from each paper were chosen for comparison here; the structure and abbreviated name of each PPC is shown in Figure 2.3.1. The cytotoxicity of each of these PPCs in several human cell lines is compared in Table 2.3.1, alongside values for cisplatin, carboplatin and oxaliplatin. The full extent of cytotoxicity data and discussions can be found in Papers I-IV.

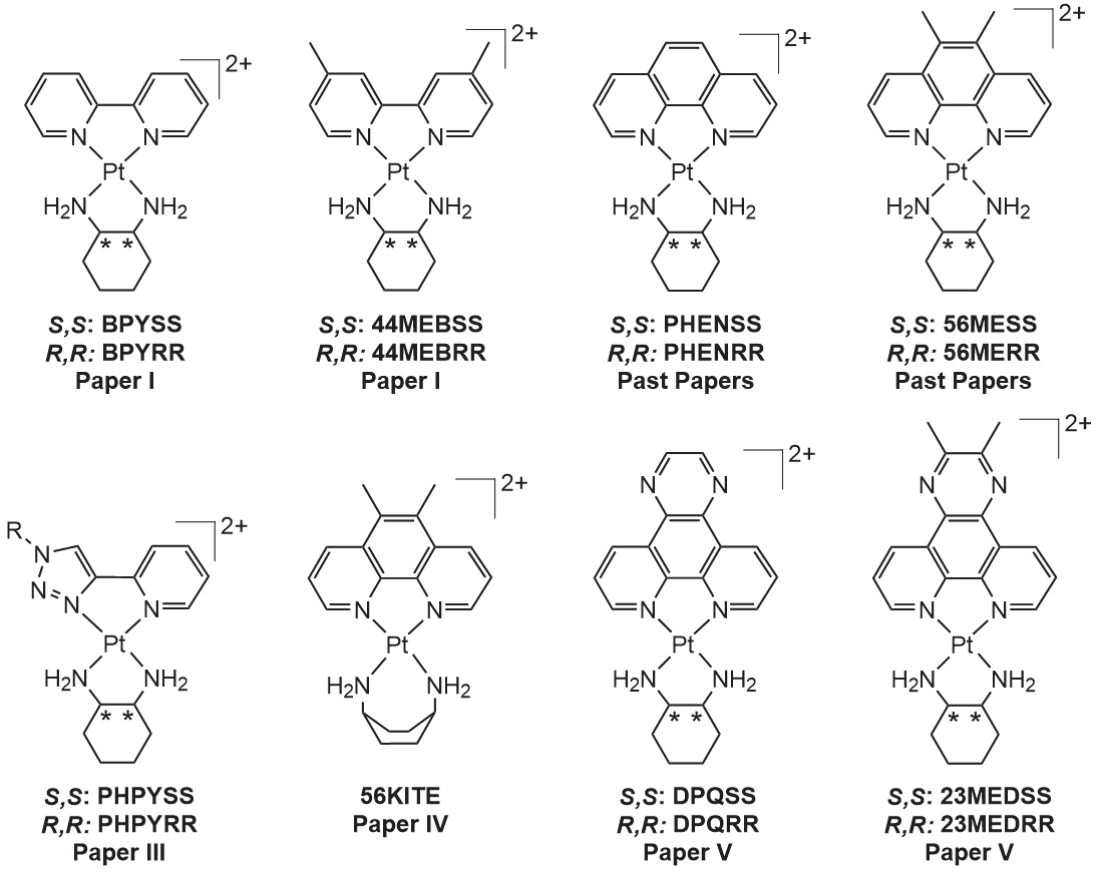

Figure 2.3.1. Chemical structures and shorthand names of several of the most cytotoxic PPCs from Papers I-V, and the published phen-based complexes used for comparison. * indicates a stereocentre, either *S* or *R*. All complexes have chloride counter-ions aside from 56KITE, which has nitrates (counter-ions not shown).

Of all the new complexes synthesised in this project, 44MEBSS and DPQSS were the most cytotoxic overall, achieving activity close to PHENSS in most cell lines. The *R*,*R* isomers DPQRR and 44MEBRR were close behind, followed by BPYSS, 56KITE, 23MEDSS and 23MEDRR, then the pyridyl triazole complexes PHPYSS and PHPYRR, along with BPYRR. The published complex 56MESS remained the most active complex by far, with IC_{50} values as low as 7 nM. Most PPCs demonstrated particularly good activity against Du145 prostate cancer and HT29 colon carcinoma lines, which indicates that they may be good choices for targeted therapy in the future. In terms of the *SS*-dach and *RR*-dach complexes, the general

trend in activity relative to P_L was 56Me$_2$phen > phen > 44Me$_2$bpy > dpq > bpy ≈ 23Me$_2$dpq > R-pytri ligands. There does not appear to be a trend relative to the size of each ligand. However, for phen and bpy ligands, the presence of terminal methyl groups does increase activity dramatically in all cases. The effect of P_L on activity is demonstrated in Figure 2.3.2, showing all *S*,*S* isomers and 56KITE.

Table 2.3.1. Summary of the *in vitro* cytotoxicity of several PCs in the HT29 colon carcinoma, U87 glioblastoma, MCF-7 breast cancer, A2780 ovarian cancer, and Du-145 prostate cancer cell lines, expressed as an IC_{50} value with standard error (1 sig. fig.). IC_{50} is the concentration at which cell growth is inhibited by 50% over 72 h.

	IC_{50} (μM)				
Complex	**HT29**[a]	**U87**[a]	**MCF-7**	**A2780**	**Du145**
BPYSS*	1.1 ± 0.2	4.0 ± 0.3	2.6 ± 0.2	2.6 ± 0.2	1.3 ± 0.4
44MEBSS	0.13 ± 0.03	0.500 ± 0.009	3.5 ± 0.7	0.9 ± 0.1	0.12 ± 0.03
44MEBRR	0.66 ± 0.07	3.9 ± 0.4	2.70 ± 0.07	5 ± 1	1.5 ± 0.3
PHENSS	0.13 ± 0.04	1.5 ± 0.4	0.5 ± 0.2	0.27 ± 0.03	0.08 ± 0.05
PHENRR	0.56 ± 0.08	8.9 ± 2.5	3.2 ± 0.2	2.70 ± 0.07	0.79 ± 0.08
56MESS	0.08 ± 0.06	0.08 ± 0.01	0.05 ± 0.02	0.030 ± 0.004	0.007 ± 0.002
56MERR	0.19 ± 0.00	2.2 ± 0.058	0.8 ± 0.1	1.1 ± 0.1	0.41 ± 0.04
PHPYSS	4.4 ± 0.3	>50	14 ± 2	4 ± 1	1.8 ± 0.5
PHPYRR	4.7 ± 0.3	>50	20 ± 4	7 ± 3	8 ± 1
56KITE	0.8 ± 0.1	47 ± 3	3.7 ± 0.6	2.9 ± 0.2	4.8 ± 0.7
DPQSS	0.59 ± 0.08	3.70 ± 0.24	1.8 ± 0.2	2.0 ± 0.1	0.44 ± 0.06
DPQRR	1.3 ± 0.2	12 ± 2.8	7.8 ± 0.8	6.5 ± 0.0	2.7 ± 0.2
23MEDSS	1.8 ± 0.3	8.2 ± 1.6	4.2 ± 0.4	3.7 ± 0.4	2.2 ± 0.1
23MEDRR	1.6 ± 0.4	16 ± 3.2	4.4 ± 0.7	2.0 ± 0.1	3 ± 1
Cisplatin	11 ± 2	4 ± 1	6.5 ± 0.8	1.0 ± 0.1	1.2 ± 0.1
Oxaliplatin	0.9 ± 0.2	1.8 ± 0.2	0.5 ± 0.1	0.16 ± 0.0	2.9 ± 0.4
Carboplatin	>50	>50	>50	9 ± 3	15 ± 1

***** Pre-screening determined that BPYRR was not active against these cell lines.

In terms of A_L, the general trend is *SS*-dach > *RR*-dach > 1,4-dach. For phen complexes, the choice of A_L impacted cytotoxicity much more than the choice of P_L; for example, 56MESS is fifty-eight times more active than 56MERR against Du145 cells, yet it is only eleven times more active than PHENSS. This was not the case for bpy complexes, as the activity of BPYSS and 44MEBRR relative to 44MEBSS are much more similar. It was harder to determine trends for the dpq complexes as there was not a clearly more active complex between 23MEDSS and 23MEDRR. The trends in activity for the 1,2-dach complexes were almost fully consistent across all cell lines tested; this indicates that the mechanism of action

of these PPCs is similar for all cancer types tested. The activity of 56KITE and the other PPCs in Paper IV was unexpectedly low. It was thought that the relatively high activity of [Pt(1,4-dach)Cl_2] (kiteplatin) over [Pt(*RR*-dach)Cl_2] would translate to polyaromatic variants; however, the cytotoxicity of 56KITE was found to be closer to BPYSS and 23MEDSS than that of 56MESS. Additionally, while demonstrating some micromolar level activity in some cell lines, 56KITE was inactive in others such as U87 glioblastoma and others (see Paper IV). This indicates that the mechanism of action of 1,4-dach PPCs is different to those of *SS*-dach and *RR*-dach. However, the mechanism must be somewhat similar as presence of terminal methyl groups on the P_L also correlated with higher activity for the 1,4-dach PPCs. Overall, the cytotoxicity of several of the newly synthesised PPCs was quite high, although not as high as the already published phen and 56Me_2phen complexes. However, nanomolar-level cytotoxicity is not a prerequisite of a good anticancer drug candidate. Many other factors must be considered, especially toxicity to healthy tissue; for example, a comparison of the *in vivo* activity of PHENSS and 56MESS revealed treatment with PHENSS to be more effective with fewer side effects, despite exhibiting lower *in vitro* cytotoxicity.[71, 155] Further *in vitro* and *in vivo* studies of the PPCs synthesised here will be necessary to determine how they truly compare to 56MESS and others in terms of anticancer activity.

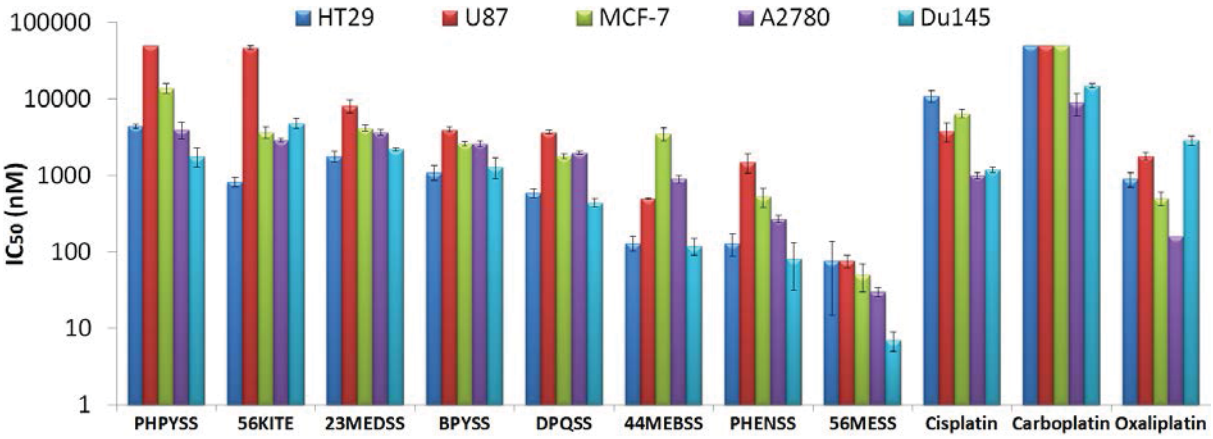

Figure 2.3.2. Comparison of the IC_{50} values of several PCs in HT29, U87, MCF-7, A2780, and Du-145 cell lines, expressed on a logarithmic scale in nanomolar with standard error. For coherency, values of ">50000 nM" are shown as 50000 nM with no error.

2.4 DNA Binding Studies

Detailed analysis of the DNA binding of several PPCs was performed across Paper II and Paper IV. The objective of Paper II was to investigate the binding of six PPCs to calf-thymus DNA (CT-DNA) using several biophysical techniques, some of which had never been applied to this family of complexes before. The complexes studied were chosen from Paper I, Paper V and previously published PPCs; BPYSS, 44MEBSS, PHENSS, 56MESS, DPQSS and

23MEDSS (structures are shown in Figure 2.3.1). These PPCs were chosen to determine the effect of the size of the P_L and the presence of methyl groups, on the DNA affinity of PPCs. The biophysical techniques utilised were UV spectroscopy, fluorescence, LD, SRCD, ITC and ESIMS; this was to determine if there are optimal techniques to study PPC-DNA binding, and if the relative DNA affinities of each compound were the same across all technique datasets. Some techniques provided more information than others, and some had limitations. Overall, the trends in DNA affinity amongst the PPCs were almost the same across all studies, meaning that any of the techniques could be used singularly to determine the relative DNA affinity of a series of compounds. The data obtained from the fluorescence and SRCD studies (examples in Figure 2.4.1), while quantitative, did not directly measure the PPC-DNA binding interaction. Instead they measured the ability of each complex to displace a competitive binder from DNA or the structure stabilisation effect of PPC binding on the DNA helix, respectively. This is useful for comparing a group of compounds within the same project, although it is more difficult to compare with other independent studies.

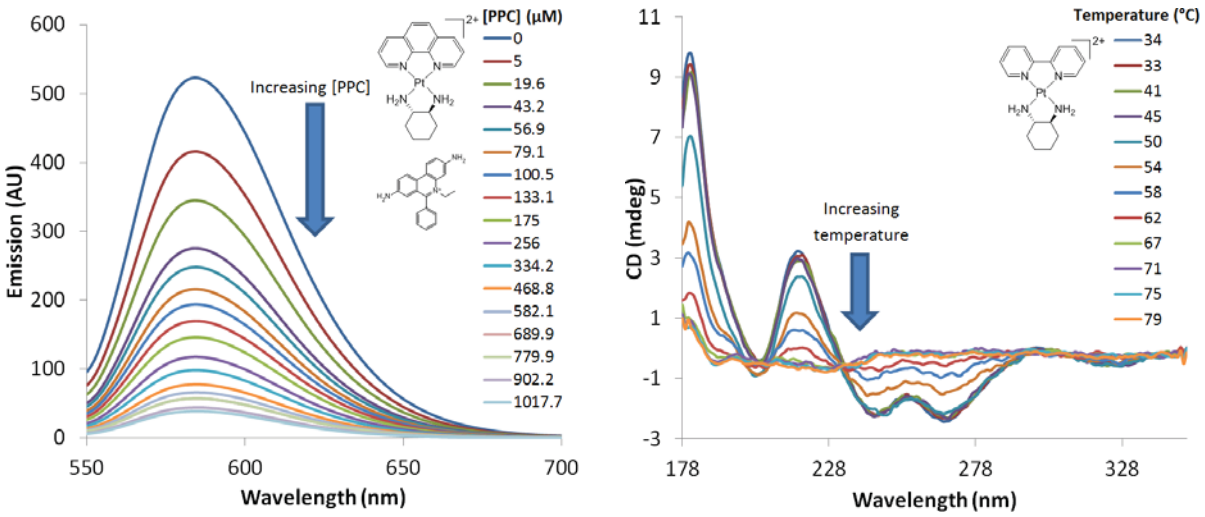

Figure 2.4.1. Representative spectra from Paper II. Left: Emission spectra of CT-DNA (150 μM base pair) bound with EtBr (75 μM) with increasing concentration of PHENSS. Right: SRCD spectra of CT-DNA (1 mM base pair) bound with BPYSS (0.5 mM) at increasing temperatures.

While the fluorescence and SRCD data were a good indication of the affinity of each compound with DNA, it was ideal to compare the results of these studies with those that directly measure PPC-DNA binding. This is what the UV, LD and ITC studies accomplished. Each of these studies determined the DNA binding constant (*K*) and number of binding sites (*n*) by monitoring the attenuation of signal and processing this attenuation data to generate *K* and other applicable parameters. Data processing was achieved through programs such as Microsoft Excel, Origin and Mathematica; further details of the processing can be found in Paper II and those within. In addition to *K* and *n*, LD also provided information on the

physical changes the DNA strand underwent during PPC binding, which in turn can suggest the binding mode. Three different binding events appeared to have occurred for each PPC, occurring at low (~5-30 μM), medium (~30-200 μM), and high (>200 μM) concentrations (relative to a DNA concentration of 150 μM base pair). In brief, the changes in LD signal at medium concentrations were very suggestive of intercalation, while it was speculated that the binding mode at low and high concentrations was partial intercalation and electrostatic groove binding, respectively. The higher concentration signal change, that is, a decrease in LD intensity, occurred at a much lower relative concentration for 56MESS and 23MEDSS; this prevented the generation of a full binding curve and the subsequent calculation of *K* for those complexes. Future experiments will attempt to elucidate the multiple binding events further. The UV study encountered no binding curve issues, and so binding data could be obtained for all complexes; however, only *K* and *n* could be obtained from this technique. Examples of LD and UV spectra are shown in Figure 2.4.2.

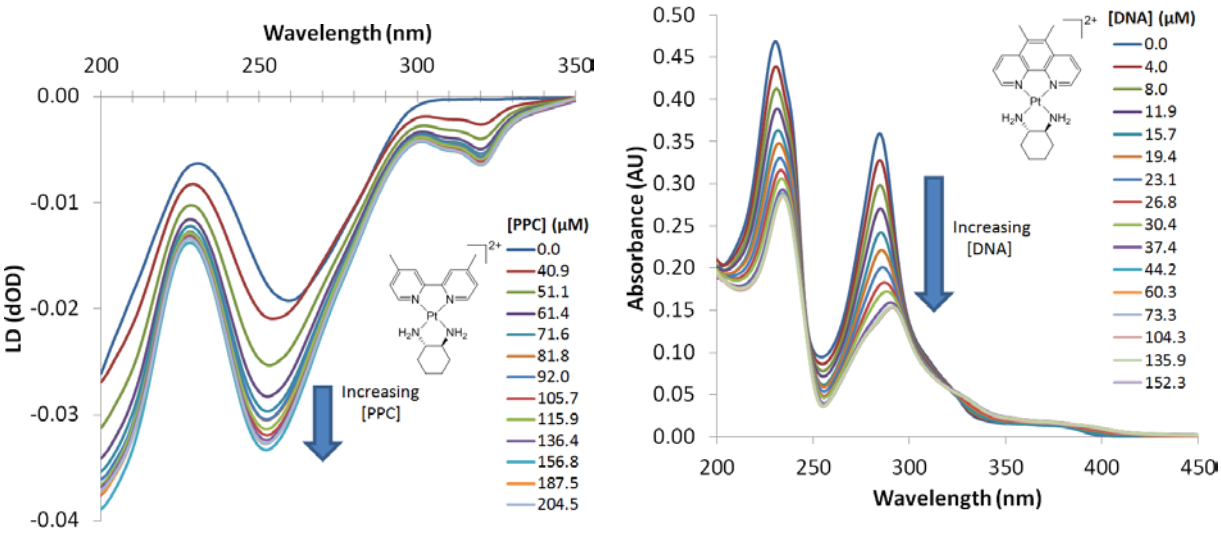

Figure 2.4.2. Representative spectra from Paper II. Left: LD spectra of CT-DNA (150 μM base pair) with increasing concentration of 44MEBSS (0-204.5 μM). Right: UV spectra of 56MESS (15 μM) with increasing concentration of CT-DNA (0-152.3 μM base pair).

The ITC experiments provided *K*, *n* and several thermodynamic parameters including the change in enthalpy (Δ*H*), entropy (Δ*S*) and Gibbs free energy (Δ*G*). ITC was determined to be the most useful method of obtaining DNA binding data, as it was able to provide *K* and *n* for all PPCs as well as additional data. The scale of binding constants and the trends between PPCs were very similar between ITC and UV, and so if both techniques are available then only ITC would preferentially be employed. LD, despite the issues with obtaining *K* for some complexes, was the only technique utilised that provided discrete binding mode data. Overall, to determine binding affinity and mode of PPCs to DNA, ITC and LD are the two techniques

that should be utilised at a minimum. The ESIMS experiments studied the binding of the six PPCs to discrete strands of DNA that consisted majorly of either adenine-thymine (AT) pairs or guanine-cytosine (GC) pairs. Each PC demonstrated a preference for the GC-rich strand over the AT-rich one (Figure 2.4.3); this information could be used in the future to study potential gene specificity of these complexes.

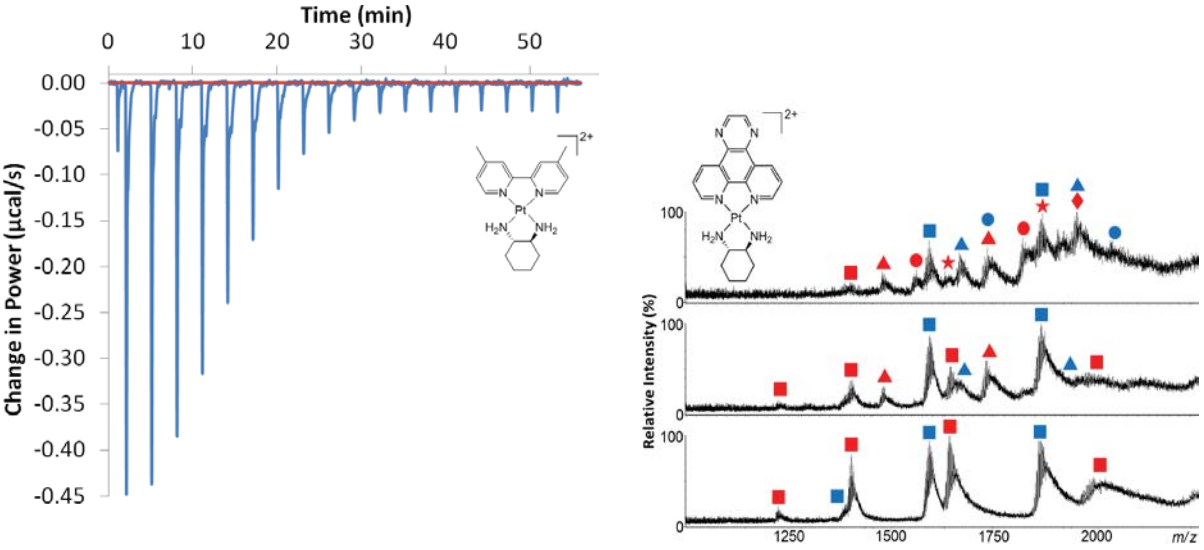

Figure 2.4.3. Representative data from Paper II. Left: ITC trace of the titration of 44MEBSS (650 µM) into CT-DNA (164 µM base pair). Right: Mass spectra of a solution of DPQSS, GC-rich strand (red symbols) and AT-rich strand (blue symbols) in the following ratios: 0:1:1 (bottom), 1:1:1 (middle) and 3:1:1 (top) (1 equivalent is 42 µM strand). Legend: square = [DNA], triangle = [DNA + 1 PPC], circle = [DNA + 2PPC], star = [DNA + 3PPC], diamond = [DNA + 4PPC].

Overall, the trends in DNA binding affinity were 56MESS > 23MEDSS ≥ DPQSS ≥ 44MEBSS = PHENSS > BPYSS (Figure 2.4.4. Full data is viewable in Paper II). The original hypothesis was that the larger aromatic P_L surface of 23MEDSS and DPQSS would result in higher intercalative DNA affinity, however 56MESS demonstrated the highest affinity. This suggested that there is an optimum P_L size for PPC-DNA interactions, and $56Me_2$phen is the closest to it of the studied P_Ls. When comparing DNA affinity to cytotoxicity, there is some correlation in that 56MESS and BPYSS are the most and least active, respectively, however there is no correlation for 23MEDSS and DPQSS. The correlation of phen and bpy complexes may suggest there is a link between DNA affinity and cytotoxicity; however, there is currently little *in vitro* evidence that DNA binding occurs in cells,[45, 72, 73] and so the primary mechanism of action of these complexes is unlikely to involve DNA intercalation.

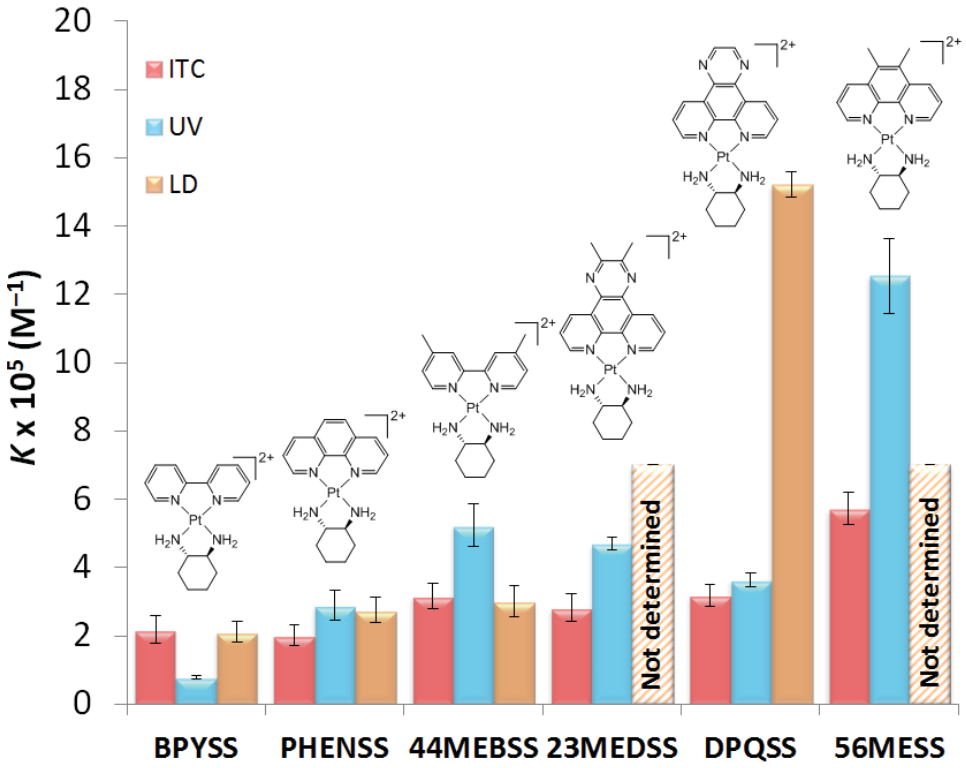

Figure 2.4.4. Comparison of the CT-DNA binding constants of the PPCs studied in Paper II, as determined by ITC (red), UV (blue) and LD (orange). Where applicable, *K* values over multiple wavelengths were averaged for LD and UV data. The error bars represent standard deviation of the values (1 sig. fig.).

In Paper IV, the CT-DNA affinity of three 1,4-dach complexes [Pt(phen)(1,4-dach)]$(NO_2)_3$ (PHENKITE), [Pt(5Mephen)(1,4-dach)]$(NO_2)_3$ (5KITE) and 56KITE was determined by ITC. The results were compared to the *SS*-dach counterparts PHENSS, 5MESS and 56MESS, and it was found that the affinity of the 1,4-dach PPCs was slightly higher than that of the *SS*-dach compounds (~0.7-2.4 × 10^5 M^{-1} higher). This suggests that the choice of A_L can have a minor effect on the affinity of PPCs to DNA. The very low cytotoxicity of the 1,4-dach complexes (Figure 2.3.2) further suggests that there is little correlation between DNA binding and cytotoxicity. While DNA binding is not likely the mechanism of action of these PPCs, past *in vitro* studies have provided some other insights. In short, these studies suggested that 56MESS: is taken up by cells more readily than cisplatin;[45] arrests the cell cycle of cancer cells in a different phase to cisplatin;[156] interferes with the accumulation and transport of copper and iron within cancer cells;[73] may suppress the biosynthesis of glutathione and other cysteine peptides.[73] Further and wider exploration of the in vitro activity of PPCs is needed to truly determine their mechanism of action.

2.5 Other Publications

The following papers indirectly contributed to this study. The laboratory work and literature research involved in the contributions to these papers makes up a significant portion of the work performed for this thesis. Brief summaries follow.

V. **Pages, B. J.**; Li, F.; Wormell, P.; Ang, D. L.; Clegg, J. K.; Kepert, C. J.; Spare, L. K.; Danchaiwijit, S.; Aldrich-Wright, J. R. Synthesis and analysis of the anticancer activity of platinum(II) complexes incorporating dipyridoquinoxaline variants. *Dalton Transactions* **2014**, 43, 15566-15575 DOI: 10.1039/C4DT02133A (Impact Factor 4.029, 19 citations). Contribution: 85%.

- This paper covered the synthesis and anticancer activity of eight complexes incorporating dpq as a P_L.
- Was based upon an honours project with some additional fluorescence and X-ray crystallography work included.
- This paper, along with Paper I, formed the synthesis base from which the final goal of DNA binding studies was achieved in Paper II.

VI. Macias, F. J.; Deo, K. M.; **Pages, B. J.**; Wormell, P.; Clegg, J. K.; Zhang, Y.; Li, F.; Zheng, G.; Sakoff, J.; Gilbert, J.; Aldrich-Wright, J. R. Synthesis and Analysis of the Structure, Diffusion and Cytotoxicity of Heterocyclic Platinum(IV) Complexes. *Chemistry – A European Journal* **2015**, 21, 16990-17001. DOI: 10.1002/chem.201502159 (Impact Factor 5.317, 10 citations). Contribution: 15%.

- Six platinum(IV) variants of polyaromatic platinum(II) complexes were synthesised and their diffusion coefficients were determined and compared with platinum(II) analogues.
- The first platinum(IV)-based paper published by the Aldrich-Wright group and the synthesis base of the work summarised in Chapter 3.

VII. **Pages, B. J**.; Ang, D. L.; Wright, E. P.; Aldrich-Wright, J. R. Metal complex interactions with DNA. *Dalton Transactions* **2015**, 44, 3505-3526. DOI: 10.1039/C4DT02700K (Impact Factor 4.029, 66 citations). Contribution: 75%.

- A comprehensive overview of the many types of binding interactions of transition metal complexes with various forms of DNA including B-DNA, G-quadruplexes and Y-junctions. The interactions of 50 complexes were covered.

VIII. Deo, K.;[†] **Pages, B.J.**;[†] Ang, D.; Gordon, C.; Aldrich-Wright, J. Transition Metal Intercalators as Anticancer Agents—Recent Advances. *International Journal of Molecular Sciences,* **2016,** 17, 1818-1834. DOI: 10.3390/ijms17111818 (Impact Factor 3.226, 9 citations). Contribution: 40%. ([†]: the authors contributed equally)

- A review of 2013-2016 advances in transition metal complexes with high anticancer activity and an intercalative binding mode with DNA.
- Provided a comprehensive overview of the potential of intercalating metal complexes as anticancer agents.

IX. **Pages, B. J.**; Garbutcheon-Singh, K. B.; Aldrich-Wright, J. R. Platinum intercalators of DNA as anticancer agents. *European Journal of Inorganic Chemistry* **2017**, 2017, 12, 1613-1624. DOI: 10.1002/ejic.201601204 (Impact Factor 2.444, 1 citation). Contribution: 80%.

- A review of the work of the Aldrich-Wright group in developing platinum(II) polyaromatic complexes as anticancer agents. Prominent PPCs from other research groups are also briefly covered.
- This provided a comprehensive understanding of the background of the Aldrich-Wright group, and also revealed potential research avenues for the future.

X. Bjelosevic, A.; **Pages, B. J.**; Spare, L. K.; Deo, K.; Ang, D. L.; Aldrich-Wright, J. R. Exposing "bright" metals: promising advances in photoactivated anticancer transition metal complexes. *Current Medicinal Chemistry* **2018**, **25**, 478-492. DOI:10.2174/0929867324666170530085123 (Impact Factor 3.249, 0 citations). Contribution: 40%.

- A review of transition metal complexes that have been used as photodynamic agents in the field of anticancer chemistry – complexes that are non-toxic to cancer cells until irradiation with light at specific wavelengths.

XI. Deo, K. M.; Ang, D. L.; McGhie, B.S.; Rajamanickam, A.; Dhiman, A.; Khoury, A.; Holland, J.; Bjelosevic, A.; **Pages, B. J.**; Gordon C.; Aldrich-Wright, J. R. Platinum Coordination Compounds with Potent Anticancer Activity. Coordination Chemistry Reviews, **2018**, Accepted. DOI: CCR112609 (Impact Factor 13.324, 0 citations). Contribution: 5%.

- A review which acknowledges that the challenges of chemotherapy demand new platinum complexes with different cancer cell-killing mechanisms of action.
- Recognizes the significant research efforts of Australian and international colleagues which have influenced the direction of modern platinum chemistry. Provides history of the development of platinum(II) and platinum(IV) complexes.

2.6 Papers I-IV in Full

Papers I-IV are shown in full starting from the next page. The supplementary information for each of these papers can be found at each of their respective websites.

Paper I – Cytotoxicity and Structural Analyses of 2,2'-Bipyridine-, 4,4'-Dimethyl-2,2'-bipyridine- and 2-(2'-Pyridyl)quinoxalineplatinum(II) Complexes

http://onlinelibrary.wiley.com/wol1/doi/10.1002/ejic.201500754/abstract

Paper II – Multifaceted Studies of the DNA Interactions and In Vitro Cytotoxicity of Anticancer Polyaromatic Platinum(II) Complexes

http://onlinelibrary.wiley.com/wol1/doi/10.1002/chem.201601221/abstract

Paper III – Investigating the cytotoxicity of platinum(II) complexes incorporating bidentate pyridyl-1,2,3-triazole "click" ligands

http://www.sciencedirect.com/science/article/pii/S0162013416301805

Paper IV – Combining the platinum(II) drug candidate kiteplatin with 1,10-phenanthroline analogues

http://pubs.rsc.org/en/content/articlelanding/2017/dt/c7dt04108j#!divAbstract

EurJIC European Journal of Inorganic Chemistry

ChemPubSoc Europe

FULL PAPER

DOI:10.1002/ejic.201500754

Cytotoxicity and Structural Analyses of 2,2′-Bipyridine-, 4,4′-Dimethyl-2,2′-bipyridine- and 2-(2′-Pyridyl)-quinoxalineplatinum(II) Complexes

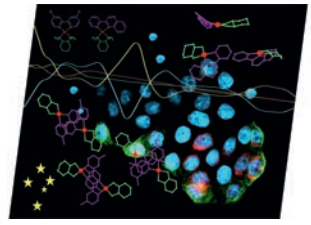

COVER PICTURE

Benjamin J. Pages,[a] Yingjie Zhang,[b] Feng Li,[a] Jennette Sakoff,[c] Jayne Gilbert,[c] and Janice R. Aldrich-Wright*[a]

Keywords: Medicinal chemistry / Antitumor agents / Cytotoxicity / Aggregation / Platinum

Platinum anticancer complexes incorporating 2,2′-bipyridine (bpy), 4,4′-dimethyl-2,2′-bipyridine (44Me$_2$bpy) or 2-(2′-pyridyl)quinoxaline (2pq) as polyaromatic ligands and the *S*,*S* or *R*,*R* isomer of 1,2-diaminocyclohexane as ancillary ligands in the form $[Pt(P_L)(A_L)]^{2+}$ have been synthesised and characterised. X-ray diffraction was used to elucidate the structure and stacking behaviour of the complexes, revealing interesting properties that may impact their biological activity. Pulsed gradient spin-echo NMR experiments elucidated the aggregation behaviour of these complexes in solution. The cytotoxicity of each complex was assessed against the L1210 murine leukaemia, HT29 human colon carcinoma and U87 human glioblastoma cell lines and compared to other complexes within this class. The complexes incorporating 44Me$_2$bpy were found to be the most potent at inhibiting cell growth with IC_{50} values for the *S*,*S* isomer (0.13–0.5 μM) less than that for cisplatin (0.36–11 μM), oxaliplatin (0.9–1.8 μM) or carboplatin (>50 μM). Most complexes were found to be very effective against HT29 colon carcinoma cells.

Introduction

The development of transition metal chemotherapeutics has been a highly active research area since the discovery of the anticancer activity of covalently binding platinum complexes (PCs) such as cisplatin,[1] although it is well-known that these complexes encounter resistance in some cancer types and have issues with dose-limiting toxicity.[2] As a result, many metal-based anticancer complexes utilising a wide variety of ligands have been, and continue to be, synthesised and tested.[3] Our group has focused on the development of platinum complexes that are capable of disrupting the activity of cancerous cells by non-covalently binding, arresting the cell cycle at a different phase to that of cisplatin, and causing cell death at nanomolar concentrations.[4] These compounds are of the type $[Pt(P_L)(A_L)]^{2+}$, in which P_L is a substituted 1,10-phenanthroline (phen) polyaromatic ligand and A_L is a chiral amine ancillary ligand such as 1*S*,2*S*-diaminocyclohexane.[5] Recently we have also reported that complexes of dipyrido[3,2-*f*:2′,3′-*h*]quinoxaline (dpq) and 2,3-dimethyl-dpq (23Me$_2$dpq) exhibit biological activity comparable to complexes with phen derivatives.[6] Here we present an expansion of the range of P_Ls via a study of complexes of 2,2′-bipyridine (bpy), 4,4′-dimethyl-bpy (44Me$_2$bpy) and 2-(2′-pyridyl)quinoxaline (2pq), with either 1*S*,2*S*-diaminocyclohexane (*SS*-dach) or 1*R*,2*R*-diaminocyclohexane (*RR*-dach) as an A_L (Figure 1).

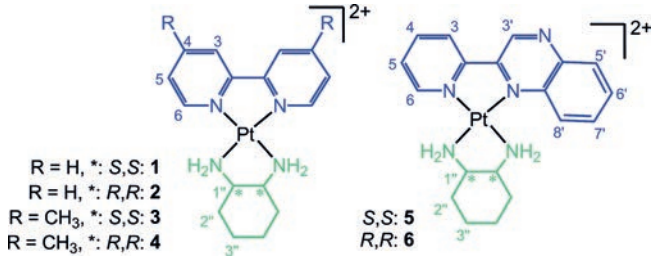

Figure 1. The general structures of complexes **1**–**6**, showing P_Ls in blue and A_Ls in green. The NMR proton numbering system is shown, and counterions have been omitted for clarity. * indicates a stereocentre, either *S* or *R*.

Bpy and its derivatives have seen use in a variety of metal complexes, such as photoswitchable complexes,[7] luminescent detectors,[8] anticancer compounds and DNA binders.[9] Similarly to phen derivatives, transition metal complexes containing terminally methyl-substituted bpy ligands have exhibited higher DNA affinity and cytotoxicity than those with regular bpy.[10] 2pq has been extensively studied as a ligand in a wide array of transition metal complexes.[11] The applications of these complexes have in-

[a] Nanoscale Organisation and Dynamics Group, University of Western Sydney,
Campbelltown, NSW 2560, Australia
E-mail: j.aldrich-wright@uws.edu.au
http://www.uws.edu.au/nanoscale/nanoscale_organisation_and_dynamics/anticancerdrugs
[b] Australian Nuclear Science and Technology Organisation, Kirrawee DC, NSW 2232, Australia
[c] Calvary Mater Newcastle,
Waratah, NSW 2298, Australia

Supporting information for this article is available on the WWW under http://dx.doi.org/10.1002/ejic.201500754.

cluded, but are not limited to: dye-sensitised solar cells;[11d] potent DNA binders;[11e,12] and nanomolar inhibitors of Platelet Activating Factor.[11f,13] The incorporation of bpy, 44Me$_2$bpy and 2pq into platinum complexes has resulted in compounds with unique physical and biological properties. The complexes studied here were [Pt(bpy)(*SS*-dach)]-Cl$_2$·1.5H$_2$O (**1**), [Pt(bpy)(*RR*-dach)]Cl$_2$·1.5H$_2$O (**2**), [Pt(44Me$_2$bpy)(*SS*-dach)]Cl$_2$·3H$_2$O (**3**), [Pt(44Me$_2$bpy)-(*RR*-dach)]Cl$_2$·3H$_2$O (**4**), [Pt(2pq)(*SS*-dach)]Cl$_2$·3H$_2$O (**5**), [Pt(2pq)(*RR*-dach)]Cl$_2$·4H$_2$O (**6**). The intermediate [Pt(2pq)Cl$_2$] (**7**) was also synthesised for the purpose of an X-ray structure comparison. X-ray crystallography and pulsed gradient spin-echo NMR (PGSE NMR) were utilised to study the stacking behaviour of these complexes, as π-stacking can play an important role in the interactions of these compounds with biomolecules such as DNA.[14] Complex cytotoxicity was determined in the L1210 murine leukaemia, HT29 human colon carcinoma and U87 human glioblastoma cell lines to facilitate structure–activity relationships. Other PCs within this archetype incorporating dpq, 23Me$_2$dpq, phen and 5,6-dimethyl-phen (56Me$_2$phen) were also tested within these cell lines.

Results and Discussion

Synthesis and Purity

The synthesis of complexes **1**–**6** was achieved using our previous methods for complexes of this type,[5b,6,15] however the yields for **5** and **6** were lower than expected. These complexes were found to decompose with heat, and so temperature of the reflux step is likely to have impeded the formation of the final coordinative product. Additionally, the elution profiles of **5** and **6** and their starting materials were found to overlap during Sep-Pak® elution, making it difficult to isolate the expected amount of pure product. Mass spectra confirmed the identity of each complex, while the NMR spectra and microanalytical data suggested only minimal impurities were present (see Table 3 in the Exp. Sect.). Complex **7** was initially synthesised as part of an alternate synthesis pathway, however the formation of easily obtainable crystals led to its use in structural comparisons. **7** had not previously been synthesised by precipitation from dimethyl sulfoxide/water,[5a,11b] and so microanalysis was employed to confirm the purity of the product.

NMR Spectral Assignment

Complexes **1**–**4** were characterised using one and two dimensional ^{1}H NMR and ^{1}H-^{195}Pt heteronuclear multiple quantum correlation (HMQC) NMR spectroscopy. The ^{1}H NMR spectrum of complex **1** is shown (Figure 2), which is also representative of the spectrum of **2**. In the aromatic region, the 8.96 ppm and 8.71 ppm doublets were assigned as H6 and H3, respectively; each of these protons would only couple with one other proton to produce a doublet, and the alpha-to-nitrogen position of H6 would result in a lower coupling constant than that of H3.[16] The COSY spectrum of complex **1** (Figure S3.1.1) revealed which of the triplets coupled to protons H3 and H6, resulting in the assignment of resonances at δ = 8.51 ppm and 7.90 ppm as H4 and H5, respectively.

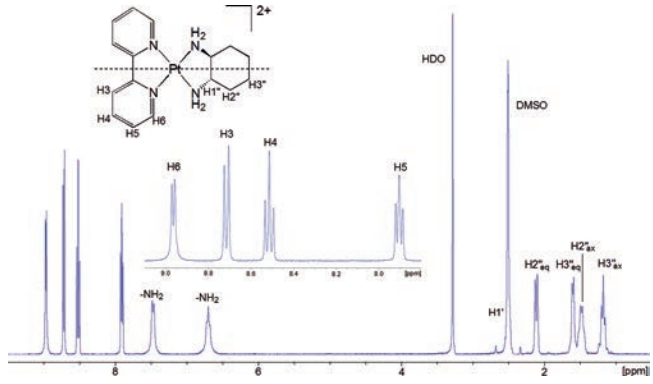

Figure 2. The ^{1}H NMR spectrum of complex **1** in [D$_6$]DMSO, showing proton assignment. Inset: a close-up of the aromatic region between 7.8 and 9 ppm. This spectrum also represents that of the enantiomer complex **2** (Figure S3.1.3).

The chemical shift and order of the aliphatic protons was the same as described for similar platinum complexes of dach in the literature,[6,17] and so assignment was identical to that of those complexes. The final resonances at δ = 7.47 and 6.70 ppm were assigned as the amines as spectrum of **1** obtained in D$_2$O (Figure S3.1.2) did not produce these peaks. For complexes **3** and **4**, the assignment of the dach resonances was identical, while that of the P$_L$ was different (Figures S3.1.4–6). The singlet at δ = 2.56 ppm was assigned as the methyl protons due to the singlet multiplicity and relative integral of 6, while the resonance at δ = 8.59 ppm was assigned as H3 by similar reasoning. In the COSY spectra of **3** and **4**, a two-bond correlation between H3 and the peak at δ = 7.73 ppm was observed, and so that resonance was assigned as H5 and the 8.76 ppm resonance as H6.

Finally, the ^{1}H-^{195}Pt HMQC spectra of complexes **1**–**4** consisted of a series of proton correlations with a platinum resonance at ca. 2786 ppm (Section S3.2). This platinum shift closely resembles that of similar complexes in the literature, and is distinct from that of the precursor [Pt(dach)-Cl$_2$] which resonates at –3283 ppm.[15,18] The correlations observed between this platinum centre and resonances in the amine and aromatic regions confirm that each ligand is coordinated to the platinum centre (Figure 3).

Assignment of the spectra of **5** and **6** was different than that of complexes **1**–**4** due to the asymmetry of the complex and the decomposition of each complex in [D$_6$]DMSO (Figure S3.1.8), meaning that the less-detailed D$_2$O spectra were used. The ^{1}H and COSY NMR spectra of complex **5** are shown as an example (Figure 4). In the aromatic region, the resonance at δ = 9.84 ppm was assigned as H3′ due to the singlet multiplicity. A NOESY spectrum of **5** (Figure 4) revealed a through-space correlation between this peak and the one at δ = 8.79 ppm, and so that resonance was assigned

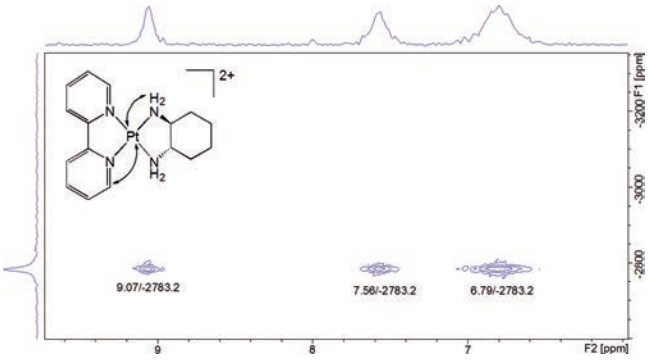

Figure 3. The ^{1}H-^{195}Pt HMQC spectrum of complex **1** in [D_6] DMSO, showing correlations of the platinum centre with the amine and H6 protons.

as H3. Tracing the correlations of the H3 resonance with those at δ = 8.59, 7.99 and 8.82 ppm within the COSY spectrum (Figure 4) lead to the assignment of H4, H5 and H6, respectively. Of the remaining protons, the resonance at δ = 8.19 ppm integrated for two protons – this was assigned as H6′/H7′ as these protons are equivalent and the resonance was coupled to two other peaks. Of these two peaks, one was merged with the H5 resonance; this was assigned as H8′ as this proton and H5 are each positioned beta to coordinated nitrogen. The remaining resonance at δ = 8.41 ppm was thus assigned as H5′.

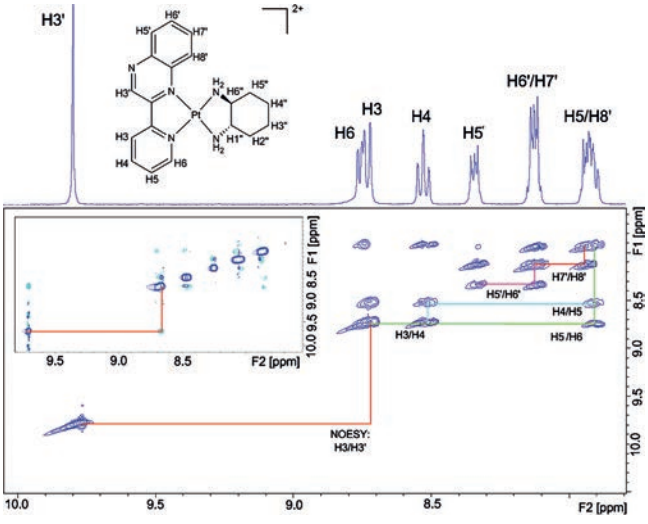

Figure 4. The ^{1}H NMR and COSY spectra of the aromatic region of complex **5** in D_2O, showing proton assignment. Inset: the NOESY spectrum of complex **5**, showing the correlation between H3′ and H3. These spectra are also representative of the enantiomer complex **6**. See S3.1.7 and S3.1.9 for full ^{1}H spectra of complexes **5** and **6**, respectively.

In the aliphatic region of complexes **5** and **6**, the resonances corresponding to each proton were partially or completely split in two, producing a range of finely-split signals for each proton (Figure 5). Each duplicate resonance was assigned as "H1′′a", "H1′′b" etc. This phenomenon occurred due to the asymmetry of the 2pq ligand. Similarly to complexes **1**–**4**, the ^{1}H-^{195}Pt NMR spectra of complexes **5** and **6** confirmed the presence of an N_4 coordination sphere (Section S3.2).

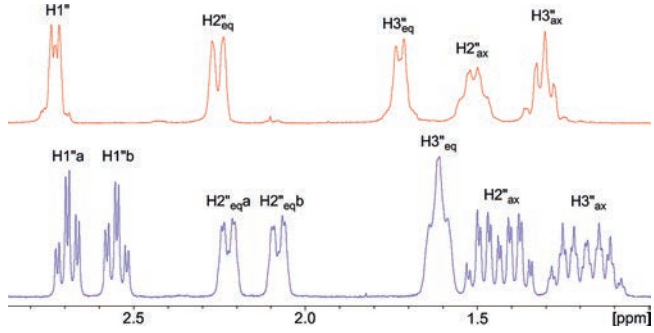

Figure 5. Comparison of the aliphatic regions of the ^{1}H NMR spectra of complexes **1** (red) and **5** (blue) in D_2O.

X-ray Crystal Structures

Crystal structure data for complexes **1**, **3**, **5**, **6** and **7** were obtained and provided the opportunity to compare the effect of the P_L and A_L on the geometry of the overall complex. The relevant data for each complex is summarised in their CDCC files. For the A_L of each complex, the chair conformation, bond lengths and angles are consistent with similar complexes in the literature.[6,19] The Pt-A_L and Pt–P_L bond angles for complexes **1** and **3** (Figures 6 and 7) were also consistent with those of previous complexes.

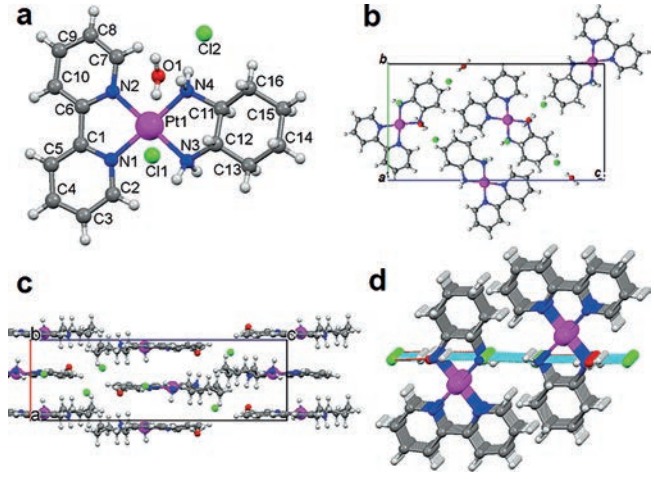

Figure 6. The X-ray structure of complex **1**, showing the atom numbering system (a), top packing view (b), side packing view (c) and double-molecular columns (d) along the *a*-axis formed by hydrogen bonding (shown in light blue).

Interestingly, the 2pq ligand of complexes **5**–**7** was found to significantly distort upon coordination (Figures 8 and 9). Compared to **1** and **3**, complexes **5**–**7** were far less planar, with N1–Pt1–N4 or N1–Pt1–Cl2 angles of ca. 172° relative to the equivalent angle of 177° for complexes **1** and **3**. This energetically unfavourable conformation resulted from ste-

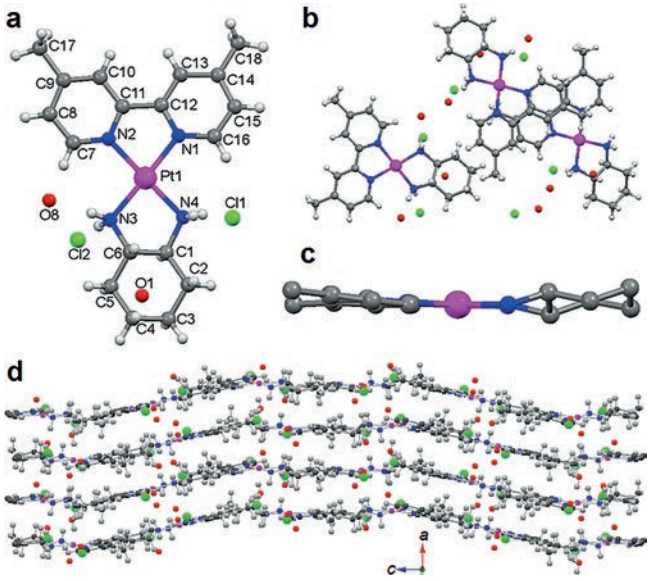

Figure 7. The X-ray structure of complex **3**, showing the atom numbering system (a) top packing view (b), planar view of a single molecule (c) and crystal packing along the *b*-axis (d).

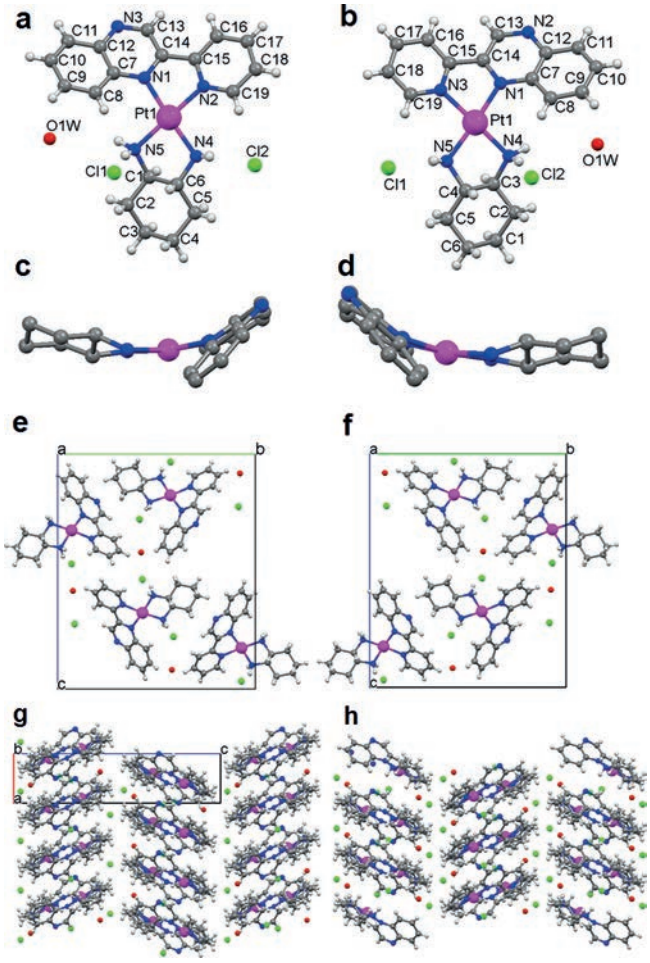

Figure 8. The X-ray structures of complexes **5** (left) and **6** (right) showing the atom numbering systems (a,b), single-molecule planar distortion (c,d), unit cell (e,f) and crystal packing views (g,h) along the *b*-axis.

ric repulsion between the quinoxaline moiety of 2pq and the opposing ligand, and may be responsible for the instability of **5**–**7** in the presence of heat and competing unidentate ligands such as DMSO. The coordinated 2pq ligand of complex **7** was not as distorted as it was in **5** and **6**, probably due to the smaller size of the unidentate chlorido ligands and less restricting coordination geometry relative to dach. This puckering of the 2pq ligand has been previously observed for complexes of platinum and palladium.[11]

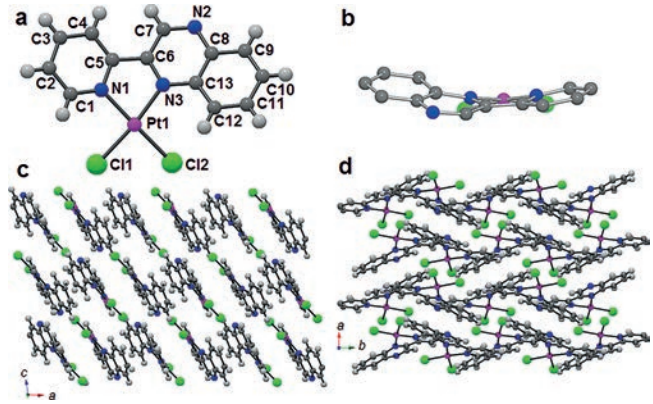

Figure 9. The X-ray structure of complex **7** showing the atom numbering system (a), planar view showing the ligand distortion (b) and packing views along the *b*-axis (c) and *c*-axis (d).

The crystal packing features of each complex warrant further discussion. Complex **3** molecules aligned their aromatic regions together with an average spacing of 3.5–3.9 Å, suggesting the presence of π-stacking interactions,[20] while complex **1** molecules stacked top-and-tail instead; this suggests that π-stacking may be a rare occurrence for bpy derivatives when compared to larger aromatic surfaces such as phen. The packing formation of **5**–**7** showed no close alignment of aromatic surfaces either, as the non-planarity of the 2pq ligand would prevent π-stacking.

Electronic Spectra

The UV spectra of each complex (Section S1) exhibited the expected π–π* transitions of the P_L and metal-to-ligand charge transfer interactions, resulting in a red-shift relative to the spectra of the free ligands. The UV spectra of complexes **1** and **2** produced strong absorption bands at approximately 245, 306 and 317 nm. Evidence of a peak below 200 nm was also observed, yet could not be resolved using this particular instrument. Complexes **3** and **4** displayed similar UV bands, although an additional peak was observed at 208 nm, supporting the possibility that a similar peak may exist for **1** and **2** under 200 nm.

The UV spectra of complexes **5** and **6** consisted of a broad peak at 256 nm with shoulder at 274 nm, and another broad peak at 367 nm. The CD spectra of each complex confirmed that the chirality of each product was con-

served from the starting materials (Section S2). Interestingly, the CD spectra of complexes **5** and **6** were much higher in complexity and signal to noise ratio than those of **1**–**4**, despite similar UV extinction coefficients (Figure 10). While the CD spectra of **1**–**4** produced broad peaks at ca. 225 and 250 nm, the spectra of **5** and **6** were dominated by sharper peaks at 252, 277 and 303 nm, as well as other broad peaks. The X-ray structures of **5** and **6** revealed that the orientation of the 2pq ligand depended on the position of the amines, which in turn depended on the chirality of the complex. The highly-absorbing 2pq ligand was therefore a source of chirality for **5** and **6**; this explains the high intensity and complexity of their CD spectra relative to **1**–**4**, which only have the less-absorbent dach as a chirality source.

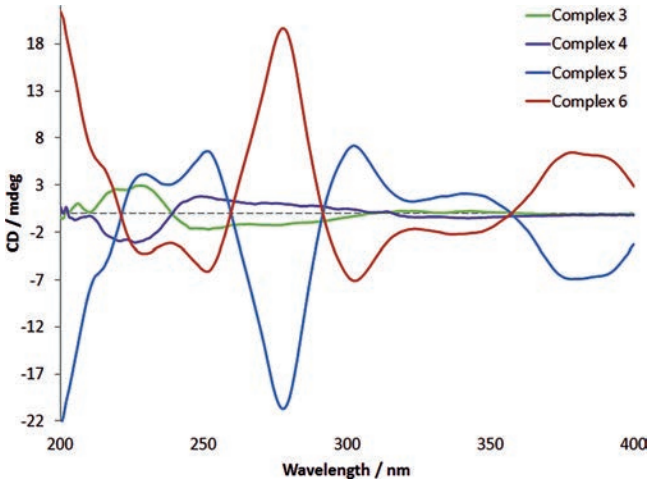

Figure 10. Comparison of the CD spectra of complexes **3**–**6** (25 μM) in water.

Pulsed Gradient Spin-Echo NMR

To further analyse the stacking behaviour of complexes **1**, **3** and **5**, PGSE NMR experiments were utilised. Over the concentration range of 1 to 25 mM, almost no change in diffusion coefficient (D) was observed (Figure 11, Table S4.1); the largest gap between values was 1.2×10^{-11} m s^{-2} for complex **1**. This suggests that no π-stacking-mediated aggregation occurred over the concentration range tested. Similar platinum(II) complexes incorporating phen ligands have been shown to aggregate over the same range,[14a] and so it is possible that the stacking exhibited by complex **3** in its X-ray structure may only occur in crystalline form, or may not be the result of π–π interaction. Stacking interactions play a role in the binding of phen complexes to biomolecules such as proteins and DNA, and so the lack of self-stacking observed for the complexes studied implies that their interactions with biomolecules may be significantly different. Meaningful correlation between self-stacking and cytotoxicity could be further investigated at physiological concentrations; however, a more sensitive technique than PGSE NMR would need to be employed.

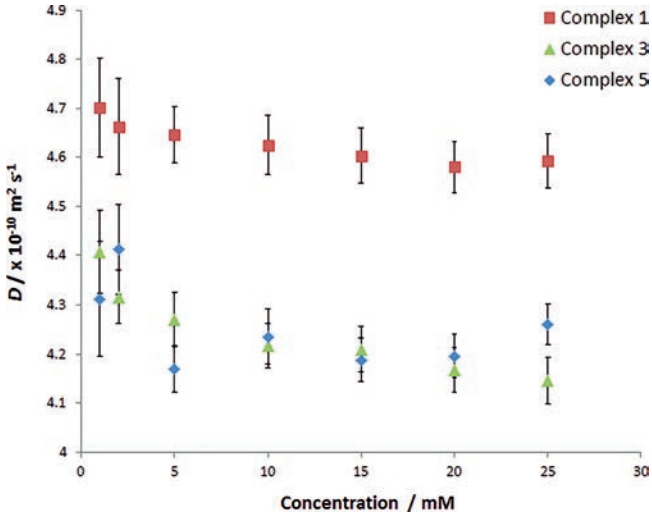

Figure 11. Combined plot of diffusion coefficient against concentration for complexes **1**, **3**, and **5**, showing error bars for each measurement.

In vitro Cytotoxicity

Cytotoxicity assays were conducted in the L1210 murine leukaemia, HT29 human colon carcinoma and U87 human glioblastoma cell lines. The compounds tested were complexes **1**–**6**, cisplatin, oxaliplatin, carboplatin, and some previously published compounds for comparison: [Pt(phen)(*SS*-dach)]Cl_2 (**8**), [Pt(phen)(*RR*-dach)]Cl_2 (**9**), [Pt(56Me$_2$phen)(*SS*-dach)]Cl_2 (**10**), [Pt(56Me$_2$phen)(*RR*-dach)]Cl_2 (**11**), [Pt(dpq)(*SS*-dach)]Cl_2 (**12**), [Pt(dpq)(*RR*-dach)]Cl_2 (**13**), [Pt(23Me$_2$dpq)(*SS*-dach)]Cl_2 (**14**), [Pt(23Me$_2$dpq)(*RR*-dach)]Cl_2 (**15**). Complex **7** was not tested due to solubility issues. The cytotoxicity values reported for **8**–**15** in L1210 cell lines are from previously published assays (see Table 1). Pre-screening tests within HT29 and U87 determined that **2**, **5** and **6** were not biologically active, and so they were excluded from further testing. The inactivity of **5** and **6** may be due to decomposition in vitro or lack of binding targets compatible with the distorted 2pq ligand. The IC_{50} values for each cell line are shown in Table 1. Across all cell lines, complexes **1**–**4** followed the same trends as **8**–**15**; those containing *SS*-dach and terminal methyl substituents exhibited higher cytotoxicity than those with *RR*-dach and no methyl. The influence of the A_L on the activity of these complexes is highlighted when comparing the HT29 and U87 IC_{50} values of complex **1** and **2**, which exhibited relatively high and no activity at all, respectively. It is clear that the bpy ligand did not contribute much to the activity of **1** and **2** in comparison to the other P_Ls studied here. The most active of those synthesised here was complex **3**, with the highest activity in all three cell lines relative to complexes **1**, **2**, **4** and cisplatin. As per previous trends,[4b,6,15] complex **10** was the most active of all of those studied, with IC_{50} values of ca. 0.1 μM in HT29 and U87 cells. Interestingly, all complexes were more effective than cisplatin and carboplatin in the HT29 line, indicating that colon carcinoma is very susceptible. The high activity of oxaliplatin

in HT29 suggests that *SS*-dach and *RR*-dach contribute to activity in this line. P_L size does appear to influence the activity of the complexes studied, as the general order of activity relative to P_L was $56Me_2$phen > phen ≅ $44Me_2$bpy > dpq > bpy > $23Me_2$dpq. This suggests that for complexes with P_Ls smaller than dpq, the greater the aromatic surface, the greater the toxicity to cancerous cells. The high activity of complexes with phen derivatives relative to those with dpq is consistent with previous trends that suggest $56Me_2$phen is the optimum P_L size for these PCs when it comes to biological activity.[6] Overall, the activity of complexes **1**, **3** and **4** was less than that of **8**–**11**, yet equal to or greater than cisplatin.

Table 1. In vitro cytotoxicity of complexes **1**–**6** in the L1210 murine leukaemia, HT29 human colon carcinoma, and U87 human glioblastoma cell lines, expressed as IC_{50} values with standard error (1 sig. fig.). A comparison with complexes **8**–**15**, cisplatin, carboplatin and oxaliplatin is included.

No.	P_L	Chirality	IC_{50}/μM		
			L1210[a]	HT29	U87
1	Bpy	*S,S*	0.6 ± 0.2	1.1 ± 0.2	4.0 ± 0.3
2	Bpy	*R,R*	5.5 ± 0.1	–	–
3	$44Me_2$bpy	*S,S*	0.36 ± 0.02	0.13 ± 0.03	0.5 ± 0.0
4	$44Me_2$bpy	*R,R*	1.8 ± 0.0	0.66 ± 0.07	3.9 ± 0.4
5	2pq	*S,S*	> 50	–	–
6	2pq	*R,R*	30 ± 10	–	–
8	Phen	*S,S*	0.10 ± 0.01	0.13 ± 0.04	1.5 ± 0.4
9	Phen	*R,R*	1.5 ± 0.1[b]	0.56 ± 0.08	9 ± 3
10	$56Me_2$phen	*S,S*	0.009 ± 0.002	0.08 ± 0.06	0.08 ± 0.01
11	$56Me_2$phen	*R,R*	0.46 ± 0.01	0.19 ± 0.00	2.20 ± 0.06
12	Dpq	*S,S*	0.19 ± 0.01	0.59 ± 0.08	3.7 ± 0.2
13	Dpq	*R,R*	0.8 ± 0.2	1.3 ± 0.2	12 ± 3
14	$23Me_2$dpq	*S,S*	1.3 ± 0.4	1.8 ± 0.3	8 ± 2
15	$23Me_2$dpq	*R,R*	6 ± 2	1.6 ± 0.4	16 ± 3
–	Cisplatin	–	0.36–1[c]	11 ± 2	4 ± 1
–	Oxaliplatin	*R,R*	–	0.9 ± 0.2	1.8 ± 0.2
–	Carboplatin	–	–	>50	>50

[a] L1210 values for **8**–**15** are from reference 6 and those within. [b] Tested as a perchlorate, rather than a chloride salt. [c] 0.36 ± 0.06 μM was the value from this publication, however higher IC_{50} valuess have been reported.[6,15]

Conclusions

Seven PCs incorporating bpy, $44Me_2$bpy or 2pq as a P_L and *SS*-dach or *RR*-dach as an A_L have been synthesised and characterised by several techniques. X-ray crystallography studies revealed that the coordination of 2pq to the platinum centre resulted in a distortion of coordination geometry and subsequent instability of **5** and **6**. X-ray and PGSE NMR experiments suggested that most synthesised complexes were unable to self-associate by π-stacking, which could impact their biological activity. Cytotoxicity assays were performed against the L1210, HT29 and U87 cell lines, with most compounds exhibiting high activity against the HT29 line. The complexes synthesised here were not as effective as those incorporating phen and $56Me_2$phen as P_Ls, although they were comparable to cisplatin, oxaliplatin, carboplatin and complexes incorporating dpq derivatives.

Experimental Section

Materials: 2pq,[11a] complexes **8**–**15**,[5b] and $[Pt(A_L)Cl_2]$,[5b] where A_L is *SS*-dach or *RR*-dach, and were synthesised using published methods. All purchased reagents were used as received and all solvents used were of analytical grade or higher. K_2PtCl_4 was obtained from Precious Metals Online. Bpy, $44Me_2$bpy, hydrochloric acid, diethyl ether and ethanol were obtained from Sigma–Aldrich chemicals. Methanol and DMSO were obtained from Lab Scan and acetone and ethanol were obtained from Chem-Supply. Sep-Pak® (20 cc, 2 g) columns were obtained from Waters. Deuterated solvents D_2O and [D_6]DMSO were obtained from Cambridge Isotope Laboratories.

Physical Measurements: Characteristic NMR spectra were obtained on a Bruker 400 MHz spectrometer, either in D_2O or [D_6]DMSO. All spectra were referenced internally to the solvent and obtained at 35 °C. ^{1}H spectra were obtained using a spectral width of 15 ppm and 256 accumulations. ^{1}H-^{195}Pt HMQC spectra were obtained using a spectral width of 2500 ppm and 256 data points for the ^{195}Pt nucleus (F1 dimension), and a spectral width of 12 ppm and 2048 data points for the ^{1}H nucleus (F2 dimension). The following abbreviations apply to spin multiplicity: s (singlet), bs (broad singlet), d (doublet), dd (doublet of doublets), t (triplet), td (triplet of doublets), and m (multiplet). The chemical shift (parts per million) of each resonance were quoted as an approximate midpoint of their multiplicity. Electronic spectra were obtained using a Cary 1E spectrophotometer using a wavelength range of 200–400 nm, using a 10 mm quartz cell. All spectra were recorded at room temperature and were automatically corrected for solvent baseline. Complexes **1**–**6** were measured in water and the starting P_Ls in ethanol. Circular dichroism spectra were recorded using a Jasco-810 spectropolarimeter at room temperature. The instrument was left to equilibrate for 30 min prior to use. Spectra were obtained in a 10 mm quartz cell, and were measured from 200–400 nm with a data pitch of 1 nm, bandwidth of 1 nm and response time of 1 second. For each spectrum, 40 accumulations were collected and a water baseline was subtracted. Mass spectra were obtained using a Thermo LCQ Classic spectrometer, using the positive electrospray ionisation mode. Sample solutions were prepared in methanol and injected with a cone voltage of 30 V and desolvation temperature of 180 °C. Spectra were collected over one minute with an *m*/*z* range of 100–1000. Microelemental analysis (C, H and N) was performed at the Chemical Analysis Facility, Department of Chemistry and Biomolecular Sciences, Macquarie University. An Elemental Analyser, Model PE2400 CHNS/O produced by Perkin–Elmer, USA, was used.

X-ray Crystallography: Single crystals of complexes **1**, **3**, **5**, and **6** were obtained via the slow diffusion of individual solutions of aqueous complex into acetone. Crystalline complex **7** was formed during synthesis. Single-crystal X-ray data for **1**, **3**, **5** and **6** were collected at 100(2) K on the MX1 beamline at the Australian Synchrotron with Silicon Double Crystal radiation (λ = 0.71070 ± 4 Å). The data were collected using BlueIce software,[21] while cell refinements and data reductions were carried out using XDS software.[22] An empirical absorption correction was then applied to each data set using SADABS.[23] The single-crystal data for **7** was collected on a Bruker kappa-II CCD diffractometer at 150 K using graphite-monochromated Mo-K_α radiation (λ = 0.71073 Å). Symmetry related absorption corrections using the program SADABS were applied and the data was corrected for Lorentz and polarisation effects using Bruker APEX2 software.[24] The structures were solved by direct methods and the full-matrix least-squares refinements were carried out using a suite of SHELX programmes.[25] The sin-

Table 2. Crystal data and refinement details for complexes **1**, **3**, **5**–**7**.

	1	**3**	**5**	**6**	**7**
Empirical formula	$C_{16}H_{24}Cl_2N_4OPt$	$C_{54}H_{80}Cl_{16}N_{12}O_9Pt_3$	$C_{19}H_{23}Cl_2N_5OPt$	$C_{19}H_{23}Cl_2N_5OPt$	$C_{13}H_9Cl_2N_3Pt$
Formula weight	554.38	1839.27	603.41	603.41	473.22
Crystal system	orthorhombic	orthorhombic	orthorhombic	orthorhombic	monoclinic
Space group	$P2_12_12_1$	$P2_12_12_1$	$P2_12_12_1$	$P2_12_12_1$	$P2_1/n$
a [Å]	6.9750(14)	7.3270(15)	5.200(1)	5.1920(10)	9.6825(4)
b [Å]	11.960(2)	17.263(5)	18.335(4)	18.348(4)	10.1544(4)
c [Å]	22.281(5)	54.778(11)	21.752(4)	21.807(4)	12.8444(5)
β [°]	90.0	90.0	90.0	90.0	97.9940(10)
Volume [Å^3]	1858.7(6)	6929(2)	2073.9(7)	2077.4(7)	1250.59(9)
Z	4	4	4	4	4
$\rho_{calcd.}$ [mg/mm^3]	1.981	1.763	1.933	1.929	2.513
μ [mm^{-1}]	7.848	6.331	7.044	7.032	11.633
$F(000)$	1072	3584	1168	1168	880
Goodness-of-fit on F^2	1.114	1.241	1.120	1.070	0.759
Final R_1[a] indexes [$I > 2\sigma(I)$]	0.0183	0.0467	0.0257	0.0252	0.0185
Final wR_2 [b] indexes [$I > 2\sigma(I)$]	0.0464	0.1552	0.0636	0.0566	0.0690
Largest diff. peak/hole/e Å^{-3}	1.29/–1.07	3.00/–3.93	1.09/–2.07	0.97/–1.50	1.29/–1.77

[a] $R_1 = \Sigma||F_o| - |F_c||/|F_o|$. [b] $wR_2 = \{\Sigma[w(F_o^2 - F_c^2)^2]/\Sigma[w(F_o^2)^2]\}^{1/2}$.

gle crystals of **1** suffered radiation damage during data collection. Consequently, the data completeness is slightly lower. In addition, no twin model was found although the Flack parameter is greater than 0. The structure of **3** was refined as a two-component inversion twin. All non-hydrogen atoms were located and refined anisotropically except a few lattice water molecules in **3** that were refined isotropically. Carbon and nitrogen bound hydrogen atoms were included in idealised positions and refined using a riding model. Lattice water hydrogen atoms could not be located and were generally not included for the final refinements.

Crystallographic data and refinement details for complexes **1**, **3**, **5**–**7** are summarised in Table 2. CCDC-1400161 (for **1**), -1400162 (for **3**), -1400163 (for **5**), -1400164 (for **6**), -1400165 (for **7**) contain the supplementary crystallographic data for this paper. These data can be obtained free of charge from The Cambridge Crystallographic Data Centre via www.ccdc.cam.ac.uk/data_request/cif.

PGSE NMR: PGSE experiments were obtained on the same 400 MHz spectrometer as above using the ^{1}H nucleus at 25 °C. Spectra were obtained using 2D Stimulated Echo experiments using bipolar gradients (stebpgp1s) with 64 scans, a spectral width of 8250 Hz, an acquisition time of 4 s and a 90° pulse of 16.75 µs. Square shaped gradient pulses were used with a Δ of 0.05 s, δ of 1 ms and 16 increments of gradient strength (5–95%). The echo attenuation for complexes **1**, **3** and **5** was determined using the resonance at δ = 7.75, 7.55 and 9.78 ppm, respectively. For each complex, seven solutions were tested ranging in concentration from 1–25 mM in D_2O. The echo attenuation (E) was plotted against gradient strength (g), and the D determined using a non-linear fit of the Equation (1):

$$E = \exp\left(-\gamma^2 g^2 \delta^2 D\left(\Delta - \frac{\delta}{3}\right)\right) \quad (1)$$

where γ is the gyromagnetic ratio (rad s^{-1} T^{-1}), g is the magnetic field gradient pulse strength (T m^{-1}), δ is the length of the gradient pulse (s), and Δ is the time between gradient pulses (s).

General Synthesis of [Pt(P$_L$)(A$_L$)]Cl$_2$ (complexes 1–6): For complexes **5** and **6**, any reduction of volume was achieved using lyophilisation instead of rotary evaporation. Using the previously established method,[6] the complex [Pt(A$_L$)Cl$_2$] (≈ 160 µmol) was suspended in water (40 mL) with the P$_L$ (1.1 equiv.) and refluxed for 48 h, resulting in a clear yellow solution. The solution volume was reduced to approximately 3 mL and filtered. A Sep-Pak® (20 cc, 2 g) column was activated with methanol (10 mL) followed by water (20 mL). The complex solution was loaded onto the column and eluted with approximately 50 mL of water. During collection, the first 5 mL of eluent were discarded and the rest collected. The

Table 3. Summary of the characterisation data of complexes **1**–**6**.

	Molecular formula	Colour (solid)	Yield [%]	ESI-MS (m/z) [M – H]$^+$ calcd. (found)	Microanalysis calcd. (found) C	H	N	UV / λ_{max}/nm (ε [mol^{-1} dm^3 cm^{-1}]) ×10^2	CD / λ_{max} [nm] (CD/mdeg L mol^{-1}) ×10^{-1}
1	[Pt(bpy)(*SS*-dach)]Cl$_2$·1.5H$_2$O	purple	84	464.1 (464.1)	34.11 (33.86)	4.47 (4.16)	9.94 (9.86)	317 (180), 306 (125), 245 (220)	209 (6), 227 (30), 254 (–20), 346 (2)
2	[Pt(bpy)(*RR*-dach)]Cl$_2$·1.5H$_2$O	purple	74	464.1 (464.1)	34.11 (34.20)	4.47 (4.62)	9.94 (9.89)	317 (180), 306 (125), 245 (220)	209 (1), 227 (–30), 254 (20), 346 (–5)
3	[Pt(44Me$_2$bpy)(*SS*-dach)]-Cl$_2$·3H$_2$O	white	81	492.2 (492.1)	34.96 (34.90)	5.22 (5.42)	9.06 (9.00)	315 (170), 303 (120), 243 (245), 206 (240)	205 (10), 210 (1), 220 (25), 227 (30), 251 (–16), 343 (2)
4	[Pt(44Me$_2$bpy)(*RR*-dach)]-Cl$_2$·3H$_2$O	white	87	492.2 (492.1)	34.96 (34.86)	5.22 (5.26)	9.06 (9.03)	315 (175), 303 (125), 243 (250), 206 (250)	205 (–7), 210 (–1), 220 (–29), 227 (–30), 251 (18), 343 (–5)
5	[Pt(2pq)(*SS*-dach)]Cl$_2$·3H$_2$O	yellow	51	515.2 (515.1)	35.58 (35.41)	4.56 (4.41)	10.92 (10.78)	367 (145), 274 (190), 256 (230)	230 (40), 252 (65), 277 (–200), 303 (71), 384 (–68)
6	[Pt(2pq)(*RR*-dach)]Cl$_2$·4H$_2$O	yellow	52	515.2 (515.1)	34.60 (34.75)	4.74 (4.25)	10.62 (10.57)	367(145), 274 (190), 256 (235)	230 (–42), 252 (–61), 277 (196), 303 (–71), 384 (62)

Table 4. Summary of NMR spectroscopic data of complexes **1**–**4** in [D_6]DMSO, showing chemical shift (ppm), integration, multiplicity and coupling constants.

Label	**1**	**2**	**3**	**4**
H3	8.71 (d, 2 H, *J* = 8.06 Hz)	8.72 (d, 2 H, *J* = 7.88 Hz)	8.59 (s, 2 H)	8.59 (s, 2 H)
H4	8.51 (t, 2 H, *J* = 7.80 Hz)	8.53 (t, 2 H, *J* = 7.94 Hz)	–	–
H5	7.90 (t, 2 H, *J* = 6.54 Hz)	7.92 (t, 2 H, *J* = 6.65 Hz)	7.73 (d, 2 H, *J* = 5.60 Hz)	7.73 (d, 2 H, *J* = 5.61 Hz)
H6	8.96 (d, 2 H, *J* = 5.40 Hz)	8.92 (d, 2 H, *J* = 5.67 Hz)	8.76 (d, 2 H, *J* = 5.93 Hz)	8.76 (d, 2 H, *J* = 5.93 Hz)
H1′′[a]	2.50 (d, 2 H)	2.51 (d, 2 H)	2.49 (d, 2 H)	2.49 (d, 2 H)
$H2''_{eq}$	2.11 (d, 2 H, *J* = 12.11 Hz)	2.10 (d, 2 H, *J* = 12.15 Hz)	2.10 (d, 2 H, *J* = 11.91 Hz)	2.10 (d, 2 H, *J* = 12.11 Hz)
$H3''_{eq}$	1.60 (d, 2 H, *J* = 8.42 Hz)	1.60 (d, 2 H, *J* = 7.88 Hz)	1.60 (d, 2 H, *J* = 8.26 Hz)	1.60 (d, 2 H, *J* = 8.16 Hz)
$H2''_{ax}$	1.48 (m, 2 H)	1.47 (m, 2 H)	1.47 (m, 2 H)	1.46 (m, 2 H)
$H3''_{ax}$	1.17 (m, 2 H)	1.19 (m, 2 H)	1.17 (m, 2 H)	1.17 (m, 2 H)
$–NH_2$	7.47 (d, 2 H, *J* = 8.51 Hz)	7.35 (d, 2 H, *J* = 9.42 Hz)	7.36 (d, 2 H, *J* = 8.80 Hz)	7.35 (d, 2 H, *J* = 8.75 Hz)
$–NH_2$	6.70 (m, 2 H)	6.61 (m, 2 H)	6.60 (m, 2 H)	6.59 (m, 2 H)
$–CH_3$	–	–	2.56 (s, 6 H)	2.56 (s, 6 H)
H6/Pt	9.07/–2783.2	9.02/–2783.9	8.80/–2790.9	8.79/–2790.9

[a] These resonances were obscured by the [D_6]DMSO peak; multiplicity is quoted from the D_2O spectrum.

remaining eluent solution was reduced under pressure and lyophilised to produce the solid product. Characterisation data for each complex is summarised in Tables 3, 4, and 5.

Table 5. Summary of NMR spectroscopic data of complexes **5** and **6** in D_2O, showing chemical shift (ppm), integration, multiplicity and coupling constants. Amine resonances were not observed due to exchange.

Label	**5**	**6**
H3	8.79 (d, 1 H, *J* = 8.47 Hz)	8.79 (d, 1 H, *J* = 8.44 Hz)
H4	8.59 (t, 1 H, *J* = 7.81 Hz)	8.59 (t, 1 H, *J* = 8.00 Hz)
H5	7.99 (m, 2 H)	7.99 (m, 2 H)
H6	8.82 (d, 1 H, *J* = 5.86 Hz)	8.81 (d, 1 H, *J* = 6.22 Hz)
H3′	9.84 (s, 1 H)	9.85 (s, 1 H)
H5′	8.41 (m, 1 H)	8.42 (m, 1 H)
H6′/H7′	8.19 (m, 2 H)	8.20 (m, 2 H)
H8′	7.99 (m, 2 H)	7.99 (m, 2 H)
H1′′a	2.81 (td, 1 H, *J* = 11.66, 4.01 Hz)	2.80 (td, 1 H, *J* = 11.62, 3.99 Hz)
H1′′b	2.68 (td, 1 H, *J* = 11.57, 3.92 Hz)	2.68 (td, 1 H, *J* = 11.62, 3.87 Hz)
$H2''_{eq}$a	2.34 (d, 1 H, *J* = 12.59 Hz)	2.34 (d, 1 H, *J* = 11.10 Hz)
$H2''_{eq}$b	2.20 (d, 1 H, *J* = 12.88 Hz)	2.20 (d, 1 H, *J* = 11.58 Hz)
$H3''_{eq}$	1.73 (m, 2 H)	1.73 (m, 2 H)
$H2''_{ax}$	1.55 (m, 2 H)	1.54 (m, 2 H)
$H3''_{ax}$	1.30 (m, 2 H)	1.30 (m, 2 H)
H6/Pt	8.92/–2712.3	8.91/–2711.2

Synthesis of [Pt(2pq)Cl_2] (Complex 7): Using the published method,[5a] a solution of K_2PtCl_4 (0.4 g, ca. 1 mmol) in DMSO/water, 4:1 was combined with a solution of with 2pq (1 equiv.) in DMSO. The solution was left at room temperature for 16 h during which dark crystals formed; these were filtered and washed with chilled HCl, water, ethanol and diethyl ether (3 × 5 mL each) to obtain brown needles (yield 93%). Elemental analysis (%): $C_{13}H_9Cl_2N_3Pt$: C, 33.00, H, 1.92, N, 8.88; found C, 33.00, H, 1.61, N, 8.84.

In Vitro Cytotoxicity: In vitro growth inhibition assays within the L1210 murine leukaemia cell line were performed at the Peter MacCallum institute in Melbourne, Victoria, Australia. Each complex was dissolved in water or DMSO before being diluted with the appropriate cell media to the required concentration. The experiments were performed in the L1210 murine leukaemia cell line using the Coulter Counting Assay. For each complex, two independent experiments were performed, each with an exposure time of 48 h. Cytotoxicity assays for the HT29 human colon carcinoma and U87 human glioblastoma cell lines were performed at the Calvary Mater Newcastle Hospital, Waratah, NSW, Australia. Test agents were prepared as 30 mM stock solutions in DMSO and stored at –20 °C. All cell lines were cultured in a humidified atmosphere 5% CO_2 at 37 °C and maintained in Dulbecco's modified Eagle's medium (Trace Biosciences, Australia) supplemented with 10% foetal bovine serum, 10 mM sodium hydrogen carbonate penicillin (100 IU/mL), streptomycin (100 μg/mL), and glutamine (4 mM). Cytotoxicity was determined by plating cells in duplicate in 100 mL medium at a density of 2,500–4,000 cells/well in 96 well plates. On day 0, (24 h after plating) when the cells were in logarithmic growth, 100 μL medium with or without the test agent was added to each well. After 72 h drug exposure growth inhibitory effects were evaluated using the MTT (3-[4,5-dimethyltiazol-2-yl]-2,5-diphenyl-tetrazolium bromide) assay and absorbance read at 540 nm. An eight point dose response curve was produced from which the IC_{50} value was calculated, representing the drug concentration at which cell growth was inhibited by 50% based on the difference between the optical density values on day 0 and those at the end of drug exposure.[26]

Acknowledgments

The authors thank the University of Western Sydney for financial support through internal research grants. B. J. P. was supported by the University of Western Sydney through an Australian Postgraduate Award and UWS Top-Up Award. The authors also thank Dr. Carleen Cullinane for her work with the L1210 cell line, Dr. Gang Zheng for his PGSE NMR assistance, Dr. Alice Klein for her assistance in characterisation and Dr. Ronald Fenton for providing 2-(2′-pyridyl)quinoxaline. The crystallographic data collections for complexes **1**, **3**, **5** and **6** were undertaken on the MX1 beamline at the Australian Synchrotron, Victoria, Australia.

[1] a) B. Rosenberg, L. Van Camp, T. Krigas, *Nature* **1965**, *205*, 698–699; b) B. W. Harper, A. M. Krause-Heuer, M. P. Grant, M. Manohar, K. B. Garbutcheon-Singh, J. R. Aldrich-Wright, *Chem. Eur. J.* **2010**, *16*, 7064–7077; c) K. B. Garbutcheon-Singh, M. P. Grant, B. W. Harper, A. M. Krause-Heuer, M. Manohar, N. Orkey, J. R. Aldrich-Wright, *Curr. Top. Med. Chem.* **2011**, *11*, 521–542.

[2] N. J. Wheate, S. Walker, G. E. Craig, R. Oun, *Dalton Trans.* **2010**, *39*, 8113–8127.

[3] a) P. C. A. Bruijnincx, P. J. Sadler, *Curr. Opin. Chem. Biol.* **2008**, *12*, 197–206; b) N. Muhammad, Z. Guo, *Curr. Opin. Chem. Biol.* **2014**, *19*, 144–153; c) B. J. Pages, D. L. Ang, E. P.

Wright, J. R. Aldrich-Wright, *Dalton Trans.* **2015**, *44*, 3505–3526.
[4] a) C. R. Brodie, J. G. Collins, J. R. Aldrich-Wright, *Dalton Trans.* **2004**, 1145–1152; b) A. M. Krause-Heuer, R. Grünert, S. Kühne, M. Buczkowska, N. J. Wheate, D. D. Le Pevelen, L. R. Boag, D. M. Fisher, J. Kasparkova, J. Malina, P. J. Bednarski, V. Brabec, J. R. Aldrich-Wright, *J. Med. Chem.* **2009**, *52*, 5474–5484; c) K. B. Garbutcheon-Singh, S. Myers, B. W. J. Harper, N. S. Ng, Q. Dong, C. Xie, J. R. Aldrich-Wright, *Metallomics* **2013**, *5*, 1061–1067.
[5] a) S. Kemp, N. J. Wheate, D. P. Buck, M. Nikac, J. G. Collins, J. R. Aldrich-Wright, *J. Inorg. Biochem.* **2007**, *101*, 1049–1058; b) N. J. Wheate, R. I. Taleb, A. M. Krause-Heuer, R. L. Cook, S. Wang, V. J. Higgins, J. R. Aldrich-Wright, *Dalton Trans.* **2007**, 5055–5064.
[6] B. J. Pages, F. Li, P. Wormell, D. L. Ang, J. K. Clegg, C. J. Kepert, L. K. Spare, S. Danchaiwijit, J. R. Aldrich-Wright, *Dalton Trans.* **2014**, *43*, 15566–15575.
[7] H. Le Bozec, V. Guerchais, *C. R. Chim.* **2013**, *16*, 1172–1182.
[8] M. Li, Q. Liang, M. Zheng, C. Fang, S. Peng, M. Zhao, *Dalton Trans.* **2013**, *42*, 13509–13515.
[9] a) B. Coban, U. Yildiz, A. Sengul, *J. Biol. Inorg. Chem.* **2013**, *18*, 461–471; b) H. Mansouri-Torshizi, S. Shahraki, Z. S. Nezami, A. Ghahghaei, S. Najmedini, A. Divsalar, H. Ghaemi, A.-A. Saboury, *Complex. Met.* **2014**, 23–31.
[10] a) J. A. Smith, J. L. Morgan, A. G. Turley, J. G. Collins, F. R. Keene, *Dalton Trans.* **2006**, 3179–3187; b) U. Śliwińska, F. P. Pruchnik, I. Pelińska, S. Ułaszewski, A. Wilczok, A. Zajdel, *J. Inorg. Biochem.* **2008**, *102*, 1947–1951; c) N. Kumar, R. Kaushal, A. Chaudhary, S. Arora, P. Awasthi, *Med. Chem. Res.* **2014**, *23*, 3897–3906.
[11] a) J. C. Plakatouras, N. Hadjiliadis, S. P. Perlepes, A. Albinati, G. Kalkanis, *Polyhedron* **1993**, *12*, 2069–2072; b) S. P. Perlepes, A. Garoufis, J. Sletten, E. G. Bakalbassis, G. Plakatouras, E. Katsarou, H. Nick, *Inorg. Chim. Acta* **1997**, *261*, 93–102; c) I. Veroni, C. A. Mitsopoulou, F. J. Lahoz, *J. Organomet. Chem.* **2008**, *693*, 2451–2457; d) G. C. Vougioukalakis, A. I. Philippopoulos, T. Stergiopoulos, P. Falaras, *Coord. Chem. Rev.* **2011**, *255*, 2602–2621; e) C. A. Mitsopoulou, C. E. Dagas, C. Makedonas, *Inorg. Chim. Acta* **2008**, *361*, 1973–1982; f) A. B. Tsoupras, A. Papakyriakou, C. A. Demopoulos, A. I. Philippopoulos, *J. Inorg. Biochem.* **2013**, *120*, 63–73.
[12] C. A. Mitsopoulou, C. E. Dagas, C. Makedonas, *J. Inorg. Biochem.* **2008**, *102*, 77–86.
[13] A. I. Philippopoulos, N. Tsantila, C. A. Demopoulos, C. P. Raptopoulou, V. Likodimos, P. Falaras, *Polyhedron* **2009**, *28*, 3310–3316.
[14] a) A. M. Krause-Heuer, N. J. Wheate, W. S. Price, J. Aldrich-Wright, *Chem. Commun.* **2009**, 1210–1212; b) B. J. Pages, *Aust. J. Chem.* **2014**, *67*, 314–315.
[15] K. B. Garbutcheon-Singh, P. Leverett, S. Myers, J. R. Aldrich-Wright, *Dalton Trans.* **2013**, *42*, 918–926.
[16] R. M. Silverstein, F. X. Webster, *Spectrometric identification of organic compounds*, Wiley, New York, USA, **1998**, .
[17] E. Bednarek, J. Sitkowski, R. Kawecki, L. Kozerski, W. Bocian, L. Pazderski, W. Priebe, *Dalton Trans.* **2008**, 4129–4137.
[18] B. M. Still, P. G. A. Kumar, J. R. Aldrich-Wright, W. S. Price, *Chem. Soc. Rev.* **2007**, *36*, 665–686.
[19] T. Koshiyama, M. Kato, *Acta Crystallogr., Sect. C: Cryst. Struct. Commun.* **2003**, *59*, m446–m449.
[20] L. M. Salonen, M. Ellermann, F. Diederich, *Angew. Chem. Int. Ed.* **2011**, *50*, 4808–4842.
[21] T. M. McPhillips, S. E. McPhillips, H. J. Chiu, A. E. Cohen, A. M. Deacon, P. J. Ellis, E. Garman, A. Gonzalez, N. K. Sauter, R. P. Phizackerley, S. M. Soltis, P. Kuhn, *J. Synchrotron Radiat.* **2002**, *9*, 401–406.
[22] W. Kabsch, *J. Appl. Crystallogr.* **1993**, *26*, 795–800.
[23] *SADABS: Empirical Absorption and Correction Software*, **1996–2008**, University of Göttingen, Germany.
[24] *APEX2*, *SAINT*, *SADABS and XSHELL*, Bruker AXS Inc., Madison, Wisconsin, USA, **2010**.
[25] a) G. M. Sheldrick, *Acta Crystallogr., Sect. A: Found. Crystallogr.* **2008**, *64*, 112–122; b) O. V. Dolomanov, L. J. Bourhis, R. J. Gildea, J. A. K. Howard, H. Puschmann, *J. Appl. Crystallogr.* **2009**, *42*, 339–341.
[26] M. Tarleton, J. Gilbert, M. J. Robertson, A. McCluskey, J. A. Sakoff, *MedChemComm* **2011**, *2*, 31–37.

Received: July 9, 2015
Published Online: August 7, 2015

ChemPubSoc Europe

DOI: 10.1002/chem.201601221

CHEMISTRY A European Journal Full Paper

Medicinal Chemistry

Multifaceted Studies of the DNA Interactions and In Vitro Cytotoxicity of Anticancer Polyaromatic Platinum(II) Complexes

Benjamin J. Pages,[a] Jennette Sakoff,[b] Jayne Gilbert,[b] Alison Rodger,[c] Nikola P. Chmel,[c] Nykola C. Jones,[d] Sharon M. Kelly,[e] Dale L. Ang,[a] and Janice R. Aldrich-Wright*[a]

Abstract: This study reports a detailed biophysical analysis of the DNA binding and cytotoxicity of six platinum complexes (PCs). They are of the type $[Pt(P_L)(SS\text{-dach})]Cl_2$, where P_L is a polyaromatic ligand and *SS*-dach is 1*S*,2*S*-diaminocyclohexane. The DNA binding of these complexes was investigated using six techniques including ultraviolet and fluorescence spectroscopy, linear dichroism, synchrotron radiation circular dichroism, isothermal titration calorimetry and mass spectrometry. This portfolio of techniques has not been extensively used to study the interactions of such complexes previously; each assay provided unique insight. The in vitro cytotoxicity of these compounds was studied in ten cell lines and compared to the effects of their *R,R* enantiomers; activity was very high in Du145 and SJ-G2 cells, with some submicromolar IC_{50} values. In terms of both DNA affinity and cytotoxicity, complexes of 5,6-dimethyl-1,10-phenanthroline and 2,2′-bipyridine exhibited the greatest and least activity, respectively, suggesting that there is some correlation between DNA binding and cytotoxicity.

Introduction

A long-standing aspiration of medicinal inorganic chemists has been the development of chemotherapeutic agents that can effectively combat cancerous cells, yet overcome the resistance and toxicity that plague current clinically used platinum agents.[1] Platinum complexes (PCs) with mechanisms of action quite different from current agents have been explored as alternatives, and have demonstrated in vitro cytotoxicity up to 100 times greater than cisplatin in several cell lines.[2] In particular, our group has focused on the development of PCs that consist of a polyaromatic ligand (P_L) and a cyclic amine ancillary ligand (A_L) in the form $[Pt(P_L)(A_L)]^{2+}$.[3] These complexes interact non-covalently with DNA, often by intercalation, rather than by forming permanent adducts. They also induce cell death by a different mechanism than cisplatin,[2a,4] and are potently cytotoxic against a variety of cell lines, including some that are cisplatin-resistant.[5] Our previous studies have been inconclusive as to whether there is a correlation between DNA affinity and cytotoxicity; however, these studies have often used only one or two spectroscopic techniques to study PC–DNA interactions.[6] Moreover, DNA binding affinity is known to vary depending on the method of measurement and the conditions used, and so separately conducted studies can often provide inconsistent results.[7] In this study, we have utilised several biophysical assays to study the interactions of six PCs with DNA (Figure 1).

The experimental conditions were kept consistent, where possible, for each assay to facilitate comparison of the binding data elucidated from the individual techniques. This allowed for definitive trends in DNA binding affinity to be determined for the six PCs. The complexes studied here incorporated 1*S*,2*S*-diaminocyclohexane (*SS*-dach) as an A_L and one of dipyrido[3,2-*d*:2′,3′-*f*]quinoxaline (dpq), 2,3-dimethyl-dpq ($23Me_2$dpq), 1,10-phenanthroline (phen), 5,6-dimethyl-phen ($56Me_2$phen), 2,2′-bipyridine (bpy) and 4,4′-dimethyl-bpy ($44Me_2$bpy) as an P_L. The use of a variety of P_Ls allowed for a comparison between the DNA affinity and aromatic surface area of these complexes; it is known that structural variations can result in different DNA binding behaviour for metal complexes.[8] Methylated variants of each P_L were included due to the proven cytotoxic and DNA binding influences of methyl substituents in our complexes,[3,5b] and *SS*-dach was chosen as the A_L as complexes of this ligand are the most active overall.[5b] The interactions of complexes **1**–**6** with calf-thymus DNA (CT-DNA) and some oligonucleotides were analysed using several methods. Firstly, linear dichroism (LD), ultraviolet spectros-

[a] *B. J. Pages, D. L. Ang, Prof. J. R. Aldrich-Wright*
Nanoscale Organisation and Dynamics Group, Western Sydney University
Campbelltown, NSW 2560 (Australia)
E-mail: j.aldrich-wright@westernsydney.edu.au

[b] *Dr. J. Sakoff, Dr. J. Gilbert*
Calvary Mater Newcastle, Waratah, NSW 2298 (Australia)

[c] *Prof. A. Rodger, Dr. N. P. Chmel*
Department of Chemistry, University of Warwick
Coventry, West Midlands CV47AL (UK)

[d] *N. C. Jones*
ISA, Department of Physics and Astronomy, Aarhus University
Aarhus 8000 (Denmark)

[e] *Dr. S. M. Kelly*
Institute of Molecular, Cell and Systems Biology
College of Medical, Veterinary and Life Sciences
University of Glasgow, Glasgow G12 8QQ (UK)

Supporting information and the ORCID identification numbers for the authors of this article can be found under http://dx.doi.org/10.1002/chem.201601221.

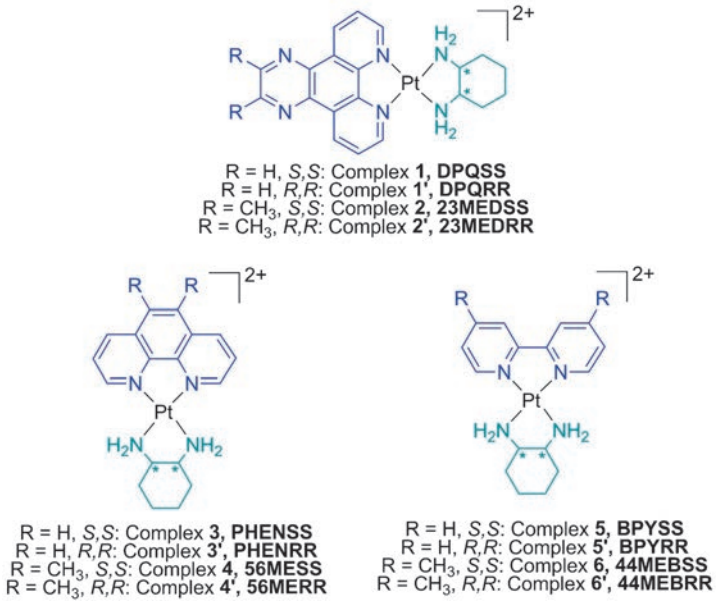

Figure 1. The structures of complexes **1**–**6** and **1**′–**6**′; each A_L is highlighted in green and each P_L in blue. Chloride counter ions have been omitted for clarity. * indicates a stereocentre, either *S* or *R*.

copy (UV) and isothermal titration calorimetry (ITC) were utilised in tandem to gain an overall picture of DNA binding mode and affinity. Secondly, fluorescent intercalator displacement assays (FIDs) and synchrotron radiation circular dichroism (SRCD) experiments were undertaken to determine the effect of DNA affinity on the ability of each complex to displace competitive binders and stabilise the DNA strand, respectively. Thirdly, electrospray ionisation mass spectrometry (ESIMS) was used to determine if **1**–**6** preferentially bind to any base-pairs. Finally, the cytotoxicity of these compounds was determined in ten human cell lines. The activity of **1**–**6** was compared to their enantiomers **1**′–**6**′ and to the DNA binding results to determine any correlations between chemical structure, DNA affinity and cytotoxicity.

Results and Discussion

Linear dichroism

The LD spectrum of CT-DNA is characterised by a large negative band at approximately 260 nm. Upon the addition of each PC in this study, this band increased in intensity, which suggests a lengthening or stiffening of the DNA strand. Additionally, negative LD signals appeared at the absorbance wavelengths of each PC, which suggests that their aromatic components have aligned perpendicular to the DNA strand. The PC signals were flattened, broadened and red-shifted relative to their absorbance bands (Figure 2). These phenomena together indicate that each PC is binding by intercalation to DNA. While the alignment of complex **6** is obvious from the LD signal at 321 nm, this complex also absorbs at 243 and 206 nm; the same region as CT-DNA. The increase of the 260 nm LD peak upon addition of **6** could therefore be due to PC alignment only and not a result of DNA lengthening.

To elucidate the cause of the signal change, the UV spectra of **6** and CT-DNA were compared to the induced LD signal of DNA + **6** (Figure 3). In the induced LD spectrum, the peak at 247 nm has a higher relative intensity than the other two; this indicates that both the alignment of **6** and the lengthening of the DNA strand are both occurring, confirming that intercalation is the binding mode. Similar absorbance contributions were observed for each of complexes **1**–**5** as they all absorb in the same region as CT-DNA. For all PCs studied, there are two regions of the titration curve at which the signal in the CT-DNA region did not consistently increase with increasing PC concentration, despite the spectral evidence for DNA lengthening and/or stiffening. The first of these was a decrease or only very small increase of DNA signal intensity at 260 nm for PC concentrations between 5 and 30 μM. This may be indicative of a partial intercalation

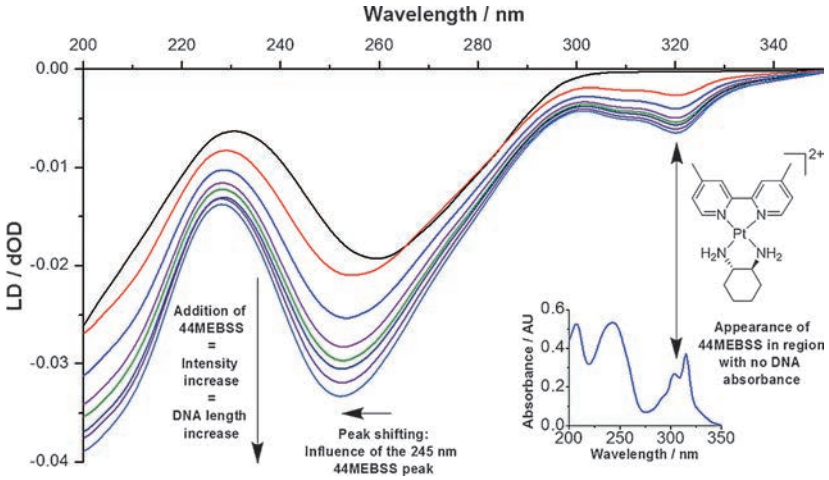

Figure 2. LD spectra of CT-DNA (150 μM) with increasing concentration of complex **6** (selected concentrations from 40–200 μM). Inset: the UV spectrum of **6**. See Figure S1.6 in the Supporting Information for spectra of the full concentration range.

mode that hinges the DNA and bends it rather than full intercalation.

The second point at which the LD signal did not increase was at high PC concentrations (85–100 μM); at this point a plateau was reached for complexes **1**, **3**, **5** and **6** before the signal began to decrease at approximately 250 μM (Figure 4). This suggests that the DNA reached saturation by intercalation before another binding mode occurred, which then caused the strand to lose its aspect ratio. An electrostatic groove binding mode of some kind is likely as the second one. The plateau allowed for a binding constant to be determined for the first or putative intercalative binding. For complexes **2** and **4**, the signal loss began to occur before any plateau was reached (at approx. 80 and 100 μM, respectively), implying that the second binding mode occurred earlier for these complexes than for the others (Figure 4). This made binding constant calculation impossible, and suggests that the difference in binding strength of the two modes is less for these complexes than it is for the others. K_{LD} was determined for **1**, **3**, **5** and **6** using binding curves from either one or two peaks in the induced spectrum; the average data are presented in Table 1 (see Table S1.2 in the Supporting Information for individual wavelength data). The points of the binding curve below 40 μM had to be removed in order to obtain a fit; this was due to the aforementioned DNA bending at these concentrations. The peak at approximately 320 nm for complexes **5** and **6** were not a result of DNA absorbance and so could be fitted with all points below 40 μM. Each complex was found to bind to DNA with high potency. The intercalative binding strength of these PCs is attributed to stabilised π–π stacking as well as the longer range charge–charge interactions of the platinum cations.[9] Complex **1** has the largest aromatic surface area and a binding constant of approximately $10^6\,M^{-1}$. The other complexes produced similar K_{LD} values of $10^5\,M^{-1}$. The *n* (number of base-pairs per PC) values were typically around 2–3, indicating that each PC could intercalate between every second or third base pair in a sequence. Despite the lack of some binding data for complexes **2** and **4**, LD has provided useful information regarding the binding activity of the PCs in this study.

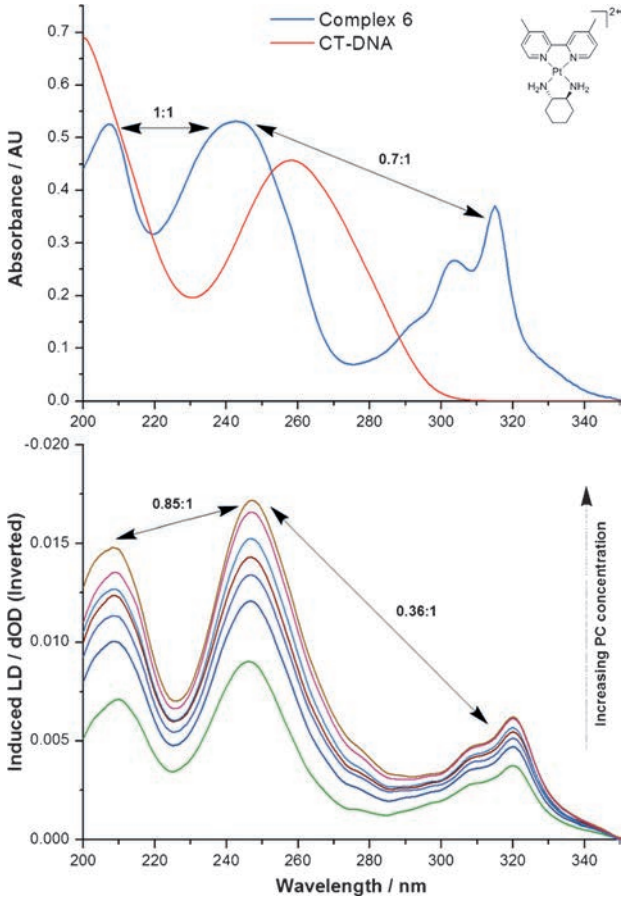

Figure 3. Top: UV spectrum of CT-DNA (red line, 35 μM) and complex **6** (blue line, 21 μM), showing ratios to the peak at 243 nm for the former. Bottom: inverted induced LD spectra of CT-DNA (150 μM) bound with **6** (selected concentrations from 50–200 μM), showing ratios to the peak at 247 nm.

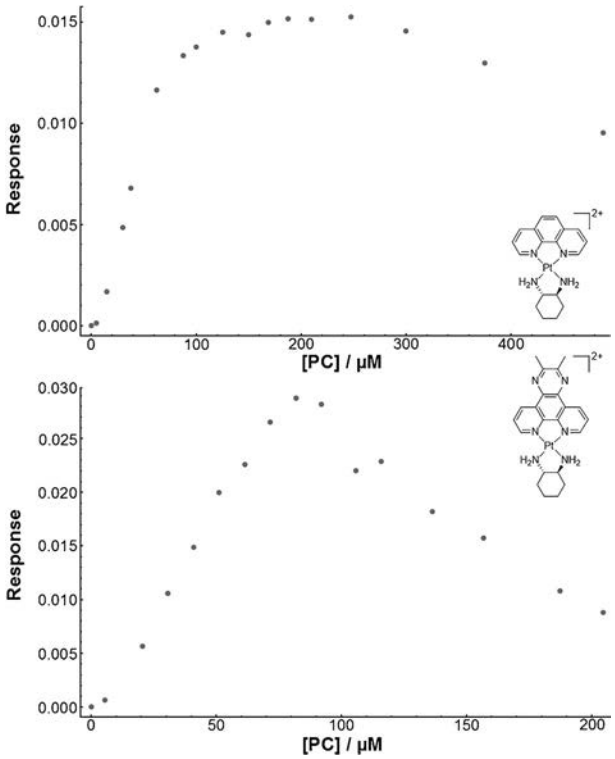

Figure 4. Plots of PC concentration against LD response of CT-DNA (150 μM) bound with increasing concentrations of complex **3** at 278 nm (4–488 μM, top) and **2** at 260 nm (5–205 μM, bottom).

UV binding assays

UV spectroscopy is a common method used to determine binding mode and affinity of metal complex–DNA interactions.[10] The addition of DNA to each of complexes **1**–**6** resulted in hypochromism, with a varying shift in wavelength between the PCs (Figure 5). The spectra of **3**–**6** were red-shifted with the effect being more subtle for **5** and **6**, while the spectra of **1** and **2** experienced a blue-shift upon the addition of CT-DNA. Typically these shifting patterns can provide information regarding the DNA binding mode;[10a] however, each of **1**–

Table 1. Summary of binding constant data obtained from LD (150 μM CT-DNA + 40–200 μM PC), UV (14 μM PC + 0–200 μM CT-DNA) and ITC (titration of 600–750 μM PC into 165 μM CT-DNA) experiments. Standard deviation values are included (1 significant figure).

	LD data		UV data		ITC data				
No.	10^{-5} K_{LD} [M^{-1}]	n	10^{-5} K_{UV} [M^{-1}]	n	10^{-5} K_{ITC} [M^{-1}]	n	ΔH [kcal mol^{-1}]	$T\Delta S$ [kcal mol^{-1}]	ΔG [kcal mol^{-1}]
1	15.2 ± 0.4	2.41 ± 0.06	3.6 ± 0.2	3.13 ± 0.09	3.2 ± 0.3	3.98 ± 0.06	−4.4 ± 0.1	3.4 ± 0.1	−7.8 ± 0.3
2[a]	n.d.	n.d.	4.7 ± 0.1	2.52 ± 0.01	2.8 ± 0.4	3.51 ± 0.08	−4.5 ± 0.1	3.2 ± 0.3	−7.7 ± 0.8
3	2.8 ± 0.4	2.2 ± 0.2	2.9 ± 0.4	3.5 ± 0.3	2.0 ± 0.3	3.7 ± 0.1	−3.7 ± 0.1	3.9 ± 0.4	−7.5 ± 0.7
4[a]	n.d.	n.d.	13 ± 1	2.32 ± 0.02	5.7 ± 0.5	3.00 ± 0.02	−5.6 ± 0.1	2.6 ± 0.2	−8.2 ± 0.6
5[b]	2.1 ± 0.3	3.1 ± 0.3	0.79 ± 0.06	4.4 ± 0.2	2.2 ± 0.4	3.4 ± 0.1	−1.3 ± 0.1	6.2 ± 0.2	−7.6 ± 0.4
6[b]	3.0 ± 0.5	2.1 ± 0.2	5.2 ± 0.6	2.87 ± 0.04	3.2 ± 0.4	3.57 ± 0.06	−3.6 ± 0.1	4.2 ± 0.1	−7.8 ± 0.2

[a] LD values could not be determined due to a decrease in LD signal at high concentrations. [b] LD data for these complexes was produced from PC concentrations of 0-200 μM. n.d. = not determined.

6 absorb in the same region as DNA and so no definitive binding mode statements could be made from these data. Unlike the LD experiments, binding constant data was obtainable for all complexes in this instance, with no removal of binding curve points required (Figure 5). The possible secondary groove binding mode that limited the binding curves in LD had no effect here, and so the K_{UV} values are likely reflective of an overall binding affinity rather than just an intercalation-related one. Due to the differences in the UV spectra of each complex, different wavelengths were chosen for each K_{UV} determination. Where applicable, up to three wavelengths were chosen to facilitate a comparison between each value obtained; only minor differences were observed, and so the values in Table 1 are averages (see Table S2.2 in the Supporting Information for individual wavelength data). The K_{UV} did not vary considerably with aromatic surface area, with most binding constants close to 10^5 M^{-1}. The only exception is complex **4**, which demonstrated higher DNA affinity with a K_{UV} of approximately 10^6 M^{-1}. This suggests that the 56Me$_2$phen ligand, despite possessing a smaller aromatic surface than dpq or 23Me$_2$dpq, is the optimum DNA-binding P_L. Despite the lack of binding mode information relative to LD, UV spectroscopy has provided binding information for all concentration ranges without being restricted to one binding event. This in turn has allowed for binding data to be obtained for complexes **2** and **4** whereas LD could not do so.

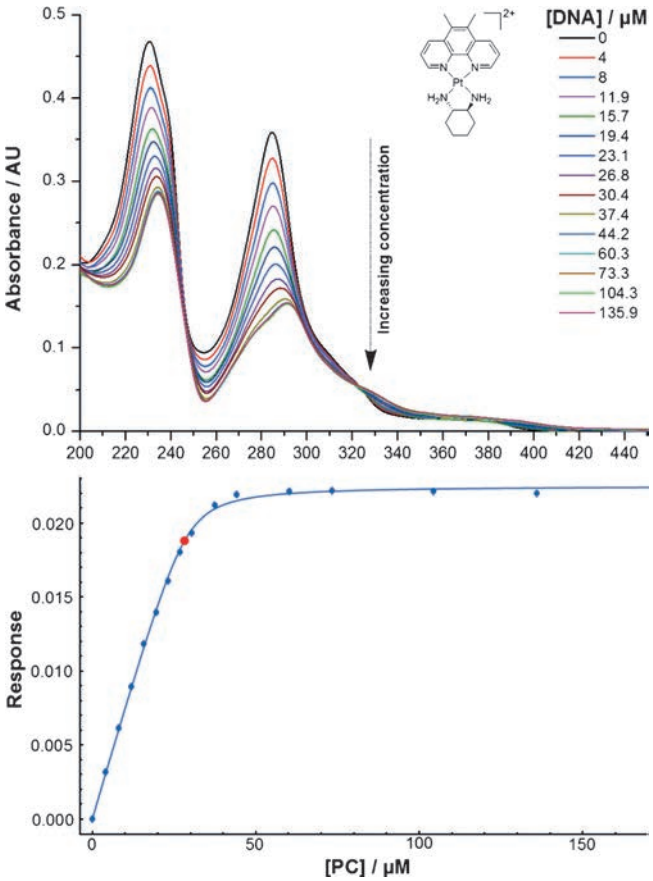

Figure 5. UV data for complex **4**: spectra of PC (14 μM) with CT-DNA (0–140 μM) (top), and fitted binding curve produced by the Mathematica script (bottom). The red dot indicates that the fit was successful.[11]

Isothermal titration calorimetry

ITC was employed here as it provides an overall picture of PC–DNA binding interaction from a calorimetric perspective.[12] The titration of each of complexes **1**–**6** was exothermic in nature, with negative μcal s^{-1} peaks present that represent DNA binding events, followed by smaller peaks from the heat of dilution once the binding sites were exhausted (Figure 6). Many titrations resulted in the appearance of two peaks rather than one, or at least evidence of two merged peaks to give the appearance of one. This suggests that binding may be biphasic in nature; the second peak may result from the ejection of solvent or sodium from the DNA sites, or from a DNA conformational adjustment post-binding, or both. The calculated thermodynamic parameters for each of **1**–**6** were similar. The binding of each complex with CT-DNA was an exothermic event, with ΔH values ranging from −1000 to −6000 cal mol^{-1} and ΔS values between 8 and 20 cal mol^{-1} deg^{-1} (Table 3). The positive ΔS is likely due to the solvation entropy that results from the ejection of solvent molecules from the grooves of DNA during PC–DNA binding.[13] The calculated ΔG values ranged between −7500 and −8500 cal mol^{-1}. Complexes **3** and **5** exhibited the lowest binding constants of approximately 2×10^5 M^{-1}, while the values for **1**, **2** and **6** were about 3×10^5 M^{-1}. The only complex that appeared to bind with a distinctly

higher affinity was complex **4** with a K_{ITC} of $(5.7\pm0.5)\times10^5\,M^{-1}$. This again suggests that $56Me_2phen$ is of an optimal size for DNA binding affinity. The number of PCs bound per base pair was between 0.25 and 0.3; converting that to *n* values reveals that approximately 3–4 binding sites are present per PC.

Binding constant data comparison

Overall, LD, UV and ITC have each provided valuable insight into the binding of complexes **1**–**6** to CT-DNA. LD has provided definitive evidence for an intercalative binding mode, however it could only provide binding constants for this interaction for four of the studied PCs. Evidence for a second electrostatic groove binding mode was also found in the LD spectra. UV spectroscopy provided binding data for all of **1**–**6** that resulted from the overall binding interaction; however no binding mode information could be obtained. ITC produced similar binding constants to the UV data, as well as additional thermodynamic information that could not be gained from the spectroscopic techniques. Each technique measures different aspects of PC–DNA binding; LD quantified the intercalation event only, whereas UV and ITC provided data that was representative of the overall interaction from a spectroscopic and calorimetric perspective, respectively. Therefore, it is not surprising that there were some differences in the calculated binding data across each technique (Table 1). More importantly, trends in DNA affinity for complexes **1**–**6** are generally the same across all studies: **4** > **2** = **1** ≥ **6** = **3** ≥ **5** (Figure 7). It is clear that these techniques are complementary and can each provide important information regarding PC–DNA binding.

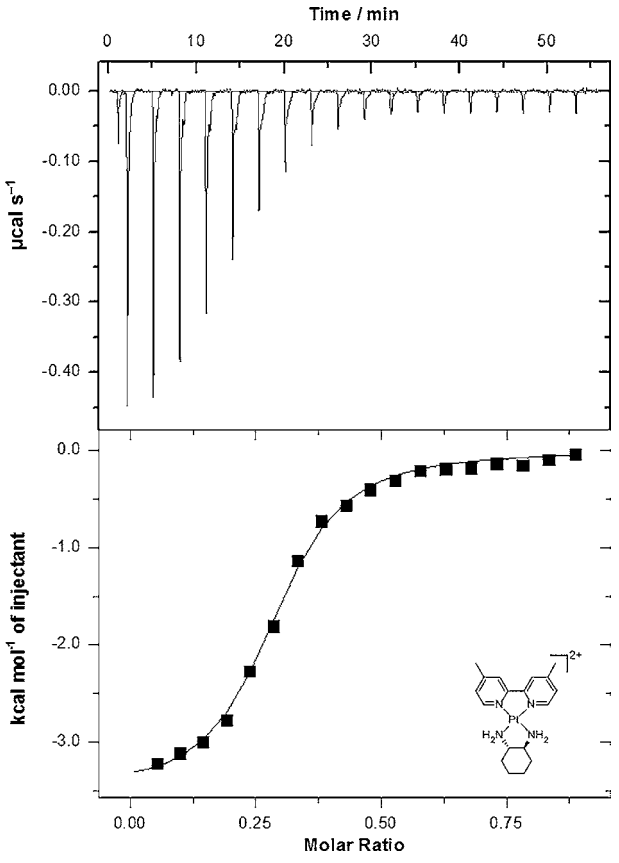

Figure 6. ITC trace and binding curve of the titration of complex **6** (650 μM) into CT-DNA (164 μM). Fits were obtained using a one-site binding model.

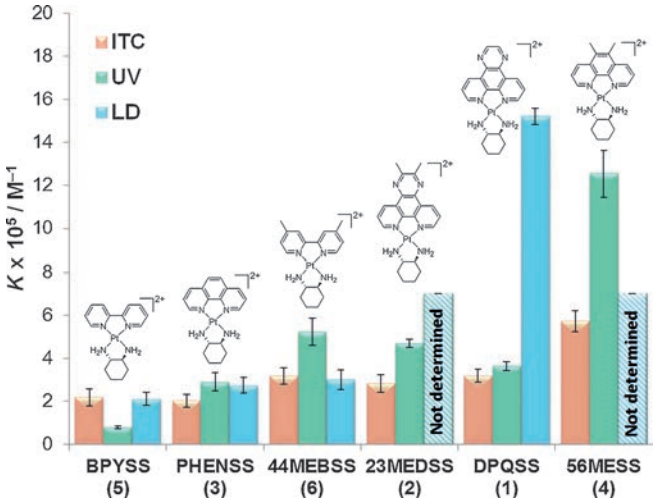

Figure 7. Comparison of the binding constants of complexes **1**–**6** with CT-DNA, as determined by ITC (red), UV (green) and LD (blue). Where applicable, *K* values over multiple wavelengths have been averaged for LD and UV data.

Fluorescent intercalator displacement (FID) assays

The ability to displace competing ligands from a target is a crucial factor in the efficacy of a drug. To study the ability of complexes **1**–**6** to competitively displace other binders from CT-DNA, fluorescent intercalator displacement assays (FIDs) were utilised. Ethidium bromide (EtBr) was used here as it is fluorescent only when bound with DNA.[14] The peak of emission for DNA-bound EtBr in this study was at 601 nm; upon the addition of each PC, the emission intensity decreased, indicating that some EtBr had been displaced from the DNA strand (Figure 8). EtBr is postulated to occupy several binding sites of DNA with an overall K_F of approximately $10^5\,M$.[15] Therefore, the determination of an accurate displacement binding constant is a difficult task as there are several possible sites occupied by EtBr that can be displaced by groove binders and intercalators alike. The binding curves obtained in this study did not reach a plateau, even at [DNA]/[PC] ratios as low as 0.15; this indicates that some ethidium molecules could not be displaced from particular binding sites. The curves could subsequently not be fitted using the same processing method as the LD and UV data, and so a simplified processing method of a previous study of ours was used (see the Experimental Section for details).[6b] The results are summarised in Figure 9 and Table 2.

Each of the PCs studied was capable of displacing EtBr from the CT-DNA strand, with K_F values between 10^2 and $10^7\,M^{-1}$. The simplified processing method means that K_F is only an indication of the ability of the complex to displace ethidium, and is not quantitatively representative of the binding affinity.

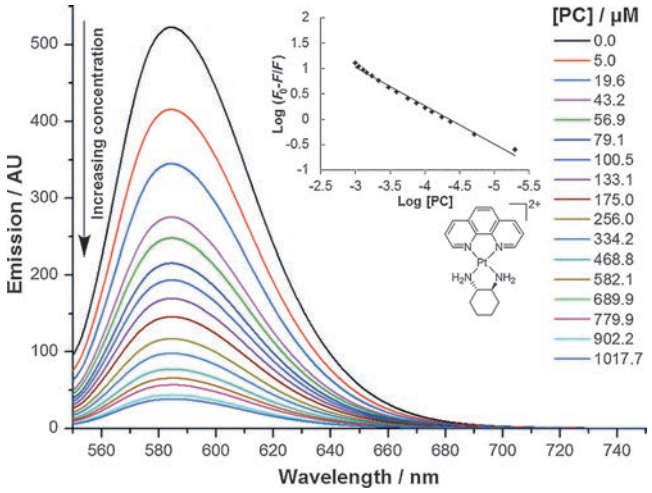

Figure 8. Emission spectra of DNA (150 μM) bound with EtBr (75 μM) with increasing concentration of complex **3** (0–1020 μM). Inset: the double-logarithm plot used to determine K_F.

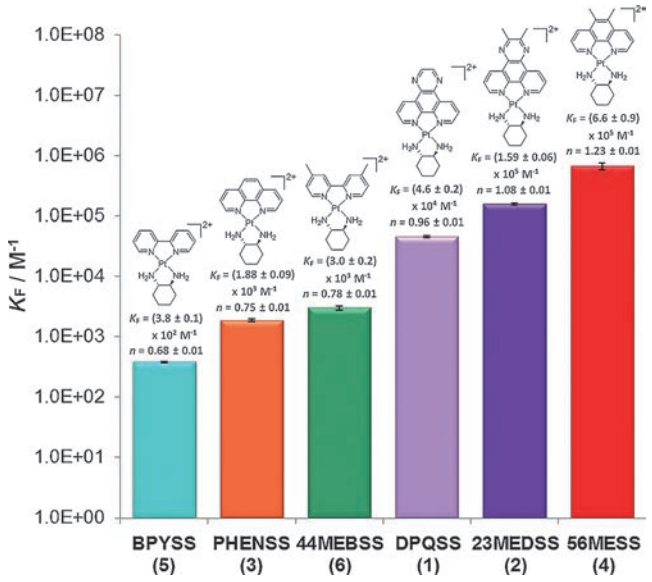

Figure 9. Comparison of the K_F and n determined for each PC, expressed on a logarithmic scale. Standard deviations (first significant figure) are included.

Table 2. Fluorescence constants calculated for complexes **1**–**6**, expressed with standard deviation (1 significant figure).

No.	10^{-5} K_q [$M^{-1}s^{-1}$]	10^{-5} K_F [M^{-1}]	n
1	2.81 ± 0.03	0.46 ± 0.02	0.96 ± 0.01
2	3.41 ± 0.02	1.59 ± 0.06	1.08 ± 0.01
3	0.539 ± 0.009	0.019 ± 0.001	0.75 ± 0.01
4	3.7 ± 0.1	6.6 ± 0.9	1.23 ± 0.01
5	0.174 ± 0.004	0.0038 ± 0.0001	0.68 ± 0.01
6	0.67 ± 0.01	0.030 ± 0.002	0.78 ± 0.01

Similarly, the calculated n values are representative of the amount of EtBr each complex can replace, rather than the number of DNA binding sites, and so it is logical that n values increased with increasing K_F. Each PC demonstrated K_q values above approximately $2\times10^{10}\,M^{-1}s^{-1}$, indicating that EtBr displacement occurred prior to the measurement of emission.[16] The trends between complexes **1**–**6** were still relatively consistent with the other data collected in this study; **4** and **5** demonstrated the highest and lowest affinity for CT-DNA, respectively. Greater differences were distinguishable between the rest of the complexes, suggesting that even the smallest differences in DNA affinity can result in large differences in competitive displacement ability that may be physiologically relevant.

Synchrotron radiation circular dichroism

SRCD has been used here to determine the effect of the binding of complexes **1**–**6** on the stability of CT-DNA. This was achieved through the determination of T_M, the temperature inflexion point at which the CD signal is lost due to a loss of secondary structure.[17] The addition of each PC to CT-DNA resulted in dramatic changes in the SRCD spectrum, presumably due to conformational changes that occurred upon binding. The wavelength maxima and minima chosen for melting analysis differed for each of **1**–**6** as each complex influenced the CT-DNA spectrum in different ways. For each DNA–PC combination, CD signal decreased with increasing temperature (Figure 10), with melting occurring at different points for each PC. For each melting curve, the T_M did not vary significantly between the wavelengths chosen. The binding of all complexes to DNA resulted in a higher T_M than the average DNA value of 55(±1) °C (Figure 11). An increase in T_M is expected for intercalative binders. It is important to note that the binding curves for complexes **2** and **4** (Section S5 in the Supporting Information) barely reached completion as the hardware could not raise the temperature above approximately 79 °C; however, ΔT_M values were consistent between replicates. The trends in T_M for each complex were almost the same as the trends of the fluorescence study; the order of DNA stabilisation was **2**≅**4** > **1** > **3**≅**6** > **5**. Similarly to the FID assays, it appears that even minor differences in the DNA affinity of these PCs has led to large differences in their ability to stabilise helical DNA against melting.

Mass spectrometry binding studies

Mass spectrometry is often used to probe ligand–biomolecule interactions at different stoichiometry.[18] The mass spectra of each of the double complementary strands 5′-GCGCATGCG-CATGCGC-3′ ("GC Strand" or GCS) and 5′-GCATATGATATCA-TATGC-3′ ("AT Strand" or ATS) are characterised by several main peaks representing different charge states of the strand (Section S6 in the Supporting Information). When binding to each strand individually, complexes **1**–**6** were found to bind to up to one in every two base-pairs. For example, for the solutions of 9:1 PC to ATS strand ratio, the mass spectra for complex **2** produced peaks corresponding to as high as [ATS+9 PC], while those for **5** only produced peaks for up to [ATS+7 PC]. Spectra and relative abundance information can be found in Section S6.2 in the Supporting Information. To determine if there

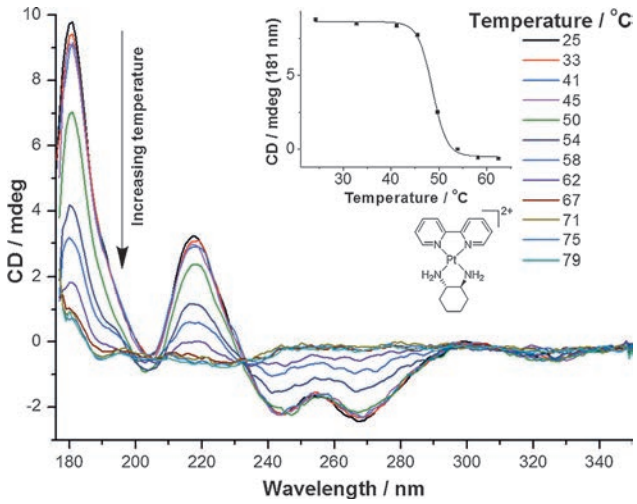

Figure 10. SRCD spectra of CT-DNA (1 mM) bound with complex 5 (0.5 mM) at various temperatures (25–79 °C). Inset: the melting curve used to generate the T_M value (points past 62 °C have been omitted for clarity).

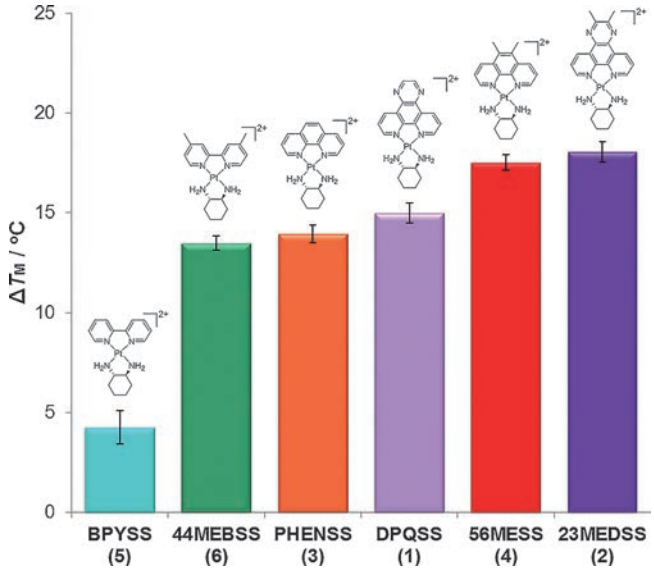

Figure 11. Comparison of the SRCD ΔT_M determined for CT-DNA bound with complexes **1**–**6**, relative to free CT-DNA (T_M = 55(±1) °C). Standard deviations (error bars) are included.

was any base-pair preference, a competitive assay was carried out in which each PC was added to a 1:1 solution of the GCS and ATS strands. All of complexes **1**–**6** demonstrated the same behaviour in these experiments and so the spectra of complex **2** will be used as an example (Figure 12). Immediate observation of the mass spectra of 1:1 GCS to ATS with one and three equivalents of complex **2** suggests that there is GC selectivity; in the 1:1:1 spectrum the peaks corresponding to unbound GCS have dropped relative to the 0:1:1 spectrum while the ATS peaks are still at large. Supporting this, the peaks at 1482 and 1741 *m/z* in this spectrum correspond to [GCS+1PC]. There is evidence for [ATS+1PC] at approximately 1670 *m/z*, however this signal is also representative of unbound GCS and so the actual intensity would be quite low. The 3:1:1 spectrum further displays the GC selectivity of complex **2** as the approximately 1400 *m/z* peak representing unbound GCS at a charge of 7− has almost disappeared, while there is still some evidence of free ATS in the peaks at approximately 1660 and about 1800 *m/z*. Peaks corresponding to [ATS+1PC] (1666 and 1953 *m/z*) and [ATS+2PC] (1730 and 2050 *m/z*) are visible, however there are also peaks representative of [GCS+3PC] (1400 and 1870 *m/z*) and [GCS+4PC] (1950 *m/z*). GC selectivity is common for DNA intercalators,[19] and these experiments were conducted within DNA/PC ratios in which only intercalation is occurring (in accordance with the LD experimental data). Abundances were not determined here as there are too many overlapping peaks; however it is clear that the PCs in this study selectively bind to GC base-pairs over AT ones.

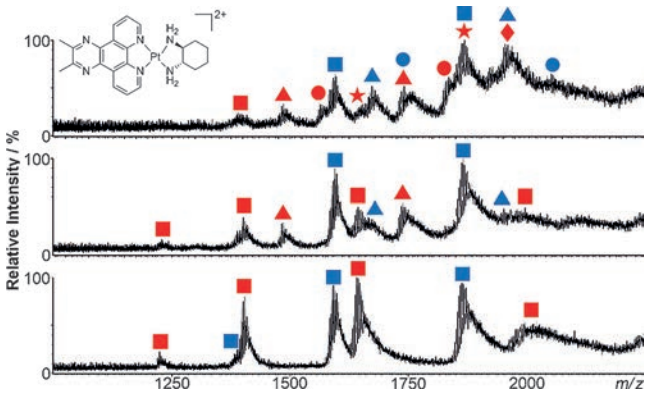

Figure 12. Mass spectra of a solution of complex **2**, GCS (red symbols) and ATS (blue symbols) in the following ratios: 0:1:1 (bottom), 1:1:1 (middle) and 3:1:1 (top) (1 equivalent is 42 μM). Legend: square = [DNA], triangle = [DNA+1PC], circle = [DNA+2PC], star = [DNA+3PC], diamond = [DNA+4PC].

In vitro cytotoxicity

As a continuation of the cytotoxicity assays performed in previous work with complexes **1**–**6** and **1′**–**6′** in the L1210 murine leukaemia, HT29 human colon carcinoma and U87 human glioblastoma cell lines,[5b] the activity of these complexes was assessed in a further ten cell lines: MCF-7 breast cancer, A2780 ovarian cancer, H460 lung cancer, A431 skin cancer, Du145 prostate cancer, BE2-C neuroblastoma, SJ-G2 human glioblastoma, MIA pancreas cancer, SMA murine glioblastoma and MCF10A breast (normal; Table 3). These experiments were conducted to gain a greater understanding of the activity of **1**–**6** and **1′**–**6′**, to relate, if possible, the DNA affinity of **1**–**6** with their in vitro activity, and to determine particularly sensitive cell lines to target in further studies. For all cell lines studied, the complexes demonstrated potent, often submicromolar activity, with complexes **3**–**6** demonstrating very high cytotoxicity in the Du145 prostate cancer (some values previously published[20]), SJ-G2 glioblastoma, and the previously published HT29 colon carcinoma[5b] lines (Figure 13). These cancer types are therefore good targets for further therapeutic studies. The lowest point of activity was in the BE2-C neuroblastoma line,

with only complexes **3** and **4** reaching submicromolar IC_{50} concentrations. Also of note is the higher cytotoxicity of all PCs in the "normal" MCF10A breast cell line relative to the MCF-7 breast cancer line. This emphasises the importance of targeted delivery of these complexes to cancerous cells. Across the majority of cell lines, the same structure-activity trends are observed as previous studies: for P_Ls, $56Me_2$phen > phen ≥ $44Me_2$bpy > dpq > bpy > $23Me_2$dpq, and for A_Ls, *SS*-dach > *RR*-dach. The fact that these trends were generally the same across all cell lines suggests that the in vitro mechanism of action of these PCs is largely independent of the cancer type, with minor differences between the mechanisms of individual complexes. A correlation between DNA affinity and cytotoxicity was observed for complexes **3**–**6**; **4** and **5** were the most and least effective in both areas, respectively, while **3** and **6** were approximately equal in both DNA affinity and cytotoxicity. Interestingly, complexes **1** and **2** exhibited mid-low biological activity despite their relatively high DNA affinity. Additionally there were large differences in activity between *R,R* and *S,S* isomers, despite their similar DNA binding affinity as determined in our previous DNA study.[6b] This reinforces the notion that the apoptotic mechanisms of these complexes involve much more than DNA binding alone.[4,21] Further studies of the in vitro interactions of these complexes are warranted.

Conclusions

The DNA binding of six anticancer PCs DPQSS, 23MEDSS, PHENSS, 56MESS, BPYSS and 44MEBSS has been studied in depth through the use of several biophysical techniques. Overall, each technique contributed unique information regarding binding behaviour; LD, UV and ITC provided PC–DNA binding constant values, as well as binding mode and thermodynamic parameters. From these data it is clear that complexes **1**–**6** are capable of binding to DNA with an affinity of approximately 10^5–$10^6\ M^{-1}$, with intercalation as the primary mode and other potential modes at higher PC concentrations. FID and SRCD experiments provided some insight into the effect of DNA affinity on the ability of the PCs to displace competing binders and to stabilise the DNA strand, respectively. Overall, 56MESS (**4**) and BPYSS (**5**) were found to be the most and least potent DNA binders, respectively. Finally, mass spectrometry studies

Table 3. Summary of the in vitro cytotoxicity of complexes **1**–**6** and **1′**–**6′** in several cell lines, expressed as an IC_{50} value with standard error (1 significant figure). IC_{50} is the concentration at which cell growth is inhibited by 50% over 72 h.

Complex		IC_{50} [μM]						
		L1210[a]	HT29[a]	U87[a]	MCF-7	A2780	H460	A431
1	DPQSS	0.19 ± 0.01	0.59 ± 0.08	3.70 ± 0.24	1.8 ± 0.2	2.0 ± 0.1	1.9 ± 0.2	3.2 ± 0.2
1′	DPQRR	0.8 ± 0.2	1.3 ± 0.2	12 ± 2.8	7.8 ± 0.8	6.5 ± 0.0	3.9 ± 0.2	7 ± 2
2	23MEDSS	1.3 ± 0.4	1.8 ± 0.3	8.2 ± 1.6	4.2 ± 0.4	3.7 ± 0.4	2.8 ± 0.1	13 ± 2
2′	23MEDRR	6 ± 2	1.6 ± 0.4	16 ± 3.2	4.4 ± 0.7	2.0 ± 0.1	8.0 ± 0.5	7 ± 2
3	PHENSS[b]	0.10 ± 0.01	0.13 ± 0.04	1.5 ± 0.4	0.5 ± 0.2	0.27 ± 0.03	0.5 ± 0.2	0.9 ± 0.3
3′	PHENRR	1.5 ± 0.1	0.56 ± 0.08	8.9 ± 2.5	3.2 ± 0.2	2.70 ± 0.07	7.2 ± 0.9	2.0 ± 0.6
4	56MESS[b]	0.009 ± 0.002	0.08 ± 0.06	0.076 ± 0.014	0.05 ± 0.02	0.030 ± 0.004	0.037 ± 0.009	0.05 ± 0.02
4′	56MERR[b]	0.46 ± 0.01	0.19 ± 0.00	2.2 ± 0.058	0.8 ± 0.1	1.1 ± 0.1	1.8 ± 0.2	0.93 ± 0.03
5	BPYSS	0.6 ± 0.2	1.1 ± 0.2	4.0 ± 0.3	2.6 ± 0.2	2.6 ± 0.2	5 ± 2	3.1 ± 0.2
5′	BPYRR[c]	5.5 ± 0.1	n.d.	n.d.	n.d.	n.d.	n.d.	n.d.
6	44MEBSS	0.36 ± 0.02	0.13 ± 0.03	0.500 ± 0.009	3.5 ± 0.7	0.9 ± 0.1	1.1 ± 0.3	0.5 ± 0.1
6′	44MEBRR	1.8 ± 0.0	0.66 ± 0.07	3.9 ± 0.4	2.70 ± 0.07	5 ± 1	5.6 ± 0.5	1.4 ± 0.4
	cisplatin	0.35–1[d]	11 ± 2	3.8 ± 1.1	6.5 ± 0.8	1.0 ± 0.1	0.9 ± 0.2	2.4 ± 0.3
	oxaliplatin	n.d.	0.9 ± 0.2	1.8 ± 0.2	0.5 ± 0.1	0.16 ± 0.0	1.6 ± 0.1	4.1 ± 0.5
	carboplatin	n.d.	> 50	> 50	> 50	9 ± 3	14 ± 1	24 ± 2

Complex		IC_{50} [μM]					
		Du145	BE2-C	SJ-G2	MIA	SMA	MCF10A
1	DPQSS	0.44 ± 0.06	2.9 ± 0.2	2.5 ± 0.3	0.62 ± 0.03	1.3 ± 0.6	1.6 ± 0.2
1′	DPQRR	2.7 ± 0.2	24 ± 3	12 ± 3	2.3 ± 0.3	7 ± 2	6 ± 1
2	23MEDSS	2.2 ± 0.1	34 ± 6	13 ± 1	0.7 ± 0.2	5.2 ± 0.4	4.3 ± 0.7
2′	23MEDRR	3 ± 1	1.80 ± 0.06	6 ± 2	1.2 ± 0.3	2.1 ± 0.6	4 ± 1
3	PHENSS[b]	0.08 ± 0.05	0.40 ± 0.05	0.45 ± 0.06	0.8 ± 0.7	0.24 ± 0.04	0.16 ± 0.07
3′	PHENRR	0.79 ± 0.08	3.8 ± 0.4	3.3 ± 0.3	2.7 ± 0.2	3.2 ± 0.3	2.4 ± 0.3
4	56MESS[b]	0.007 ± 0.002	0.100 ± 0.002	0.07 ± 0.02	0.015 ± 0.002	0.032 ± 0.007	0.020 ± 0.005
4′	56MERR[b]	0.41 ± 0.04	2.3 ± 0.2	2.2 ± 0.2	0.45 ± 0.006	1.6 ± 0.5	0.39 ± 0.01
5	BPYSS	1.3 ± 0.4	3 ± 1	1.8 ± 0.3	2.5 ± 0.1	3.1 ± 0.8	1.6 ± 0.3
5′	BPYRR[c]	n.d.	n.d.	n.d.	n.d.	n.d.	n.d.
6	44MEBSS	0.12 ± 0.03	1.0 ± 0.5	0.55 ± 0.04	3 ± 1	0.29 ± 0.03	0.27 ± 0.02
6′	44MEBRR	1.5 ± 0.3	5.2 ± 0.4	3.0 ± 0.2	3.4 ± 0.2	2.7 ± 0.2	2.0 ± 0.3
	cisplatin	1.2 ± 0.1	1.9 ± 0.2	0.4 ± 0.1	8 ± 1	1.2 ± 0.1	n.d.
	Oxaliplatin	2.9 ± 0.4	0.9 ± 0.2	3 ± 1	0.9 ± 0.2	1.4 ± 0.1	n.d.
	Carboplatin	15 ± 1	19 ± 1	5.7 ± 0.2	> 50	14.3 ± 0.7	n.d.

[a] Quoted from reference [5b] and those within. [b] Values for these complexes were also previously reported in reference [20]. [c] Pre-screening determined this complex was not active in most Calvary Mater cell lines. [d] Values also retrieved from references [6b] and [22]. n.d. = not determined.

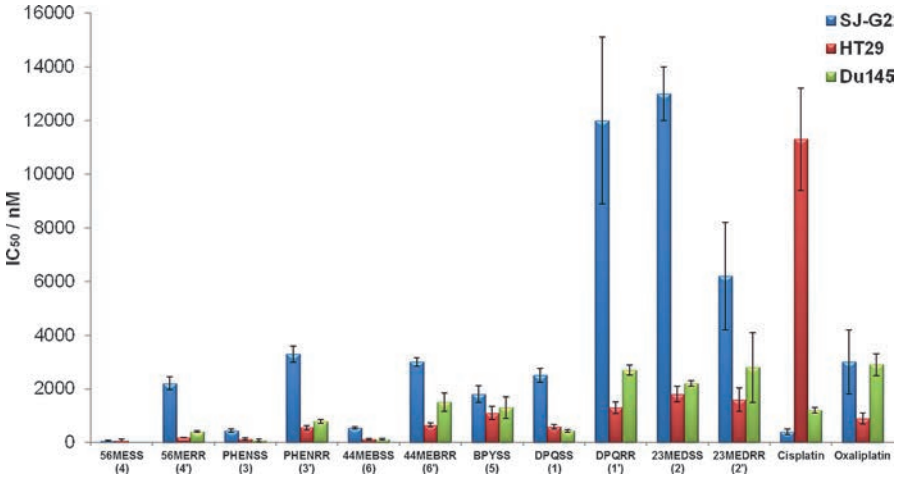

Figure 13. Comparison of the cytotoxicity of complexes **1**–**6** and **1**′–**6**′ in the SJ-G2 human glioblastoma (blue), HT29 colon carcinoma (red) and Du145 prostate cancer (green) cell lines, expressed as nanomolar IC_{50} values with standard error. Carboplatin and BPYRR (**5**′) values have been omitted for clarity.

revealed that each PC preferentially binds to GC base-pairs over AT ones. The unique information gleaned from each of these biophysical methods, and the minor differences in trends observed from each, clearly reveal that in order for one to have a complete understanding of the binding of small molecules to DNA, multiple techniques of analysis should be utilised. Complexes **1**–**6** and **1**′–**6**′ demonstrated high in vitro activity across a large range of human cancer cell lines with particularly high efficacy in Du145 prostate cancer and SJ-G2 glioblastoma cells. PCs of dpq and $23Me_2$dpq, despite demonstrating relatively high DNA affinity, were among the least active biologically. For complexes of bpy, $44Me_2$bpy, phen and $56Me_2$phen, DNA affinity does appear to correlate with cytotoxicity, suggesting that DNA binding plays a role in the apoptotic activity of these complexes. However, the large difference in activity between enantiomers suggests that further studies of other, non-DNA interactions are needed to determine the overall mechanism of action.

Experimental Section

Materials and preparation

All reagents were used as received and all solvents used were of analytical grade or higher. Complexes **1**–**6** and **1**′–**6**′ were prepared as per previous publications.[5b,6b,22] Dipotassium hydrogen orthophosphate, potassium dihydrogen orthophosphate, ammonium acetate, sodium fluoride, sodium chloride, D-10-camphorsulfonic acid, calf-thymus DNA and ethidium bromide (EtBr) were obtained from Sigma–Aldrich chemicals. Pora-Pak™ Rxn CX cartridges (20cc, 2 g) were obtained from Waters. The HPLC-purified DNA oligonucleotides 5′-GCGCATGCGCATGCGC-3′ ("GC Strand" or GCS) and 5′-GCATATGATATCATATGC-3′ ("AT Strand or ATS") were obtained from Integrated DNA Technologies (IDT). Further purification and ion exchange of each strand was achieved by dissolution in 150 mM ammonium acetate and elution through a Pora-Pak™ Rxn CX cartridge (20cc, 2 g) followed by lyophilisation. Annealing was achieved by heating solutions of each oligonucleotide in 150 mM ammonium acetate to 95 °C in a water bath for 3 min before being left to cool overnight. Oligonucleotide concentrations were determined through UV absorbance, using the IDT-provided extinction coefficients of 254000 and 283000 $M^{-1}cm^{-1}$ per double strand at 260 nm for GCS and ATS, respectively. CT-DNA concentration was confirmed using the 260 nm extinction coefficient of 13200 $M^{-1}cm^{-1}$ per base pair.[23] EtBr concentration was determined using the extinction coefficient of $\varepsilon_{476} = 5680\ M^{-1}cm^{-1}$,[24] and PC concentrations were determined using their respective extinction coefficients (Table 4).[5b,6b,25]

Table 4. Wavelength maxima and extinction coefficients of complexes **1**–**6**.

No.	P_L	λ_{max} [nm]	ε [$M^{-1}cm^{-1}$]
1	Dpq	258	50000
2	$23Me_2$dpq	261	45000
3	Phen	226	35000
4	$56Me_2$phen	230	37000
5	Bpy	245	22000
6	$44Me_2$bpy	243	24500

Linear dichroism

LD spectra were obtained using a Jasco 810 spectropolarimeter using a quartz capillary LD couette flow cell built by Crystal Precision Optics. Experiments at temperatures close to physiological resulted in DNA shearing, and so experiments were performed at 20 °C rather than 37 °C. The instrument was allowed to equilibrate for 30 min prior to use, and nitrogen gas flow was kept at approximately 10 L min^{-1}. A series of about 17 solutions consisting of CT-DNA (150 μM), K_2HPO_4/KH_2PO_4 (10 mM, pH 7.3), NaCl (10 mM) and various amounts of each PC were prepared according to Table S1.1 in the Supporting Information. NaCl concentration was relatively low due to the strong absorption of chloride salts at low wavelengths.[26] For each solution, spectra were obtained over the range of 200–350 nm using a scan rate of 200 nm min^{-1}, data pitch of 1 nm, response time of 1 s and rotation speed of 3000 rpm. Two accumulations were collected and a baseline non-rotating spectrum was subtracted from each data set. The change of the DNA signal in proportion to the PC concentration was used to elucidate PC–DNA binding information, and to determine the binding constant for LD (K_{LD}). To determine the binding constants, the induced

response of the LD signal was plotted against PC concentration, and fitted to the following equation using the published Wolfram Mathematica script,[11] which utilises the binding model of Ismail and Stootman et al. [Eq. (1)]:[11,27]

$$\varepsilon = 0.5R_B\left(\frac{1}{K}+\frac{B_T}{n}+L_T-\sqrt{\left(\frac{1}{K_{LD}}+\frac{B_T}{n}+L_T\right)^2-\frac{4B_TL_T}{n}}\right) \quad (1)$$

where L_T is the total PC concentration, B_T is the total number of DNA bases, K_{LD} is the binding constant and n is the number of base-pairs per PC. R_B is the response of the instrument as a result of the binding of PC to DNA (whose concentration is denoted L_B) and ε is an experimental measurement that relates to L_B via Equation (2):

$$\varepsilon = R_BL_B \quad (2)$$

K_{LD} was calculated for each wavelength peak in the induced spectrum of complexes **1**, **3**, **5** and **6**. For complexes **1** and **3**, the points of the binding curve corresponding to PC concentrations below 40 μM had to be removed in order to fit the data. Experiments were performed in triplicate for each PC.

UV spectroscopy

Absorbance spectra were obtained using a Jasco V-660 UV/Vis spectrometer operating at 37 °C. The wavelength range chosen was 200–450 nm, and the scan rate was 400 nm min^{-1}, data interval was 1 nm and averaging time was 0.1 s. The spectrum of each PC (≈14 μM) in K_2HPO_4/KH_2PO_4 (10 mM, pH 7.3) and NaCl (50 mM) buffer was initially obtained, followed by the titration of CT-DNA (1–2 mM) according to Table S2.1 in the Supporting Information. The same amount of DNA and buffer was added to the reference cell to account for the absorbance of DNA. After each titration, the solutions were gently mixed and allowed to incubate for 2 min before measurement. The attenuation of signal at various wavelengths for each PC was used to determine the binding constant (K_{UV}) for each complex. The binding of each PC to CT-DNA was studied quantitatively using the same Wolfram Mathematica script as the LD experiments, to determine the binding constant (K_{UV}) and number of binding sites (n). Experiments were performed in triplicate for each PC.

Isothermal titration calorimetry assays

ITC traces were obtained using a MicroCal iTC 200 calorimeter operating at 37 °C. Each PC (600–750 μM) was titrated into a solution of CT-DNA (165 μM) in K_2HPO_4/KH_2PO_4 (10 mM, pH 7.3) and NaCl (50 mM) buffer. Each PC was also titrated into buffer without DNA for use as a baseline. The titration program consisted of one 0.4 μL addition followed by 18 titrations of 2 μL, with a spacing of 180 s, reference power of 6 μcal s^{-1} and stirring speed of 750 rpm. Data were analysed using Origin 7.0 (MicroCal version) using 200 iterations of a one-site binding model using the following equations. Experiments were performed in duplicate for each PC [Eqs. (3) and (4)]:

$$\Delta G = -RT\ln K \quad (3)$$

$$\Delta S = \frac{\Delta H-\Delta G}{T} \quad (4)$$

Fluorescent intercalator displacement assays

Emission spectra for the FIDs were collected using a Jasco FP-2500 fluorimeter operating at 37 °C. The wavelength range chosen was 550–750 nm with an excitation wavelength of 480 nm, scan rate of 600 nm min^{-1}, data interval of 1 nm and averaging time of 0.1 s. The emission and excitation slits were each set to 5 nm. A solution of EtBr (75 μM) and CT-DNA (150 μM) in K_2HPO_4/KH_2PO_4 (10 mM, pH 7.3) and NaCl (50 mM) buffer was initially measured, followed by the titration of PC (various concentrations) according to Tables S4.1 and S4.2 in the Supporting Information. After each titration the solution was gently mixed and incubated for 3 min before measurement. The attenuation of signal at 601 nm from each successive titration was used to calculate the binding constant for fluorescence (K_F). To determine the quenching mode, the Stern–Volmer equation [Eq. (5)] was used:[28]

$$\frac{F_0}{F} = 1+K_q\tau_0[PC] = 1+K_{SV}[PC] \quad (5)$$

where F_0 is the fluorescence of the binding site in the absence of quencher, F is the fluorescence of the site containing the PC, K_q is the bimolecular quenching constant, τ_0 is the lifetime of the chromophore in the absence of the quencher ($\approx 22\times10^{-9}$ s for ethidium-bound DNA),[29] and K_{SV} is the Stern–Volmer quenching constant. A plot of F_0/F against [PC] using experimental values allows for the determination of K_q and K_{SV} from the slope. To determine K_F, the double-logarithm expression derived in our previous work was used to determine a binding constant for the PC–DNA interaction [Eq. (6)]:[6b]

$$\log_{10}\left(\frac{F_0-F}{F}\right) = n\log_{10}[PC]+\log_{10}K_F \quad (6)$$

where n is the number of ethidium compounds displaced per PC. It is important to note that this expression is a simplification of the true binding interaction as the effect of EtBr on the binding equilibrium is ignored;[30] however, the results obtained are still comparable between complexes of the same study.[6b] A plot of $\log_{10}[(F_0-F)/F)]$ against $\log_{10}[PC]$ is used to determine K_F and n from the intercept and slope, respectively. Experiments were performed in triplicate for each PC.

Synchrotron radiation circular dichroism

Experiments were performed at the AU-CD beamline on ASTRID2[31] at ISA, Aarhus University. ASTRID2 operates in top-up mode with a current of 120 mA. The AU-CD beam-line operates in the wavelength range of 125 to 450 nm, with a bandwidth of 0.6 nm. The beam size on the sample is 2 (vert.)×6 mm (horz.), with a sample to detector distance of 25 mm. All SRCD experiments were performed using a suprasil quartz cuvette with a 0.01 cm path-length. Temperature control was achieved through the use of a Eurotherm temperature regulator. Calibration of the spectropolarimeter was assessed through daily measurement of the CD spectrum of D-10-camphorsulfonic acid. Each melting solution consisted of a PC (0.5 mM) and CT-DNA (1 mM) in K_2HPO_4/KH_2PO_4 (10 mM, pH 7.3) and NaF (50 mM) buffer. NaF was used due

to the strong absorption of chloride salts at low wavelengths.[26] Solutions of CT-DNA with no PC present were also measured. Temperature scans were performed as follows: the cell temperature began at 25 °C, was raised to 45 °C in 10 °C increments and then raised from 45–90 °C in 5 °C increments. The heating rate was 1 °C min^{-1}. For each temperature increment, the cell was allowed to equilibrate for 5 min before a spectrum was recorded; these were collected from 350–170 nm with a 1 nm increment and three accumulations. Prior to each melting experiment, a baseline spectrum of the PC in phosphate buffer was obtained to partially eliminate the effects of PC chirality from the SRCD spectra. Experiments were performed in duplicate for each PC. For each wavelength, SRCD intensity was plotted against temperature, and a Boltzmann curve was fitted to the plot using Origin Pro 8.5 (Origin Labs) to determine the T_M. The CT-DNA concentration used here was much higher than that for other biophysical assays due to the lower path length of the cell used. To prevent the chirality of the PCs from affecting the CD spectrum of DNA, the PCs were included in the baseline solutions and the DNA/PC ratio was consistently kept at 2:1 and no higher.

Electrospray ionisation mass spectrometry

DNA–PC solutions were analysed by negative-mode ESIMS using a Waters XEVO QToF ESI mass spectrometer with a *Z*-spray ionisation source. Mass spectra were obtained with a MCP potential of 2400 V, a cone voltage of 25 V and a capillary tip potential of 2.4 kV. The desolvation gas flow was 300 L h^{-1} at a desolvation temperature of 150 °C with the source temperature at 70 °C. The collision energy was set to off. Spectra were obtained over a mass/charge (*m/z*) range of 50–4000. A Hamilton 250 μL model 1725RN gastight syringe was loaded with 25 μL of solution and infused into the mass spectrometer source using a KD Scientific model 100 syringe pump set to 5 μL min^{-1}, achieving 5 min of data acquisition. Between each run the syringe was cleaned thoroughly and the mass spectrometer was flushed with MilliQ-purified water.

In-vitro cytotoxicity

Cytotoxicity assays were performed at the Calvary Mater Newcastle Hospital, Waratah, NSW, Australia. The cell lines tested were MCF-7 breast cancer, A2780 ovarian cancer, H460 lung cancer, A431 skin cancer, Du145 prostate cancer, BE2-C neuroblastoma, SJ-G2 glioblastoma, MIA pancreas cancer, SMA murine glioblastoma and the non-tumour derived MCF10A breast cell lines. All test agents were prepared as 30 mM stock solutions in DMSO and stored at −20 °C. Cell lines were cultured in a humidified atmosphere 5% CO_2 at 37 °C and maintained in Dulbecco's modified Eagle's medium (Trace Biosciences, Australia) supplemented with 10% foetal bovine serum, 10 mM sodium bicarbonate penicillin (100 IU mL^{-1}), streptomycin (100 μg mL^{-1}), and glutamine (4 mM). Cytotoxicity was determined by plating cells in duplicate in 100 mL medium at a density of 2500–4000 cells per well in 96-well plates. On day 0 (24 h after plating) when the cells were in logarithmic growth, 100 μL medium with or without the test agent was added to each well. After 72 h drug exposure growth inhibitory effects were evaluated using the MTT (3-[4,5-dimethyltiazol-2-yl]-2,5-diphenyl-tetrazolium bromide) assay and absorbance read at 540 nm. An eight-point dose-response curve was produced from which the IC_{50} value was calculated, representing the drug concentration at which cell growth was inhibited by 50% based on the difference between the optical density values on day 0 and those at the end of drug exposure.[32]

Acknowledgements

The authors thank ISA, Aarhus University for synchrotron beam time and Australian Synchrotron for providing International Synchrotron Access project travel funds. We also thank Western Sydney University for its financial support through internal research grants. B.J.P. and D.L.A. were supported by an Australian Postgraduate Award and Western Sydney University Top-Up Award. B.J.P. was also supported by an Endeavour Fellowship.

Keywords: Anticancer agents · biophysical chemistry · DNA · platinum · spectroscopy

[1] a) B. H. Harper, F. Li, R. Beard, K. B. Garbutcheon-Singh, N. S. Ng, J. R. Aldrich-Wright, in *Biomolecular Interactions of Platinum Complexes* (Ed.: H. J. Schneider), RSC, Cambridge, **2013**; b) A. Callejo, L. Sedó-Cabezón, I. D. Juan, J. Llorens, *Toxics* **2015**, *3*, 268–293.

[2] a) A. M. Krause-Heuer, R. Grünert, S. Kühne, M. Buczkowska, N. J. Wheate, D. D. Le Pevelen, L. R. Boag, D. M. Fisher, J. Kasparkova, J. Malina, P. J. Bednarski, V. Brabec, J. R. Aldrich-Wright, *J. Med. Chem.* **2009**, *52*, 5474–5484; b) L. A. Graham, J. Suryadi, T. K. West, G. L. Kucera, U. Bierbach, *J. Med. Chem.* **2012**, *55*, 7817–7827.

[3] C. R. Brodie, J. G. Collins, J. R. Aldrich-Wright, *Dalton Trans.* **2004**, 1145–1152.

[4] K. B. Garbutcheon-Singh, S. Myers, B. W. J. Harper, N. S. Ng, Q. Dong, C. Xie, J. R. Aldrich-Wright, *Metallomics* **2013**, *5*, 1061–1067.

[5] a) K. B. Garbutcheon-Singh, B. W. J. Harper, S. Myers, J. R. Aldrich-Wright, *Metallomics* **2014**, *6*, 126–131; b) B. J. Pages, Y. Zhang, F. Li, J. Sakoff, J. Gilbert, J. R. Aldrich-Wright, *Eur. J. Inorg. Chem.* **2015**, 4167–4175.

[6] a) S. Kemp, N. J. Wheate, D. P. Buck, M. Nikac, J. G. Collins, J. R. Aldrich-Wright, *J. Inorg. Biochem.* **2007**, *101*, 1049–1058; b) B. J. Pages, F. Li, P. Wormell, D. L. Ang, J. K. Clegg, C. J. Kepert, L. K. Spare, S. Danchaiwijit, J. R. Aldrich-Wright, *Dalton Trans.* **2014**, *43*, 15566–15575.

[7] a) D. Z. M. Coggan, I. S. Haworth, P. J. Bates, A. Robinson, A. Rodger, *Inorg. Chem.* **1999**, *38*, 4486–4497; b) S. M. Kelly, T. J. Jess, N. C. Price, *Biochim. Biophys. Acta Proteins Proteomics* **2005**, *1751*, 119–139; c) N. Shahabadi, L. Heidari, *Spectrochim. Acta Part A* **2014**, *128*, 377–385.

[8] B. J. Pages, D. L. Ang, E. P. Wright, J. R. Aldrich-Wright, *Dalton Trans.* **2015**, *44*, 3505–3526.

[9] B. Norden, A. Rodger, T. Dafforn, *Linear Dichroism and Circular Dichroism: A Textbook on Polarised-Light Spectroscopy*, RSC, London, **2010**, p. 304.

[10] a) T. Biver, *Appl. Spectrosc. Rev.* **2012**, *47*, 272–325; b) M. R. Gill, D. Cecchin, M. G. Walker, R. S. Mulla, G. Battaglia, C. Smythe, J. A. Thomas, *Chem. Sci.* **2013**, *4*, 4512–4519.

[11] D. L. Ang, N. C. Jones, F. Stootman, B. Ghadirian, J. R. Aldrich-Wright, *Analyst* **2015**, *140*, 4162–4169.

[12] N. C. Garbett, J. B. Chaires, *Expert Opin. Drug Discovery* **2012**, *7*, 299–314.

[13] J. A. D'Aquino, E. Freire, L. M. Amzel, *Proteins Struct. Funct. Bioinf.* **2000**, *41*, 93–107.

[14] R. W. Sabnis, *Handbook of Biological Dyes and Stains: Synthesis and Industrial Applications*, Wiley, New Jersey, **2010**, p. 544.

[15] a) J. B. Lepecq, C. Paoletti, *J. Mol. Biol.* **1967**, *27*, 87–106; b) R. R. Monaco, *J. Biomol. Struct. Dyn.* **2007**, *25*, 119–125.

[16] W. R. Ware, *J. Phys. Chem.* **1962**, *66*, 455–458.

[17] D. L. Ang, B. W. J. Harper, L. Cubo, O. Mendoza, R. Vilar, J. Aldrich-Wright, *Chem. Eur. J.* **2015**, *22*, 2317–2325.

[18] a) S. M. Meier, M. Hanif, Z. Adhireksan, V. Pichler, M. Novak, E. Jirkovsky, M. A. Jakupec, V. B. Arion, C. A. Davey, B. K. Keppler, C. G. Hartinger, *Chem. Sci.* **2013**, *4*, 1837–1846; b) K. J. Davis, C. Richardson, J. L. Beck, B. M. Knowles, A. Guedin, J.-L. Mergny, A. C. Willis, S. F. Ralph, *Dalton Trans.* **2015**, *44*, 3136–3150.

[19] a) K. X. Chen, N. Gresh, B. Pullman, *FEBS Lett.* **1987**, *224*, 361–364; b) R. Nanjunda, W. D. Wilson, in *Binding to the DNA Minor Groove by Hetero-*

cyclic Dications: From AT Specific Monomers to GC Recognition with Dimers, Wiley, New York, **2012**.

[20] F. J. Macias, K. M. Deo, B. J. Pages, P. Wormell, J. K. Clegg, Y. Zhang, F. Li, G. Zheng, J. Sakoff, J. Gilbert, J. R. Aldrich-Wright, *Chem. Eur. J.* **2015**, *21*, 16990 – 17001.

[21] a) S. Wang, M. J. Wu, V. J. Higgins, J. R. Aldrich-Wright, *Metallomics* **2012**, *4*, 950 – 959; b) K. J. Davis, J. A. Carrall, B. Lai, J. R. Aldrich-Wright, S. F. Ralph, C. T. Dillon, *Dalton Trans.* **2012**, *41*, 9417 – 9426.

[22] N. J. Wheate, R. I. Taleb, A. M. Krause-Heuer, R. L. Cook, S. Wang, V. J. Higgins, J. R. Aldrich-Wright, *Dalton Trans.* **2007**, 5055 – 5064.

[23] T. Maniatis, E. F. Fritsch, J. Sambrook, *Molecular Cloning: A Laboratory Manual*, Cold Spring Harbor Laboratory, NY, **1982**, p. 545.

[24] C. Y. Lee, H.-W. Ryu, T.-S. Ko, *Bull. Korean Chem. Soc.* **2001**, *22*, 87 – 89.

[25] K. B. Garbutcheon-Singh, P. Leverett, S. Myers, J. R. Aldrich-Wright, *Dalton Trans.* **2013**, *42*, 918 – 926.

[26] S. M. Kelly, N. C. Price, *Curr. Protein Pept. Sci.* **2000**, *1*, 349 – 384.

[27] a) M. A. Ismail, K. J. Sanders, G. C. Fennell, H. C. Latham, P. Wormell, A. Rodger, *Biopolymers* **1998**, *46*, 127 – 143; b) F. H. Stootman, D. M. Fisher, A. Rodger, J. R. Aldrich-Wright, *Analyst* **2006**, *131*, 1145 – 1151.

[28] O. Stern, M. Volmer, *Phys. Z.* **1919**, *20*, 183 – 188.

[29] D. P. Heller, C. L. Greenstock, *Biophys. Chem.* **1994**, *50*, 305 – 312.

[30] a) W. C. Tse, D. L. Boger, *Acc. Chem. Res.* **2004**, *37*, 61 – 69; b) B. K. S. Yeung, W. C. Tse, D. L. Boger, *Bioorg. Med. Chem. Lett.* **2003**, *13*, 3801 – 3804; c) S. P. Sau, P. Kumar, P. K. Sharma, P. J. Hrdlicka, *Nucleic Acids Res.* **2012**, *40*, e162.

[31] a) A. J. Miles, S. V. Hoffmann, Y. Tao, R. W. Janes, B. A. Wallace, *Spectroscopy* **2007**, *21*, 245 – 255; b) A. J. Miles, R. W. Janes, A. Brown, D. T. Clarke, J. C. Sutherland, Y. Tao, B. A. Wallace, S. V. Hoffmann, *J. Synchrotron Radiat.* **2008**, *15*, 420 – 422.

[32] M. Tarleton, J. Gilbert, M. J. Robertson, A. McCluskey, J. A. Sakoff, *MedChemComm* **2011**, *2*, 31 – 37.

Received: March 15, 2016
Published online on May 24, 2016

Journal of Inorganic Biochemistry 165 (2016) 92–99

Contents lists available at ScienceDirect

Journal of Inorganic Biochemistry

journal homepage: www.elsevier.com/locate/jinorgbio

Investigating the cytotoxicity of platinum(II) complexes incorporating bidentate pyridyl-1,2,3-triazole "click" ligands

Benjamin J. Pages [a], Jennette Sakoff [b], Jayne Gilbert [b], Yingjie Zhang [c], Feng Li [a], Dan Preston [d], James D. Crowley [d], Janice R. Aldrich-Wright [a,*]

[a] Nanoscale Organisation and Dynamics Group, Western Sydney University, Campbelltown, NSW 2560, Australia
[b] Calvary Mater Newcastle, Waratah, NSW 2298, Australia
[c] Australian Nuclear Science and Technology Organisation, Locked Bag 2001, Kirrawee DC, NSW 2232, Australia
[d] Department of Chemistry, University of Otago, P.O. Box 56, Dunedin 9054, New Zealand

ARTICLE INFO

Article history:
Received 3 March 2016
Received in revised form 16 May 2016
Accepted 14 June 2016
Available online 15 June 2016

Keywords:
Platinum
Click
Triazole
Cell growth inhibition
X-ray crystal structure

ABSTRACT

Six platinum(II) complexes of the type $[Pt(P_L)(A_L)]^{2+}$, where P_L is a bidentate pyridyl-1,2,3-triazole "click" ligand and A_L is the *R*,*R* or *S*,*S* isomer of 1.2-diaminocyclohexane, have been synthesised and characterised by several methods including elemental microanalysis, proton NMR spectroscopy and X-ray crystallography. The *in vitro* cytotoxicity of each complex was assessed in eleven cell lines, revealing moderate to good activity for complexes incorporating 2-(1-phenyl-1H-1,2,3-triazol-4-yl)pyridine.

1. Introduction

The study of anticancer metal complexes that can overcome the toxicity and resistance limitations of current agents such as cisplatin continues to be a developing field. Many complexes have been identified with different biological behaviour to cisplatin yet also demonstrate equivalent or higher potential to kill cancerous cells [1–5]. Platinum complexes (PCs) continue to be at the forefront of this field; our group is focused upon compounds of the type $[Pt(P_L)(A_L)]^{2+}$, where P_L is one of several polyaromatic heterocyclic ligands such as 2,2′-bipyridine (bpy), 1,10-phenanthroline (phen) or dipyrido[3,2-*f*:2′,3′-*h*]quinoxaline (dpq), and A_L is one of several chiral diamines such as diaminocyclohexane (dach) [6–8]. These PCs induce cell death in a different way to cisplatin, partly due to non-covalent binding interactions [9,10], and exhibit cytotoxicity at concentrations as low as 7 nM in a variety of cell lines [11]. In a previous report on the potential of ligands with wider polyaromatic surface than our typical archetypes of 1,10-phenanthroline, 2-(2-pyridyl)quinoxaline (2pq) was incorporated as a P_L to synthesise complexes with the potential for novel activity [8]. Unexpectedly, the conformation of the coordinated 2pq ligand resulted in PCs that were unstable in solution and inactive in cancerous cell lines. Here we have successfully synthesised PCs that incorporate atypical P_Ls with no stability issues. The PCs incorporate 2-(1-phenyl-1H-1,2,3-triazol-4-yl)pyridine (phpytri), 2-(1-benzyl-1H-1,2,3-triazol-4-yl)pyridine (bnpytri), or 2-(1-octyl-1H-1,2,3-triazol-4-yl)pyridine (octpytri) as the P_L and 1*S*,2*S*-diaminocyclohexane (*SS*-dach) or 1*R*,2*R*-diaminocyclohexane (*RR*-dach) as the A_L (Fig. 1).

These pyridyl-1,2,3-triazole (R-pytri) ligands have recently emerged as readily functionalised analogues of the common bidentate chelators bpy and phen. The utility of the copper(I) catalysed azide alkyne "click" reaction has allowed for a diverse variety of R-pytri ligands such as the ones in this study [12–14], and the corresponding metal complexes have been synthesised and examined in a range of applications [15–17]. In particular there is a growing interest in using functionalised R-pytri ligands for the development of metal complexes for biomedical purposes. A number of authors have coordinated inert octahedral ions such as Re(I) [18–28], Tc(I) [19,26,27], Ru(II) [29] and Ir(III) [29–31] to functionalised R-pytri ligands and exploited the resulting complexes as infrared, luminescent and radiolabelled bioprobes. Additionally, some of these octahedral R-pytri complexes have displayed respectable cytotoxicity [21,24,25,27,31,32]. Square planar

Abbreviations: 2pq, 2-(2-pyridyl)quinoxaline; bnpytri, 2-(1-benzyl-1H-1,2,3-triazol-4-yl)pyridine; bpy, 2,2′-bipyridine; dach, diaminocyclohexane; DMEM, Dulbecco's modified Eagle's medium; dpq, dipyrido[3,2-*f*:2′,3′-*h*]quinoxaline; HMQC, heteronuclear multiple quantum correlation; ESIMS, electrospray ionisation mass spectrometry; octpytri, 2-(1-octyl-1H-1,2,3-triazol-4-yl)pyridine; PC, platinum complex; phen, 1,10-phenanthronline; phpytri, 2-(1-phenyl-1H-1,2,3-triazol-4-yl)pyridine; *R*-pytri, pyridyl-1,2,3-triazole; *RR*-dach, 1*R*,2*R*-diaminocyclohexane; *SS*-dach, 1*S*,2*S*-diaminocyclohexane.

* Corresponding author.
E-mail address: J.Aldrich-Wright@westernsydney.edu.au (J.R. Aldrich-Wright).

http://dx.doi.org/10.1016/j.jinorgbio.2016.06.017
0162-0134/

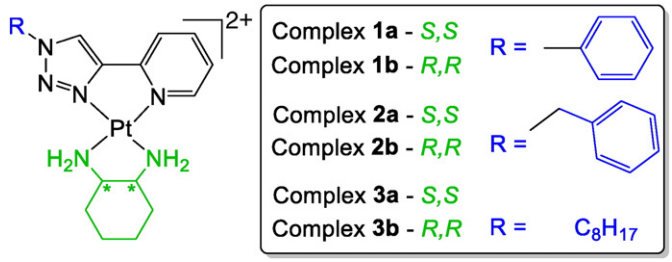

Fig. 1. General structure of complexes **1–3**. Counter-ions have been omitted for clarity, and * indicates a stereocentre, either *S* or *R*.

palladium and platinum chloride R-pytri complexes have also been reported to display moderate anticancer activity [33–35]. Some of us have examined the use of dimetallic R-pytri complexes as anti-bacterial [36,37] and anti-fungal [38] agents with modest success. Additionally, derivatives of the R-pytri ligands alone have demonstrated potent inhibition of NMRPTase [39] and macrophage migration inhibitory factor [40]. Herein, we show that combining the "click" ligands bnpytri, phpytri and octpytri with *SS*-dach and *RR*-dach ligands resulted in a series of new PCs with moderate anticancer activity.

2. Experimental section

2.1. Materials

The ligands phpytri, bnpytri and octpytri [41], and $[Pt(A_L)Cl_2]$ [6], where A_L is *SS*-dach or *RR*-dach, were prepared using previously reported methods. All purchased reagents were used as received and all solvents used were of analytical grade or higher. Methanol and acetone were obtained from Honeywell, while ethanol was obtained from Chem Supply. Sep-Pak® (20 cc, 2 g) columns were obtained from Waters. Deuterated solvents D_2O and DMSO-d_6 were obtained from Cambridge Isotope Laboratories.

2.2. Physical measurements

Characteristic NMR spectra were obtained using a 400 MHz Bruker Avance nuclear magnetic resonance spectrometer. All spectra were referenced internally to the solvent (either D_2O or DMSO-d_6) and obtained at room temperature. ^1H spectra were obtained using a spectral width of 15 ppm and 128 accumulations. ^1H-^{195}Pt heteronuclear multiple quantum correlation (HMQC) spectra were obtained using a spectral width of 2500 ppm and 256 data points for the ^{195}Pt nucleus (F1 dimension), and a spectral width of 12 ppm and 2048 data points for the ^1H nucleus (F2 dimension). The following abbreviations apply to spin multiplicity: s (singlet), bs (broad singlet), d (doublet), t (triplet), and m (multiplet). The chemical shift (parts per million) of each resonance was quoted as an approximate midpoint of its multiplicity.

Electronic spectra were obtained on a Cary 1E spectrophotometer at a wavelength range of 200–350 nm, using a 10 mm quartz cell. All spectra were recorded at room temperature and were automatically corrected for solvent baseline.

Circular dichroism spectra were recorded using a Jasco-810 spectropolarimeter at room temperature. The instrument was left to equilibrate for 30 min prior to use. Spectra were obtained in a 10 mm quartz cell, and were measured from 200 to 400 nm with a data pitch of 1 nm, bandwidth of 1 nm and response time of 1 s. For each spectrum, 40 accumulations were collected and a water baseline was subtracted.

Positive-mode electrospray ionisation mass spectrometry (ESIMS) experiments were performed using a Waters TQ-MS triple quadrupole mass spectrometer fitted with an ESI source. Spectra were recorded in positive ion mode from analyte solutions injected (10 μL) into 0.1% formic acid in 50% aqueous methanol flowing at 0.1 mL min^{-1}. A capillary voltage of 3.0 kV, cone voltage of 30 V, desolvation temperature of 300 °C and desolvation flow rate (nitrogen) of 500 L h^{-1} were employed. Spectra were collected over 1 min with an *m/z* range of 100–1000.

Microelemental analysis (C, H and N) was performed at the Chemical Analysis Facility, Department of Chemistry and Biomolecular Sciences, Macquarie University. An Elemental Analyser, Model PE2400 CHNS/O produced by PerkinElmer, USA, was used.

2.3. Synthesis of $[Pt(P_L)(A_L)]^{2+}$

Using the previously established method [7], the complex $[Pt(A_L)Cl_2]$ (1 equiv), where A_L is either *SS*-dach or *RR*-dach, was suspended in water with the P_L (1.1 equiv) and refluxed for 24 h, resulting in a clear solution. The solution volume was reduced to approximately 3 mL and filtered. A Sep-Pak® (20 cc, 2 g) column was activated with methanol (10 mL) followed by water (20 mL). The complex solution was loaded onto the column and eluted with water. The fractions containing product were combined, reduced under pressure and lyophilised to produce a solid white product. Yield and characterisation data are presented in Table 1, while NMR chemical shifts are presented in Table 2.

2.4. X-ray crystallography

Crystals of complex **2a** were obtained *via* slow diffusion of acetone into a concentrated solution of **2a** in water. Single Crystal data for **2a** was collected at 100 K on the MX1 beamline at the Australian Synchrotron with an energy equivalent to Mo-Kα radiation (17.4 keV, λ =

Table 1
Summary of the characterisation data of complexes **1–3**.

No.	Molecular formula	Yield (%)	ESI-MS (*m/z*) $[M-H]^+$ Calc.(found)	Microanalysis Calc.(found)			UV/λ_{max} (nm) (ε/$mol^{-1}\cdot dm^3$ cm^{-1})	CD/λ_{max} (nm) (CD/mdeg. $L\cdot mol^{-1}$)
				C	H	N	$\times 10^2$	$\times 10^{-1}$
1a	$[Pt(phpytri)(SS\text{-dach})]Cl_2\cdot 4H_2O$	75	530.2 (530.2)	33.83 (33.96)	4.78 (4.74)	12.46 (12.48)	260 (205), 235 (245)	325 (5), 283 (−11), 246 (−11), 220 (15)
1b	$[Pt(phpytri)(RR\text{-dach})]Cl_2\cdot 4H_2O$	79	530.2 (530.4)	33.83 (34.06)	4.78 (4.82)	12.46 (12.57)	259 (200), 235 (240)	327 (−5), 279 (16), 245 (17), 215 (−11)
2a	$[Pt(bnpytri)(SS\text{-dach})]Cl_2\cdot 3.5H_2O$	76	544.2 (544.4)	35.35 (35.19)	4.90 (4.86)	12.37 (12.21)	292 (95), 230 (260)	323 (6), 288 (−7), 244 (−17), 219 (17),
2b	$[Pt(bnpytri)(RR\text{-dach})]Cl_2\cdot 3.5H_2O$	68	544.2 (544.3)	35.35 (35.15)	4.90 (4.89)	12.37 (12.39)	292 (90), 230 (250)	323 (−6), 288 (11), 244 (18), 222 (−18)
3a	$[Pt(octpytri)(SS\text{-dach})]Cl_2\cdot 4H_2O$	68	567.2 (567.1)	35.49 (35.79)	6.24 (6.14)	11.83 (11.85)	292 (85), 230 (220)	328 (4), 290 (−9), 246 (−16), 224 (14)
3b	$[Pt(octpytri)(RR\text{-dach})]Cl_2\cdot 4.5H_2O$	69	567.2 (567.2)	35.05 (35.16)	6.30 (6.39)	11.68 (11.64)	292 (85), 230 (225)	324 (−4), 291 (13), 245 (20), 222 (−11)

Table 2
Summary of the proton and platinum NMR chemical shifts (ppm) of complexes **1–3** in D_2O.

Type	Label	**1a**	**1b**	**2a**	**2b**	**3a**	**3b**
Pyridyl-triazole	H3	8.10 (1H, d, $J = 7.9$ Hz)	8.04 (1H, d, $J = 8.0$ Hz)	7.97 (1H, d, $J = 7.9$ Hz)	7.99 (1H, d, $J = 8.0$ Hz)	8.04 (1H, d, $J = 7.8$ Hz)	8.04 (1H, d, $J = 7.9$ Hz)
	H4	8.30 (1H, t, $J = 7.9$ Hz)	8.22 (1H, t, $J = 7.8$ Hz)	8.22 (1H, t, $J = 7.9$ Hz)	8.23 (1H, t, $J = 7.5$ Hz)	8.25 (1H, td, $J = 1.2, 7.9$ Hz)	8.25 (1H, td, $J = 1.1, 7.9$ Hz)
	H5	7.64 (1H, t, $J = 7.3$ Hz)	7.54 (1H, m)	7.56 (1H, t, $J = 7.0$ Hz)	7.57 (1H, t, $J = 6.9$ Hz)	7.57 (1H, t, $J = 6.8$ Hz)	7.58 (1H, t, $J = 6.8$ Hz)
	H6	8.52 (1H, d, $J = 5.7$ Hz)	8.45 (1H, d, $J = 5.5$ Hz)	8.48 (1H, d, $J = 5.7$ Hz)	8.48 (1H, d, $J = 5.8$ Hz)	8.48 (1H, d, $J = 5.7$ Hz)	8.49 (1H, d, $J = 5.6$ Hz)
	H^T	9.27 (1H, s)	9.18 (1H, s)	8.72 (1H, s)	8.72 (1H, s)	8.75 (1H, s)	8.75 (1H, s)
Hexane ring	H1″	2.63 (2H, m)	2.54 (2H, m)	2.59 (2H, m)	2.58 (2H, m)	2.58 (2H, m)	2.59 (2H, m)
	$H2''_{eq}$	2.17 (2H, t, $J = 10.2$ Hz)	2.07 (2H, t, $J = 11.5$ Hz)	2.13 (2H, t, $J = 13.3$ Hz)	2.13 (2H, t, $J = 13.2$ Hz)	2.13 (2H, t, $J = 11.9$ Hz)	2.14 (2H, t, $J = 11.7$ Hz)
	$H3''_{eq}$	1.63 (2H, d, $J = 7.1$ Hz)	1.53 (2H, d, $J = 6.9$ Hz)	1.60 (2H, d, $J = 7.0$ Hz)	1.60 (2H, d, $J = 6.8$ Hz)	1.60 (2H, d, $J = 6.6$ Hz)	1.61 (2H, d, $J = 6.8$ Hz)
	$H2''_{ax}$	1.44 (2H, m)	1.33 (2H, m)	1.39 (2H, m)	1.38 (2H, m)	1.39 (2H, m)	1.39 (2H, m)
	$H3''_{ax}$	1.20 (2H, m)	1.11 (2H, m)	1.18 (2H, m)	1.17 (2H, m)	1.19 (2H, m)	1.19 (2H, m)
Benzyl or phenyl	H^M	–	–	5.68 (2H, s)	5.71 (2H, s)	–	–
	H2′–H6′	–	–	7.40 (5H, m)	7.42 (5H, m)	–	–
	H2′/H6′	7.80 (2H, d, $J = 7.3$ Hz)	7.74 (2H, d, $J = 7.3$ Hz)	–	–	–	–
	H3′–H5′	7.54 (3H, m)	7.52 (3H, m)	–	–	–	–
Octyl chain	H1′	–	–	–	–	4.52 (2H, t, $J = 7.0$ Hz)	4.52 (2H, t, $J = 7.0$ Hz)
	H2′	–	–	–	–	1.93 (m, 2H)	1.93 (m, 2H)
	H3′–H4′	–	–	–	–	1.26 (m, 4H)	1.26 (m, 4H)
	H5′–H7′	–	–	–	–	1.19 (m, 6H)	1.19 (m, 6H)
	H8′	–	–	–	–	0.76 (3H, t, $J = 6.8$ Hz)	0.77 (3H, t, $J = 6.7$ Hz)
Pt	$^1H/^{195}Pt$	8.61/−2865.4	8.63/−2870.0	8.56/−2875.7	8.57/−2877.8	8.57/−2878.8	8.57/−2878.8

0.7108 Å). Data collection was controlled using the BluIce software package [42]. Data indexing and integration were conducted using the program XDS [43]. The structure was solved by direct methods using SHELXT [44,45] and refined with SHELXL-2014 [46,47] using $Olex^2$ as an interface [48]. All non-hydrogen atoms were located on the electron density map and refined with anisotropic displacement parameters. Hydrogen atoms attached to carbon, nitrogen and oxygen atoms of the water molecules were placed in calculated positions and refined using a riding model. Crystallographic refinement details are summarised in Table 3. CCDC 1455173 contains the supplementary crystallographic data for **2a**. These data can be obtained free of charge *via* http://www.ccdc.cam.ac.uk/conts/retrieving.html, or from the Cambridge Crystallographic Data Centre, 12 Union Road, Cambridge CB2 1EZ, UK; fax: (+44) 1223-336-033; or e-mail: deposit@ccdc.cam.ac.uk.

Table 3
Crystallographic data and structure refinement details for complex **2a**.

Parameters	Values
Empirical formula	$C_{20}H_{34}Cl_2N_6O_4Pt$
Formula weight	688.52
Temperature/K	100(2)
Crystal system	orthorhombic
Space group	$P2_12_12_1$
a/Å	7.1930(14)
b/Å	12.992(3)
c/Å	27.096(5)
Volume/Å^3	2532.2(9)
Z	4
ρ_{calc}/mg mm^{-3}	1.806
μ/mm^{-1}	5.790
$F(000)$	1360.0
Crystal size/mm	0.025 × 0.005 × 0.005
2Θ range for data collection/°	4.344 to 55.858
Index ranges	$-9 \le h \le 9, -17 \le k \le 17, -35 \le l \le 35$
Reflections collected	41,225
Independent reflections	6021 [$R_{int} = 0.0371$, $R_{sigma} = 0.0205$]
Data/restraints/parameters	6021/0/311
Goodness-of-fit on F^2	1.091
Final R indexes [$I >= 2\sigma(I)$]	$R_1 = 0.0206$, w$R_2 = 0.0503$
Final R indexes [all data]	$R_1 = 0.0211$, w$R_2 = 0.0505$
Largest diff. peak/hole/e Å^{-3}	0.67/−0.74
Flack parameter	0.002(2)

2.5. In vitro cytotoxicity

Cytotoxicity assays were performed at the Calvary Mater Newcastle Hospital, Waratah, NSW, Australia. The cell lines tested were HT29 colon carcinoma, U87 human glioblastoma, MCF-7 breast cancer, A2780 ovarian cancer, H460 lung cancer, A431 skin cancer, Du145 prostate cancer, SJ-G2 glioblastoma, MIA pancreas cancer, SMA murine glioblastoma and the non-tumour derived MCF10A breast line. All test agents were prepared as 30 mM stock solutions in water and stored at −20 °C. All cell lines were cultured in a humidified atmosphere 5% CO_2 at 37 °C. The cancer cell lines were maintained in Dulbecco's modified Eagle's medium (DMEM) (Trace Biosciences, Australia) supplemented with 10% foetal bovine serum, 10 mM sodium bicarbonate penicillin (100 IU mL^{-1}), streptomycin (100 μg mL^{-1}), and glutamine (4 mM). The non-cancer MCF10A cell line was cultured in DMEM:F12 (1:1) cell culture media, 5% heat inactivated horse serum, supplemented with penicillin (50 IU mL^{-1}), streptomycin (50 μg mL^{-1}), 20 mM Hepes, L-glutamine (2 mM), epidermal growth factor (20 ng mL^{-1}), hydrocortisone (500 ng mL^{-1}), cholera toxin (100 ng mL^{-1}), and insulin (10 μg mL^{-1}). Cytotoxicity was determined by plating cells in duplicate in 100 mL medium at a density of 2500–4000 cells per well in 96 well plates. On day 0, (24 h after plating) when the cells were in logarithmic growth, 100 μL medium with or without the test agent was added to each well. After 72 h compound exposure growth inhibitory effects were evaluated using the MTT (3-[4,5-dimethyltiazol-2-yl]-2,5-diphenyl-tetrazolium bromide) assay and absorbance read at 540 nm. An eight point dose response curve was produced from which the IC_{50} value was calculated, representing the drug concentration at which cell growth was inhibited by 50% based on the difference between the optical density values on day 0 and those at the end of drug exposure [49].

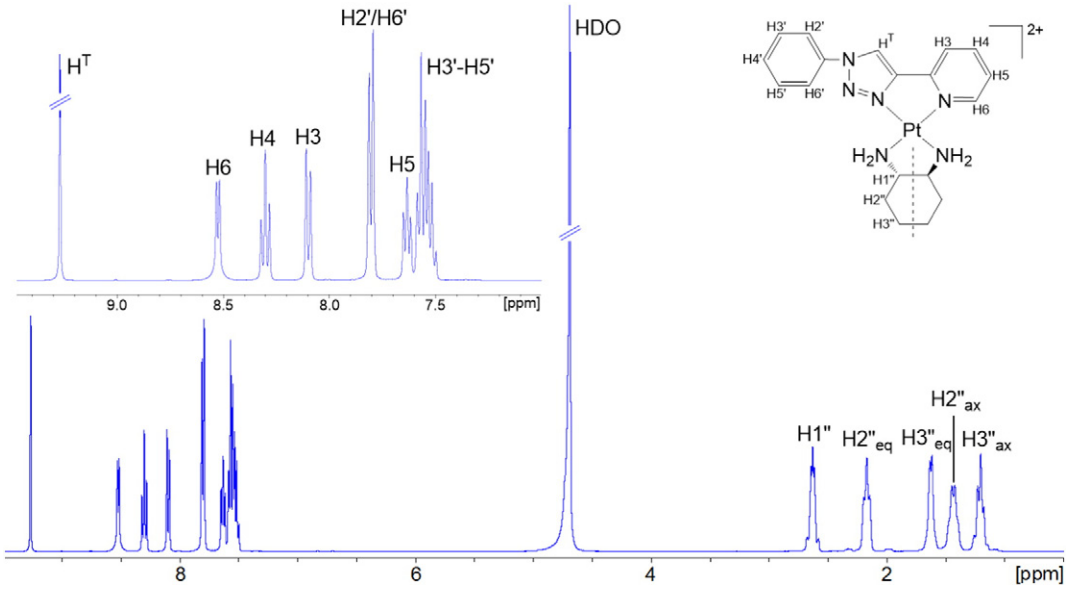

Fig. 2. ^{1}H NMR spectrum of complex **1a** in D_2O, showing proton assignment. Inset: enlarged view of the aromatic region. This spectrum is also representative of complex **1b**.

3. Results and discussion

3.1. Synthesis and characterisation

Synthesis of complexes **1–3** was accomplished through our established method for complexes of this type [8]. The only difference was in the Sep-Pak® purification step, in which approximately 200–300 mL of water were required to elute complexes **3a** and **3b**, rather than 50–100 mL; these complexes were retained on the column for much longer due to the octyl chain present on the P_L. NMR spectra, mass spectra and microanalytical data confirmed the identity and purity of each product. The electronic transitions in the UV spectra (Section S1) of **1–3** were comparable with those of similar bpy analogues, although they were blue-shifted relative to such complexes [8]. This phenomenon has been observed in other R-pytri metal complexes and is attributed to a higher-energy LUMO of R-pytri ligands relative to bpy [15]. Finally, the CD spectra of each complex confirmed that the chirality of the products was conserved during synthesis (Section S2).

3.2. NMR spectral assignment

Complexes **1–3** were characterised using one and two-dimensional ^{1}H NMR and ^{1}H-^{195}Pt HMQC NMR spectroscopy. The NMR spectra of complex **1a** will be used as an example. The proton spectrum of **1a** reveals several peaks in the aromatic region corresponding to the phpytri P_L (Fig. 2). The resonance at 9.27 ppm was assigned as the triazole proton (H^T) as it is the only proton of **1a** that would produce a singlet. The two doublets at 8.52 and 8.04 ppm were assigned H6 and H3, respectively, as the lower coupling constant of the 8.52 ppm resonance corresponds with the alpha-to-nitrogen position of H6 [50]. The H4 and H5 resonances were then assigned based upon the COSY spectrum of complex **1a** (Fig. S3.1.3). Finally, the doublet at 7.80 ppm and multiplet at 7.54 ppm were assigned to the phenyl substituent protons due to their relative integrals of two and three and their COSY coupling. H2′/H6′ was assigned to the higher ppm doublet as these two protons are in equivalent positions and are coupled to only one other proton each. Interestingly, the H^T proton of complexes **1a**, **1b**, **3a** and **3b** were

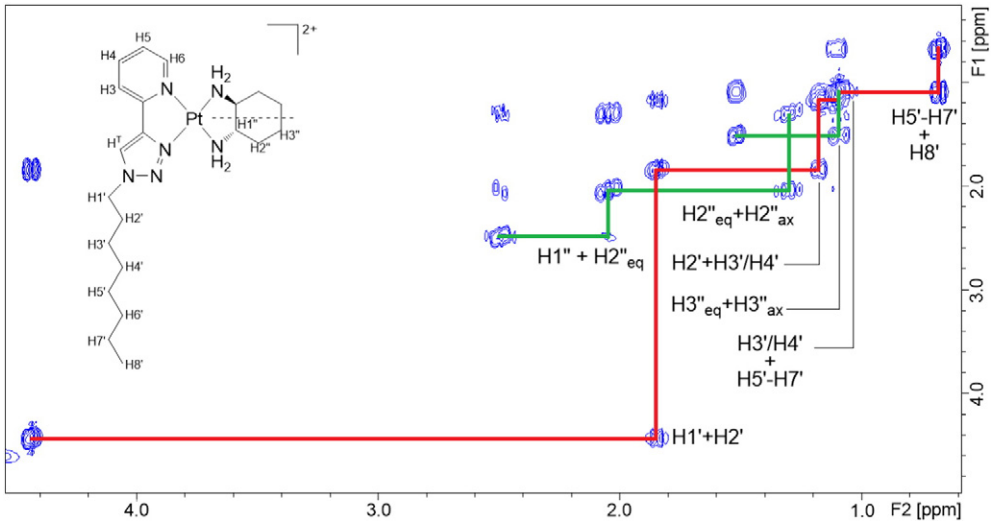

Fig. 3. The aliphatic region of the COSY NMR spectrum of complex **3a**, showing cross-peak assignment. The octyl chain and *SS*-dach peaks are represented by green and red lines, respectively. This spectrum is also representative of complex **3b**.

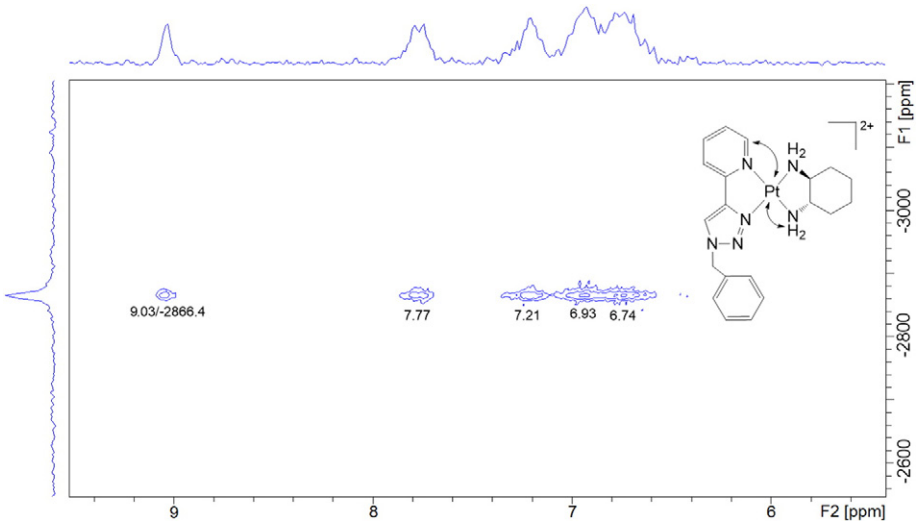

Fig. 4. The ^{1}H-^{195}Pt HMQC spectrum of complex **2a** in DMSO-d_6, showing cross peak assignment of the platinum centre and proton resonances. This is also representative of complex **2b**.

found to exchange in D_2O (Fig. S3.1.1); the proton is likely to be acidic due to its proximity of the proton to the triazole nitrogens, as well as the conjugated and large alkyl substituents, respectively.

The aliphatic proton region was assigned to the *SS*-dach or *RR*-dach protons, consistent with previous works [7,8]. The lower symmetry of the P_L in complexes **1–3** resulted in some minor splitting of the dach resonances, although it was not to the same extent as previously synthesised low symmetry complexes (Fig. S3.1.2) [8]. The most obvious example of splitting was the amine resonances in the DMSO-d_6 spectra; three or four amine peaks were observed rather than the usual two (Figs. S3.1.4, 8, 12). Assignment of the other complexes in this study was achieved in the same way with some minor differences. In the spectra of Complexes **2–3** (Figs. S3.1.6–S3.1.13), the H^T resonance was further upfield due to the lack of electron resonance delocalisation with the triazole ring, and for **2a** and **2b** there was a peak at ~5.7 ppm corresponding to the methylene linker protons (H^M) of the benzyl substituent. The aliphatic region of complexes **3a** and **3b** (Figs. S3.1.10 and S3.1.13) included the resonances of the octyl chain. Each of protons H1′ to H8′was assigned based upon the relative integral values, proximity to the triazole ring and COSY coupling pattern (Fig. 3).

Finally, to confirm the coordination of each ligand to the platinum centre, the ^{1}H-^{195}Pt NMR spectra of **1–3** were obtained in D_2O and DMSO-d_6. These spectra demonstrated a series of proton correlations with a platinum resonance at *ca.* −2800 to −2900 ppm. For example, the ^{1}H-^{195}Pt NMR spectrum of complex **2a** (Fig. 4) revealed a correlation between H6 and Pt at 9.03 ppm, as well as four correlations between the amine resonances and Pt at 7.77–6.74 ppm. Complexes **1a** and **1b** were only sparingly soluble in DMSO-d_6, and so a ^{1}H-^{195}Pt spectrum could not be obtained; however, the Pt chemical shift of ~2870 ppm in the D_2O spectrum is consistent with complexes **2–3**, confirming that the coordination sphere is the same. Additionally the Pt chemical shifts of **1–3** are close to similar complexes of dpq and bpy (*ca.* −2800 and −2786 ppm, respectively) [7,8].

To determine the stability of these complexes relative to the previously-synthesised 2pq complexes, complex **4** and [Pt(2pq)(*RR*-dach)]Cl_2 were each dissolved in DMSO-d_6 and their proton spectra

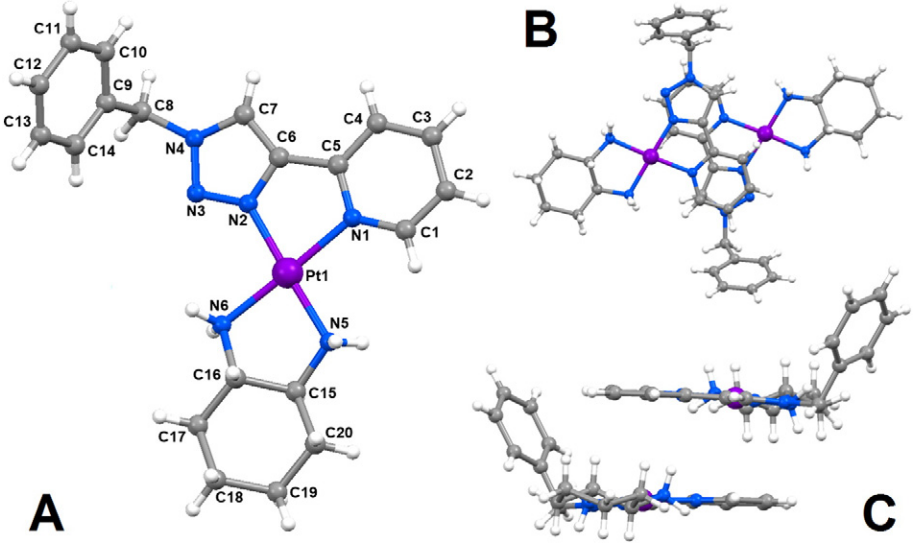

Fig. 5. X-ray crystal structure of [Pt(bnpytri)(*SS*-dach)]$Cl_2 \cdot 4H_2O$: the atom numbering system (A), and stacking views from a top-down (B) and side (C) view. Platinum centres are shown in purple, nitrogens in green, carbon in grey and hydrogens in white. Chloride counter-ions and waters of hydration have been removed for clarity.

Table 4
Selected bond lengths, angles and torsion angles for [Pt(bnpytri)(*SS*-dach)]$Cl_2 \cdot 4H_2O$ as determined by X-ray crystallography. Standard deviations are shown in parentheses.

Bond distances (Å)			
Pt1—N1	2.058(4)	Pt1—N5	2.038(4)
Pt1—N2	1.992(4)	Pt1—N6	2.040(4)
Bond angles and torsion angles (°)			
N1—Pt1—N2	79.6(2)	N5—Pt1—N6	83.5(2)
N1—Pt1—N5	99.0(2)	N2—Pt1—N6	98.0(2)
N1—Pt1—N6	177.0(2)	N2—Pt1—N5	177.7(2)
N1—C5—C6—N2	−2.0(6)	N5—C15—C16—N6	53.6(5)
N4—C8—C9	111.9(4)		

monitored for 12 h. Complex **4** showed no signs of degradation while [Pt(2pq)(*RR*-dach)]Cl_2 produced spectra demonstrating decomposition, both immediately and gradually over 12 h (Fig. S3.1.14). This indicates that the R-pytri PCs synthesised here are stabile relative to the previously synthesised 2pq complexes.

3.3. X-ray crystal structure of [Pt(bnpytri)(SS-dach)]$Cl_2 \cdot 4H_2O$

Complex **2a** crystallised in the orthorhombic space group $P2_12_12_1$ with four molecules in the unit. The PC consists of a square-planar platinum(II) centre with an N_4 coordination sphere (Fig. 5). The relevant bond lengths, bond angles and torsion angles are shown in Table 4. The N—Pt—N bond angles between the bnpytri and *SS*-dach ligand and the platinum centre were 79.6° and 83.5°, respectively. **2a** is relatively planar, with cross-ligand N—Pt—N angles of 177° and 177.7°. The average Pt—N bond length for the bnpytri ligand was 2.025 Å, and for *SS*-dach it was 2.039 Å. As has been observed in related R-pytri complexes [51–53], the N_{tri}—Pt bond length (1.992(4) Å) was slightly shorter than the N_{py}—Pt (2.058(4) Å, Table 4). The N—C—C—N torsion angle for bnpytri was −2.0°, indicating there was little distortion of the ligand upon coordination to platinum. The ligand was planar, aside from the benzyl substituent, which was projected from the triazole moiety at an N—C—C angle of 111.9°. The *SS*-dach torsion angle was 53.6°, which is typical of a puckered six-membered ring in the δ-conformation (stable chair). The positive sign of this angle confirms the chirality as *S*,*S*. These lengths and angles of **2a** are consistent with similar complexes of dpq and bpy [7,8]. The stacking pattern of **2a** is of interest, as bnpytri ligands aligned themselves so that their pyridyl and triazole moieties were overlapping, with the benzyl substituents aligning in the same direction (Fig. 5). The distance separating the ligands was between 3.4 and 4.0 Å, indicating that the stacking is stabilised by π-π and hydrogen bonding interactions [54]. The amine groups of the *SS*-dach ligand form several hydrogen bonds with the solvent water molecules and chloride counter anions. Additionally, the acidic C—H triazole proton of the R-pytri ligands also interacts with one of the chloride counter anions *via* a hydrogen bonding interaction (C7—Cl1 3.609(6) Å, H7—Cl1 2.812 Å, C7—H7—Cl1 144.31°) [52]. The closest distance between the platinum(II) ions of adjacent complexes is 6.747(1) Å precluding the presence of any stabilising Pt—Pt interactions in the solid state [55].

3.4. In vitro cytotoxicity

The *in vitro* cytotoxicity of complexes **1–3** were tested in a panel of cell lines in order to determine their potential anticancer efficacy and to compare with previously studied polyaromatic PCs. Overall, **1–3** were the most active in HT29 and Du145 lines (Table 5), which have previously shown vulnerability to polyaromatic PCs [9]. However, contrary to previous trends, very little activity was observed in the majority of the other cell lines for complexes **2–3**. **1a** and **2a** were clearly the most active of the PCs studied here, as they were the only complexes that demonstrated sub-ten-micromolar IC_{50} values outside of HT29 and Du145. **1a** was by far the most effective, as it was the only complex to inhibit live cell growth complex completely in some cell lines (Fig. 6, Section S4). Despite this, a comparison of the activity of **1a** to the similarly-structured [Pt(2,2′-bipyridine)(*SS*-dach)]Cl_2 (**4a**, BPYSS), as well as the highly active [Pt(5,6-dimethyl-1.10-phenanthroline)(*SS*-dach)]Cl_2 (**5a**, 56MESS), its enantiomer (**5b**, 56MERR), and the clinically used cisplatin, oxaliplatin and carboplatin reveals low relative activity for a complex of this type (Table 5) [9]. The only instance in which **1a** was more effective than some other complexes was in the MIA pancreatic cancer cell line, with an IC_{50} of 1.4 ± 0.4 μM relative to **4a**'s 2.5 ± 0.1 μM. It is clear that the size, in particular the width, of the P_L has an effect on the activity of complexes **1–3**, as the general trend in activity

Table 5
Summary of the *in vitro* cytotoxicity of complexes **1**–**6** and **1′**–**6′** in several cell lines, expressed as an IC_{50} value with standard error (1 sig. fig.). IC_{50} is the concentration at which cell growth is inhibited by 50% over 72 h.

IC_{50} (μM)											
Complex		HT29	U87	MCF-7	A2780	H460	A431	Du145	SJ-G2	MIA	SMA	MCF10A
1a	PHPYSS	4.4 ± 0.3	>50	14 ± 2	4 ± 1	16 ± 1	19 ± 3	1.8 ± 0.5	22 ± 2	1.4 ± 0.4	2.3 ± 0.8	7.7 ± 0.8
1b	PHPYRR	4.7 ± 0.3	>50	20 ± 4	7 ± 3	34 ± 11	19 ± 1	8 ± 1	15 ± 6	13 ± 2	12 ± 4	21 ± 2
2a	BNPYSS	14 ± 1	>50	>50	38 ± 2	>50	>50	14 ± 5	37 ± 8	>50	36 ± 5	>50
2b	BNPYRR	22 ± 2	53 ± 3	38 ± 6	12.0 ± 0.3	46 ± 10	>50	17 ± 3	17 ± 2	20 ± 2	31 ± 3	>50
3a	OTPYSS	6.3 ± 0.7	>50	>50	>50	>50	>50	7 ± 4	>50	>50	7 ± 2	>50
3b	OTPYRR	6 ± 1	>50	>50	>50	>50	>50	13 ± 6	>50	>50	18 ± 11	>50
4a	BPYSS[a,b]	1.1 ± 0.2	4.0 ± 0.3	2.6 ± 0.2	2.6 ± 0.2	5 ± 2	3.1 ± 0.2	1.3 ± 0.4	1.8 ± 0.3	2.5 ± 0.1	3.1 ± 0.8	1.6 ± 0.3
5a	56MESS[a]	0.08 ± 0.06	0.08 ± 0.01	0.05 ± 0.02	0.030 ± 0.004	0.037 ± 0.009	0.05 ± 0.02	0.007 ± 0.002	0.07 ± 0.02	0.015 ± 0.002	0.032 ± 0.007	0.020 ± 0.005
5b	56MERR[a]	0.19 ± 0.00	2.20 ± 0.06	0.8 ± 0.1	1.1 ± 0.1	1.8 ± 0.2	0.93 ± 0.03	0.41 ± 0.04	2.2 ± 0.2	0.45 ± 0.006	1.6 ± 0.5	0.39 ± 0.01
	Cisplatin[a]	11 ± 2	3.8 ± 1.1	6.5 ± 0.8	1.0 ± 0.1	0.9 ± 0.2	2.4 ± 0.3	1.2 ± 0.1	0.4 ± 0.1	8 ± 1	1.2 ± 0.1	nd
	Oxaliplatin[a]	0.9 ± 0.2	1.8 ± 0.2	0.5 ± 0.1	0.16 ± 0.0	1.6 ± 0.1	4.1 ± 0.5	2.9 ± 0.4	3 ± 1	0.9 ± 0.2	1.4 ± 0.1	nd
	Carboplatin[a]	>50	>50	>50	9 ± 3	14 ± 1	24 ± 2	15 ± 1	5.7 ± 0.2	>50	14.3 ± 0.7	nd

[a] Quoted from ref. [9] and those within.
[b] Pre-screening determined that the *R*,*R* isomer of this complex was not active in most cell lines.

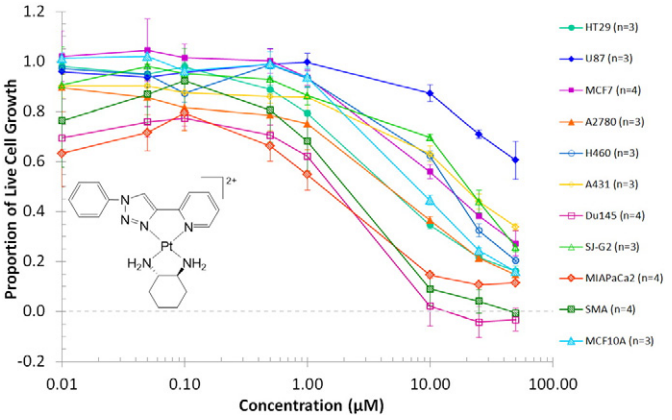

Fig. 6. Dose-response curves for *in vitro* cells treated with complex **1a**, including standard errors and number of repetitions.

was **1** > **2** > **3**. The hydrophobicity of complexes **1–3** may also influence their activity as it is inversely proportional to their cytotoxicity.

The typical trend of the *S,S*-isomer being more active than the *R,R*-isomer is not observed for complexes **2–3**, and it is in fact the opposite for **2a** and **2b**; this suggests that the intracellular mechanisms of **2–3** are very different from **4** to **5**, while there may be some similarities between the latter and complexes **1a** and **1b**. It is possible that the wider P_L of **2–3** is preventing them from binding to critical intracellular sites such as DNA base-pairs. **1a** and **1b**, having the smaller P_L of the synthesised complexes, may still be able to interact with some of the same targets as **4–5**, although this is not the case for all cancer cell types as evidenced by the lack of significant activity in U87, MCF-7, H460, A431 and SJ-G2. Overall, complexes **1a** and **1b** have demonstrated some potential as anticancer agents while **2–3** demonstrated very little activity relative to other polyaromatic PCs.

4. Conclusions

Six new platinum(II) anticancer agents incorporating bidentate pyridyl-1,2,3-triazole "click" ligands have been synthesised with good yields and characterised through several spectroscopic techniques, including X-ray crystallography. The *in vitro* cytotoxicity of complexes **1–3** was assessed in a panel of cell lines, revealing good efficacy against HT29 and Du145 cells with little activity observed elsewhere for **2–3**. Complexes **1a** and **1b** demonstrated low micromolar activity in many other cell lines including A2870 ovarian and MIA pancreatic cancers, suggesting that these phenyl substituted pyridyl-1,2,3-triazole PCs have some potential as anticancer compounds. Having identified a lead compound, we are now attempting to exploit the CuAAC "click" reaction to generate a family of structurally related phenyl substituted pyridyl-1,2,3 complexes that exhibit higher cytotoxicity.

Acknowledgments

We thank Western Sydney University and the Department of Chemistry, University of Otago for providing financial support through internal research grants. B.J.P. was supported by an Australian Postgraduate Award and a Western Sydney University Top-Up Award. D.P. thanks the University of Otago for a doctoral scholarship. The crystallographic data for complex **2a** were collected on the MX1 beamline at the Australian Synchrotron, Victoria, Australia, through a collaborative access program (AS161/MXCAP9733/10589). Lastly we thank the National Institutes of Health and National Cancer Institute for grant 1R13CA200223-01A1 (Conference Organization support, 1st International Symposium on Clinical and Experimental Metallodrugs in Medicine: Cancer Chemotherapy, CEMM).

Appendix A. Supplementary data

Supplementary data to this article can be found online at http://dx.doi.org/10.1016/j.jinorgbio.2016.06.017.

References

[1] E.J. Peterson, V.R. Menon, L. Gatti, R. Kipping, D. Dewasinghe, P. Perego, L.F. Povirk, N.P. Farrell, Mol. Pharm. 12 (2015) 287–297.
[2] A.K. Renfrew, N.S. Bryce, T. Hambley, Chem. Eur. J. 21 (2015) 15224–15234.
[3] A.J. Millett, A. Habtemariam, I. Romero-Canelón, G.J. Clarkson, P.J. Sadler, Organometallics 34 (2015) 2683–2694.
[4] C. Nardon, F. Chiara, L. Brustolin, A. Gambalunga, F. Ciscato, A. Rasola, A. Trevisan, D. Fregona, ChemistryOpen 4 (2015) 183–191.
[5] F. Liu, J. Suryadi, U. Bierbach, Chem. Res. Toxicol. 28 (2015) 2170–2178.
[6] N.J. Wheate, R.I. Taleb, A.M. Krause-Heuer, R.L. Cook, S. Wang, V.J. Higgins, J.R. Aldrich-Wright, Dalton Trans. (2007) 5055–5064.
[7] B.J. Pages, F. Li, P. Wormell, D.L. Ang, J.K. Clegg, C.J. Kepert, L.K. Spare, S. Danchaiwijit, J.R. Aldrich-Wright, Dalton Trans. 43 (2014) 15566–15575.
[8] B.J. Pages, Y. Zhang, F. Li, J. Sakoff, J. Gilbert, J.R. Aldrich-Wright, Eur. J. Inorg. Chem. 2015 (2015) 4167–4175.
[9] B.J. Pages, J. Sakoff, J. Gilbert, A. Rodger, N.P. Chmel, N.C. Jones, S.M. Kelly, D.L. Ang, J.R. Aldrich-Wright, Chem. Eur. J. 22 (2016) 8943–8954.
[10] K.B. Garbutcheon-Singh, S. Myers, B.W.J. Harper, N.S. Ng, Q. Dong, C. Xie, J.R. Aldrich-Wright, Metallomics 5 (2013) 1061–1067.
[11] F.J. Macias, K.M. Deo, B.J. Pages, P. Wormell, J.K. Clegg, Y. Zhang, F. Li, G. Zheng, J. Sakoff, J. Gilbert, J.R. Aldrich-Wright, Chem. Eur. J. 21 (2015) 16990–17001.
[12] V.V. Rostovtsev, L.G. Green, V.V. Fokin, K.B. Sharpless, Angew. Chem. Int. Ed. 41 (2002) 2596–2599.
[13] C.W. Tornoe, C. Christensen, M. Meldal, J. Org. Chem. 67 (2002) 3057–3064.
[14] L. Liang, D. Astruc, Coord. Chem. Rev. 255 (2011) 2933–2945.
[15] P.I.P. Elliott, Organometallic chemistry, R. Soc. Chem. 39 (2014) 1–25.
[16] C. Kluba, T. Mindt, Molecules 18 (2013) 3206.
[17] H. Struthers, T.L. Mindt, R. Schibli, Dalton Trans. 39 (2010) 675–696.
[18] A. Boulay, A. Seridi, C. Zedde, S. Ladeira, C. Picard, L. Maron, E. Benoist, Eur. J. Inorg. Chem. 2010 (2010) 5058–5062.
[19] A. Seridi, M. Wolff, A. Boulay, N. Saffon, Y. Coulais, C. Picard, B. Machura, E. Benoist, Inorg. Chem. Commun. 14 (2011) 238–242.
[20] S. Clede, F. Lambert, C. Sandt, Z. Gueroui, M. Refregiers, M.-A. Plamont, P. Dumas, A. Vessieres, C. Policar, Chem. Commun. 48 (2012) 7729–7731.
[21] R. Huang, G. Langille, R.K. Gill, C.M.J. Li, Y. Mikata, M.Q. Wong, D.T. Yapp, T. Storr, J. Biol. Inorg. Chem. 18 (2013) 831–844.
[22] E.C. Mattson, M. Unger, S. Clede, F. Lambert, C. Policar, A. Imtiaz, R. D'Souza, C.J. Hirschmugl, Analyst 138 (2013) 5610–5618.
[23] M. Wolff, L. Munoz, A. Francois, C. Carrayon, A. Seridi, N. Saffon, C. Picard, B. Machura, E. Benoist, Dalton Trans. 42 (2013) 7019–7031.
[24] H.C. Bertrand, S. Clede, R. Guillot, F. Lambert, C. Policar, Inorg. Chem. 53 (2014) 6204–6223.
[25] S. Clède, F. Lambert, R. Saint-Fort, M.-A. Plamont, H. Bertrand, A. Vessières, C. Policar, Chem. Eur. J. 20 (2014) 8714–8722.
[26] T.U. Connell, D.J. Hayne, U. Ackermann, H.J. Tochon-Danguy, J.M. White, P.S. Donnelly, J. Label. Compd. Radiopharm. 57 (2014) 262–269.
[27] A. Francois, C. Auzanneau, V. Le Morvan, C. Galaup, H.S. Godfrey, L. Marty, A. Boulay, M. Artigau, B. Mestre-Voegtle, N. Leygue, C. Picard, Y. Coulais, J. Robert, E. Benoist, Dalton Trans. 43 (2014) 439–450.
[28] S. Hostachy, J.M. Swiecicki, C. Sandt, N. Delsuc, C. Policar, Dalton Trans. 45 (2016) 2791–2795.
[29] T.U. Connell, J.L. James, A.R. White, P.S. Donnelly, Chem. Eur. J. 21 (2015) 14146–14155.
[30] A. Baschieri, S. Muzzioli, V. Fiorini, E. Matteucci, M. Massi, L. Sambri, S. Stagni, Organometallics 33 (2014) 6154–6164.
[31] S.C. Hockey, G.J. Barbante, P.S. Francis, J.M. Altimari, P. Yoganantharajah, Y. Gibert, L.C. Henderson, Eur. J. Med. Chem. 109 (2016) 305–313.
[32] J.A. Czaplewska, F. Theil, E. Altuntas, T. Niksch, M. Freesmeyer, B. Happ, D. Pretzel, H. Schaefer, M. Obata, S. Yano, U.S. Schubert, M. Gottschaldt, Eur. J. Inorg. Chem. 2014 (2014) 6290–6297.
[33] S. Deepthi, R. Trivedi, P. Sujitha, C. Kumar, B. Sridhar, S. Bhargava, J. Chem. Sci. 124 (2012) 1405–1413.
[34] S. Yano, H. Ohi, M. Ashizaki, M. Obata, Y. Mikata, R. Tanaka, T. Nishioka, I. Kinoshita, Y. Sugai, I. Okura, S.-i. Ogura, J.A. Czaplewska, M. Gottschaldt, U.S. Schubert, T. Funabiki, K. Morimoto, M. Nakai, Chem. Biodivers. 9 (2012) 1903–1915.
[35] S.B. Deepthi, R. Trivedi, L. Giribabu, P. Sujitha, C.G. Kumar, Inorg. Chim. Acta 416 (2014) 164–170.
[36] S.V. Kumar, W.K.C. Lo, H.J.L. Brooks, J.D. Crowley, Inorg. Chim. Acta 425 (2015) 1–6.
[37] S.V. Kumar, W.K.C. Lo, H.J.L. Brooks, L.R. Hanton, J.D. Crowley, Aust. J. Chem. (2015).
[38] S. Vellas, J. Lewis, M. Shankar, A. Sagatova, J. Tyndall, B. Monk, C. Fitchett, L. Hanton, J. Crowley, Molecules 18 (2013) 6383–6407.
[39] G. Colombano, C. Travelli, U. Galli, A. Caldarelli, M.G. Chini, P.L. Canonico, G. Sorba, G. Bifulco, G.C. Tron, A.A. Genazzani, J. Med. Chem. 53 (2010) 616–623.
[40] P. Dziedzic, J.A. Cisneros, M.J. Robertson, A.A. Hare, N.E. Danford, R.H.G. Baxter, W.L. Jorgensen, J. Am. Chem. Soc. 137 (2015) 2996–3003.
[41] J.D. Crowley, P.H. Bandeen, L.R. Hanton, Polyhedron 29 (2010) 70–83.

[42] T.M. McPhillips, S.E. McPhillips, H.J. Chiu, A.E. Cohen, A.M. Deacon, P.J. Ellis, E. Garman, A. Gonzalez, N.K. Sauter, R.P. Phizackerley, S.M. Soltis, P. Kuhn, J. Synchrotron Radiat. 9 (2002) 401–406.
[43] W. Kabsch, J. Appl. Crystallogr. 26 (1993) 795–800.
[44] G.M. Sheldrick, Acta Crystallogr. Sect. A: Found. Crystallogr. 64 (2008) 112–122.
[45] G.M. Sheldrick, SHELXS-2014, University of Göttingen, 2014.
[46] G.M. Sheldrick, Acta Crystallogr. Sect. C: Cryst. Struct. Commun. 71 (2015) 3–8.
[47] G.M. Sheldrick, SHELXL-2014, University of Göttingen, 2014.
[48] O.V. Dolomanov, L.J. Bourhis, R.J. Gildea, J.A.K. Howard, H. Puschmann, J. Appl. Crystallogr. 42 (2009) 339–341.
[49] M. Tarleton, J. Gilbert, M.J. Robertson, A. McCluskey, J.A. Sakoff, Med. Chem. Commun. 2 (2011) 31–37.
[50] R.M. Silverstein, F.X. Webster, Spectrometric Identification of Organic Compounds, sixth ed. Wiley, New York, USA, 1998.
[51] D. Schweinfurth, R. Pattacini, S. Strobel, B. Sarkar, Dalton Trans. (2009) 9291–9297.
[52] D. Schweinfurth, S. Strobel, B. Sarkar, Inorg. Chim. Acta 374 (2011) 253–260.
[53] W.K.C. Lo, G.S. Huff, J.R. Cubanski, A.D.W. Kennedy, C.J. McAdam, D.A. McMorran, K.C. Gordon, J.D. Crowley, Inorg. Chem. 54 (2015) 1572–1587.
[54] L.M. Salonen, M. Ellermann, F. Diederich, Angew. Chem. Int. Ed. 50 (2011) 4808–4842.
[55] L.H. Doerrer, Dalton Trans. 39 (2010) 3543–3553.

Dalton Transactions

PAPER

View Article Online
View Journal

Cite this: DOI: 10.1039/c7dt04108j

Combining the platinum(II) drug candidate kiteplatin with 1,10-phenanthroline analogues†

Benjamin J. Pages,[a] Jennette Sakoff,[b] Jayne Gilbert,[b] Yingjie Zhang,[c] Sharon M. Kelly,[d] James D. Hoeschele[e] and Janice R. Aldrich-Wright *[a]

Received 31st October 2017,
Accepted 27th November 2017

DOI: 10.1039/c7dt04108j

rsc.li/dalton

Platinum complexes of the type $[Pt(P_L)(A_L)]^{2+}$ where P_L is a derivative of 1,10-phenanthroline and A_L is *cis*-1,4-diaminocyclohexane (1,4-dach), have been synthesised and characterised by ultraviolet spectroscopy, elemental microanalysis, nuclear magnetic resonance and X-ray crystallography. The calf-thymus DNA binding affinity of these complexes was determined by isothermal titration calorimetry, revealing higher DNA affinity than their 1*S*,2*S*-diaminocyclohexane analogues. *In vitro* cytotoxicity was assessed in eleven human cell lines, revealing unexpectedly low activity for the 1,4-dach complexes.

1. Introduction

Cancer is a globally prominent disease in western civilisation; it is the second-highest cause of death and has a lifetime diagnostic rate of 40–50% in Australia and the USA.[1,2] Chemotherapy remains a widely-used treatment option, and large portion of treatment programs incorporate platinum drugs.[3,4] The globally approved drugs cisplatin, carboplatin and oxaliplatin are used in these programs; they kill cancerous cells by forming covalent adducts with DNA.[5] However, these drugs do have drawbacks; treatment results in toxic side effects such as nephrotoxicity, neurotoxicity and myelotoxicity, and there are many cancer types that they are not effective against.[3,6] These drawbacks have inspired the development of new platinum complexes (PCs) as chemotherapy agents; one example is the complex kiteplatin, which incorporates the ligand *cis*-1,4-diaminocyclohexane (1,4-dach) in the form $[Pt(1,4\text{-dach})Cl_2]$ (Fig. 1).[7] Kiteplatin is active against several cell lines that are resistant to cisplatin and oxaliplatin, and is at least as active as oxaliplatin against cells that are sensitive to current agents.[8] Part of the reason for this may be that the 1,2-GG intrastrand adducts formed by kiteplatin inhibit DNA polymerase more than the adducts formed by cisplatin.[9,10]

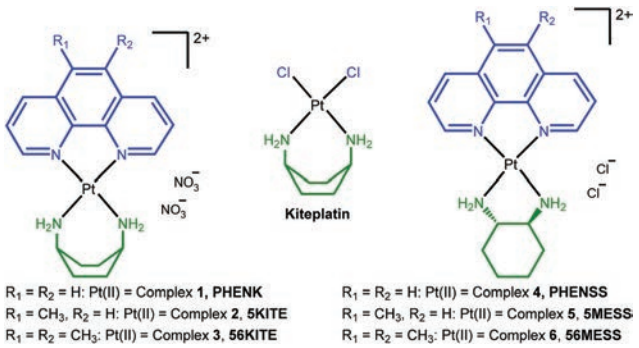

Fig. 1 Chemical structures of: 1,4-dach complexes **1–3** (left), 1,2-dach complexes **4–6** (right) and kiteplatin (middle).

Research into kiteplatin has recently resurged, with many labs investigating the DNA binding activity of kiteplatin and synthesising platinum(IV) derivatives to improve cytotoxicity.[11–17]

Another promising class of PC with potent activity against cisplatin-resistant cells are polyaromatic PCs; these incorporate a polyaromatic ligand (P_L), typically a 1,10-phenanthroline (phen) analogue, and a diamine ancillary ligand (A_L) in the form $[Pt(P_L)(A_L)]^{2+}$. The A_L is usually a 1,2-diaminocyclohexane (1,2-dach) analogue, either 1*S*, 2*S* (*SS*-dach) or 1*R*, 2*R* (*RR*-dach). These PCs are active against cisplatin-resistant cell lines,[18] induce cell death in cancerous cells by a caspase-independent mechanism,[18–20] and bind to DNA through non-covalent intercalation.[21] In particular, the lead complex [Pt(5,6-dimethyl-phen)(*SS*-dach)]Cl_2 (56MESS, Fig. 1) is up to 100 times more active than cisplatin in several cell lines, with nanomolar activity against L1210 murine leukaemia and Du145 prostate cancer cells.[21] These polyaromatic PCs and kiteplatin each have demonstrated great potential as platinum

[a]*Nanoscale Organisation and Dynamics Group, Western Sydney University, Campbelltown, NSW 2560, Australia. E-mail: J.Aldrich-Wright@westernsydney.edu.au*
[b]*Calvary Mater Newcastle, Waratah, NSW 2298, Australia*
[c]*Australian Nuclear Science and Technology Organisation, Locked Bag 2001, Kirrawee DC, NSW 2232, Australia*
[d]*Institute of Molecular, Cell and Systems Biology, College of Medical, Veterinary and Life Sciences, University of Glasgow, Glasgow, G128QQ, UK*
[e]*Department of Chemistry, Eastern Michigan University, Ypsilanti, MI 48197, USA*
† Electronic supplementary information (ESI) available. CCDC 1583091. For ESI and crystallographic data in CIF or other electronic format see DOI: 10.1039/c7dt04108j

drug candidates, due to their different cellular mechanisms and enhanced DNA repair inhibition, respectively, and due to their outperformance of cisplatin in several cell lines. These factors, in addition to kiteplatin's higher activity than that of [Pt(1*R*,2*R*-dach)Cl_2],[8] prompted the development of polyaromatic PCs incorporating 1,4-dach as an A_L and phen, 5-methylphen (5Mephen) and 5,6-dimethyl-phen (56Me_2phen) as a P_L (to produce complexes **1**, **2** and **3** respectively, Fig. 1). Here we present a comparative study between complexes **1–3** and their 1,2-dach analogues (including PHENSS, complex **4**, 5MESS, complex **5** and 56MESS, complex **6**, Fig. 1) in terms of calf-thymus DNA (CT-DNA) binding by isothermal titration calorimetry (ITC) and *in vitro* cytotoxicity in a panel of human cancer cell lines.

2. Experimental section

2.1. Materials

[Pt(1,4-dach)Cl_2] (Kiteplatin) was synthesised *via* previously reported methods.[22] All purchased reagents were used as received and all solvents used were of analytical grade or higher. Silver nitrate was obtained from BDH chemicals. Dimethyl formamide (DMF) was obtained from Merck. Phen, 5Mephen, 56Me_2phen, dipotassium hydrogen phosphate, potassium dihydrogen phosphate, sodium chloride and CT-DNA were obtained from Sigma-Aldrich. Methanol was obtained from Chem Supply. Deuterium oxide (D_2O) was obtained from Cambridge Isotope Laboratories.

2.2. Characterisation measurements

NMR spectra were obtained using a 400 MHz Bruker Avance nuclear magnetic resonance spectrometer. All spectra were referenced internally to D_2O and were obtained at room temperature. ^{1}H spectra were obtained using a spectral width of 15 ppm and 128 accumulations. ^{1}H–^{195}Pt heteronuclear multiple quantum correlation (HMQC) spectra were obtained using a spectral width of 2500 ppm and 256 data points for the ^{195}Pt nucleus (F1 dimension), and a spectral width of 12 ppm and 2048 data points for the ^{1}H nucleus (F2 dimension). The following abbreviations apply to spin multiplicity: s (singlet), bs (broad singlet), d (doublet), dd (doublet of doublets), pt (pseudotriplet), and m (multiplet). The chemical shift (parts per million) of each resonance were quoted as an approximate midpoint of their multiplicity.

Electronic spectra were obtained on a Cary 1E spectrophotometer at a wavelength range of 200–350 nm, using a 10 mm quartz cell. All spectra were recorded at room temperature and were automatically corrected for solvent baseline. Extinction coefficients were obtained through titration of 1 M solution of PC (10 μL) into 2400 μL of water.

Positive-mode electrospray ionisation mass spectrometry (ESIMS) experiments were performed using a Waters TQ-MS triple quadrupole mass spectrometer fitted with an ESI source. Spectra were recorded in positive ion mode from analyte solutions injected (10 μL) into 0.1% trifluoroacetic acid in 50% aqueous acetonitrile flowing at 0.1 mL min^{-1}. A capillary voltage of 1.6 kV, cone voltage of 25 V, desolvation temperature of 300 °C and desolvation flow rate (nitrogen) of 500 L h^{-1} were employed. Spectra were collected over one minute with an *m*/*z* range of 50–1000.

Microelemental analysis (C, H and N) was performed at the Chemical Analysis Facility, Department of Chemistry and Biomolecular Sciences, Macquarie University. An Elemental Analyser, Model PE2400 CHNS/O produced by PerkinElmer, USA, was used.

2.3. Synthesis of [Pt(P_L)(1,4-dach)]$^{2+}$

Using a modification of a previously established method,[23] kiteplatin (~60 mg, 1 equiv.) was dissolved in DMF (~4 mL). Silver nitrate (2 equiv.) was added and the solution stirred for 16 h at room temperature with light excluded. The resultant silver chloride precipitate was removed by centrifugation. P_L (2 equiv.) was added to the supernatant and the solution stirred for 16 h at 50 °C, again with light excluded. Another equivalent of P_L was then added and the solution stirred again without light for 16 h at 50 °C. The DMF solution was removed through rotary evaporation, the crude product suspended in water and this suspension was filtered. The filtrate was then added to a separatory funnel and washed twice with dichloromethane (20 mL each). The aqueous layer was reduced to a volume of approx. 2.5 mL through rotary evaporation. Purification was achieved through a Sep-Pak® (20 cc, 5 g) column connected to a pump apparatus with UV detector (Bio-Rad, EM-1 Econo™ UV Monitor). The column was activated with methanol (~15 mL) and then flushed with water (~40 mL) until absorbance had equilibrated. The crude product solution was then loaded onto the column and eluted with water at a flow rate of 1 mL min^{-1}. The product was collected, reduced in volume and the Sep-Pak® purification process repeated. Fractions were collected and their contents determined using ^{1}H NMR. The fractions containing product were combined, reduced under pressure and lyophilised to produce a pale yellow solid. Yield and characterisation data are presented in Table 1, while NMR chemical shifts are presented in Table 2.

2.4. X-ray crystallography

Single crystals of complex **1** were obtained by dissolving a sample in the minimum amount of hot water and allowing the solution to cool to room temperature. Single crystal data for **1** was collected on the MX1 beamline at the Australian Synchrotron using Si<111> monochromated synchrotron X-ray radiation (λ = 0.71074). Data collection was performed at 100(2) K using BlueIce software[24] and corrected for polarisation and Lorentz effects using XDS software.[25] The absorption correction was then applied to the data using SADABS.[26] The structure was solved with direct methods using SHELXT[27,28] and full-matrix least-squares refinement was performed using SHELXL-2014[27,29] *via* the Olex^2 interface.[30] Two diffractions affected by beam stops were removed in the final structure refinement. All non-hydrogen atoms with occupancies over 0.5 were located from the electron density map and were refined

Table 1 Summary of the characterisation data of complexes **1–3**

No	Molecular formula	Yield (%)	ESI-MS (m/z) $[M - H]^+$ calc. (found)	Microanalysis calc. (found) C	H	N	UV/λ_{max} (nm) (ε/mol^{-1} dm^3 cm^{-1}) × 10^2
1	[Pt(phen)(1,4-dach)] $(NO_3)_2 \cdot 0.25H_2O$	70	488.2 (487.8)	34.98 (34.84)	3.67 (3.44)	13.60 (13.53)	278 (280), 226 (345)
2	[Pt(5Mephen)(1,4-dach)]$(NO_3)_2 \cdot$ $1.5H_2O$	62	502.2 (501.9)	34.86 (34.96)	4.16 (3.76)	12.84 (12.96)	281 (330), 229 (405)
3	[Pt(56Me$_2$phen)(1,4-dach)] $(NO_3)_2 \cdot 1.5H_2O$	71	516.2 (515.8)	35.93 (35.91)	4.37 (3.97)	12.57 (12.59)	285 (340), 231 (450)

Table 2 Summary of the proton and platinum NMR chemical shifts (ppm) of complexes **1–3** and **1′–3′** in D_2O

Label	**1**	**2**	**3**
H4	8.87 (2H, d, J = 8.2 Hz)	8.73 (1H, d, J = 8.3 Hz)	8.86 (2H, d, J = 8.6 Hz)
H7	—	8.94 (1H, d, J = 8.5 Hz)	—
H2	8.72 (2H, d, J = 5.5 Hz)	8.63 (1H, d, J = 5.6 Hz)	8.61 (2H, d, J = 5.4 Hz)
H9	—	8.70 (1H, d, J = 5.6 Hz)	—
H5	8.11 (2H, s)	7.86 (1H, s)	—
H3	8.04 (2H, dd, J = 8.6, 5.6 Hz)	7.99 (1H, dd, J = 8.5, 5.5 Hz)	8.0 (2H, dd, J = 8.8, 5.5 Hz)
H8	—	8.06 (1H, dd, J = 8.5, 5.5 Hz)	—
CH_3	—	2.78 (3H, s)	2.56 (6H, s)
H1′	3.65 (2H, pt, $^3J_{Pt-H}$ = 87.0 Hz)	3.65 (2H, pt, $^3J_{Pt-H}$ = 84.1 Hz)	3.67 (2H, pt, $^3J_{Pt-H}$ = 76.8 Hz)
HA′	1.90 (4H, m)	1.90 (4H, m)	1.91 (4H, m)
HA′	1.79 (4H, m)	1.78 (4H, m)	1.79 (4H, m)
$^1H/^{195}Pt$	8.83, 2760	8.82, 2690	8.83, 2700

anisotropically. The disordered lattice water molecule was modelled and refined isotropically without added hydrogen atoms, causing a B-level alert in the checkCIF. Hydrogen atoms bound to carbon and nitrogen were added in ideal positions and refined using a riding model. Crystallographic refinement parameters are summarised in Table 3. Supplementary crystallographic data for **1** can be found under CCDC 1583091.†

2.5. Isothermal titration calorimetry – DNA binding

CT-DNA binding was assessed using a MicroCal ITC 200 calorimeter operating at 37 °C. Each platinum complex (564–750 μM) was titrated into a solution of CT-DNA (160 μM) in K_2HPO_4/KH_2PO_4 (10 mM, pH 7.0) and NaCl (50 mM) buffer. For a baseline, each PC was titrated into buffer alone, and this trace was subtracted from the PC-DNA binding trace. The titration program consisted of one 0.4 μL addition followed by 18 titrations of 2 μL, with a spacing of 180 s, reference power of 6 μcal s^{-1} and stirring speed of 750 rpm. Data was analysed using Origin 7.0 (MicroCal version) using 200 iterations of a one-site binding model, and binding constants were calculated using the following equations. Experiments were performed in duplicate for each PC.

$$\Delta G = -RT \ln K$$

$$\Delta S = \frac{\Delta H - \Delta G}{T}$$

Table 3 Crystallographic data and structure refinement details for complex **1**

Parameters	Values
Empirical formula	$C_{18}H_{22}N_6O_{7.25}Pt$
Formula weight	633.50
Temperature/K	100(2)
Crystal system	Monoclinic
Space group	$C2/c$
a/Å	13.864(3)
b/Å	25.762(5)
c/Å	6.5990(13)
β/°	110.57(3)
Volume/Å^3	2206.7(9)
Z	4
ρ_{calc}/mg mm^{-3}	1.907
μ/mm^{-1}	6.412
F(000)	1232
Crystal size/mm	0.12; 0.03; 0.03
2θ range for data collection/°	1.581 to 27.499°
Index ranges	$-18 \le h \le 18$, $-33 \le k \le 33$, $-8 \le l \le 8$
Reflections collected	17 054
Independent reflections	2471 [R_{int} = 0.0419, R_σ = 0.0211]
Data/restraints/parameters	2469/0/152
Goodness-of-fit on F^2	1.065
Final R indexes [$I \ge 2\sigma(I)$]	R_1 = 0.0380, wR_2 = 0.1066
Final R indexes [all data]	R_1 = 0.0384, wR_2 = 0.1070
Largest diff. peak/hole/e Å^{-3}	1.63/−2.24

2.6. *In vitro* cytotoxicity

Cytotoxicity assays were performed at the Calvary Mater Newcastle Hospital, Waratah, NSW, Australia. The cell lines tested were HT29 colon carcinoma, U87 glioblastoma, MCF-7

breast cancer, A2780 ovarian cancer, H460 lung cancer, A431 skin cancer, Du145 prostate cancer, BE2-C neuroblastoma, SJ-G2 glioblastoma, MIA pancreas cancer, and the non-tumour derived MCF10A breast line. All test agents were prepared as 30 mM stock solutions in water and stored at −20 °C. All cell lines were cultured in a humidified atmosphere 5% CO_2 at 37 °C. The cancer cell lines were maintained in Dulbecco's modified Eagle's medium (DMEM) (Trace Biosciences, Australia) supplemented with 10% foetal bovine serum, 10 mM sodium bicarbonate penicillin (100 IU mL^{-1}), streptomycin (100 μg mL^{-1}), and glutamine (4 mM). The non-cancer MCF10A cell line was cultured in DMEM : F12 (1 : 1) cell culture media, 5% heat inactivated horse serum, supplemented with penicillin (50 IU mL^{-1}), streptomycin (50 μg mL^{-1}), 20 mM Hepes, L-glutamine (2 mM), epidermal growth factor (20 ng mL^{-1}), hydrocortisone (500 ng mL^{-1}), cholera toxin (100 ng mL^{-1}), and insulin (10 μg mL^{-1}). Cytotoxicity was determined by plating cells in duplicate in 100 mL medium at a density of 2500–4000 cells per well in 96 well plates. On day 0, (24 h after plating) when the cells were in logarithmic growth, 100 μL medium with or without the test agent was added to each well. After 72 h drug exposure growth inhibitory effects were evaluated using the MTT (3-[4,5-dimethylthiazol-2-yl]-2,5-diphenyl-tetrazolium bromide) assay and absorbance read at 540 nm. An eight point dose response curve was produced from which the IC_{50} value was calculated, representing the drug concentration at which cell growth was inhibited by 50% based on the difference between the optical density values on day 0 and those at the end of drug exposure.

3. Results and discussion

3.1. Synthesis and characterisation

Synthesis of complexes **1–3** could not be achieved through the typical reflux used for complexes of this type.[31] NMR experiments suggested that much of the 1,4-dach was detached from the platinum centre, with only minor amounts of the final product formed. Instead, a gentler synthesis was undertaken to keep the 1,4-dach ligand coordinated. The addition of silver nitrate in DMF resulted in the conversion of [Pt(1,4-dach)Cl_2] to the intermediate [Pt(1,4-dach)$(DMF)_2$]$(NO_3)_2$; the leaving groups of this product are more labile, allowing the reaction with phen derivatives to take place at 50 °C rather than 100 °C. The phen addition was slow and incomplete with only one equivalent, and so two equivalents were used instead, with a third added the next day to ensure that as much of the product formed as possible. Scheme 1 summarises the synthesis process.

The filtering and DCM washes removed most of the excess P_L, while the column purification removed the rest. During Sep-Pak® purifications in our previous work, the [Pt(1,2-dach)Cl_2] intermediate typically eluted before the final product, with minor overlap of elution profiles. Here, the elution profile of the [Pt(1,4-dach)$(DMF)_2$]$(NO_3)_2$ intermediate overlapped with the product to a much greater extent. To maximise separation, the flow rate was set to 1 mL min^{-1}, which was the lowest

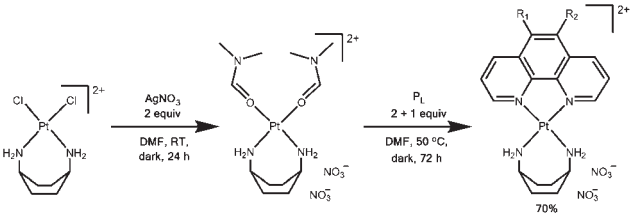

Scheme 1 General synthesis of complexes **1–3**. R_1 and R_2 are either H, CH_3, or a mixture of the two.

speed achievable without allowing diffusion to occur in the column. Even so, it typically took two runs through the column to separate most of the product from impurities. The gentler reaction conditions and difficult separation are thought to be the reasons for the relatively low yields of ~70% compared to the typical yields of 80–85% of similar complexes.[32,33] The identity and purity of these complexes was confirmed through NMR spectra, mass spectra and elemental analysis. The electronic transitions in the UV spectra (section S1†) of **1–3** were comparable with those of similar phen platinum(II) analogues;[33] the presence of methyl substituents on the phenanthroline resulted in a red-shift of each peak and the appearance of a shoulder in the peak at approx. 280 nm.

3.2. NMR spectral assignment

Characterisation of all complexes was achieved using ^1H NMR and ^1H–^{195}Pt HMQC NMR. The NMR spectra of complex **3** are shown as an example (Fig. 2 and 3). For all complexes, the aromatic region signals of the phen derivatives exhibited the expected chemical shifts and multiplicities as per previous studies.[33] In the aliphatic region, the 1,4-dach signals were similar to that of kiteplatin; the H1′ proton presented a pseudo triplet due to platinum satellites at 3.67 ppm, and the multiplets corresponding to the other aliphatic protons (HA′) were present from approx. 1.95–1.75 ppm. The amine protons

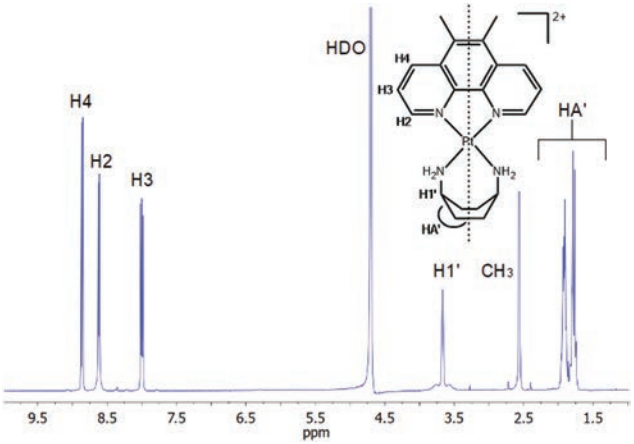

Fig. 2 ^1H NMR spectrum of complex **3** in D_2O, showing proton assignment. Inset: The structure of **1**, showing proton NMR number assignment. Amine protons are not present due to D_2O exchange.

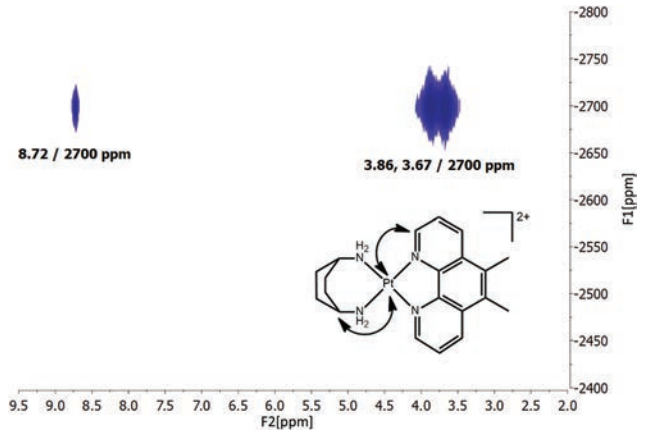

Fig. 3 The $^{1}H–^{195}Pt$ HMQC spectrum of complex **3** in D_2O, showing cross peak assignment of the platinum centre and proton resonances.

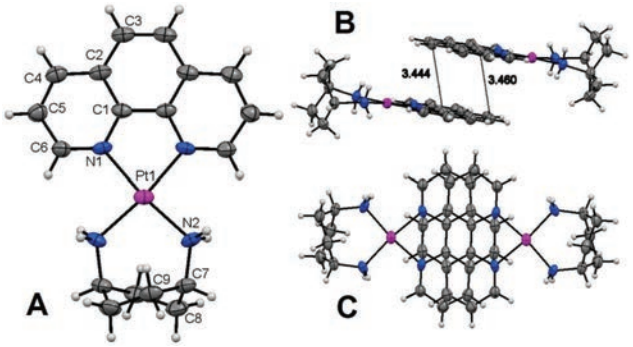

Fig. 4 Crystal structure of complex **1**: an ellipsoidal plot (probability 50%) showing the atom numbering system (A) and stacking views from a side (B) and top-down (C) perspective. Colour code: Pt in purple, N in blue, C in grey and H in white. Nitrate counter-ions and lattice water molecules have been omitted for clarity. Selected bond lengths (Å): Pt1–N1: 2.062(4), Pt1–N2: 2.072(4). Selected bond angles and torsion angles (°): N1–Pt1–N1: 81.7(2), N1–Pt1–N2: 172.6(2), N2–Pt1–N2: 96.3(3), Pt1–N2–C7: 125.6(4), N1–C1–C1–N1: 0.7(8).

were not present due to exchange with D_2O. To confirm the coordination of each ligand to the platinum centre, the $^{1}H–^{195}Pt$ NMR spectra of all complexes were obtained. These spectra demonstrated a series of proton correlations with a platinum resonance at approx. −2700 ppm. For example, the $^{1}H–^{195}Pt$ NMR spectrum of complex **3** (Fig. 3) revealed a correlation between the 56Me$_2$phen proton H2 and Pt at 8.72 ppm, as well as between the 1,4-dach proton H1′ and Pt at 3.86 and 3.67 ppm. The Pt chemical shifts of **1–3** were slightly higher than those reported for phen complexes of 1,2-dach (approx. −2800 ppm).[34] This kind of platinum peak difference was observed for complexes of 1,2-diaminocyclopentane (approx. −2550 ppm), which was attributed to the ring strain of the pentane.[33] This suggests that a similar phenomenon has occurred here with complexes **1–3**, although to a lesser extent, and demonstrates the sensitivity of the platinum nucleus to changes in chemical environment.[35]

3.3. X-ray crystal structure of complex 1

The crystal data and structural refinement details are summarised in Table 3 and selected bond lengths, angles and torsion angles are listed in the Fig. 4 caption. The asymmetric unit of **1** contains a half molecule and the full structure is generated by a two-fold symmetry expansion. The complex consists of a PtN_4 coordination sphere with a square-planar coordination geometry for the platinum metal centre (Fig. 4). The bond lengths and angles related to the phen ligand and platinum are consistent with the previously published polyaromatic PCs.[32,33] The 1,4-dach ligand adopted a twist-boat conformation similar to that seen in previous 1,4-dach complexes,[7,15,36] with a N2–Pt1–N2 bond angle of 96.3(3)° and Pt1–N2–C7 angle of 125.6(4)°. The N–Pt–N angle is approximately 13° larger than that of previous 1,2-dach complexes that adopt a chair conformation.[32,33] Relative to complexes of 1,2-dach, the large bite angle of the coordinated 1,4-dach ligand appears to have had no effect on the conformation of the opposing phen ligand. Adjacent phen ligands stack along the *c* axis, with carbon–carbon distances between 3.4–3.5 Å (Fig. 4B). This correlates with π–π interactions.[37]

3.4. DNA binding studies

The DNA binding of **1–3** was assessed to determine if there were any differences in affinity between the 1,4-dach complexes and those of *S*,*S*-dach (complexes **4–6**). **5a**, the nitrate salt of **5**, was also tested to determine if the counter-ion had any effect. The thermodynamic parameters of each PC-DNA interaction are summarised in Table 4, and the ITC trace of **3** is shown as an example (Fig. 5). Similar to previous experiments with **6**,[21] the binding of **1–3** with CT-DNA resulted in two peaks per titration rather than one, again suggesting that the binding was biphasic

Table 4 Isothermal titration calorimetry data for complexes **1–6** and **5a**

No	Complex	10^{-5} K [M^{-1}]	N	ΔH [kcal mol^{-1}]	$T\Delta S$ [kcal mol^{-1}]	ΔG [kcal mol^{-1}]
1[a]	PHENK	2.87 ± 0.04	0.257 ± 0.006	−2.5 ± 0.1	5.2 ± 0.1	−7.7 ± 0.1
2[a]	5KITE	6.2 ± 0.4	0.31 ± 0.01	−3.8 ± 0.1	4.2 ± 0.1	−8.1 ± 0.2
3[a]	56KITE	7.7 ± 0.8	0.325 ± 0.005	−6.0 ± 0.1	2.1 ± 0.2	−8.1 ± 0.2
4[b,c]	PHENSS	2.0 ± 0.3	0.27 ± 0.01	−3.7 ± 0.1	3.9 ± 0.4	−7.5 ± 0.7
5[b]	5MESS	3.8 ± 0.2	0.271 ± 0.004	−3.5 ± 0.2	4.3 ± 0.1	−7.8 ± 0.2
6[b,c]	56MESS	5.7 ± 0.5	0.33 ± 0.01	−5.6 ± 0.1	2.6 ± 0.2	−8.2 ± 0.6
5a[a]	5MESS	3.2 ± 0.3	0.265 ± 0.004	−3.4 ± 0.1	4.3 ± 0.1	−7.7 ± 0.2

[a] Tested as a nitrate salt. [b] Tested as a chloride salt. [c] Values from ref. 21.

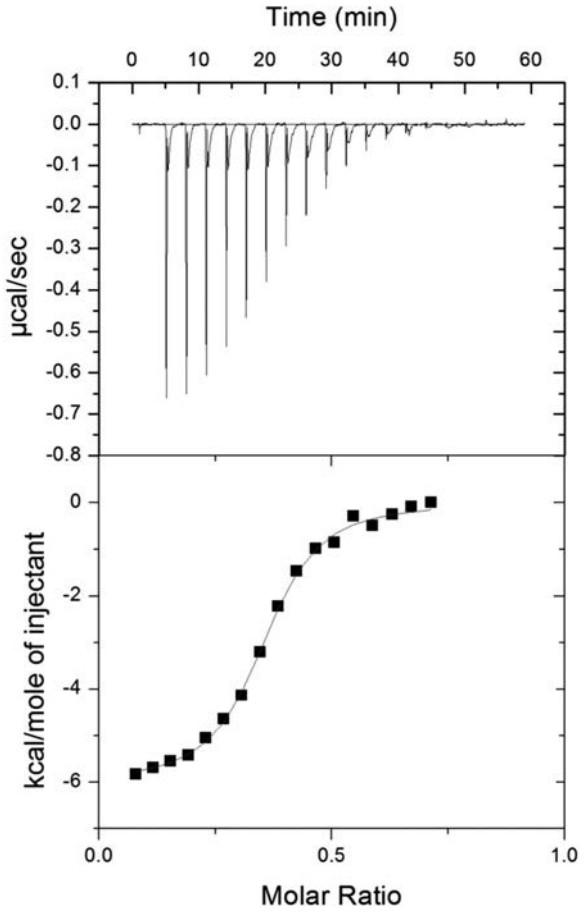

Fig. 5 ITC trace and binding curve of the titration of complex **3** (564 µM) into CT-DNA (160 µM). Fits were obtained using a one-site binding model.

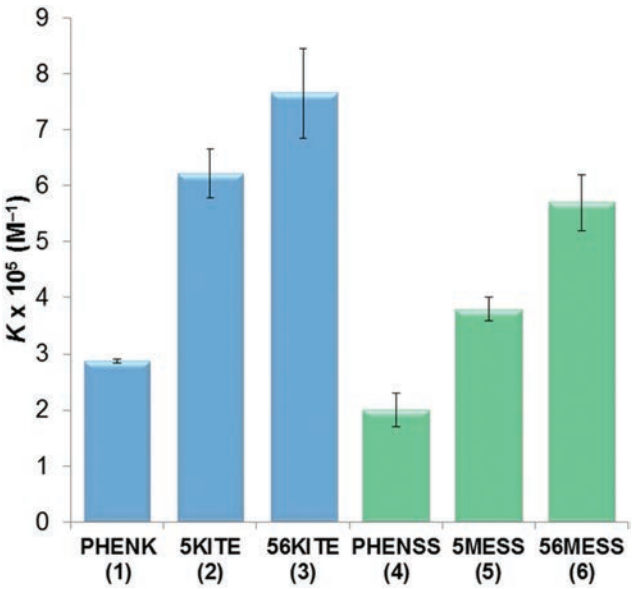

Fig. 6 Comparison of the DNA binding constants of **1–3** (1,4-dach, blue) and **4–6** (*SS*-dach, green), as determined by ITC.

in nature. All binding was spontaneous, with negative changes in enthalpy and overall negative Gibbs free energy. The affinity of **5** was found to be slightly higher than that of **5a**, which suggests that the presence of chloride counter-ions results in a slightly higher DNA affinity than complexes with nitrates. The ΔH and $T\Delta S$ differences between **5** and **5a** are too small to make any meaningful statement regarding thermodynamics, and so the reason behind this difference in affinity is unknown. Counter-ions were recently shown to effect DNA affinity to a larger extent for a pair of cobalt complexes,[38] so this phenomenon is not unusual. Regardless, the affinity of complexes **1–3** were found to be ~0.7–2.4 × 10^5 M^{-1} higher than that of their *SS*-dach counterparts (Fig. 6). This suggests that the 1,4-dach ligand does impact the DNA binding of these PCs to some extent, and minor changes in DNA binding behaviour based upon A_L have been observed previously.[23] The P_L trend of 56Me_2phen > 5Mephen > phen was observed for **1–3**, although the affinity of **2** relative to **3** was slightly higher than expected.

3.5. *In vitro* cytotoxicity

The *in vitro* cytotoxicity of complexes **1–3** was assessed using the MTT assay in ten human cancer cell lines and one "normal" cell line. These data were compared with those of **4–6** and their *R*,*R* isomers (**4′–6′**), as well as those of cisplatin, carboplatin and oxaliplatin (Table 5). **5** and **5′** had not previously been tested in this panel of cell lines; the activity of **5** relative to **6** is consistent with previous cytotoxicity studies in that **6** is more active yet **5** is still very cytotoxic.[23] In most cell lines **6** is approx. 1.5–3 times more active than **5**, although **5** is more active than **6** against HT29 cells with an IC_{50} of 0.02 ± 0.01 µM. In contrast, **6** is approx. 15–60 times more active than **6′** in most cell lines; this reaffirms that while both the presence of methyl groups on the P_L and *SS*-dach as an A_L each improve cytotoxicity, the latter makes much more of a difference. The activity of **1–3** was lower than anticipated, with **1** being inactive in most lines and equivalent to cisplatin against HT29 cells. Complex **2** demonstrated notable activity in HT29 cells only, and was relatively inactive in most other cell lines. Complex **3** was more active than cisplatin in MIA cells, equivalent to cisplatin in A431 cells, and was comparable to **4′** against HT29, MCF-7, A2780 and BE2-C lines (Fig. 7). The low cytotoxicity of **1–3** despite their high DNA affinity shows that DNA is not likely their target, or that the complexes are unable to reach nuclear DNA *in vitro*. It is clear that the improvement in cytotoxicity that 1,4-dach provides for kiteplatin over [Pt(*RR*-dach)Cl_2] is not transferrable to $[Pt(P_L)(A_L)]^{2+}$ complexes. Considering that 56MESS is known to disrupt cellular machinery through several methods unrelated to DNA,[18,20,39] and that the proposed mechanism of action of kiteplatin is the formation of DNA adducts that are harder to remove than those of cisplatin,[10] it is possible that the benefits of 1,4-dach over 1,2-dach only apply to the formation of covalent platinum-DNA adducts, which are not relevant for polyaromatic PCs.

Table 5 Summary of the *in vitro* cytotoxicity of complexes **1–3** in several cell lines, determined by the MTT assay and expressed as an IC_{50} value with standard error (1 sig. fig.). The activity of complexes **4–6** and **4′–6′**, as well as that of cisplatin, oxaliplatin and carboplatin is also included. IC_{50} is the concentration at which cell growth is inhibited by 50% over 72 h

	IC_{50} (μM)										
Complex	HT29	U87	MCF-7	A2780	H460	A431	Du145	BE2-C	SJ-G2	MIA	MCF10A
1 PHENK	10 ± 1	>50	>50	25 ± 3	>50	>50	>50	46 ± 4	>50	>50	>50
2 5KITE	2.1 ± 0.4	>50	14 ± 2	7 ± 1	>50	12 ± 2	43 ± 4	15.0 ± 0.3	30 ± 2	17 ± 2	50 ± 20
3 56KITE	0.8 ± 0.1	47 ± 3	3.7 ± 0.6	2.9 ± 0.2	29 ± 5	4.4 ± 0.5	4.8 ± 0.7	5.7 ± 0.7	17 ± 2	4.0 ± 0.4	5 ± 1
4 PHENSS[a]	0.13 ± 0.04	1.5 ± 0.4	0.5 ± 0.2	0.27 ± 0.03	0.5 ± 0.2	0.9 ± 0.3	0.08 ± 0.05	0.40 ± 0.05	0.45 ± 0.06	0.8 ± 0.7	0.16 ± 0.07
4′ PHENRR[a]	0.56 ± 0.08	8.9 ± 2.5	3.2 ± 0.2	2.70 ± 0.07	7.2 ± 0.9	2.0 ± 0.6	0.79 ± 0.08	3.8 ± 0.4	3.3 ± 0.3	2.7 ± 0.2	2.4 ± 0.3
5 5MESS	0.02 ± 0.01	0.21 ± 0.04	0.08 ± 0.02	0.04 ± 0.01	0.07 ± 0.03	0.11 ± 0.04	0.02 ± 0.01	0.3 ± 0.1	0.15 ± 0.03	0.10 ± 0.07	0.03 ± 0.01
5′ 5MERR	0.19 ± 0.01	3.8 ± 0.4	1.3 ± 0.2	1.0 ± 0.2	2.8 ± 0.0	0.8 ± 0.2	1.3 ± 0.3	2.9 ± 0.2	2.9 ± 0.4	1.7 ± 0.2	1.6 ± 0.4
6 56MESS[a]	0.08 ± 0.06	0.08 ± 0.01	0.05 ± 0.02	0.030 ± 0.004	0.037 ± 0.009	0.05 ± 0.02	0.007 ± 0.002	0.10 ± 0.02	0.07 ± 0.02	0.015 ± 0.002	0.020 ± 0.005
6′ 56MERR[a]	0.19 ± 0.00	2.2 ± 0.058	0.8 ± 0.1	1.1 ± 0.1	1.8 ± 0.2	0.93 ± 0.03	0.41 ± 0.04	2.3 ± 0.2	2.2 ± 0.2	0.45 ± 0.006	0.39 ± 0.01
Cisplatin[a]	11 ± 2	4 ± 1	6.5 ± 0.8	1.0 ± 0.1	0.9 ± 0.2	2.4 ± 0.3	1.2 ± 0.1	1.9 ± 0.2	0.4 ± 0.1	8 ± 1	nd
Oxaliplatin[a]	0.9 ± 0.2	1.8 ± 0.2	0.5 ± 0.1	0.16 ± 0.0	1.6 ± 0.1	4.1 ± 0.5	2.9 ± 0.4	0.9 ± 0.2	3 ± 1	0.9 ± 0.2	nd
Carboplatin[a]	>50	>50	>50	9 ± 3	14 ± 1	24 ± 2	15 ± 1	19 ± 1	5.7 ± 0.2	>50	nd

[a] Reported in ref. 21 and those within.

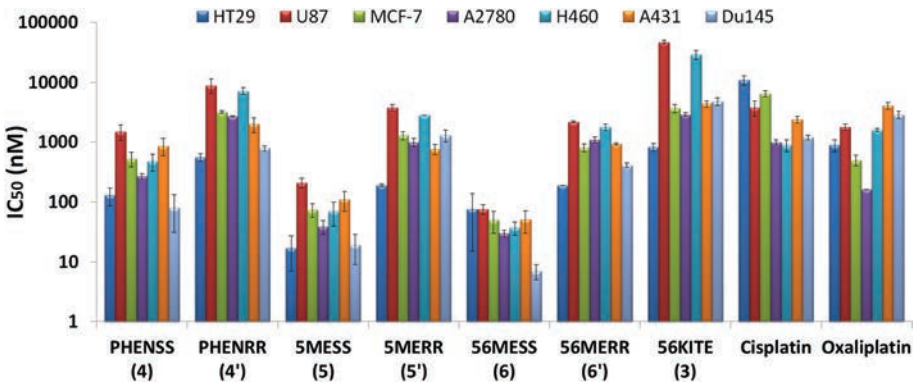

Fig. 7 MTT assay-determined IC_{50} values of complexes **3–6**, **4′–6′**, cisplatin and oxaliplatin in several human cancer cell lines, expressed on a logarithmic scale in nanomolar with standard error. Complexes **1**, **2** and carboplatin were not included for clarity.

4. Conclusions

Three new platinum(II) derivatives of kiteplatin incorporating phen derivatives and 1,4-dach have been synthesised and characterised through several spectroscopic techniques. The CT-DNA binding of complexes **1–3** was assessed through ITC and compared to 1,2-dach analogues, revealing slightly higher DNA affinity for the former. The *in vitro* cytotoxicity of complexes **1–3** was found to be unexpectedly low in several human cell lines, with complex **3** demonstrating some results comparable with cisplatin. The results here indicate that the addition of 1,10-phenanthroline analogues to kiteplatin does not result in an improvement of anticancer activity and that DNA binding is not the primary mechanism of action of this type of complex.

Conflicts of interest

There are no conflicts to declare.

Acknowledgements

We thank Western Sydney University for providing financial support through internal research grants. B. J. P. was supported by an Australian Postgraduate Award and a Western Sydney University Top-Up Award. Crystallographic data collection was undertaken on the MX1 beamline at Australian Synchrotron, Victoria, Australia.

References

1 Australian Institute of Health and Welfare and Australasian Association of Cancer Registries, *Cancer in Australia 2017*, Australian Institute of Health and Welfare, Canberra, 2017.
2 R. L. Siegel, K. D. Miller and A. Jemal, *Ca–Cancer J. Clin.*, 2017, **67**, 7–30.
3 N. J. Wheate, S. Walker, G. E. Craig and R. Oun, *Dalton Trans.*, 2010, **39**, 8113–8127.

4 M. G. Apps, E. H. Y. Choi and N. J. Wheate, *Endocr.–Relat. Cancer*, 2015, **22**, R219–R233.
5 B. H. Harper, F. Li, R. Beard, K. B. Garbutcheon-Singh, N. S. Ng and J. R. Aldrich-Wright, in *Supramolecular Systems in Biomedical Fields*, ed. H. J. Schneider, Royal Society of Chemistry, Cambridge, UK, 1st edn, 2013, ch. 9.
6 A.-M. Florea and D. Büsselberg, *Cancers*, 2011, **3**, 1351–1371.
7 J. D. Hoeschele, H. D. H. Showalter, A. J. Kraker, W. L. Elliott, B. J. Roberts and J. W. Kampf, *J. Med. Chem.*, 1994, **37**, 2630–2636.
8 N. Margiotta, C. Marzano, V. Gandin, D. Osella, M. Ravera, E. Gabano, J. A. Platts, E. Petruzzella, J. D. Hoeschele and G. Natile, *J. Med. Chem.*, 2012, **55**, 7182–7192.
9 J. Kasparkova, T. Suchankova, A. Halamikova, L. Zerzankova, O. Vrana, N. Margiotta, G. Natile and V. Brabec, *Biochem. Pharmacol.*, 2010, **79**, 552–564.
10 V. Brabec, J. Malina, N. Margiotta, G. Natile and J. Kasparkova, *Chem. – Eur. J.*, 2012, **18**, 15439–15448.
11 E. Petruzzella, N. Margiotta, G. Natile and J. D. Hoeschele, *Dalton Trans.*, 2014, **43**, 12851–12859.
12 N. Margiotta, E. Petruzzella, J. A. Platts, S. T. Mutter, R. J. Deeth, R. Ranaldo, P. Papadia, P. A. Marzilli, L. G. Marzilli, J. D. Hoeschele and G. Natile, *Dalton Trans.*, 2015, **44**, 3544–3556.
13 S. Mutter, N. Margiotta, P. Papadia and J. Platts, *J. Biol. Inorg. Chem.*, 2015, **20**, 35–48.
14 J. Kasparkova, H. Kostrhunova, V. Novohradsky, J. Pracharova, A. Curci, N. Margiotta, G. Natile and V. Brabec, *Dalton Trans.*, 2017, **46**, 14139–14148.
15 N. Margiotta, S. Savino, C. Marzano, C. Pacifico, J. D. Hoeschele, V. Gandin and G. Natile, *J. Inorg. Biochem.*, 2016, **160**, 85–93.
16 N. Margiotta, S. Savino, N. Denora, C. Marzano, V. Laquintana, A. Cutrignelli, J. D. Hoeschele, V. Gandin and G. Natile, *Dalton Trans.*, 2016, **45**, 13070–13081.
17 A. Curci, N. Denora, R. M. Iacobazzi, N. Ditaranto, J. D. Hoeschele, N. Margiotta and G. Natile, *Inorg. Chim. Acta*, 2017, DOI: 10.1016/j.ica.2017.1007.1019.
18 S. Wang, V. Higgins, J. Aldrich-Wright and M. Wu, *J. Chem. Biol.*, 2012, **5**, 51–61.
19 A. M. Krause-Heuer, R. Grünert, S. Kühne, M. Buczkowska, N. J. Wheate, D. D. Le Pevelen, L. R. Boag, D. M. Fisher, J. Kasparkova, J. Malina, P. J. Bednarski, V. Brabec and J. R. Aldrich-Wright, *J. Med. Chem.*, 2009, **52**, 5474–5484.
20 K. B. Garbutcheon-Singh, S. Myers, B. W. J. Harper, N. S. Ng, Q. Dong, C. Xie and J. R. Aldrich-Wright, *Metallomics*, 2013, **5**, 1061–1067.
21 B. J. Pages, J. Sakoff, J. Gilbert, A. Rodger, N. P. Chmel, N. C. Jones, S. M. Kelly, D. L. Ang and J. R. Aldrich-Wright, *Chem. – Eur. J.*, 2016, **22**, 8943–8954.
22 R. Ranaldo, N. Margiotta, F. P. Intini, C. Pacifico and G. Natile, *Inorg. Chem.*, 2008, **47**, 2820–2830.
23 S. Kemp, N. J. Wheate, D. P. Buck, M. Nikac, J. G. Collins and J. R. Aldrich-Wright, *J. Inorg. Biochem.*, 2007, **101**, 1049–1058.
24 T. M. McPhillips, S. E. McPhillips, H. J. Chiu, A. E. Cohen, A. M. Deacon, P. J. Ellis, E. Garman, A. Gonzalez, N. K. Sauter, R. P. Phizackerley, S. M. Soltis and P. Kuhn, *J. Synchrotron Radiat.*, 2002, **9**, 401–406.
25 W. Kabsch, *J. Appl. Crystallogr.*, 1993, **26**, 795–800.
26 *SADABS: Empirical Absorption and Correction Software*, University of Göttingen, 1998.
27 G. M. Sheldrick, *Acta Crystallogr., Sect. C: Cryst. Struct. Commun.*, 2015, **71**, 3–8.
28 G. M. Sheldrick, *SHELXT-2014*, University of Göttingen, 2014.
29 G. M. Sheldrick, *SHELXL-2014*, University of Göttingen, 2014.
30 O. V. Dolomanov, L. J. Bourhis, R. J. Gildea, J. A. K. Howard and H. Puschmann, *J. Appl. Crystallogr.*, 2009, **42**, 339–341.
31 B. J. Pages, J. Sakoff, J. Gilbert, Y. Zhang, F. Li, D. Preston, J. D. Crowley and J. R. Aldrich-Wright, *J. Inorg. Biochem.*, 2016, **165**, 92–99.
32 B. J. Pages, F. Li, P. Wormell, D. L. Ang, J. K. Clegg, C. J. Kepert, L. K. Spare, S. Danchaiwijit and J. R. Aldrich-Wright, *Dalton Trans.*, 2014, **43**, 15566–15575.
33 K. B. Garbutcheon-Singh, P. Leverett, S. Myers and J. R. Aldrich-Wright, *Dalton Trans.*, 2013, **42**, 918–926.
34 S. Kemp, N. J. Wheate, M. J. Pisani and J. R. Aldrich-Wright, *J. Med. Chem.*, 2008, **51**, 2787–2794.
35 B. M. Still, P. G. A. Kumar, J. R. Aldrich-Wright and W. S. Price, *Chem. Soc. Rev.*, 2007, **36**, 665–686.
36 A. R. Khokhar, S. Shamsuddin and Q. Xu, *Inorg. Chim. Acta*, 1994, **219**, 193–197.
37 L. M. Salonen, M. Ellermann and F. Diederich, *Angew. Chem., Int. Ed.*, 2011, **50**, 4808–4842.
38 B. N. Anila, N. M. K. Muraleedharan, J. Sreedharan and V. P. Sylas, *Asian J. Chem.*, 2017, **29**, 691–702.
39 S. Wang, M. J. Wu, V. J. Higgins and J. R. Aldrich-Wright, *Metallomics*, 2012, **4**, 950–959.

CHAPTER 3. POLYAROMATIC PLATINUM(IV) COMPLEXES

3.1 Foreword

This chapter is a collection of mostly unpublished work regarding the synthesis of platinum(IV) polyaromatic PCs, the optimisation of the synthetic method and efforts to conjugate the PCs to the moiety known as DCL that can target PSMA. The synthesis and characterisation of platinum(IV) dihydroxido complexes will be detailed first, followed by those utilised for the DCL project. Some of method development of the dihydroxido complexes mentioned here contributed to Paper VI. The other method optimisation and novel synthesised compounds will be published as part of a future platinum(IV)-based manuscript. The PSMA targeting project will continue and eventually be incorporated into a paper in collaboration with the Trevor Hambley group at Sydney University when completed.

3.2 Materials

All reagents used were of laboratory grade and were used without further purification. Platinum(II) complexes PHENSS, 5MESS, 56MESS, and their enantiomers PHENRR, 5MERR and 56MERR were synthesised using the methods described in Paper V and others.[70, 142] Acetone, acetic acid, acetonitrile, ammonium chloride, dioxanes, *N*,*N*-diisopropylethylamine (DIPEA), dichloromethane (DCM), diethyl ether, ethyl acetate, hexane, 1-Hydroxybenzotriazole (HOBt), HBTU, hydrochloric acid, lithium hydroxide, monomethyl hydrogen succinate, ninhydrin, silver acetate, silver nitrate, sodium chloride, sodium sulphate, triethylamine (TEA) and triphosgene were obtained from Sigma-Aldrich. Hydrogen peroxide was obtained from VWR. Methanol was obtained from Honeywell. *L*-Glutamic acid di-*tert*-butyl ester hydrochloride and *N*ε-benzyloxycarbonyl-L-lysine *tert*-butyl ester hydrochloride were obtained from Combi-Blocks. 7-azidoheptanoic acid was obtained from ChemPep. Sep-Pak® C18 20 cc cartridges were obtained from Waters. Silica gel 60 (40 – 63 μm) was obtained from Grace Davison. Silica thin-layer chromatography (TLC) plates were obtained from Merck. A CatCart 70 mm Pd/C 10% cartridge was obtained from ThalesNano.

3.3 Instrumentation

A 400 MHz Bruker Avance NMR spectrometer was used to obtain all NMR spectra. Deuterium oxide (D_2O) was used as a solvent and all spectra were obtained at room temperature. Proton spectra were obtained using 128 accumulations and a spectral width of 15 ppm. ^{1}H-^{195}Pt heteronuclear multiple quantum correlation (HMQC) spectra were obtained using 2048 data points and a spectral width of 12 ppm for the ^{1}H nucleus, and 256 data points and a spectral width of 2500 ppm for the ^{195}Pt nucleus. Spin multiplicity abbreviations are as follows: s (singlet), d (doublet), dd (doublet of doublets), and m (multiplet). Chemical shifts

are quoted as an approximate midpoint of each multiplicity in parts per million. ESIMS experiments, in the positive mode, were performed using a Waters TQ-MS triple quadrupole mass spectrometer. Sample solutions (10 μL) were injected into 0.1% trifluoroacetic acid in 50% aqueous acetonitrile, and were flowed at 0.1 mL/min. A desolvation temperature of 300 ^{o}C, desolvation flow rate (nitrogen) of 500 L/hr, a cone voltage of 25 V and capillary voltage of 1.6 kV were utilised. Spectra were collected over varied *m/z* ranges depending on the target mass.

3.4 Polyaromatic Platinum(IV) Dihydroxido Complexes

3.4.1 Introduction

The synthesis of platinum(IV) dihydroxido complexes is important as they are intermediates for the further functionalisation of PPCs. In this project, the method of synthesising these complexes was further developed and optimised to maximise yield and purity, using the method described in Paper VI as the base. To demonstrate the utility of the final method, it was used to oxidise the most cytotoxic platinum(II) PPCs: PHENSS, PHENRR, 5MESS, 5MERR, 56MESS and 56MERR (Figure 3.4.1). In the future, these complexes will be used as the base from which platinum(IV) PPCs with higher functionality will be synthesised.

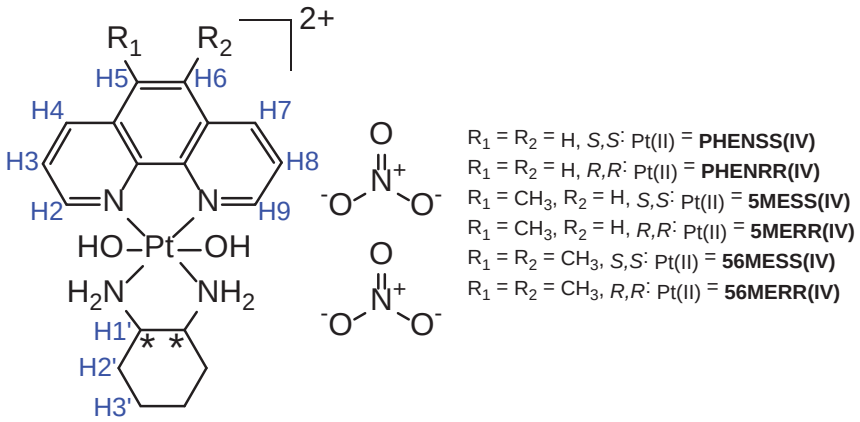

Figure 3.4.1. General structure of the dihydroxido PPCs, showing the proton numbers used for NMR assignment in blue. * indicates a stereocentre, either *S* or *R*. Amine and hydroxido protons were not assigned due to exchange in D_2O.

3.4.2 Synthesis of $[Pt(P_L)(A_L)(OH)_2](NO_3)_2$

Counter-ion conversion

$[Pt(P_L)(A_L)]Cl_2$ (1 equiv) was dissolved in the minimum amount of water and silver nitrate (2 equiv) was added. The solution was stirred in the dark overnight, and then syringe filtered to produce $[Pt(P_L)(A_L)](NO_3)_2$ (95% yield).

Preliminary method 1

$[Pt(P_L)(A_L)](NO_3)_2$ (49 μmol) was dissolved in 30% hydrogen peroxide (60 mL, 585 mmol peroxide). This solution was stirred in the dark for 2 h and then lyophilised. The crude solid was then dissolved in the minimum amount of water, followed by fifteen times as much acetonitrile, resulting in a white precipitate. This precipitate was filtered and washed with acetonitrile to produce the product as a white to cream solid (~83% yield).

Preliminary method 2

$[Pt(P_L)(A_L)](NO_3)_2$ (80 μmol) was dissolved in 30% hydrogen peroxide (1 mL, 9.75 mmol peroxide). The solution was heated to 70 °C for 2 hours in the dark. The solution was removed from heat and immediately added to 13 mL of acetonitrile. The solution was centrifuged to isolate the product as a white pellet (~60% yield).

Final method

$[Pt(P_L)(A_L)](NO_3)_2$ (80 μmol) was dissolved in water (5.8 mL) and heated to 70 °C on a water bath. 30% hydrogen peroxide solution (820 μL, 8 mmol peroxide) was added and the solution stirred at 70 °C in the dark for 2 h. The resulting reaction solution was immediately frozen and lyophilised. To purify, a Sep-Pak® (20 cc, 5 g) column was used, which was connected to a pump apparatus with UV detector (Bio-Rad, EM-1 Econo™ UV Monitor). Methanol (~15 mL) was used to activate the column and it was then flushed with water (~40 mL) until UV absorbance reached equilibrium. The crude lyophilised platinum(IV) product was dissolved in the minimum amount of water, loaded onto the column, and was eluted at 1 mL/min using water. Once absorbance began to increase, the first 2-3 mLs to elute were collected and discarded. The rest of the product was collected together as a colourless band. The product solution was reduced to approx. 1-2 mL and was purified through the Sep-Pak® process again. The final solution was reduced to approx. 3-5 mL and lyophilised to produce a white solid (96% yield). The NMR characterisation data for each complex are presented in Table 3.4.1.

Table 3.4.1. Summary of the NMR data of the dihydroxido platinum(IV) PPCs, showing chemical shift (ppm), integration, multiplicity and coupling constants. Experiments were performed in D_2O, and so amine resonances were not observed due to proton exchange.

Label	Complex					
	PHENSS(IV)	PHENRR(IV)	5MESS(IV)	5MERR(IV)	56MESS(IV)	56MERR(IV)
H2	9.09 (2H, d, *J* = 8.42 Hz)	9.09 (2H, d, *J* = 8.34 Hz)	8.95 (1H, d, *J* = 8.42 Hz)	8.95 (1H, d, *J* = 8.50 Hz)	9.20 (2H, d, *J* = 8.67 Hz)	9.20 (2H, d, *J* = 8.64 Hz)
H3	8.27 (2H, dd, *J* = 8.37, 5.56 Hz)	8.27 (2H, dd, *J* = 8.35, 5.57 Hz)	8.20 (1H, dd, *J* = 8.36, 5.52 Hz)	8.20 (1H, dd, *J* = 8.32, 5.53 Hz)	8.24 (2H, dd, *J* = 8.64, 5.51 Hz)	8.24 (2H, dd, *J* = 8.60, 5.47 Hz)
H4	9.23 (2H, d, *J* = 5.58 Hz)	9.22 (2H, d, *J* = 5.48 Hz)	9.13 (1H, d, *J* = 5.63 Hz)	9.13 (1H, d, *J* = 5.53 Hz)	9.12 (2H, d, *J* = 5.54 Hz)	9.13 (2H, d, *J* = 5.52 Hz)
H5	8.35 (2H, s)	8.35 (2H, s)	-	-	-	-
H6	-	-	8.15 (1H, s)	8.15 (1H, s)	-	-
H7	-	-	9.17 (1H, d, *J* = 8.59 Hz)	9.17 (1H, d, *J* = 8.54 Hz)	-	-
H8	-	-	8.29 (1H, dd, *J* = 8.57, 5.53 Hz)	8.28 (1H, dd, *J* = 8.55, 5.54 Hz)	-	-
H9	-	-	9.21 (1H, d, *J* = 5.59 Hz)	9.21 (1H, d, *J* = 5.62 Hz)	-	-
H1'	3.18 (2H, d, *J* = 9.07 Hz)	3.18 (2H, d, *J* = 9.08 Hz)	3.17 (2H, d, *J* = 8.83 Hz)	3.17 (2H, d, *J* = 8.86 Hz)	3.17 (2H, d, *J* = 9.03 Hz)	3.17 (2H, d, *J* = 9.02 Hz)
$H2'_{eq}$	2.39 (2H, d, *J* = 10.95 Hz)	2.39 (2H, d, *J* = 10.86 Hz)	2.38 (2H, d, *J* = 10.93 Hz)	2.38 (2H, d, *J* = 10.87 Hz)	2.38 (2H, d, *J* = 10.83 Hz)	2.38 (2H, d, *J* = 10.69 Hz)
$H3'_{eq}$/ $H2'_{ax}$	1.69 (4H, m)	1.69 (4H, m)	1.68 (4H, m)	1.68 (4H, m)	1.68 (4H, m)	1.68 (4H, m)
$H3'_{ax}$	1.31 (2H, m)	1.31 (2H, m)	1.30 (2H, m)	1.30 (2H, m)	1.31 (2H, m)	1.30 (2H, m)
$-CH_3$	-	-	2.90 (3H, s)	2.90 (3H, s)	2.84 (6H, s)	2.84 (6H, s)
$^{1}H/^{195}Pt$	9.33/434	9.32/434	9.31/436	9.31/436	9.22/422	9.22/421

3.4.3 Results and discussion

The synthesis of the symmetric dihydroxido products of the type $[Pt(P_L)(A_L)(OH)_2](NO_3)_2$ was achieved through the well-established method of hydrogen peroxide oxidation.[157] During this oxidation reaction, it is known that one of the hydroxido ligands originates from the coordination and electron transfer of the peroxide to the platinum centre, and the other originates from the solvent, in this case water.[157] Several methods were investigated to oxidise the PPCs in this project until the most effective was identified and developed. Firstly, the platinum(II) starting material was usually converted to the nitrate salt prior to oxidation; attempts to oxidise the chloride salts of these PPCs resulted in platinum(IV) impurities, possibly due to chloride coordination. The main characteristic of preliminary method 1 was the use of a very large excess of peroxide and small amounts of platinum(II) starting material (30-40 mg) to ensure that the reaction was driven towards the product. While the platinum(II) complexes are soluble in both water and acetonitrile, the platinum(IV) complexes are not acetonitrile soluble, and so precipitation in acetonitrile was used as for purification. This approach was used for the complexes published in Paper VI; however, it was only successful in small batches and used a large amount of peroxide solution. Preliminary method 2 was developed in an attempt to reduce the amount of peroxide needed, using only 1 mL for 50-60 mg of starting material. To compensate for the reduced amount of peroxide, heat was employed to increase the rate of reaction. For each set of reaction conditions, monitoring of the relative ratio of starting material and product was achieved through high-performance liquid chromatography (HPLC). The conditions required to convert the starting material to the product in the shortest time were identified as 70 °C for 2 hours. Aside from reducing hydrogen peroxide costs, another advantage to using a reaction solution of only 1 mL was that the volume was small enough to immediately precipitate the product from acetonitrile; this removed the need for lyophilisation. Each oxidation method is summarised in Figure 3.4.2.

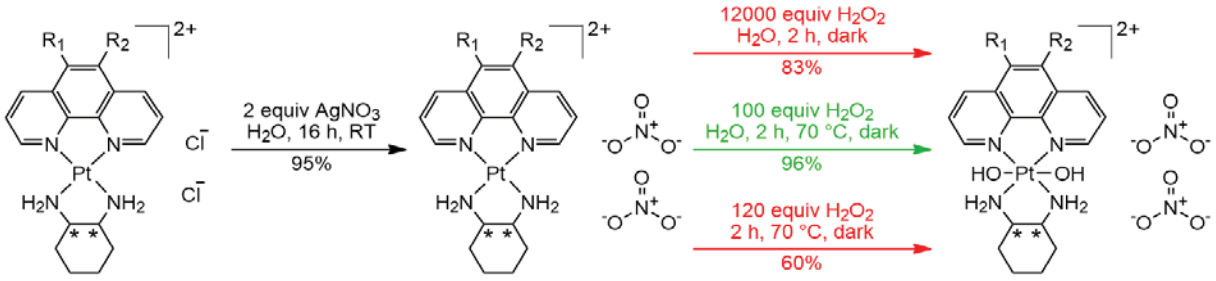

Figure 3.4.2. Reaction scheme of the synthesis of dihydroxido platinum(IV) PPCs. Preliminary methods 1 and 2 are shown in red while the final method is shown in green. R_1 and R_2 are either hydrogen, methyl, or a mixture of both. * indicates a stereocentre, either *S* or *R*.

While this method did result in the formation of product, some impurities were also formed that could not be removed, and yields were much lower than preliminary method 1. This lead to the final modification of the synthesis method, based upon a published method for oxidising kiteplatin.[158] A similar amount of peroxide solution was used; however it was diluted with water. Initially the products of this method were isolated through acetonitrile precipitation, and produced a sufficiently pure product according to ^{1}H and ^{1}H-^{195}Pt NMR. However, precipitation was subsequently replaced by Sep-Pak® purification, alone. Originally it was accepted that the platinum(IV) PPCs were white, yet turned pale yellow when dissolved; however, when the crude 56MESS(IV) reaction solution was purified through a Sep-Pak® and UV detector, the product eluted as a colourless band which was closely followed by a bright yellow band, resulting in some overlap. The yellow band did not produce a UV detectable signal and the NMR spectrum of the yellow band showed a variety of peaks too small to characterise. When the colourless 56MESS(IV) band was concentrated, a slight yellow tinge remained. This was removed by a second Sep-Pak® elution that produced a colourless solution and a white product upon lyophilisation. Despite the need to column the crude product twice, the yield was 96% for 56MESS(IV); this yield was consistent for the other platinum(IV) PPCs synthesised through this method. Characteristic NMR spectra were obtained for each of the platinum(IV) PPC products to confirm that the final oxidation method produced the correct products in high purity. Considering that some of these PPCs were published in Paper VI, and that the rest of the PPCs will be published in a future paper by the same primary authors, other characterisation data was not obtained for these complexes by this author. Comparison of the NMR spectra of PHENSS(IV) with PHENSS(II) reveals the typical changes in proton signals upon oxidation:[159] the chemical shift of all proton resonances is increased upon oxidation, the doublet corresponding to H4 exhibited shoulders, and the peaks corresponding to H3'$_{eq}$ and H2'$_{ax}$ were merged (Figure 3.4.3). All proton peaks were assigned as detailed in Papers I-VI. The platinum(IV) chemical shift of PHENSS(IV) was approx. 434 ppm (Figure 3.4.4), which is consistent with the reported shift in Paper VI. It is difficult to obtain true evidence of the identity of the axial ligand of these complexes, as hydroxido ligands will exchange in protic solvents and these PPCs are insoluble in aprotic ones. However, the theory of direct oxidative addition of peroxides and solvent to platinum(II) complexes is well-established,[157] there are no other likely axial ligands in the reaction solution (nitrate counter ions are very weak binders), and hydroxido species are the only likely ligands that would produce a platinum species with a positive ^{195}Pt chemical shift.[160] The NMR spectra of the other synthesised PPCs demonstrated the same phenomena (Table 3.4.1).

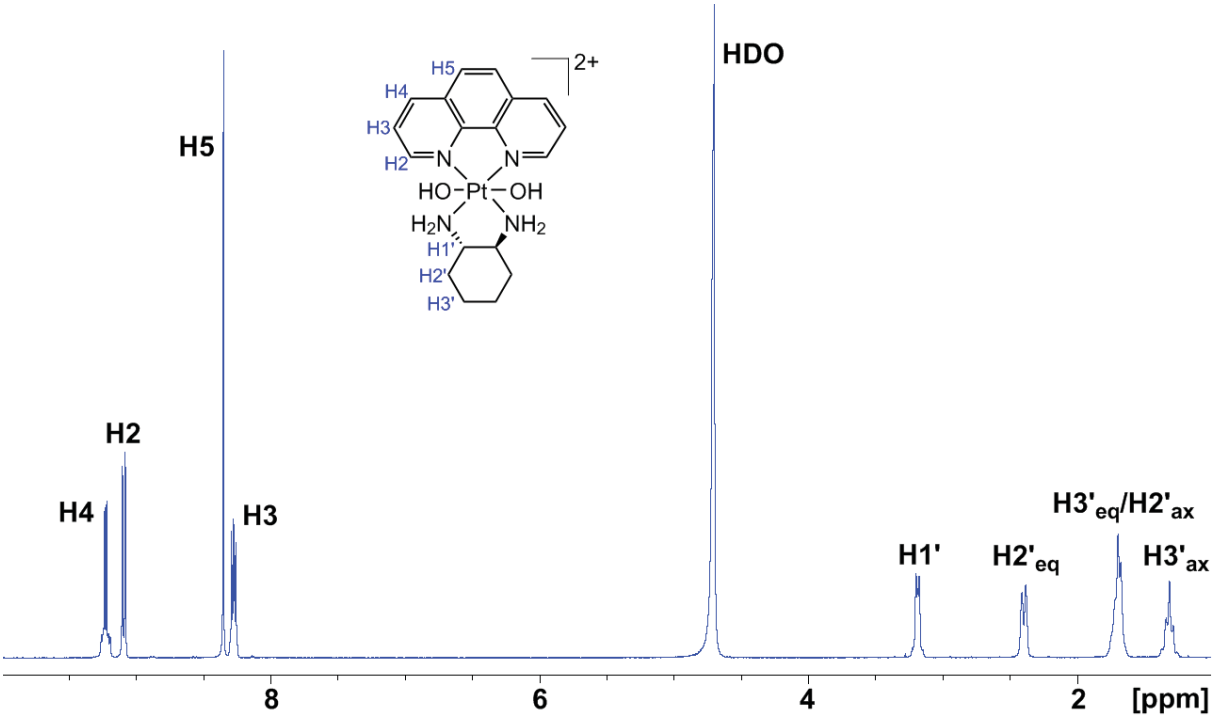

Figure 3.4.3. Proton NMR spectrum of PHENSS(IV) in D_2O, showing proton assignment. Amine and hydroxido resonances are not observed due to exchange with D_2O.

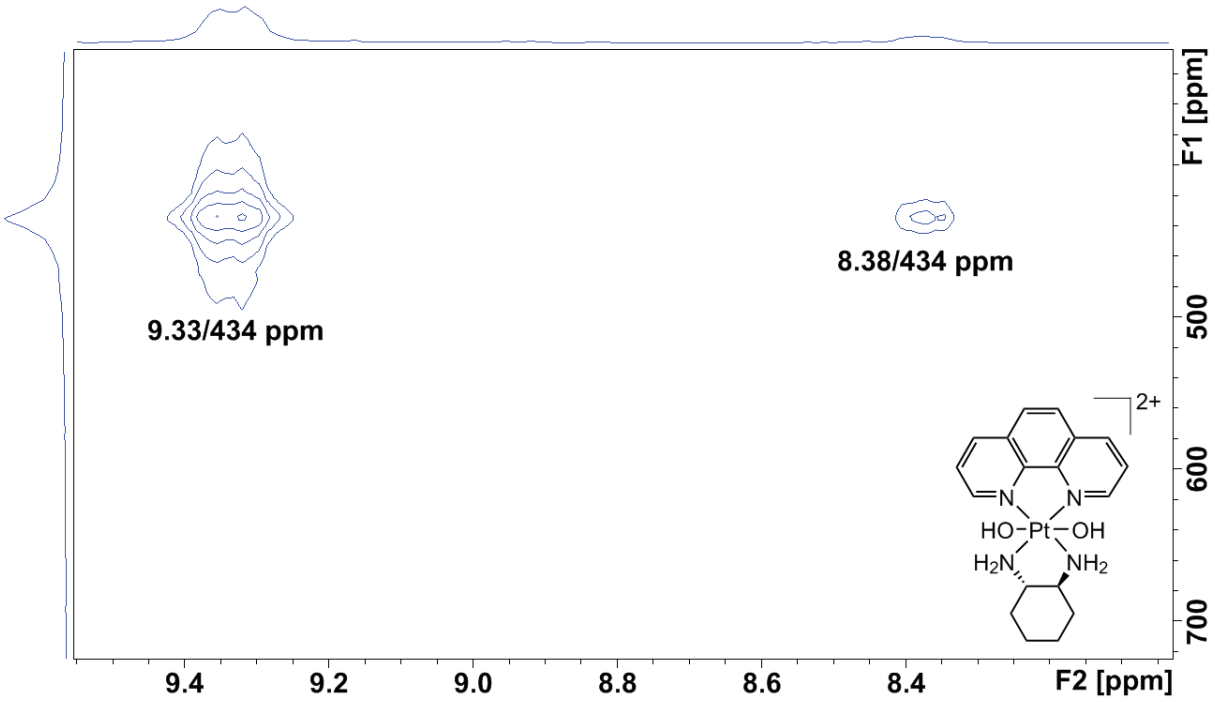

Figure 3.4.4. ^{1}H-^{195}Pt HMQC NMR spectrum of PHENSS(IV) in D_2O, showing cross-peak assignment.

3.5 A PSMA-Targeting Platinum(IV) Complex

3.5.1 Introduction

This project was undertaken to conjugate a PSMA-targeting ligand with a polyaromatic platinum(IV) complex. PHENSS was chosen as the base platinum(II) complex as it is less expensive to synthesise yet still has good biological activity *in vitro* and *in vivo*.[71] The work was performed at Sydney University in collaboration with Prof Trevor Hambley's group, who have been working with the PSMA targeting moiety DCL for several years. The final goal of the project was to synthesise a conjugated PHENSS-DCL complex that could be tested for viability in prostate cancer cell lines (both with and without expression of PSMA) and in 3D tumour models. The proposed mechanism of such a complex *in vivo* would be as follows: the three carboxylic acids of the DCL moiety would deprotonate at physiological pH, resulting in an overall negative charge that would discourage the drug from passively diffusing into non-target cells. Once the target prostate cancer cell was reached, the DCL moiety would be recognised by PSMA and the drug would be endocytosed. Intracellular reductants would then reduce the prodrug to PHENSS(II), which would subsequently kill the cell. Unfortunately, the synthesis of the final product could not be completed within the time frame of this candidature; however, the successful realisation of the last step of the synthesis did prove that the conjugation is possible. The synthetic route, so far, is summarised and discussed here. Considering that these experiments were to determine if conjugated PHENSS-DCL could be synthesised, and it was expected to be purified using preparative HPLC, only ESIMS was utilised to confirm the identity of each intermediate before proceeding to the next synthetic step. However, NMR spectra were obtained for the product described in Section 3.5.8.

3.5.2 Synthesis of (*S*)-2-(3-((*S*)-5-Benzyloxycarbonylamino-1-*tert*-butoxycarbonylpentyl)ureido)pentanedioic acid di-*tert*-butyl ester (DCL 1)

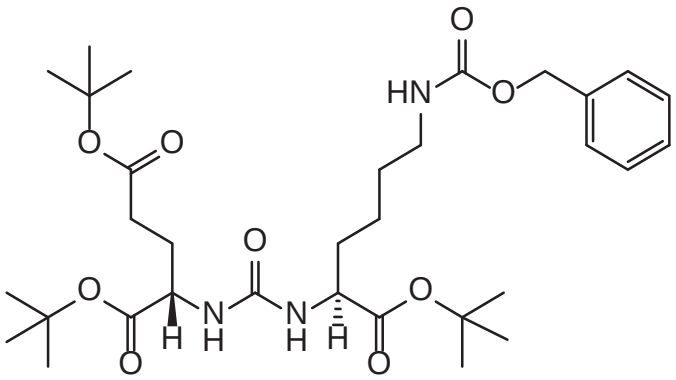

Triphosgine (0.37 g, 1.2 mmol) was dissolved in DCM (10 mL) and stirred at -10 ^{o}C (1:1 v/v ice to acetone bath). A solution of *L*-Glutamic acid di-*tert*-butyl ester hydrochloride (1 g, 3.38 mmol) and DIPEA (1.3 mL, 7.7 mmol) in DCM (20 mL) was added drop-wise over ~4 h. A

solution of *N*ε-benzyloxycarbonyl-*L*-lysine *tert*-butyl ester hydrochloride (1.26 g, 3.38 mmol) and DIPEA (1.3 mL) in DCM (20 mL) was then added in its entirety. The solution was allowed to warm to room temperature and stir for 16 h before the solvent was removed under pressure. The resultant oil was dissolved in ethyl acetate (50 mL) and washed with saturated ammonium chloride (2 × 50 mL) and brine (50 mL). The solvent was removed under pressure and the crude product re-dissolved in minimum ethyl acetate. Purification was achieved *via* silica gel chromatography (gradient elution from 30:70 to 50:50 ethyl acetate/hexane). Column progress was tracked using TLC (30:70 ethyl acetate/hexane, ninhydrin stain). The product was a colourless oil which solidified to a white solid upon standing. Yield: 75%. ESIMS: *m/z* calculated for $C_{32}H_{51}N_3O_9Na$ ($M+Na^+$): 644.4, found 643.9.

3.5.3 Synthesis of (*S*)-2-(3-((*S*)-5-amino-1-*tert*-butoxycarbonylpentyl)ureido)pentanedioic acid *di*-*tert*-butyl ester (DCL 2)

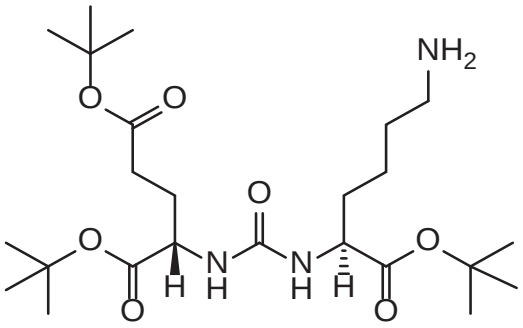

DCL 1 (880 mg, 1.4 mmol) was dissolved in methanol (20 mL) and flowed through a H-Cube Pro™ system utilising a 70 mm Pd/C 10% CatCart® cartridge. Experimental parameters included a flow rate of 1 mL/min, temperature of 50 ^oC, full hydrogen capacity and 1 atm of pressure. The eluted methanol solution was collected, and the solvent removed under pressure to yield DCL 2 (95% yield). ESIMS: *m/z* calculated for $C_{24}H_{45}N_3O_7$ ($M+H^+$): 487.3, found 488.0.

3.5.4 Synthesis of (*S*)-2-(3-((*S*)-5-(7-azidoheptanamido)-1-*tert*-butoxycarbonylpentyl)ureido)pentanedioic acid di-*tert*-butyl ester (DCL 3)

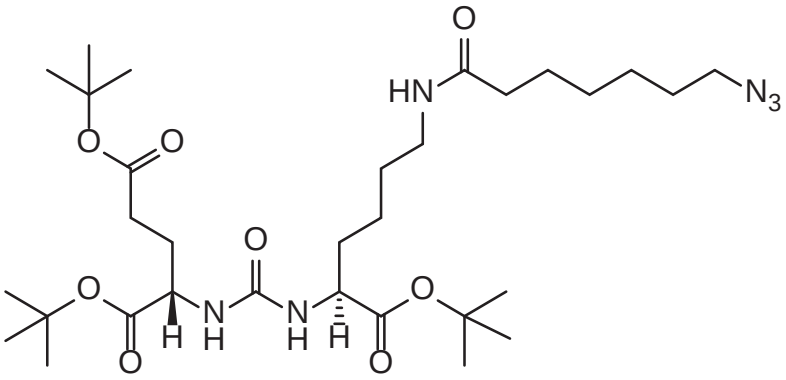

A round-bottomed flask was charged with HBTU (704 mg, 1.86 mmol) and HOBt (251 mg, 1.86 mmol). DCL 2 (823 mg, 1.69 mmol) in acetonitrile (20 mL), 7-azidoheptanoic acid (292 µL, 1.69 mmol) and DIPEA (592 µL, 3.4 mmol) were then added and the solution stirred for 16 h at room temperature. All solvent was removed and the crude product taken up in the minimum amount of ethyl acetate. A silica gel column (20 × 3 cm) was prepared and the product eluted with 50:50 ethyl acetate/hexane. Column progress was tracked using TLC (50:50 ethyl acetate/hexane, ninhydrin stain). Reduction of fraction volumes revealed a yellow oil, DCL 3 (53 % yield). ESIMS: *m/z* calculated for $C_{31}H_{56}N_6O_8$ ($M+H^+$): 640.4, found 640.1.

3.5.5 Synthesis of (*S*)-2-(3-((*S*)-5-(7-aminoheptanamido)-1-*tert*-butoxycarbonylpentyl)ureido)pentanedioic acid di-*tert*-butyl ester (DCL 4)

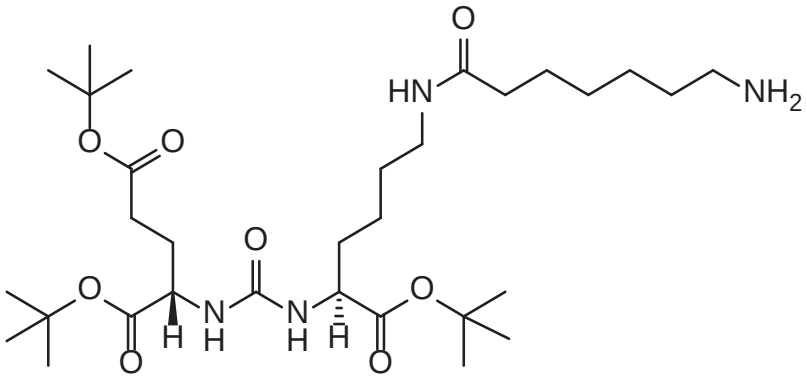

DCL 3 (500 mg, 0.78 mmol) was dissolved in methanol (20 mL) and flowed through a H-Cube Pro™ utilising a 70 mm Pd/C 10% CatCart® cartridge. Experimental parameters included a flow rate of 1 mL/min, temperature of 50 ^oC, full hydrogen capacity and 1 atm of pressure. The eluted methanol solution was collected and the solvent removed under pressure to yield DCL 4 (95% yield). ESIMS: *m/z* calculated for $C_{31}H_{58}N_4O_8$ ($M+H^+$): 614.4, found 614.2.

3.5.6 Synthesis of (*S*)-2-(3-((*S*)-5-(7-(4-methoxybutanamido)heptanamido)-1-*tert*-butoxycarbonylpentyl)ureido)pentanedioic acid di-*tert*-butyl ester (DCL 5)

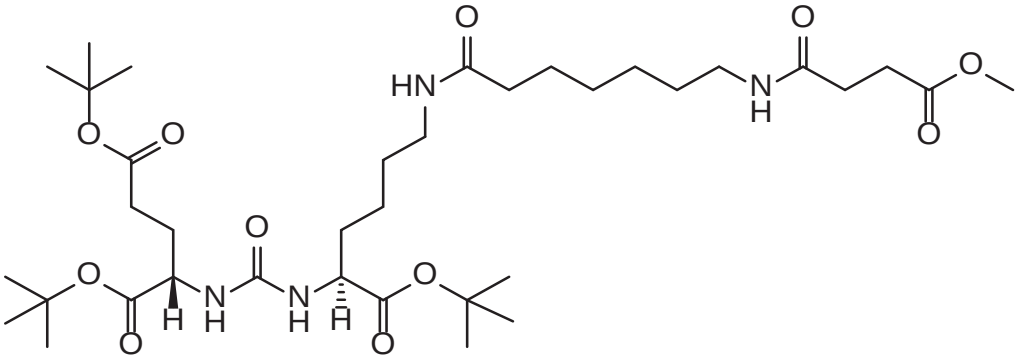

A round-bottomed flask was charged with HBTU (379 mg, 1 mmol), HOBt (135 mg, 1 mmol) and monomethyl hydrogen succinate (121 mg, 0.91 mmol). DCL 4 (560 mg, 0.91 mmol) in acetonitrile (20 mL) and DIPEA (317 μL, 1.82 mmol) were then added and the solution stirred for 16 h. All solvent was removed and the crude product taken up in the minimum amount of DCM. A silica gel column (20 × 3 cm) was prepared and the product eluted with methanol in DCM (5% v/v). Column progress was tracked using TLC (5% methanol in DCM, ninhydrin stain). Reduction of fraction volumes revealed a yellow oil, DCL 5 (82 % yield). ESIMS: *m/z* calculated for $C_{36}H_{64}N_4NaO_{11}$ ($M+Na^+$): 751.5, found 751.3.

3.5.7 Synthesis of (*S*)-2-(3-((*S*)-5-(7-(4-hydroxybutanamido)heptanamido)-1-*tert*-butoxycarbonyl pentyl)ureido)pentanedioic acid di-*tert*-butyl ester (DCL 6)

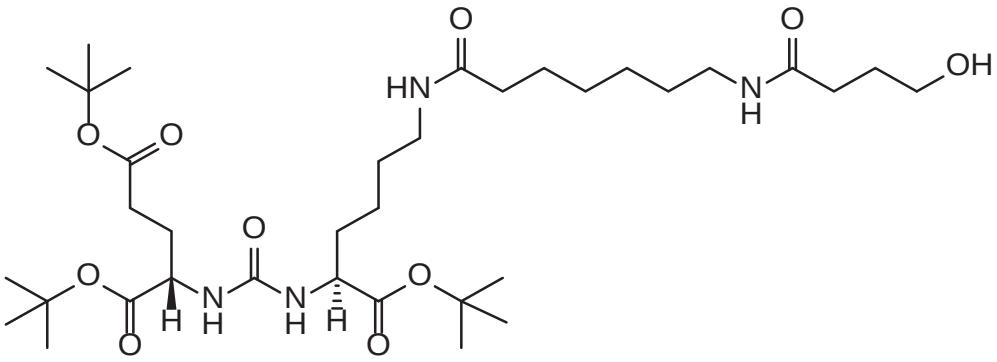

LiOH (4.1 mg, 171 μmol) was suspended in dioxanes (2 mL) and added to DCL 5 (31.3 mg 42.9 μmol). The solution was stirred for 16 h before the addition of another 1.5 mg of LiOH and continued stirring for 24 h. The solvent was removed under pressure and the crude product suspended in water. The solution was acidified with hydrochloric acid and extracted with ethyl acetate. The extracts were dried over sodium sulphate and the solvent removed to produce a yellow oil, DCL 6 (58% yield). ESIMS: *m/z* calculated for $C_{35}H_{62}N_4NaO_{11}$ ($M+Na^+$): 737.4, found 736.1.

3.5.8 Synthesis of [Pt(phen)(*SS*-dach)(OH)(OAc)](OAc)$_2$ (PHENSS(IV)A)

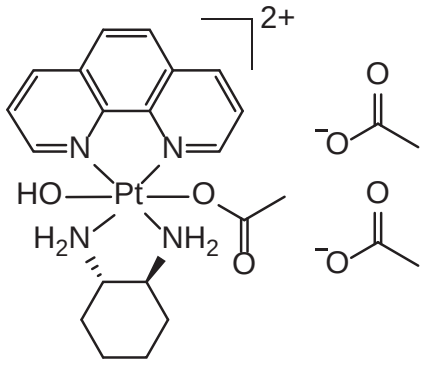

Counter-ion conversion

PHENSS chloride (100 mg, 178 μmol) was dissolved in water (20 mL) and silver acetate (59.5 mg, 356 μmol) was added. The solution was stirred in the dark for 2 h, and then syringe filtered to produce PHENSS acetate.

Oxidation method 1

PHENSS acetate (33.7 mg, 55.5 μmol) was dissolved in acetic acid (7 mL). 30% hydrogen peroxide solution (68 μL, 665 μmol peroxide) was added and the solution stirred in the dark for two hours. The solvent was removed under nitrogen to produce the crude product. This solid product was used without further purification. ESIMS: *m/z* calculated for $C_{20}H_{26}N_4O_3Pt$ ($M\text{-}H^+$): 564.2, found 563.8.

Oxidation method 2

PHENSS acetate (50 mg, 82.3 μmol) was dissolved in acetic acid (1.5 mL). 30% hydrogen peroxide solution (30 μL, 294 μmol peroxide) was added and the solution stirred in the dark for 48 h. The solution was added dropwise to diethyl ether (~100 mL) and cooled to ~4 °C for 16 h. The solution was then centrifuged to produce a pale yellow pellet. Yield could not be recorded (see 3.5.10). ^{1}H NMR (400 MHz, D_2O) δ: 9.24 (2H, dd, *J* = 17.5, 5.5 Hz), 9.06 (2H, dd, *J* = 8.3, 2.6 Hz), 8.31 (2H, s), 8.24 (2H, dd, *J* = 8.3, 5.6 Hz), 3.48 (2H, dd, *J* = 14.3, 7.1 Hz), 3.19 (2H, d, *J* = 5.9 Hz), 2.38 (2H, d, *J* = 11.0 Hz), 1.9 (13H, s), 1.68 (7H, m), 1.29 (2H, m), 1.09 (t, *J* = 7.11 Hz). ^{1}H-^{195}Pt HMQC NMR (400/86 MHz, D_2O) δ: 9.3/542, 8.3/542.

3.5.9 Synthesis of [Pt(phen)(*SS*-dach)(DCL 6)(OAc)](OAc)$_2$ (PHENSS(IV)DCL)

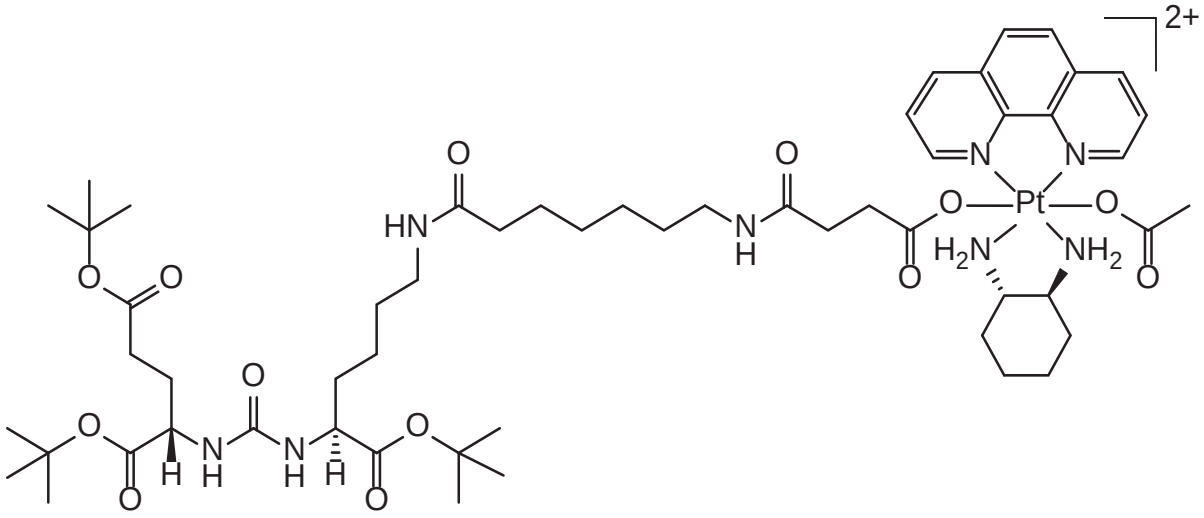

PHENSS(IV)A (11.5 mg, 16.8 μmol), DCL 6 (18 mg, 25.1 μmol) and HBTU (9.5 mg, 25.1 μmol) were combined in methanol (3 mL). TEA (3.5 μL, 25.1 umol) was then added and the solution stirred in the dark for 16 h. Solvent was removed under nitrogen to produce the crude product. ESIMS: *m/z* calculated for $C_{55}H_{86}N_8O_{13}Pt$ ($M\text{-}H^+$): 1261.6, found 1260.8.

3.5.10 Results and discussion

The synthesis of DCL 1, the *tert*-butyl-protected analogue of the active DCL component, was based upon the method of the Hambley group and others.[161-163] This is the most sensitive step of the process. Triphosgene is a symmetrical reagent and is very reactive; to prevent glutamic acid from reacting with both sides of triphosgene, the reagent was added very slowly and the reaction vessel kept below 0 °C. Once all the glutamic acid was bound, by-product risk was minimalised and so the protected lysine could be added all at once. Deprotection of the carboxybenzyloxy group of the lysine was achieved through flow hydrogenation on the H-Cube Pro™. This method was employed over traditional batch hydrogenation methods as all hydrogen is safely internalised in the H-cube system, and the use of a CatCart® cartridge meant no catalyst remained that needed filtering. The peptide coupling reactions that produced DCL 3 and DCL 5 were achieved using the well-established HBTU/HOBt process,[164] and the deprotection of the azide of DCL 3 was achieved through the same method as DCL 1. The deprotection of the methyl group from DCL 5 was initially attempted using the H-Cube Pro™; some DCL 5 was dissolved in dioxanes and was flowed through a lithium hydroxide CatCart® cartridge. However, lithium hydroxide appeared to leak from the cartridge and co-elute with the product. Due to this, the batch chemistry method described in Section 3.5.7 was used instead to remove the methyl group. The full synthesis scheme is shown in Figure 3.5.1.

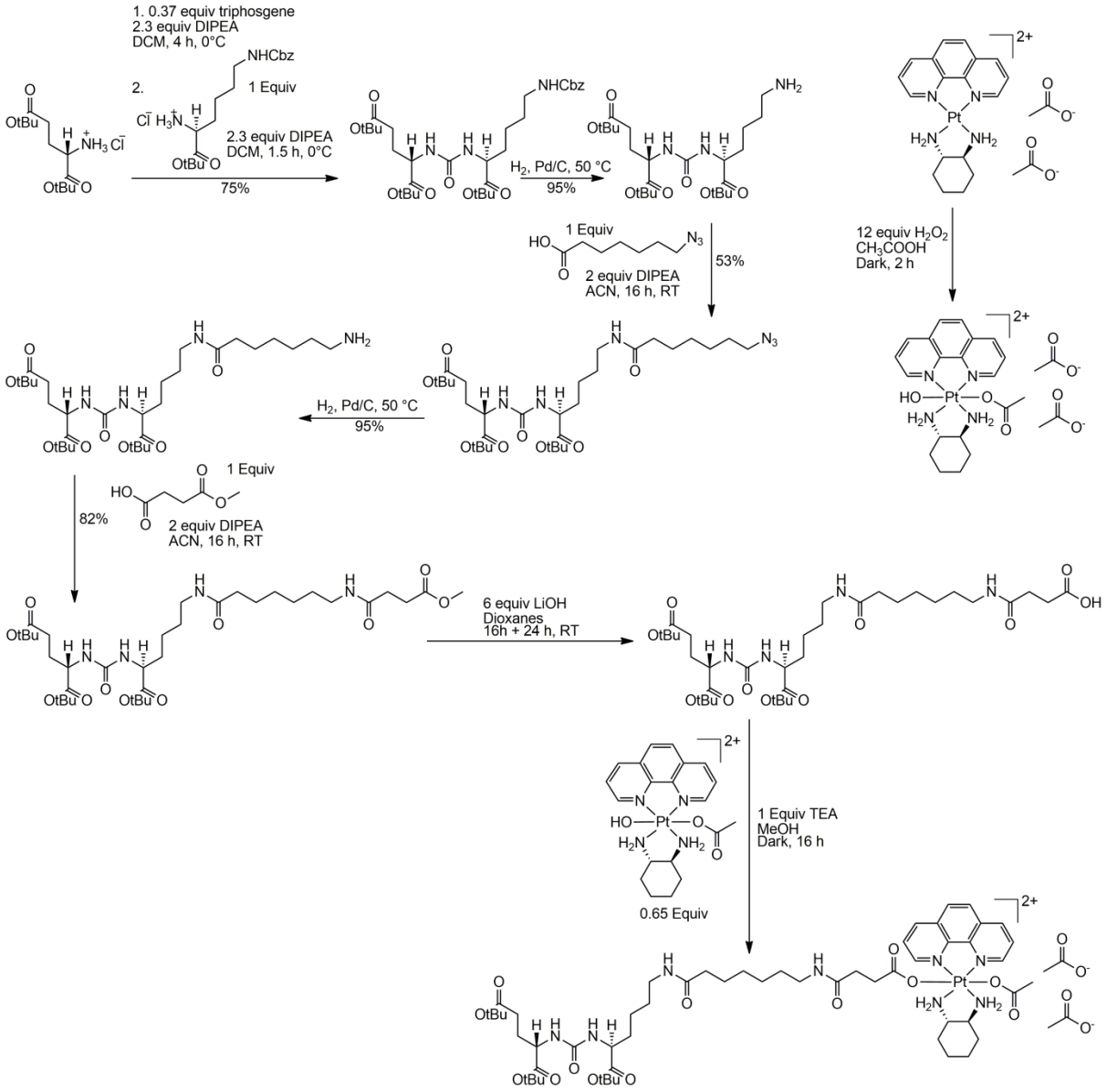

Figure 3.5.1. Full reaction scheme showing progression from DCL 1 to DCL 6, as well as the oxidation of PHENSS acetate to PHENSS(IV)A, and the conjugation of PHENSS(IV)A with DCL 6. Coupling agents HBTU and HOBt have been excluded for clarity.

To simplify the DCL-PHENSS conjugation process, it was decided that rather than two hydroxido ligands, the platinum(IV) reagent would incorporate one hydroxido and one acetato ligand. If PHENSS(IV) dihydroxido was used in the DCL coupling reaction, it would be difficult to ensure that the products were not a mixture of PHENSS(IV) with one hydroxido and one DCL ligand and PHENSS(IV) with two DCL ligands. To prevent this occurrence, the asymmetric complex PHENSS(IV)A was synthesised. The acetato ligand was expected to be relatively unreactive and so would prevent the DCL ligand from binding twice. The oxidation of PHENSS to the asymmetric complex PHENSS(IV)A was achieved through a similar process to that which produced the symmetric dihydroxido complexes in Section 3.4. The reaction took place in acetic acid as this would be the source of the acetate axial ligand as described by the oxidation mechanism in Section 3.4.2.[157] To ensure that no mixed-counter-

ion products were produced, PHENSS was converted to an acetate salt prior to oxidation. Method 1 was used to synthesise the PHENSS(IV)A that would be coupled to the DCL ligand in Reaction 3.5.9. PHENSS(IV)A was used here without further purification, as Reaction 3.5.9 was performed to determine if the final product could be made. Method 2 was developed in an attempt to isolate and purify PHENSS(IV)A. To halt the reaction immediately and crash the product out of solution, a smaller amount of acetic acid was used so that the product could immediately be precipitated in diethyl ether. The proton NMR spectrum of PHENSS(IV)A (Figure 3.5.2) shows the typical upfield shift of proton signals that occurs when oxidised. The platinum chemical shift of the product was at approx. 541 ppm, which is shifted higher than the dihydroxido peaks of ~430 ppm. Minor impurities were visible and likely correspond to the diacetato complex; some proton peaks that are slightly upfield of the main product are present, and the ^{1}H-^{195}Pt HMQC spectrum of the crude product showed a minor peak at ~720 ppm (Figure 3.5.3). There is also a peak corresponding to unbound acetic acid at approximately 1.91 ppm, and two peaks at ~3.48 and 1.10 corresponding to diethyl ether. Yield could not be record as the product could not be fully isolated; if the acetic acid was removed – either through washing with more diethyl ether or when dissolving the sample in water and lyophilising it – the sample reduced to platinum(II). Due to time restrictions, no further attempts were made to isolate PHENSS(IV)A.

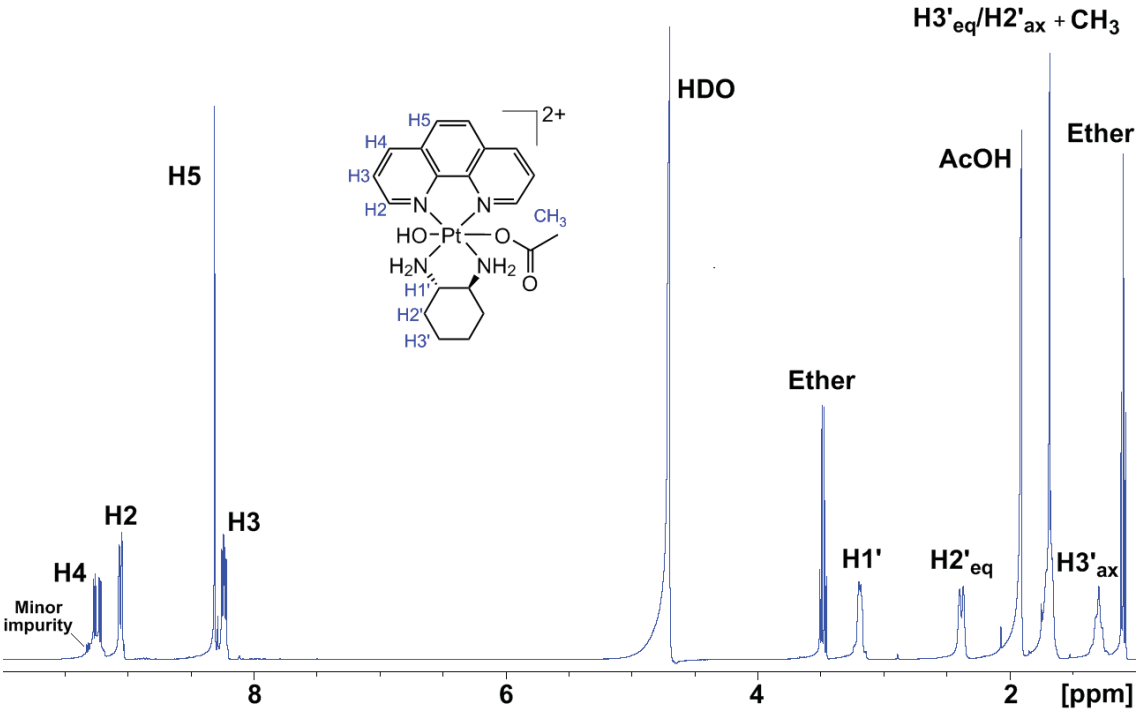

Figure 3.5.2. Proton NMR spectrum of PHENSS(IV)A in D_2O, showing proton assignment. Amine and hydroxido resonances are not observed due to exchange with D_2O.

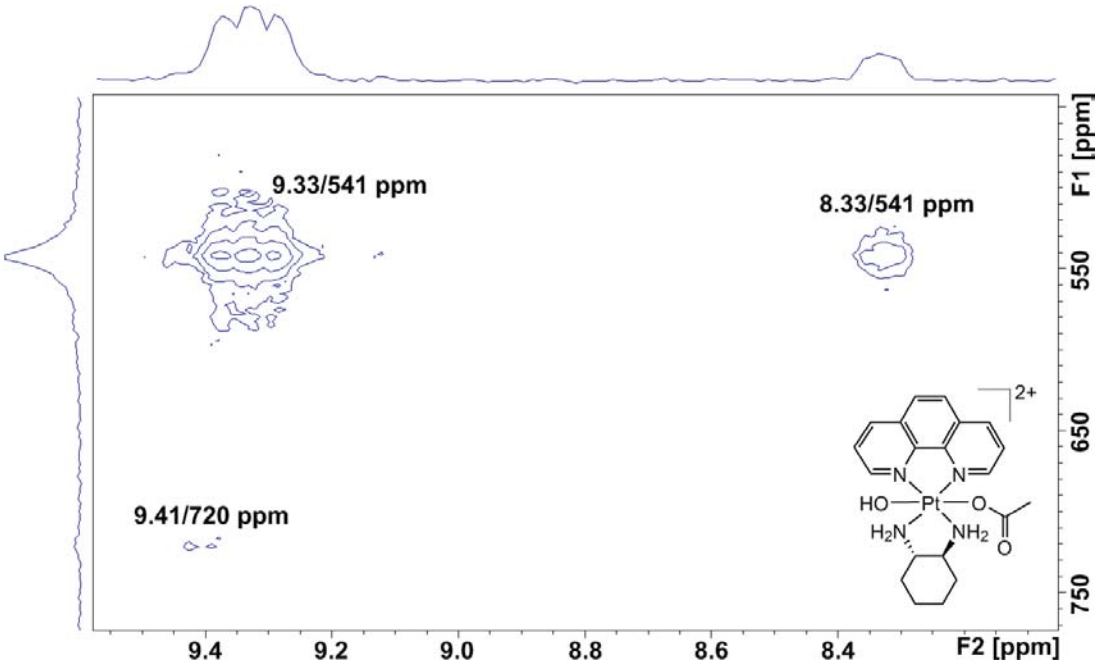

Figure 3.5.3. ^{1}H-^{195}Pt HMQC NMR spectrum of PHENSS(IV)A in D_2O, showing cross-peak assignment.

The final reaction to produce PHENSS(IV)-DCL used HBTU to activate the terminal carboxylic acid and TEA to deprotonate the hydroxido group of PHENSS(IV)A. The reaction was moderately successful as the *m/z* peak corresponding to the product was visible in the mass spectrum of the crude product solution (Figure 3.5.4). Unfortunately, the reaction scale was too small to attempt isolation of the product *via* preparative HPLC, and time restrictions prevented this series of reactions from being optimised. However, these results confirm that it is possible to couple the DCL moiety to a PPC using a carboxylic acid link.

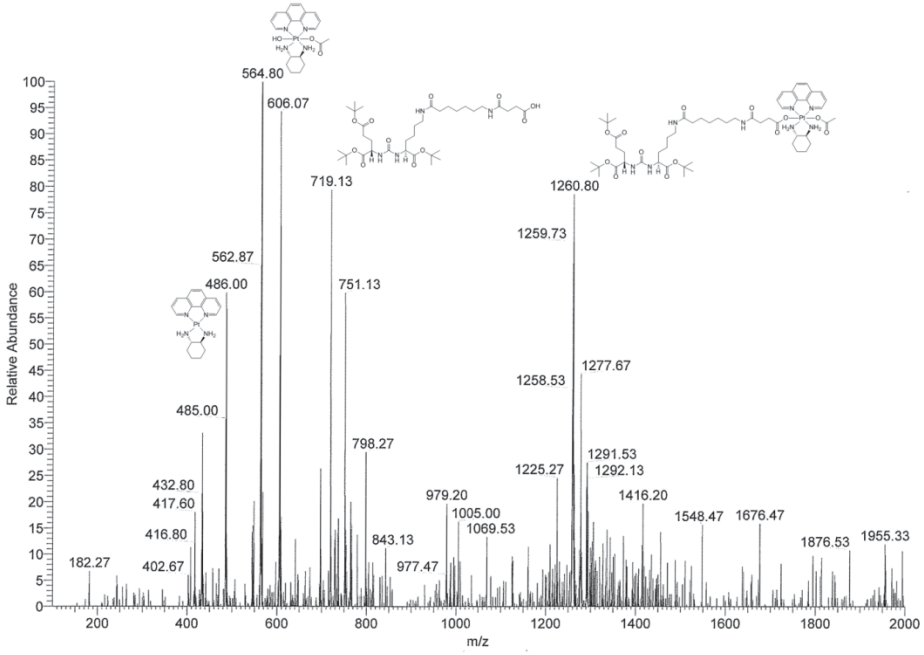

Figure 3.5.4. Mass spectrum of PHENSS(IV)DCL crude product, with major peaks corresponding to product and starting materials identified.

CHAPTER 4. CONCLUSIONS

Four papers have been published based upon the synthesis of PPCs and the analysis of their DNA binding. In total, fifteen PPCs were synthesised, fourteen of which were novel. The PPCs were of the type $[Pt(P_L)(A_L)](X)_2$. P_L is a polyaromatic ligand, one of bpy, $44Me_2bpy$, or 2pq (Paper I), an R-pytri ligand (Paper III) or phen, 5Mephen, or $56Me_2phen$ (Paper IV). A_L is a diamine ancillary ligand, either *SS*-dach or *RR*-dach (Papers I and III) or 1,4-dach (Paper IV), while X is either chloride (Papers I and III) or nitrate (Paper IV). Synthesis was achieved through the modification of the published reflux method (Papers I and III) or the silver nitrate exchange method (Paper IV) which resulted in highly pure complexes with moderately high yields. This work provides the foundation for many more P_L and A_L combinations that will be explored in the future, and the synthetic method to be further optimised to achieve higher yields.

All complexes synthesised were tested for cytotoxicity in several human cell lines. Aside from the R-pyrtri and 1,4-dach derived complexes and BPYRR, all PPCs demonstrated notable activity in all cell lines tested, with many complexes surpassing the activity of chemotherapeutic agents cisplatin, carboplatin and oxaliplatin. The PPCs studied were particularly potent against Du145 prostate cancer, HT29 colon carcinoma and SJ-G2 glioblastoma cells. Overall, 56MESS is the most cytotoxic complex, with the A_L of each complex having much more of an effect on activity of the PPC than the choice of P_L. The DNA binding of the PPCs BPYSS, 44MEBSS, PHENSS, 56MESS, DPQSS and 23MEDSS was assessed through several biophysical assays. The experiments revealed that each complex binds with CT-DNA through intercalation, with binding constants within the range of 10^5 M^{-1}. While all biophysical techniques provided unique information, the prominent ones to use at a minimum were determined to be ITC and LD. Despite 23MEDSS and DPQSS incorporating a larger P_L, the complex with the highest DNA affinity was 56MESS; this suggests that there is an optimum P_L size for PPC-DNA interactions and the $56Me_2phen$ ligand is close to that size. DNA affinity and cytotoxicity were correlated for 56MESS, PHENSS, 44MEBSS and BPYSS; this suggests that DNA affinity may affect cytotoxicity, although DNA binding is not likely the primary mechanism of action for these complexes. In order to truly understand the mechanism of action of these PPCs, further biological studies, such as proteomics and genomics assays and 3D tumour model studies, need to be undertaken.

The synthesis of six dihydroxido platinum(IV) complexes PHENSS(IV), PHENRR(IV), 5MESS(IV), 5MERR(IV), 56MESS(IV) and 56MERR(IV) was achieved through optimisation of the hydrogen peroxide oxidation method affording high yield and purity. It was found that lowering the concentration of peroxide and using heat allowed for larger scale

reactions to be carried out, and that column chromatography could be used to successfully remove coloured impurities. These complexes can now be consistently synthesised and subsequently used to create more complicated and highly functionalised platinum(IV) prodrugs. The application of this methodology was assessed with the asymmetric acetato-hydroxido platinum(IV) complex PHENSS(IV)A, which was synthesised and conjugated to the PSMA-targeting moiety DCL through a peptide chain. While the final products could not be isolated within the timeframe of this candidature, the reactions confirm that linking DCL to a platinum centre is possible, and that polyaromatic platinum(IV) complexes have the potential to become potent targeted prodrugs. In the future, a wide variety of targeting agents and other ligands can be coordinated in the axial position to expand the functionality of our PPCs, leading to prodrug candidates that can withstand *in vivo* conditions, find their target and deliver a highly cytotoxic platinum payload to cancerous tumours.

References

1. Australian Institute of Health and Welfare and Australasian Association of Cancer Registries, *Cancer in Australia 2017*, Australian Institute of Health and Welfare, Canberra, 2017.
2. R. L. Siegel, K. D. Miller and A. Jemal, *CA. Cancer J. Clin.*, 2017, **67**, 7-30.
3. H. Joensuu, *Lancet Oncol.*, 2008, **9**, 304-304.
4. N. J. Wheate, S. Walker, G. E. Craig and R. Oun, *Dalton Trans.*, 2010, **39**, 8113-8127.
5. P. Nygren, *Acta Oncol.*, 2001, **40**, 166-174.
6. R. Pazdur, K. A. Camphausen, L. D. Wagman and W. J. Hoskins, *Cancer Management: A Multidisciplinary Approach*, Cmp United Business Media, 2008.
7. T. Talarico, D. Phillips, G. Deacon, S. Rainone and L. Webster, *Invest. New Drugs*, 1999, **17**, 1-15.
8. P. Saraon, K. Jarvi and E. P. Diamandis, *Clin. Chem.*, 2011, **57**, 1366-1375.
9. R. J. Kumar, A. Barqawi and E. D. Crawford, *Rev. Urol.*, 2005, **7**, S37-S43.
10. B. A. Weber, B. L. Roberts, N. R. Chumbler, T. L. Mills and C. B. Algood, *Urol. Nurs.*, 2007, **27**, 527-533.
11. I. F. Tannock , R. de Wit , W. R. Berry , J. Horti , A. Pluzanska , K. N. Chi , S. Oudard , C. Théodore , N. D. James , I. Turesson , M. A. Rosenthal and M. A. Eisenberger *New Engl. J. Med.*, 2004, **351**, 1502-1512.
12. D. P. Petrylak , C. M. Tangen , M. H. A. Hussain , P. N. J. Lara , J. A. Jones , M. E. Taplin , P. A. Burch , D. Berry , C. Moinpour , M. Kohli , M. C. Benson , E. J. Small , D. Raghavan and E. D. Crawford *New Engl. J. Med.*, 2004, **351**, 1513-1520.
13. S. S. Chang, D. S. O'Keefe, D. J. Bacich, V. E. Reuter, W. D. W. Heston and P. B. Gaudin, *Clin. Cancer Res.*, 1999, **5**, 2674-2681.
14. D. A. Silver, I. Pellicer, W. R. Fair, W. D. Heston and C. Cordon-Cardo, *Clin. Cancer Res.*, 1997, **3**, 81-85.
15. A. Ghosh and W. D. W. Heston, *J. Cell. Biochem.*, 2004, **91**, 528-539.
16. J. S. Ross, C. E. Sheehan, H. A. G. Fisher, R. P. Kaufman, P. Kaur, K. Gray, I. Webb, G. S. Gray, R. Mosher and B. V. S. Kallakury, *Clin. Cancer Res.*, 2003, **9**, 6357-6362.
17. M. J. Burger, M. A. Tebay, P. A. Keith, H. M. Samaratunga, J. Clements, M. F. Lavin and R. A. Gardiner, *Int. J. Cancer.*, 2002, **100**, 228-237.
18. M. Santoni, M. Scarpelli, R. Mazzucchelli, A. Lopez-Beltran, L. Cheng, S. Cascinu and R. Montironi, *J. Biol. Regul. Homeostatic Agents*, 2014, **28**, 555-563.
19. H. Liu, A. K. Rajasekaran, P. Moy, Y. Xia, S. Kim, V. Navarro, R. Rahmati and N. H. Bander, *Cancer Res.*, 1998, **58**, 4055-4060.
20. T. Liu, L. Y. Wu, M. Kazak and C. E. Berkman, *The Prostate*, 2008, **68**, 955-964.
21. S. M. Hillier, K. P. Maresca, F. J. Femia, J. C. Marquis, C. A. Foss, N. Nguyen, C. N. Zimmerman, J. A. Barrett, W. C. Eckelman, M. G. Pomper, J. L. Joyal and J. W. Babich, *Cancer Res.*, 2009, **69**, 6932-6940.
22. S. R. Banerjee, C. A. Foss, M. Castanares, R. C. Mease, Y. Byun, J. J. Fox, J. Hilton, S. E. Lupold, A. P. Kozikowski and M. G. Pomper, *J. Med. Chem.*, 2008, **51**, 4504-4517.
23. S. Jayaprakash, X. Wang, W. D. Heston and A. P. Kozikowski, *ChemMedChem*, 2006, **1**, 299-302.
24. B. Rosenberg, L. Van Camp and T. Krigas, *Nature*, 1965, **205**, 698-699.
25. B. Rosenberg, L. Van Camp, J. E. Trosko and V. H. Mansour, *Nature*, 1969, **222**, 385-386.
26. M. G. Apps, E. H. Y. Choi and N. J. Wheate, *Endocr.-Relat. Cancer*, 2015, **22**, R219-R233.
27. M. D. Hall, M. Okabe, D.-W. Shen, X.-J. Liang and M. M. Gottesman, *Annu. Rev. Pharmacol. Toxicol.*, 2008, **48**, 495-535.
28. E. R. Jamieson and S. J. Lippard, *Chem. Rev.*, 1999, **99**, 2467-2498.
29. A. V. Klein and T. W. Hambley, *Chem. Rev.*, 2009, **109**, 4911-4920.
30. M. S. Davies, S. J. Berners-Price and T. W. Hambley, *Inorg. Chem.*, 2000, **39**, 5603-5613.
31. B. H. Harper, F. Li, R. Beard, K. B. Garbutcheon-Singh, N. S. Ng and J. R. Aldrich-Wright, in *Supramolecular Systems in Biomedical Fields*, ed. H. J. Schneider, Royal Society of Chemistry, Cambridge, UK, 1st edn., 2013, ch. 9.
32. T. W. Hambley, *Coord. Chem. Rev.*, 1997, **166**, 181-223.

33. L. Kelland, *Nat. Rev. Cancer*, 2007, **7**, 573-584.
34. F. Puisset, A. Schmitt and E. Chatelut, *Anticancer Res.*, 2014, **34**, 465-470.
35. D. Wang and S. J. Lippard, *Nat. Rev. Drug Discov.*, 2005, **4**, 307-320.
36. J. D. Hoeschele, H. D. H. Showalter, A. J. Kraker, W. L. Elliott, B. J. Roberts and J. W. Kampf, *J. Med. Chem.*, 1994, **37**, 2630-2636.
37. R. Ranaldo, N. Margiotta, F. P. Intini, C. Pacifico and G. Natile, *Inorg. Chem.*, 2008, **47**, 2820-2830.
38. J. Kasparkova, T. Suchankova, A. Halamikova, L. Zerzankova, O. Vrana, N. Margiotta, G. Natile and V. Brabec, *Biochem. Pharmacol.*, 2010, **79**, 552-564.
39. V. Brabec, J. Malina, N. Margiotta, G. Natile and J. Kasparkova, *Chem. - Eur. J.*, 2012, **18**, 15439-15448.
40. N. Margiotta, C. Marzano, V. Gandin, D. Osella, M. Ravera, E. Gabano, J. A. Platts, E. Petruzzella, J. D. Hoeschele and G. Natile, *J. Med. Chem.*, 2012, **55**, 7182-7192.
41. M. J. Piccart, H. Lamb and J. B. Vermorken, *Ann. Oncol.*, 2001, **12**, 1195-1203.
42. M. Kartalou and J. M. Essigmann, *Mutat. Res-Fund. Mol. M.*, 2001, **478**, 23-43.
43. P. C. A. Bruijnincx and P. J. Sadler, *Curr. Opin. Chem. Bio.*, 2008, **12**, 197-206.
44. G. Momekov, A. Bakalova and M. Karaivanova, *Curr. Med. Chem.*, 2005, **12**, 2177-2191.
45. A. M. Krause-Heuer, R. Grünert, S. Kühne, M. Buczkowska, N. J. Wheate, D. D. Le Pevelen, L. R. Boag, D. M. Fisher, J. Kasparkova, J. Malina, P. J. Bednarski, V. Brabec and J. R. Aldrich-Wright, *J. Med. Chem.*, 2009, **52**, 5474-5484.
46. C. R. Brodie, J. G. Collins and J. R. Aldrich-Wright, *Dalton Trans.*, 2004, 1145-1152.
47. L. A. Graham, J. Suryadi, T. K. West, G. L. Kucera and U. Bierbach, *J. Med. Chem.*, 2012, **55**, 7817-7827.
48. J. Reedijk, *Metallomics*, 2012, **4**, 628-632.
49. K. Suntharalingam, O. Mendoza, A. A. Duarte, D. J. Mann and R. Vilar, *Metallomics*, 2013, **5**, 514-523.
50. S. Komeda, *Metallomics*, 2011, **3**, 650-655.
51. L. S. Lerman, *J. Mol. Biol.*, 1961, **3**, 18-30.
52. G. Arena, L. M. Scolaro, R. F. Pasternack and R. Romeo, *Inorg. Chem.*, 1995, **34**, 2994-3002.
53. E. Meggers, G. E. Atilla-Gokcumen, K. Grundler, C. Frias and A. Prokop, *Dalton Trans.*, 2009, 10882-10888.
54. M. V. Keck and S. J. Lippard, *J. Am. Chem. Soc.*, 1992, **114**, 3386-3390.
55. R. R. Monaco, *Nucleic Acids Res.*, 2010, **2010**, 685-691.
56. M. Ardhammar, B. Norden and T. Kurucsev, in *Circular Dichroism: Principles and Applications*, eds. N. Berova, K. Nananishi and R. W. Woody, Wiley-VCH, New York, 2nd edn., 2000.
57. D. Wilmanska, M. Czyz, K. Studzian, M. K. Piestrzeniewicz and M. Gniazdowski, *Z. Naturforsch., C: J. Biosci.*, 2001, **56**, 886-891.
58. P. Dervan, A. Poulin-Kerstien, E. Fechter and B. Edelson, in *DNA Binders and Related Subjects*, eds. M. Waring and J. Chaires, Springer Berlin Heidelberg, 2005, vol. 253, ch. 1, pp. 1-31.
59. B. Neto and A. Lapis, *Molecules*, 2009, **14**, 1725-1746.
60. D. A. Nicholas and G. Brian, *Curr. Med. Chem.*, 2017, **24**, 1504-1519.
61. K. W. Jennette, S. J. Lippard, G. A. Vassiliades and W. R. Bauer, *Proc. Nat. Acad. Sci.*, 1974, **71**, 3839-3843.
62. W. D. McFadyen, L. P. G. Wakelin, I. A. G. Roos and V. A. Leopold, *J. Med. Chem.*, 1985, **28**, 1113-1116.
63. J. Suryadi and U. Bierbach, *Chem. - Eur. J.*, 2012, **18**, 12926-12934.
64. S. J. Lippard, *Acc. Chem. Res.*, 1978, **11**, 211-217.
65. K. S. Lovejoy and S. J. Lippard, *Dalton Trans.*, 2009, 10651-10659.
66. A. L. Harris, X. Yang, A. Hegmans, L. Povirk, J. J. Ryan, L. Kelland and N. P. Farrell, *Inorg. Chem.*, 2005, **44**, 9598-9600.
67. S. Kemp, N. J. Wheate, D. P. Buck, M. Nikac, J. G. Collins and J. R. Aldrich-Wright, *J. Inorg. Biochem.*, 2007, **101**, 1049-1058.
68. K. J. Davis, J. A. Carrall, B. Lai, J. R. Aldrich-Wright, S. F. Ralph and C. T. Dillon, *Dalton Trans.*, 2012, **41**, 9417-9426.
69. S. Kemp, N. J. Wheate, M. J. Pisani and J. R. Aldrich-Wright, *J. Med. Chem.*, 2008, **51**, 2787-2794.

70. K. B. Garbutcheon-Singh, P. Leverett, S. Myers and J. R. Aldrich-Wright, *Dalton Trans.*, 2013, **42**, 918-926.
71. D. M. Fisher, R. R. Fenton and J. R. Aldrich-Wright, *Chem. Commun.*, 2008, 5613-5615.
72. S. Wang, M. J. Wu, V. J. Higgins and J. R. Aldrich-Wright, *Metallomics*, 2012, **4**, 950-959.
73. S. Wang, V. Higgins, J. Aldrich-Wright and M. Wu, *J. Chem. Biol.*, 2012, **5**, 51-61.
74. M. D. Hall and T. W. Hambley, *Coord. Chem. Rev.*, 2002, **232**, 49-67.
75. M. D. Hall, H. R. Mellor, R. Callaghan and T. W. Hambley, *J. Med. Chem.*, 2007, **50**, 3403-3411.
76. S. Dhar, N. Kolishetti, S. J. Lippard and O. C. Farokhzad, *Proc. Nat. Acad. Sci.*, 2011, **108**, 1850-1855.
77. N. Graf and S. J. Lippard, *Adv. Drug Delivery Rev.*, 2012, **64**, 993-1004.
78. W. H. Ang, I. Khalaila, C. S. Allardyce, L. Juillerat-Jeanneret and P. J. Dyson, *J. Am. Chem. Soc.*, 2005, **127**, 1382-1383.
79. S. Dhar, Z. Liu, J. Thomale, H. Dai and S. J. Lippard, *J. Am. Chem. Soc.*, 2008, **130**, 11467-11476.
80. C. F. Chin, Q. Tian, M. I. Setyawati, W. Fang, E. S. Q. Tan, D. T. Leong and W. H. Ang, *J. Med. Chem.*, 2012, **55**, 7571-7582.
81. M. D. Hall, R. A. Alderden, M. Zhang, P. J. Beale, Z. Cai, B. Lai, A. P. J. Stampfl and T. W. Hambley, *J. Struct. Biol.*, 2006, **155**, 38-44.
82. M. Clavel, S. Monfardini, S. Gundersen, S. Kaye, P. Siegenthaler, J. Renard, G. M. van and H. M. Pinedo, *Eur. J. Cancer Clin. Oncol.*, 1988, **24**, 1345-1348.
83. H. Anderson, J. Wagstaff, D. Crowther, R. Swindell, M. J. Lind, J. McGregor, M. S. Timms, D. Brown and P. Palmer, *Eur. J. Cancer Clin. Oncol.*, 1988, **24**, 1471-1479.
84. R. J. Schilder, F. P. LaCreta, R. P. Perez, S. W. Johnson, J. M. Brennan, A. Rogatko, S. Nash, C. McAleer, T. C. Hamilton, D. Roby, R. C. Young, R. F. Ozols and P. J. O'Dwyer, *Cancer Res.*, 1994, **54**, 709-717.
85. T. J. O'Rourke, G. R. Weiss, P. New, H. A. Burris, III, G. Rodriguez, J. Eckhardt, J. Hardy, J. G. Kuhn, S. Fields, G. M. Clark and D. D. Von Hoff, *Anti-Cancer Drugs*, 1994, **5**, 520-526.
86. J. Cetnar, G. Wilding, D. McNeel, N. K. LoConte, T. A. McFarland, J. Eickhoff and G. Liu, *Urol. Oncol.: Semin. Orig. Invest.*, 2013, **31**, 436-441.
87. W. D. Figg, C. H. Chau, R. A. Madan, J. L. Gulley, R. Gao, T. M. Sissung, S. Spencer, M. Beatson, J. Aragon-Ching, S. M. Steinberg and W. L. Dahut, *Clin. Genitourin. Cancer*, 2013, **11**, 229-237.
88. P. D. Braddock, T. A. Connors, M. Jones, A. R. Khokhar, D. H. Melzack and M. L. Tobe, *Chem.-Biol. Interact.*, 1975, **11**, 145-161.
89. R. J. Brandon and J. C. Dabrowiak, *J. Med. Chem.*, 1984, **27**, 861-865.
90. J. F. Vollano, S. Al-Baker, J. C. Dabrowiak and J. E. Schurig, *J. Med. Chem.*, 1987, **30**, 716-719.
91. C. M. Giandomenico, M. J. Abrams, B. A. Murrer, J. F. Vollano, M. I. Rheinheimer, S. B. Wyer, G. E. Bossard and J. D. Higgins, *Inorg. Chem.*, 1995, **34**, 1015-1021.
92. M. Galanski and B. K. Keppler, *Inorg. Chem.*, 1996, **35**, 1709-1711.
93. M. Galanski and B. K. Keppler, *Met.-Based Drugs*, 1995, **2**, 57-63.
94. J. Z. Zhang, P. Bonnitcha, E. Wexselblatt, A. V. Klein, Y. Najajreh, D. Gibson and T. W. Hambley, *Chem. - Eur. J.*, 2013, **19**, 1672-1676.
95. M. Reithofer, M. Galanski, A. Roller and B. K. Keppler, *Eur. J. Inorg. Chem.*, 2006, **2006**, 2612-2617.
96. K. R. Barnes, A. Kutikov and S. J. Lippard, *Chem. Biol.*, 2004, **11**, 557-564.
97. Q. He, C. H. Liang and S. J. Lippard, *Proc. Nat. Acad. Sci.*, 2000, **97**, 5768-5772.
98. S. Mukhopadhyay, C. M. Barnes, A. Haskel, S. M. Short, K. R. Barnes and S. J. Lippard, *Bioconjug Chem.*, 2008, **19**, 39-49.
99. L. Gaviglio, A. Gross, N. Metzler-Nolte and M. Ravera, *Metallomics*, 2012, **4**, 260-266.
100. S. Somaï, A. Gompel, W. Rostène and P. Forgez, *Biochem. Biophys. Res. Commun.*, 2002, **295**, 482-488.
101. A. C. Antony, *Blood*, 1992, **79**, 2807-2820.
102. J. Yang, W. Liu, M. Sui, J. Tang and Y. Shen, *Biomaterials*, 2011, **32**, 9136-9143.
103. I. K. Kwon, S. C. Lee, B. Han and K. Park, *J. Controlled Release*, 2012, **164**, 108-114.
104. N. Kolishetti, S. Dhar, P. M. Valencia, L. Q. Lin, R. Karnik, S. J. Lippard, R. Langer and O. C. Farokhzad, *Proc. Nat. Acad. Sci.*, 2010, **107**, 17939–17944.

105. R. P. Feazell, N. Nakayama-Ratchford, H. Dai and S. J. Lippard, *J. Am. Chem. Soc.*, 2007, **129**, 8438-8439.
106. B. Norden, A. Rodger and T. Dafforn, *Linear dichroism and circular dichroism – A textbook on polarised-light spectroscopy*, The Royal Society of Chemistry, London, 2010.
107. B. M. Bulheller, A. Rodger and J. D. Hirst, *Phys. Chem. Chem. Phys.*, 2007, **9**, 2020-2035.
108. M. Urbanová, *Chirality*, 2009, **21**, E215-E230.
109. H. Khachfe and D. Atkinson, *Eur. Biophys. J.*, 2012, **41**, 639-646.
110. E. Iakubovskaya, I. Kudelina, A. Feofanov, A. Gabibov, I. Bronstein, G. Dodson and I. Nabiev, in *Spectroscopy of Biological Molecules: Modern Trends*, eds. P. Carmona, R. Navarro and A. Hernanz, Springer Netherlands, 1997, ch. 73.
111. M. Hicks, N. Orkey, M. Pisani, J. Collins, N. Wheate and J. Aldrich-Wright, in *Methods for Studying Nucleic Acid/Drug Interactions*, eds. M. Wanunu and Y. Tor, CRC Press, 2011, ch. 1.
112. D. M. Nejat and P. Lincoln, *J. Fluoresc.*, 2013, **23**, 813-821.
113. P. Zhang, J. Chen and Y. Liang, *Acta Biochim. Biophys. Sin.*, 2010, **42**, 440-449.
114. A. M. Krause-Heuer, W. S. Price and J. R. Aldrich-Wright, *J. Chem. Biol.*, 2012, **5**, 105-113.
115. B. J. Pages, Y. Zhang, F. Li, J. Sakoff, J. Gilbert and J. R. Aldrich-Wright, *Eur. J. Inorg. Chem.*, 2015, **2015**, 4167-4175.
116. A. J. Miles and B. A. Wallace, *Chem. Soc. Rev.*, 2006, **35**, 39-51.
117. N. J. Wheate, C. R. Brodie, J. G. Collins, S. Kemp and J. R. Aldrich-Wright, *Mini-Rev. Med. Chem.*, 2007, **7**, 627-648.
118. S. Balakrishnan and S. Jaldappagari, *J. Lumin.*, 2013, **142**, 17-22.
119. B. Harper, PhD Thesis, University of Western Sydney, 2013.
120. C.-W. Hsu, C.-F. Kuo, S.-M. Chuang and M.-H. Hou, *Biometals*, 2013, **26**, 1-12.
121. G. Rodrigo, Z. Yan, I. Vassili and Z. Giovanni, *J. Phys. Condens. Mat.*, 2009, **21**, 34-102.
122. Q. Cao, Y. Li, E. Freisinger, P. Z. Qin, R. K. O. Sigel and Z.-W. Mao, *Inorg. Chem. Front.*, 2017, **4**, 10-32.
123. D. L. Ang, B. W. J. Harper, L. Cubo, O. Mendoza, R. Vilar and J. Aldrich-Wright, *Chem. - Eur. J.*, 2015, 2317-2325.
124. D. T. Clarke, M. A. Bowler, B. D. Fell, J. V. Flaherty, A. F. Grant, G. R. Jones, M. L. Martin-fernandez, D. A. Shaw, B. Todd, B. A. Wallace and E. Towns-Andrews, *Synchrotron Radiat. News*, 2000, **13**, 21-27.
125. D. T. Clarke and G. Jones, *J. Synchrotron Radiat.*, 2004, **11**, 142-149.
126. B. A. Wallace, *Nat. Struct. Biol.*, 2000, **7**, 708-709.
127. M. R. Hicks, A. Rodger, Y.-p. Lin, N. C. Jones, S. V. Hoffmann and T. R. Dafforn, *Anal. Chem.*, 2012, **84**, 6561-6566.
128. K. Razmkhah, N. P. Chmel, M. I. Gibson and A. Rodger, *Analyst*, 2014, **139**, 1372-1382.
129. R. Marrington, T. R. Dafforn, D. J. Halsall, J. I. MacDonald, M. Hicks and A. Rodger, *Analyst*, 2005, **130**, 1608-1616.
130. H.-K. Kim, J.-M. Kim, S. K. Kim, A. Rodger and B. Nordén, *Biochem.*, 1996, **35**, 1187-1194.
131. B. Valeur and M. N. Berberan-Santos, *Molecular Fluorescence: Principles and Applications*, Wiley-VCH, Weinheim, Germany, 2013.
132. J. M. Belitsky, S. J. Leslie, P. S. Arora, T. A. Beerman and P. B. Dervan, *Bioorg. Med. Chem.*, 2002, **10**, 3313-3318.
133. V. W.-W. Yam, K. M.-C. Wong, L.-L. Hung and N. Zhu, *Angew. Chem., Int. Ed.*, 2005, **44**, 3107-3110.
134. R. C. Evans, P. Douglas and C. J. Winscom, *Coord. Chem. Rev.*, 2006, **250**, 2093-2126.
135. J. Nygren, N. Svanvik and M. Kubista, *Biopolymers*, 1998, **46**, 39-51.
136. E. Grueso, G. López-Pérez, M. Castellano and R. Prado-Gotor, *J. Inorg. Biochem.*, 2012, **106**, 1-9.
137. S. Shi, H.-L. Huang, X. Gao, J.-L. Yao, C.-Y. Lv, J. Zhao, W.-L. Sun, T.-M. Yao and L.-N. Ji, *J. Inorg. Biochem.*, 2013, **121**, 19-27.
138. R. W. Sabnis, *Handbook of Biological Dyes and Stains: Synthesis and Industrial Applications*, John Wiley & Sons, New Jersey, 2010.
139. W. C. Tse and D. L. Boger, *Acc. Chem. Res.*, 2003, **37**, 61-69.
140. A. Alonso, M. J. Almendral, Y. Curto, J. J. Criado, E. Rodríguez and J. L. Manzano, *Anal. Biochem.*, 2006, **355**, 157-164.
141. A. Banerjee, J. Singh and D. Dasgupta, *J. Fluoresc.*, 2013, **23**, 745-752.

142. B. J. Pages, F. Li, P. Wormell, D. L. Ang, J. K. Clegg, C. J. Kepert, L. K. Spare, S. Danchaiwijit and J. R. Aldrich-Wright, *Dalton Trans.*, 2014, **43**, 15566-15575.
143. E. Freire, O. L. Mayorga and M. Straume, *Anal. Chem.*, 1990, **62**, 950A-959A.
144. M. Kandeel, W. Elgazar and Y. Kitade, *Indian J. Pharm. Sci.*, 2012, **74**, 592-596.
145. J. I. Loch, P. Bonarek, A. Polit, S. Swiatek, M. Dziedzicka-Wasylewska and K. Lewinski, *J. Mol. Recognit.*, 2013, **26**, 357-367.
146. H. Ertan, K. S. Siddiqui, J. Muenchhoff, T. Charlton and R. Cavicchioli, *Biochim.*, 2012, **94**, 1221-1231.
147. A. Szabó, R. A. Flowers, B. J. Carter and S. A. Lee, *Phys. Rev. E*, 1998, **58**, 7754-7760.
148. H. Xu, Y. Liang, P. Zhang, F. Du, B.-R. Zhou, J. Wu, J.-H. Liu, Z.-G. Liu and L.-N. Ji, *J. Biol. Inorg. Chem.*, 2005, **10**, 529-538.
149. I. Haq, P. Lincoln, D. Suh, B. Norden, B. Z. Chowdhry and J. B. Chaires, *J. Am. Chem. Soc.*, 1995, **117**, 4788-4796.
150. C. Metcalfe, I. Haq and J. A. Thomas, *Inorg. Chem.*, 2004, **43**, 317-323.
151. C. Rajput, R. Rutkaite, L. Swanson, I. Haq and A. Thomas Jim, *Chem. - Eur. J.*, 2006, **12**, 4611-4619.
152. T. Wiseman, S. Williston, J. F. Brandts and L.-N. Lin, *Anal. Biochem.*, 1989, **179**, 131-137.
153. P. E. Morin and E. Freire, *Biochem.*, 1991, **30**, 8494-8500.
154. B. A. Williams and E. J. Toone, *J. Org. Chem.*, 1993, **58**, 3507-3510.
155. J. Moretto, B. Chauffert, F. Ghiringhelli, J. Aldrich-Wright and F. Bouyer, *Invest. New Drugs*, 2011, **29**, 1164-1176.
156. K. B. Garbutcheon-Singh, S. Myers, B. W. J. Harper, N. S. Ng, Q. Dong, C. Xie and J. R. Aldrich-Wright, *Metallomics*, 2013, **5**, 1061-1067.
157. S. O. Dunham, R. D. Larsen and E. H. Abbott, *Inorg. Chem.*, 1993, **32**, 2049-2055.
158. N. Margiotta, S. Savino, C. Marzano, C. Pacifico, J. D. Hoeschele, V. Gandin and G. Natile, *J. Inorg. Biochem.*, 2016, **160**, 85-93.
159. F. J. Macias, K. M. Deo, B. J. Pages, P. Wormell, J. K. Clegg, Y. Zhang, F. Li, G. Zheng, J. Sakoff, J. Gilbert and J. R. Aldrich-Wright, *Chem. - Eur. J.*, 2015, **21**, 16990-17001.
160. B. M. Still, P. G. A. Kumar, J. R. Aldrich-Wright and W. S. Price, *Chem. Soc. Rev.*, 2007, **36**, 665-686.
161. R. P. Murelli, A. X. Zhang, J. Michel, W. L. Jorgensen and D. A. Spiegel, *J. Am. Chem. Soc.*, 2009, **131**, 17090-17092.
162. K. P. Maresca, S. M. Hillier, F. J. Femia, D. Keith, C. Barone, J. L. Joyal, C. N. Zimmerman, A. P. Kozikowski, J. A. Barrett, W. C. Eckelman and J. W. Babich, *J. Med. Chem.*, 2009, **52**, 347-357.
163. A. V. Klein, PhD Thesis, Sydney University, 2013.
164. R. Knorr, A. Trzeciak, W. Bannwarth and D. Gillessen, *Tetrahedron Letters*, 1989, **30**, 1927-1930.